THE CORAL *CLADOCORA CAESPITOSA* AS A

HIGH RESOLUTION PALAEOCLIMATE ARCHIVE

Samuel H Royle

March 2015

A thesis presented to the School of Environmental

Sciences, University of East Anglia, in candidate for

the degree of Doctor of Philosophy

Abstract

High resolution proxy data (stable isotopes, trace elements) from coral skeletons is an established method to reconstruct seawater growth temperatures for palaeoenvironmental studies. In this work the temperate, colonial, Mediterranean scleractinian coral *Cladocora caespitosa* was investigated. First modern Adriatic corals from Mljet (Croatia) where growth temperatures were known were studied. A clear sinusoidal cyclicity is present in both the $\delta^{18}O$ and trace element (Sr, Mg, U, etc.) composition of the modern coral skeletons. Cyclicity approximately matches the number of seasonal growth band pairs in each corallite, implying a genetic link between these cycles and factors that determine seasonal growth band development, in this case mainly water temperature. It is found that *C. caespitosa* do not calcify in equilibrium with seawater in respect to any of the proxies analysed. Much intra-site variation is observed in trace element composition between coral colonies so this is not useful for production of a reliable palaeothermometer. For $\delta^{18}O$ and Δ_{47} however, the offset, from what would be expected for aragonite precipitated in equilibrium with water, appears constant and so it was possible to derive a species-specific $\delta^{18}O$-temperature calibration equation, although more work needs to be done on Δ_{47}. The $\delta^{18}O$-temperature calibration equation was applied to well-preserved corals collected from late Pleistocene deposits, MIS 1, 5, 7, in central Greece. The fossils contain 'similar to modern' $\delta^{18}O$ values and variability in all proxies preserving growth environment seasonal signatures. MIS 5e, which has the best supporting contextual palaeoclimatic information, was found to be the warmest period studied with a lower than modern seasonal temperature range. The Early-Mid Holocene probably

experienced the coolest temperatures while conditions in MIS 7a/c were probably the wettest with most freshwater input into the Gulf.

Table of contents

List of figures

2. BACKGROUND TO CURRENT RESEARCH

3. METHODOLOGY

4. STABLE ISOTOPIC ANALYSIS - RESULTS AND DISCUSSION

5. CLUMPED ISOTOPIC ANALYSIS - RESULTS AND DISCUSSION

6. HIGH RESOLUTION TRACE ELEMENT ANALYSIS - RESULTS AND DISCUSSION

7. DISCUSSION AND REVIEW

List of Tables

5. CLUMPED ISOTOPIC ANALYSIS - RESULTS AND DISCUSSION

6. HIGH RESOLUTION TRACE ELEMENT ANALYSIS - RESULTS AND DISCUSSION

Acknowledgements

1. Introduction

1.1. Overview

1.1.1. Aims and objectives

The purpose of this research was to study the potential of the Mediterranean coral *Cladocora caespitosa* as a multi-proxy palaeoclimate archive for the interglacials of the late Pleistocene back to Marine Isotope Stage (MIS) 7. To complete this aim, the specific objectives were:

- To obtain stable isotope, clumped isotope and trace element data from modern samples of *C. caespitosa* collected from an environment where growth conditions were known.

- To use the modern data to assess the water temperature dependence of potential proxies and the reliability of *C. caespitosa* as a palaeoclimate archive.

- To use any proxies that prove reliably linked to water temperature, along with the known modern growth conditions, to calibrate species-specific proxy-temperature relationships, with the aim of producing palaeothermometers.

- To obtain stable isotope, clumped isotope and trace element data from well preserved fossil samples of *C. caespitosa* collected from a range of well dated sites around the Perachora Peninsula, Greece.

- To apply the modern *C. caespitosa* calibrated palaeothermometers to the fossil samples to attempt to reconstruct quantitative seasonal

palaeoclimate conditions for the interglacials of the late Pleistocene and Holocene in this area.

1.1.2.   Thesis structure

In this thesis the background to the current research is discussed first: the study covers a broad range of disciplines and techniques and each is introduced individually. The science of sclerochronology is summarised as a whole and the target of this study, the coral species *Cladocora caespitosa*, is introduced. The theory behind each analytical method/temperature proxy is discussed along with a brief overview of why it is potentially suitable for use to fulfil the aims of this study. The methods section includes the sample sites and field localities, along with detailed methodologies for each analytical technique used. The results of each technique and an analysis and discussion of their individual meanings for this work are contained within their own chapters; this allows each proxy, with its own advantages or disadvantages, to be kept separate initially. The discussion chapter summarises and brings together the findings of the individual techniques with a summary of the outcomes achieved that improve our understanding of Mediterranean climate through the last few interglacials: there is also a discussion on the potential causes of the observed disequilibrium calcification in *C. caespitosa.* The thesis is concluded with an overview of the main findings and potential avenues for future work.

2. Background to current research

Due to the relatively wide scope of fields and techniques (i.e. branches of geology, biology, chemistry and physics) brought together in this research it is necessary to review the literature relevant to these main topics. This section provides an overview on the main topics and theories underpinning the current research.

2.1. Sclerochronology

Sclerochronology is the study of time-series data contained within the mineralised tissues of plants and animals which were deposited by accretion over time. This technique is very similar to dendrochronology, as the growth increments in carbonate skeletons can be very similar to tree rings in both appearance and content. Due to the mineralogical nature of the study material it is possible to use geochemical time-series data (e.g. stable isotope or trace element composition) to facilitate both the measurement of elapsed time and examine environmental changes throughout the life of the studied individual/colony (Toland et al., 2000; Johnson et al., 2009).

The subjects of sclerochronological studies range from modern bivalves (Stecher III et al., 1996; Schöne et al., 2003; Schöne et al., 2005) to dinosaurs (Sander and Klein, 2005). However, probably the most common group of organisms for this kind of research, and the topic of this thesis, are the scleractinian corals. These aragonite skeletoned organisms are ideally suited to this kind of technique due to their longevity (some colonies can provide unbroken records of growth going back hundreds of years (e.g. Dunbar et al., 1994; Quinn et al., 1998)) and fast growth rate (with species such as

Montastrea annularis reaching up to 9 cm yr^{-1} (Gladfelter et al., 1978)) allowing data on a sub-monthly scale to be resolved (e.g. Montagna et al., 2007). Numerous studies have therefore been able to show the potential of scleractinian corals as high resolution palaeoenvironmental archives by comparing various environmental proxies of living corals to both laboratory controlled (Armid et al., 2011) and natural measured (Montagna et al., 2007) growth conditions and looking for significant relationships that can be used to back calculate the conditions in which ancient corals grew.

2.2. *Cladocora caespitosa*

The species of coral used in this research was *Cladocora caespitosa* (Figure 2.2.1). This species was chosen due to its relative abundance around the Mediterranean region both now and through the late Pleistocene to mid Holocene (Bernasconi et al., 1997; Peirano et al., 1998; Kružić, 2002; Montagna et al., 2007).

Figure 2.2.1 Living *C. caespitosa* with open polyps (photograph from www.pagurus.it)

2.2.1.   Ecology

C. caespitosa is a temperate colonial scleractinian coral of the family *Faviidae* (Linnaeus, 1767). According to the classification scheme of Schuhmacher & Zibrowius (1985); *C. caespitosa* is an ahermatypic, constructional, zooanthellate coral. This means that although it is not considered a reef building coral, in the sense of tropical reef builders (such as *Porites*), it is said to be physiologically and ecologically close to them (Schuhmacher and Zibrowius, 1985; Schiller, 1993). Where abundant, *C. caespitosa* may still form large formations or 'banks' which can up to a metre in height and cover several square metres in surface area (Peirano et al., 1998). Mostly, however, *C. caespitosa* is found as separate, distinct sub-spherical colonies, 15-60cm in diameter, and where abundant these form 'beds' (Aguirre and Jimenez, 1998; Peirano et al., 1998; Peirano et al., 2005). Because it is a zooanthellate (i.e. lives with symbiotic photosynthetic algae) *C. caespitosa* is restricted to living in the photic zone and

is most common at depths of 7-25 m, although it can be found down to 40 m where the waters are clear enough for sunlight to penetrate (Rodolfo-Metalpa et al., 2008), which usefully constrains the depth of deposition of fossil assemblages.

2.2.2.   Distribution

As shown in Figure 2.2.2, *C. caespitosa* is most commonly found in the Mediterranean; however, there are records of colonies also being found in the East Atlantic, southern Portugal and Morocco (Peirano et al., 1998). Extensive biostromes of *C. caespitosa* are very rare today; the largest known living *C. caespitosa* bank, and the only one truly comparable to a tropical reef, is found in Lake Veliko Jezero ('Big Lake'), Mljet National Park, Croatia (Kružić et al., 2008; Kružić and Benković, 2008). However, extensive fossil deposits show that large banks dominated by this species were much more widespread in the previous interglacials of the late Pleistocene to mid Holocene (Bernasconi et al., 1997; Pirazzoli et al., 1997; Houghton et al., 2003; Leeder et al., 2003; Mastronuzzi et al., 2003; Peirano et al., 2009). This is especially true around southern Italy and the Gulf of Corinth, Greece. Here they have been used extensively to date uplifted marine terraces by ^{234}Uranium-^{230}Thorium methods (Pirazzoli et al., 1997; Houghton et al., 2003; Leeder et al., 2003; Leeder et al., 2005; Peirano et al., 2009; Roberts et al., 2009). This means there is plenty of readily accessible study material from deposits that have already been dated by other studies.

It has been suggested that the recent reduction in the distribution of *C. caespitosa* is related to climate change and human activity (Laborel, 1987); however, it seems likely that conditions were more favourable to this species

proliferation during past interglacials compared to the present, with or without anthropogenic effects.

C. caespitosa can occupy a wide variety of habitats; from sandy to rocky substrates and from areas with high turbulence to more sheltered settings. This is possible as the morphotype of colonies is adaptable to different conditions. In low energy areas they can grow taller and have an inverted cone morphology; whereas in higher energy areas (e.g. beach facies) they are flatter and have more rounded outlines (Aguirre and Jimenez, 1998; Peirano et al., 1998); which are presumably less susceptible to breakage. Unlike most species of coral, *C. caespitosa* is commonly found around estuaries, being well adapted to living in turbid waters with a high content of particulate organic matter and zooplankton food sources, and being able to survive purely by heterotrophy for weeks at a time (Tremblay et al., 2011). It may well be this adaptability that has allowed this species to be so dominant in the fossil record and makes it such a promising target for palaeoclimate research.

Figure 2.2.2 Known distribution of modern and fossil (late Pleistocene - mid Holocene) *C. caespitosa* colonies in the NW Mediterranean (Chassefi and Kremer, 1972; Schiller, 1993; Chintiroglou, 1996; Fornos et al., 1996; Mauz et al., 1997; Pirazzoli et al., 1997; Aguirre and Jimenez, 1998; Stamatopoulos et al., 1998; Peirano et al., 2001; Kružić and Požar-Domac, 2002; Pedley and Grasso, 2002; Houghton et al., 2003; Zecchin et al., 2004; Peirano et al., 2005; Goy et al., 2006; Montagna et al., 2007; Kružić and Benković, 2008; Roberts et al., 2009; Santoro et al., 2009; Zecchin et al., 2010)

2.2.3.   Growth

C. caespitosa corallites have an average growth rate of 1.36 to 5.20 mmyr^{-1} (Peirano et al., 1998; Peirano et al., 1999). Growth of the corallites occurs by two processes: the lengthening of the corallite wall and the internal fusion of skeletal elements. The dominance of these two processes differs between times of the year leading to the formation of annual pairs of visible growth bands. Growth by corallite wall lengthening is more dominant in the summer and produces low density bands, whilst the process of internal fusion dominates during the winter producing high density bands. This has been shown to be related to the seasonal change in water temperature and irradiation, and appears to be unrelated to the growth depth of the colony (Peirano et al., 1999).

These seasonal changes in growth patterns are believed to be a response to the seasonality of the Mediterranean. There are more nutrients available to the coral in the winter (due to increased runoff from high rainfall and re-suspension of bottom sediments) providing both an increased food source for the coral polyps and nutrients for the zooxanthellae. This is suggested to allow a greater rate of carbonate precipitation and thus allows the formation of a denser skeleton (Peirano et al., 1999; Rodolfo-Metalpa et al., 2008). During the summer, because of the regular occurrences of dangerously high irradiance and temperature, the coral polyp builds longer and less dense calyx walls which it is able to completely recede into in times of high stress (Peirano et al., 2005).

2.2.4.   Suitability for a high resolution sclerochronology

The suitability of modern *C. caespitosa* for high resolution sclerochronology has already been proven by the studies of Silenzi et al. (2005) and Montagna et al. (2007) and this thesis aims to build upon their work.

Like all other shallow-water scleractinian corals, *C. caespitosa* secretes an aragonite skeleton as it grows. Although this species grows slowly in comparison to tropical reef building corals, it is a major carbonate producer in the Mediterranean (Laborel, 1987).

As with many species of tropical reef-building corals (Lea et al., 1989; Mitsuguchi et al., 1996; Allison and Finch, 2004; Correge, 2006; Armid et al., 2011), both the stable isotope and trace elemental compositions of *C. caespitosa* have been shown to represent a natural archive for the physical and chemical features of the surrounding environment at both low (seasonal (Silenzi et al., 2005)) and high (weekly to fortnightly (Montagna et al., 2007)) resolutions. Both of these studies showed that, although (like other corals) *C. caespitosa* does not precipitate its skeleton in equilibrium with the surrounding sea water (presumably due to some biological control or 'vital effect' (Weber and Woodhead, 1972)), trends seen in oxygen isotope ratios and trace element concentrations are significantly correlatable with sea surface temperature (SST).

This study is novel in taking these ideas and applying them to fossil and sub-fossil samples of *C. caespitosa* dating back to previous interglacials as far back as MIS 7.

2.3. Stable isotope theory

Stable isotope ratios are commonly used in palaeoclimate research and stable isotope theory is one of the major principles on which a large section of this thesis is founded.

Isotopes are species of an element that are identical in their numbers of protons and electrons but differ in their number of neutrons. This means that they have the same atomic number and thus exhibit almost identical chemical behaviour. However, due to their differing number of neutrons, they have different masses (atomic weights) and so have subtly different physical and chemical properties (Hoefs, 2004).

Stable isotopes do not break down by radioactive decay. In most cases where an element has multiple isotopes, there is one stable isotope that is much more common than the others (Hoefs, 2004); for example ^{16}O has a natural abundance of 99.76% while ^{17}O and ^{18}O are only present at 0.04% and 0.20% respectively (Nier, 1950).

2.3.1. Isotopic fractionation

The subtle chemical and physical differences between isotopes of the same element lead to fractionation of the isotopes when there is exchange of isotopes between two pools/substrates through chemical or physical processes (Urey, 1947).

The fractionation factor (α) quantifies the degree of isotope distribution between two end member pools and this is described by Equation 2.3.1. In this equation A and B are the two end members that isotope exchange is occurring between

while R_A and R_B are the least to the most abundant (generally the heavy to the light) ratios of isotopes in the two end members, A and B, respectively.

$$\propto = \frac{R_A}{R_B}$$

<div align="right">**Equation 2.3.1**</div>

Fractionation happens through both mass-dependent and mass-independent processes, however only mass-dependent fractionation is relevant to the current study:

Equilibrium fractionation occurs between two substances in chemical equilibrium. The strength of bonds containing heavier isotopes are higher than in the bonds containing lighter isotopes (Faure and Mensing, 2005). This is because the bonds between heavier isotopes need more vibrational energy (in the form of latent heat) to be broken. Because of this heavier isotopes become relatively concentrated in solid phases (as these have higher bond forces) while lighter isotopes will concentrate in gas phases. In the reaction most relevant to this study, between liquid water (H_2O) and solid aragonite ($CaCO_3$) the isotopes ^{16}O and ^{18}O will most readily partition themselves between these 2 phases to concentrate (heavy) ^{18}O in the aragonite and (light) ^{16}O in the water:

$$H_2{}^{18}O + Ca^{12}C^{16}O_3 \leftrightarrow H_2{}^{16}O + Ca^{12}C^{18}O^{16}O^{18}O$$
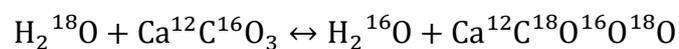
<div align="right">**Equation 2.3.2**</div>

The equilibrium constant (K) for this reaction is:

$$K = \frac{\left(Ca^{12}C^{18}O^{16}O^{18}O\right) \cdot \left(H_2{}^{16}O\right)}{\left(Ca^{12}C^{16}O_3\right) \cdot \left(H_2{}^{18}O\right)}$$

<div align="right">**Equation 2.3.3**</div>

This can be simplified, as the exchange concerns just a single nuclide, to:

$$\frac{\left(^{18}O/^{16}O\right)_{CaCO_3}}{\left(^{18}O/^{16}O\right)_{H_2O}} = \propto^O_{H_2O/CaCO_3}(T,P)$$

Equation 2.3.4

The fractionation constant $\propto^O_{H_2O/CaCO_3}(T,P)$ replaces the equilibrium partition constant K to signal that the exchange concerns just a single element (O) and is dependent on temperature and pressure (T, P). Fractionation factors and their relationships to temperature and pressure have been defined for many stable isotope pairs between varied phases as well as the $^{16}O/^{18}O$; $H_2O/CaCO_3$ relationship looked at here (which was calculated by Epstein et al. (1953)). As the molar volumes of the different stable isotopes of an element are very similar this relationship is actually virtually independent of pressure (Clayton et al., 1975) so that the main controlling factor is temperature, with equilibrium fractionation being strongest at lower temperatures.

Kinetic fractionation is also mass dependent. Lighter isotopes react quicker than heavier isotopes and at high reaction rates equilibrium cannot be reached so that the light isotopes, requiring lower energies to react, are exchanged more rapidly (Hoefs, 2004). This is important in geobiochemistry as organisms (by use of enzymes and other metabolic processes) speed up reaction rates. This leads to organic molecules becoming significantly enriched in light isotopes in comparison to both the environment in which they formed and abiological minerals formed under similar environmental conditions.

Together, the processes of equilibrium and kinetic fractionation form the basis of the most widely used isotope palaeothermometers.

The largest differences in behaviour are in the light elements as there are greater relative differences in their isotope's atomic weights than for the heavier elements. For example ^{2}H has approximately twice as much mass as ^{1}H, while ^{208}Pb is only 0.48% heavier than ^{207}Pb. Because of this it is the lighter isotopes that fractionate more readily and so are more studied for palaeoclimate work.

2.3.2.   Delta notation and standards

Measuring the absolute abundances of isotopes in a sample is difficult; instead, relative isotope abundances are measured with respect to an internal standard to allow the comparison of measurements of isotope abundances between different materials and different laboratories.

The delta notation expresses the abundance of a given isotope in a sample relative to the abundance of that isotope in a standard material with a delta value arbitrarily set to zero. This delta value of a sample is expressed as:

$$\delta(‰) = \left(\frac{R_{sample}}{R_{standard}} - 1 \right)$$

Equation 2.3.5

Where R is the heavy to light isotopic abundance ratio of the sample and standard respectively. Due to the small variations in isotopic abundance studied; the delta values are reported in per mil (‰) or parts per thousand. Positive δ values indicate that the sample is enriched in the heavy isotope with respect to the standard, while negative δ values indicate that the sample is depleted in the heavy isotope with respect to the standard.

Relevant to this study, the international standard for carbon and oxygen isotopic analysis of carbonate is the Vienna Pee Dee Belemnite (VPDB) and the one for

hydrogen isotope analysis of water is Vienna Standard Mean Ocean Water (VSMOW).

2.3.3. The carbonate-water δ^{18}O palaeothermometer

Early studies such as Urey et al. (1947), McCrea (1950) and Epstein et al. (1953) showed that there was a clear relationship between the oxygen isotopic composition of both inorganically and organically precipitated carbonates and temperature (due to the fractionation processes discussed above). This led to the development of the carbonate-water isotope temperature scale which has been one of the most widely used palaeothermometers.

This palaeothermometer is based around a heterogeneous isotope exchange reaction where oxygen isotopes are exchanged between calcium carbonate (aragonite or calcite) and water (Eiler, 2011) in the form:

$$H_2{}^{18}O + CaC^{16}O_3 \leftrightarrow H_2{}^{16}O + CaC^{18}O^{16}O_2$$
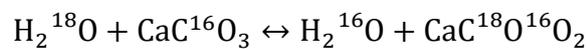
Equation 2.3.6

Experimental work has shown that, for calcite precipitated in isotopic equilibrium with the water, the degree of fractionation of the oxygen isotopes is related to temperature. The original work by Epstein et al. (1953) has been modified by Craig (1965) and Anderson and Arthur (1983) to produce the palaeotemperature equation for calcite precipitating in isotopic equilibrium:

$$T = 16.0 - 4.14(\delta^{18}O_C - \delta^{18}O_W) + 0.13(\delta^{18}O_C - \delta^{18}O_W)^2$$

Equation 2.3.7

More relevant to the corals studied here, the Grossman and Ku (1986) palaeotemperature equation for aragonite precipitated in isotopic equilibrium, modified by Goodwin et al. (2001):

$$T = 20.60 - 4.34(\delta^{18}O_A - (\delta^{18}O_W - 0.20)$$

Equation 2.3.8

These equations clearly show that to calculate temperature (T, in degrees Celsius), for the carbonate-water thermometer, we need to know both the oxygen isotopic composition (‰, VPDB) of the calcite ($\delta^{18}O_C$) or aragonite ($\delta^{18}O_A$) and the oxygen isotopic composition (‰, VSMOW) of the water it precipitated from ($\delta^{18}O_w$). For the majority of palaeotemperature and mineral formation studies the $\delta^{18}O$ of the water is a relative unknown and so an assumption must be made. Usually if dealing with marine carbonates the seawater is assumed to have been 0‰, however this is not always an accurate assumption, especially in areas where water masses are not well mixed with the open ocean (such as the Mediterranean (Gat et al., 1996; Pierre, 1999)) or during periods when global sea level and glacial extent have been different to modern (Thompson and Goldstein, 2005; Thompson and Goldstein, 2006). This introduces some uncertainty and a margin of error into the technique.

As well as the unknown oxygen isotopic value of the waters, this palaeothermometer also relies on equilibrium fractionation being the only process occurring during precipitation. In corals, however, isotopic fractionation does not occur in equilibrium with the water, the isotopic values of coralline aragonite being generally isotopically lower relative to inorganically precipitated carbonates.

This offset is called the "vital effect" (Weber and Woodhead, 1972) and is believed to be due to the kinetic (affected by rates of precipitation) and metabolic (affected by respiration and photosynthesis) effects caused by the coral altering its preferential uptake of oxygen isotopes from seawater into carbonate. At the site of calcification, carbonate is believed to gradually move towards isotopic equilibrium with the water that is present in the calcifying fluid, which will be in equilibrium with the seawater. Therefore, as calcification rate increases, the isotopic disequilibrium with seawater is more marked (McConnaughey, 1989a): this is thus partially controlled by growth rate (de Villiers et al., 1995). It has also been suggested that the disequilibrium also varies with pH variations in the microenvironment at the site of precipitation (Rollion-Bard et al., 2003a; 2003b). However, if the amount of disequilibrium caused by the vital effect is constant, and can be corrected for, then a coral's isotope composition may still be a useful indicator of palaeotemperature (Weil et al., 1981).

2.4. Carbonate clumped isotope thermometry

Isotopologues are molecules that are chemically identical but differing in their isotope composition (as opposed to isotopes which are solitary atoms with differing isotope compositions); see Table 2.4.1 for all carbonate and carbon dioxide isotopologues and their natural abundances.

2.4.1. Theory of carbonate clumped isotope thermometry

Carbonate clumped isotope thermometry is a relatively new technique which is less well established than, but has clear advantages over, the traditional carbonate $\delta^{18}O$ thermometer discussed above.

Carbonate clumped isotope thermometry is based on the temperature induced ordering of the heavy stable isotopes of carbon and oxygen, into bonds with each other in the same carbonate molecule (e.g. ^{13}C – ^{18}O). Carbonate minerals contain 20 different (stable) isotopologues of the carbonate ion group (Table 2.4.1). The most abundant of these, present at around 98.2%, $^{12}C^{16}O_3^{2-}$ contains no rare (heavy) stable isotopes, the next 3 are only singularly substituted (i.e. only containing one rare isotope) – and together these 4 make up around 99.99% of all the carbonate ions in a natural carbonate mineral, thus controlling their bulk isotopic compositions. It is the remaining approximately 0.01% of the ions which are the 'heavy' clumped isotopologues, with their double, triple and quadruple substituted bonds, which this technique exploits (Ghosh et al., 2006).

Table 2.4.1 Abundances of isotopologues of CO_2 and CO_3, assuming bulk $^{13}C/^{12}C$ ratios equal to PDB, bulk $^{18}O/^{17}O/^{16}O$ ratios equal to SMOW, and a random distribution of isotopes (after Ghosh et al., 2006)

CO_3 Isotopologue	Mass	Abundance
$^{12}C^{16}O^{16}O^{16}O$	60	98.20%
$^{13}C^{16}O^{16}O^{16}O$	61	1.10%
$^{12}C^{17}O^{16}O^{16}O$	61	0.11%
$^{12}C^{18}O^{16}O^{16}O$	62	0.60%
$^{13}C^{17}O^{16}O^{16}O$	62	12 ppm
$^{12}C^{17}O^{17}O^{16}O$	62	405 ppb
$^{13}C^{18}O^{16}O^{16}O$	63	67 ppm
$^{12}C^{17}O^{18}O^{16}O$	63	4.4 ppm
$^{13}C^{17}O^{17}O^{16}O$	63	4.54 ppb
$^{12}C^{17}O^{17}O^{17}O$	63	50 ppt
$^{12}C^{18}O^{18}O^{16}O$	64	12 ppm
$^{13}C^{17}O^{18}O^{16}O$	64	50 ppb
$^{12}C^{17}O^{17}O^{18}O$	64	828 ppt
$^{13}C^{17}O^{17}O^{17}O$	64	0.5 ppt
$^{13}C^{18}O^{18}O^{16}O$	65	138 ppb
$^{12}C^{17}O^{18}O^{18}O$	65	4.5 ppb
$^{13}C^{17}O^{17}O^{18}O$	65	9 ppt
$^{12}C^{18}O^{18}O^{18}O$	66	8 ppb
$^{13}C^{17}O^{18}O^{18}O$	66	51 ppt
$^{13}C^{18}O^{18}O^{18}O$	67	94 ppt
CO_2 Isotopologue	Mass	Abundance
$^{16}O^{12}C^{16}O$	44	98.40%
$^{16}O^{13}C^{16}O$	45	1.10%
$^{17}O^{12}C^{16}O$	45	730 ppm
$^{18}O^{12}C^{16}O$	46	0.40%
$^{17}O^{13}C^{16}O$	46	8.19 ppm
$^{17}O^{12}C^{17}O$	46	135 ppb
$^{18}O^{13}C^{16}O$	47	45 ppm
$^{17}O^{12}C^{18}O$	47	1.5 ppm
$^{17}O^{13}C^{17}O$	47	1.5 ppb
$^{18}O^{12}C^{18}O$	48	4.1 ppm
$^{17}O^{13}C^{18}O$	48	16.7 ppb
$^{18}O^{13}C^{18}O$	49	46 ppb

The heavy isotopes have a preference of bonding with each other, i.e. 'clumping' together, which becomes stronger at lower temperatures. Therefore, the abundance of the 'heavy' isotopologues in a growing carbonate has an inverse relationship with temperature, with the degree of clumping tending towards a random distribution as temperature increases (Thiagarajan et al., 2011). This phenomenon exists due to a thermodynamically controlled homogeneous (within only minerals of the same phase: carbonate) isotope equilibrium reaction in the forming carbonate mineral. The reaction which

produces the most common (and therefore the one measured for thermometry) doubly substituted isotopologue, $^{13}C^{18}O^{16}O_2^{2-}$, progresses as such:

$$^{13}C^{16}O_3^{2-} + {}^{12}C^{18}O^{16}O_2^{2-} \leftrightarrow {}^{13}C^{18}O^{16}O_2^{2-} + {}^{12}C^{16}O_3^{2-}$$
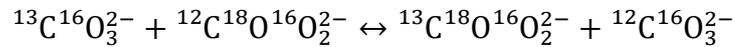
Equation 2.4.1

And is such biased towards the right hand side to show this slight preference towards producing heavier clumped isotopologues. Even in the most extreme cases this preference is less than 0.8% different from a random distribution, however, with modern mass spectrometers, this is still measureable.

The proportion of this most common rare heavy isotopologue in a carbonate sample can be measured through similar techniques to normal carbonate bulk $\delta^{13}C$, $\delta^{18}O$ mass spectrometry (Huntington et al., 2009; Eiler, 2011). The abundance of the doubly substituted isotopologue $^{13}C^{18}O^{16}O$, with mass-47, in the CO_2 has been shown to be proportional to the abundance of $^{13}C-^{18}O$ bonds in the digested carbonate (Ghosh et al., 2006). So by analysing the produced ion beams corresponding to masses 44 to 47 and measuring the ratio of mass-47 to mass-44 ($^{13}C^{18}O^{16}O$: $^{12}C^{16}O_2$) the deviation of the mass-47 over what would be expected from a random distribution can be calculated, this variable is known as Δ_{47} and is expressed in per mil (‰) (Ghosh et al., 2006; Eiler, 2011). Other masses, such as mass-48 and mass-49 can be reported as deviation from stochastic distribution ($\Delta_{48,49}$) in the same way.

The theoretical relationship between carbonate Δ_{47} and temperature, with Δ_{47} tending towards a stochastic distribution as temperature increases, is described by the polynomial equation by Guo et al. (2009a):

$$\Delta_{47} = -\frac{3.33040 \cdot 10^9}{T^4} + \frac{2.32415 \cdot 10^7}{T^3} - \frac{2.91282 \cdot 10^3}{T^2} - \frac{5.54042}{T} + 0.23252$$

<div align="right">**Equation 2.4.2**</div>

Plotting Equation 2.4.2 (fitted to the absolute reference frame of Dennis et al., (2011) to allow for inter-laboratory data comparison) over the temperature range experienced by near surface carbonates of 0-100°C, Figure 2.4.1, shows that over this range the relationship of carbonate Δ_{47} and temperature can be approximated by a straight line; described by Equation 2.4.3.
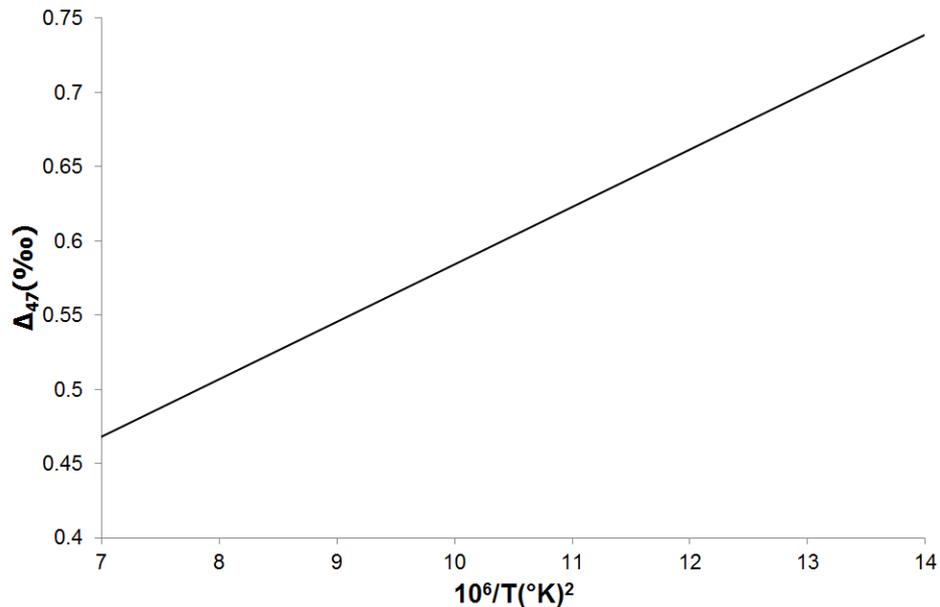
Figure 2.4.1 Plot of the Guo et al. (2009a) theoretical relationship between carbonate Δ_{47} and temperature with the polynomial approximating a straight line between 0-100°C (fitted to the absolute reference frame of Dennis et al., (2011)).

$$\Delta_{47} = 0.0375 \cdot \frac{10^6}{T^2} + 0.210$$

<div align="right">**Equation 2.4.3**</div>

Therefore, this enrichment can be used as a palaeothermometer. However, across the most commonly used 0-50°C range, Δ_{47} only ranges from around 0.5-0.7‰ (Ghosh et al., 2006) with a temperature sensitivity of −0.00289‰/°C (Guo et al., 2009a), leaving little margin for error.

2.4.2. Advantages over the δ^{18}O carbonate-water palaeothermometer

The main advantage of this method (over the traditional δ^{18}O carbonate palaeothermometer) is that the temperature of carbonate formation can be calculated without needing to know the δ^{18}O of the water it precipitated from. This is possible as the controlling isotope exchange reaction (Equation 2.4.1) is homogeneous; equilibrium is obtained through exchange among components of a single phase – calcium carbonate. Whereas the traditional carbonate-water thermometer examines a heterogeneous isotope exchange reaction between components of separate phases – calcium carbonate and water (Equation 2.3.6). By gaining temperatures of precipitation through clumped isotope thermometry and also measuring $\delta^{18}O_{carbonate}$ (and assuming equilibrium) it is actually possible to use a re-arranged carbonate-water palaeotemperature equation (such as Equation 2.3.7) to back calculate $\delta^{18}O_{water}$. In some situations this could prove a valuable proxy for estimating sea levels, ice volume, or better understanding the environment in which the carbonates were precipitated (e.g. Guo and Eiler, 2007).

Early work suggested that the majority of biologically precipitated carbonates do not exhibit any vital effects in their Δ_{47} values. Figure 2.4.2 is a summary diagram from a review by Eiler (2011) bringing together calibrations for the carbonate clumped isotope thermometer from a wide range of studies. What can clearly be seen is that almost all of the data points lie on or near the same calibration line as the synthetic calcites of Ghosh et al. (2006).
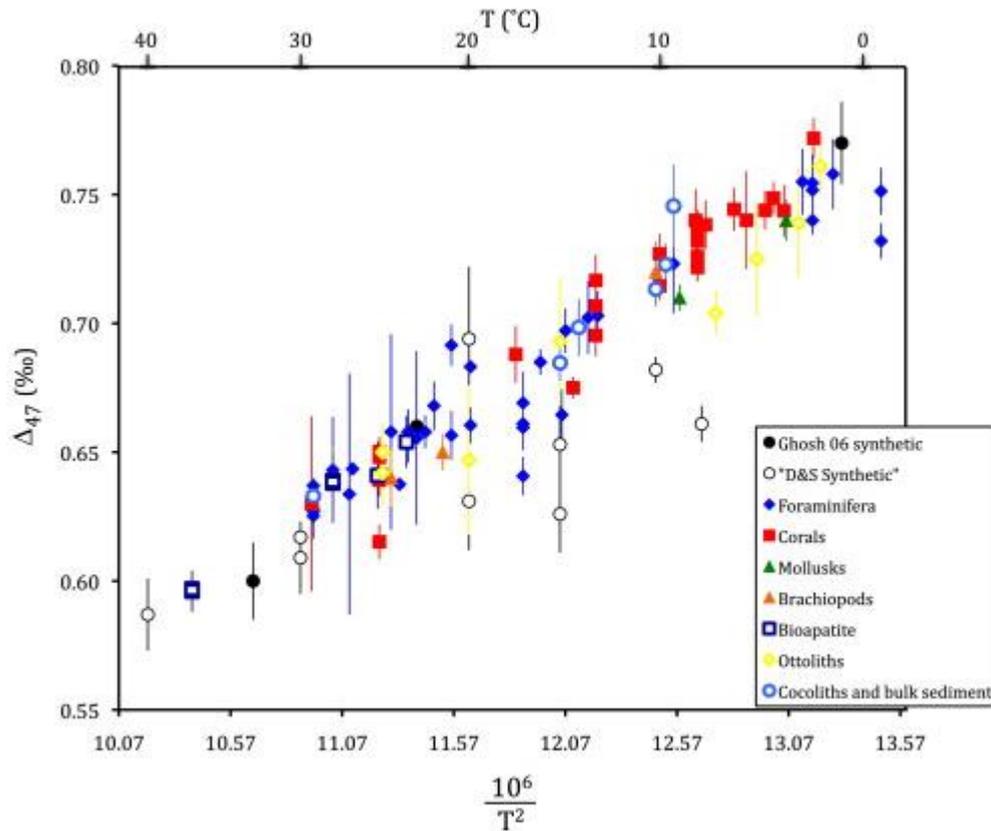
Figure 2.4.2 Summary of published calibrations of the carbonate clumped isotope thermometer between 0 and 40°C compiled by Eiler (2011). Data sources: Ghosh et al. (2006) – synthetic calcite and corals; Came et al. (2007) – molluscs and brachiopods; Ghosh et al. (2007) – otoliths; Dennis and Schrag (2010) – 'D&S synthetics'; Eagle et al. (2010) – bioapatite; Tripati et al. (2010) – foraminifera, coccoliths and bulk sediment (marine carbonates); Thiagarajan et al. (2011) – corals.

The collection of data that makes up the clearly visible trend in Figure 2.4.2 includes calcite, aragonite and carbonate-apatite, minerals that were grown both inorganically and biologically, and from a wide range of phyla from marine, freshwater and terrestrial environments. Therefore, this data set clearly suggests that (under very wide ranging circumstances) the calibration for this thermometer is independent of mineral, environmental condition and species. This was the view when this current study was begun and so it was originally hypothesised that clumped isotope analysis of *C. caespitosa* would provide

accurate temperatures without the complications of 'vital effects'; a major advantage over both $\delta^{18}O$ and trace element based carbonate thermometers.

2.5. Trace elements

2.5.1. Incorporation into coralline aragonite

As a growing coral (such as *C. caespitosa*) precipitates its aragonitic skeleton, various trace elements are incorporated so that the composition of the precipitated calcium carbonate is not pure $CaCO_3$.

Numerous studies (e.g. Kinsman and Holland, 1969; Weber, 1973; Lea et al., 1989; Beck et al., 1992; Rong Min et al., 1995; Alibert and McCulloch, 1997; McCulloch et al., 2003; Silenzi et al., 2005; Lewis et al., 2007; Montagna et al., 2007; LaVigne et al., 2010; Armid et al., 2011; Trotter et al., 2011) have shown experimentally and theoretically how the variation in the amount of a particular trace element incorporated into the precipitating aragonite will vary depending on various environmental and biological factors (such as temperature, precipitation rate, nutrient availability, rainfall, upwelling, pH), thus providing a record of changes in these parameters over the growth of the carbonate in a similar way to the fractionation of stable isotopes (discussed above).

However, there has been much debate on how the trace elements are incorporated into the crystal lattice and what processes control their uptake.

It is generally agreed that the partitioning of trace elements between seawater and the precipitating carbonate is not consistent with either equilibrium thermodynamics or kinetic fractionations (Gaetani and Cohen, 2006) and so is more complex than fractionation of the stable isotopes.

These trace elements may actually be incorporated into the molecular framework of the aragonite substituting for Ca^{2+} ions (Finch and Allison, 2007), with the models invoked for the relationships between trace element/Ca and temperature of precipitation assuming that trace elements substitute ideally for Ca (i.e. with no deformation of the aragonite molecular structure) as shown in Figure 2.5.1.
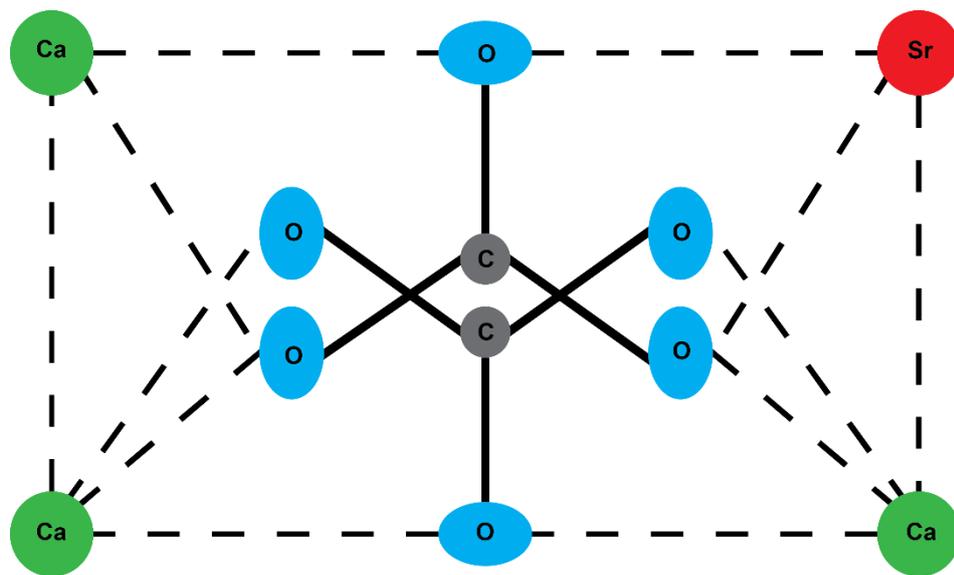
Figure 2.5.1 Aragonite (CaCO$_3$) molecular structure with calcium (Ca), carbon (C), oxygen (O) and a substituted element (strontium, Sr, in this example) in a site normally occupied by calcium (modified from Bevan et al., 2002)

However, due to the varying atomic radii of different elements (e.g. Ca: 197pm, Mg: 160pm, Sr: 215pm), crystal structures must accommodate trace elements through dilation or contraction of the ion site which alters strain fields and may cause far-reaching deformation throughout the molecular lattice (Finch and Allison, 2007). Hence ion exchange may be far from ideal, involving complex interactions between molecules which are not thoroughly understood, partially explaining why the partitioning of trace elements is not consistent with either equilibrium thermodynamics or kinetic fractionations.

Also, not all trace elements may be lattice bound, instead forming organo-metal complexes, being adsorbed onto crystal faces (Amiel et al., 1973), co-precipitating with the aragonite by occlusion, being trapped in crystal defects or in micro-domains (Sinclair, 2005).

By studying the skeletal composition of the 'brain' coral *Diplora labyrinthiformis* and comparing it with results from precipitation experiments to determine partition coefficients of various trace elements (Mg^{2+}, Ca^{2+}, Sr^{2+}, Ba^{2+}) into aragonite, Gaetani and Cohen (2006) concluded that the systematic change in partitioning with temperature is most likely due to the process of surface entrapment of Watson and Liang (1995) and Watson (2004). In this model the concentration of a particular trace-element (or stable isotope) is determined by both the concentration of the particular element in the near-surface region of the crystal and the relative rates of crystal growth (which can trap surface enrichments of elements in the crystal lattice) and ion-migration in the near-surface regions (which attempts to rid the lattice of impurities), i.e. '*a growing crystal assumes the composition of its surface unless diffusion in the near-surface region is effective during growth*' (Watson, 2004). This can cause the crystal's trace element and stable isotope composition to deviate from thermodynamic equilibrium when growth occurs quickly or where mobility of ions in the near surface region is limited, by low temperature for example. Because of this, it is especially relevant for the rapid growth of coralline aragonite crystals in the relatively low temperatures of ambient seawater.

Gaetani and Cohen (2006) also concluded that the calcifying fluid at the site of precipitation actually has a relatively constant Sr/Ca ratio comparable to that of seawater, but is depleted in Mg and Ba, and that variations in the trace

element/Ca ratio recorded in the aragonite are due to fluctuations in the precipitation efficiency of the aragonite, which governs growth rate. These authors go on to suggest that the seasonal fluctuations in the precipitation efficiency (growth rate) are caused by changes in the environmental conditions, most likely driven by variations in efficiency of the Ca-ATPase enzyme pump or ion channel transport in response to changes in light and/or temperature. Therefore, the combined effects of surface entrapment during aragonite growth and seasonal fluctuations in 'precipitation efficiency' likely forms the basis for the temperature information recorded in the aragonite skeletons of Scleractinian corals.

Despite this lack of agreement on the exact processes at work, numerous studies have still managed to use the trace elemental compositions of corals (and other carbonate producing organisms) for thermometry.

2.5.2.   Trace element palaeothermometry

Many studies have found a strong co-variance between the trace elemental composition of coralline aragonite and the temperature of precipitation (or SST) with annual-scale cycles in trace element to calcium ratios being a general feature in well preserved primary coralline aragonite (Rong Min et al., 1995).

The main trace elements used for coral palaeothermometry are strontium (Weber, 1973; Beck et al., 1992; de Villiers et al., 1994; Alibert and McCulloch, 1997; Marshall and McCulloch, 2002; Silenzi et al., 2005; Montagna et al., 2007; Sayani et al., 2011) and magnesium (Mitsuguchi et al., 1996; Sinclair et al., 1998; Silenzi et al., 2005; Montagna et al., 2007), as these are some of the most abundant trace elements in both seawater and coralline aragonite (Silenzi

et al., 2005). However, similar temperature dependencies have been found with barium (Lea et al., 1989; Montaggioni et al., 2006), boron (Montagna et al., 2007; Trotter et al., 2011), lithium (Marriott et al., 2004; Montagna et al., 2006a) and uranium (Rong Min et al., 1995; Sinclair et al., 1998; Montagna et al., 2007).

As noted above, corals do not calcify completely in equilibrium with seawater due to trace elemental uptake occurring by numerous processes and some biological controls or 'vital effects' as found with stable isotope uptake. The degree to which the trace element/Ca concentration - temperature relationship differs from equilibrium in shallow water corals appears to differ between different studies, different species and different localities (even between the same species in the same study (de Villiers et al., 1994)). This is demonstrated by the variability between a selection of the published Sr/Ca thermometer calibration equations shown in Table 2.5.1.

Table 2.5.1 Published Sr/Ca thermometer calibration equations for various shallow water scleractinian coral species

Study	Coral	Technique	Sr/Ca (mmol/mol)
Silenzi et al. (2005)	*Cladocora caespitosa*	ICP-Atomic Emission Spectroscopy (on winter growth bands)	$11.25(\pm0.38) - 0.079(\pm0.026) \cdot SST(\text{℃})$
Montagna et al. (2007)	*Cladocora caespitosa*	Laser Ablation – ICP-MS	$10.50(\pm0.13) - 0.073(\pm0.006) \cdot SST(\text{℃})$
Alibert & McCulloch (1997)	*Porites sp.*	Thermal Ionisation MS	$10.48(\pm0.01) - 0.0615(\pm0.004) \cdot SST(\text{℃})$
Marshall & McCulloch (2002)	*Porites sp.*	Isotope Dilution Thermal Ionisation MS	$10.40(\pm0.016) - 0.0575(\pm0.0005) \cdot SST(\text{℃})$
Sinclair et al. (1998)	*Porites mayeri*	LA-ICP-MS	$10.80(\pm0.10) - 0.070(\pm0.004) \cdot SST(\text{℃})$
Rong Min et al. (1995)	*Porites sp.*	Thermal Ionisation MS	$16.81 - 0.1881 \cdot SST(\text{℃})$
Mitsuguchi et al. (1996)	*Porites sp.*	ICP-Atomic Emission Spectroscopy	$10.50 - 0.0608 \cdot SST(\text{℃})$
Beck et al. (1992)*	*Porites lobata*	Thermal Ionisation MS	$16.013 - 0.167 \cdot SST(\text{℃})$
Armid et al. (2011)	*Porites cylindrica*	ICP-Atomic Emission Spectroscopy	$10.214(\pm0.229) - 0.0642(\pm0.00897) \cdot T(\text{℃})$
Alibert et. al (2003)	*Porites lutrea*	Thermal Ionisation MS	$10.29(\pm0.02) - 0.0537(\pm0.0006) \cdot SST(\text{℃})$
Alibert et. al (2003)	*Porites mayeri*	Thermal Ionisation MS	$10.46(\pm0.02) - 0.060(\pm0.0001) \cdot SST(\text{℃})$

*corrected by the authors

3. Methodology

3.1. Fieldwork localities and sample collection

Both modern and fossil samples of *C. caespitosa* were collected from numerous sites around the Mediterranean. This section describes the sampling localities, the methods of sample selection and the material collected.

3.1.1. Modern corals

The majority of the modern corals analysed were from the *C. caespitosa* bank in Lake Veliko Jezero, on the Island of Mljet, Croatia (42°46'08''N; 17°22' 26''E) (Figure 3.1.1 and Figure 3.1.2). This is the largest known living bank of *C. caespitosa*, approximately 650 m^2 in areal extent in water depths of 4-18 m (Kružić, 2002; Kružić and Požar-Domac, 2003; Kružić and Benković, 2008).

Living corallites, along with water samples, were collected alive by Dr Petar Kružić of the University of Zagreb, Croatia on the 21/09/2012.

Figure 3.1.1 Locality map of the *C. caespitosa* bank on the island of Mljet, Croatia
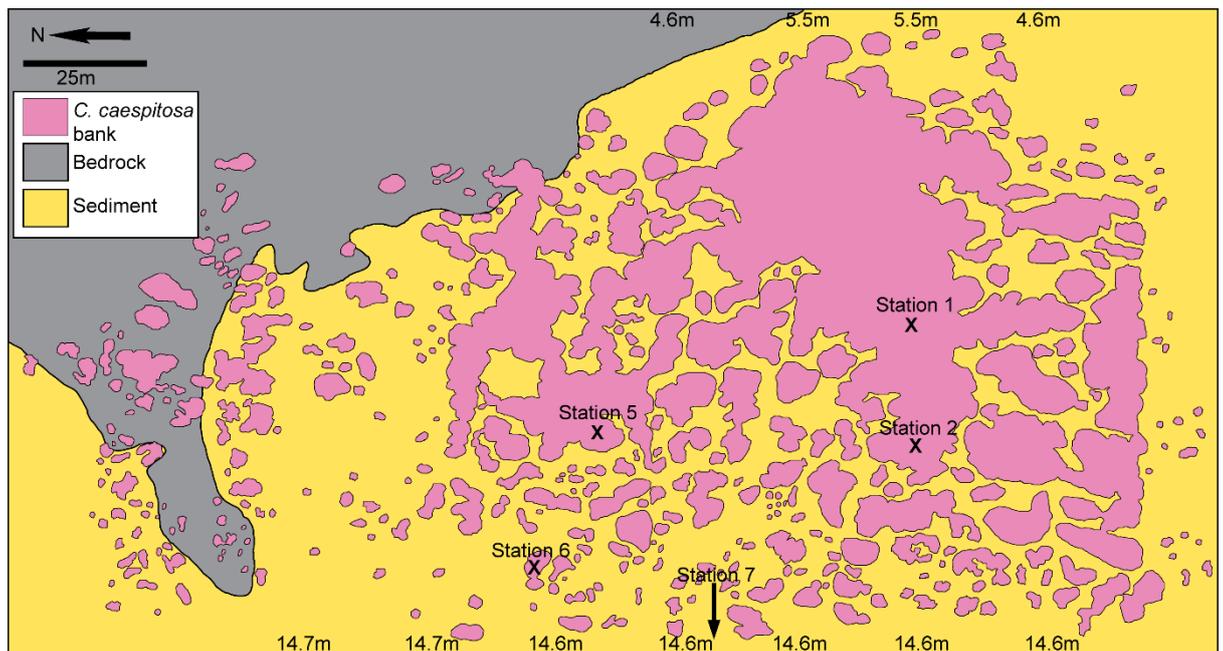
Figure 3.1.2 Mljet *C. caespitosa* bank showing monitoring stations where samples were collected from. Depths of the lake bed are shown to show gradient of slope (modified from original map by P. Kružić)

Modern samples were also sourced from Fiascherino (44°07'09''N; 09°55'02''E)

and Capo di Montenero (44°05.4'N; 09°44.1'E) in the Gulf of La Spezia, Italy

(Figure 3.1.3). These were provided by Dr Andrea Peirano and were leftover

31

from previous studies (Peirano et al., 1999; Peirano et al., 2001; Peirano et al., 2009).

The Fiascherino samples were collected (alive) on the 05/08/2003 with the Montenero samples collected (alive) on the 23/11/1994.

Figure 3.1.3 The Gulf of La Spezia, Northern Italy, showing sampling localities

3.1.2.   **Fossil Greek samples**

Fossil and subfossil coral and shell samples were collected from various localities around the Perachora Peninsula, Gulf of Corinth, Greece (Figure 3.1.4) in November 2011 on a field campaign with Dr Jenni Turner.
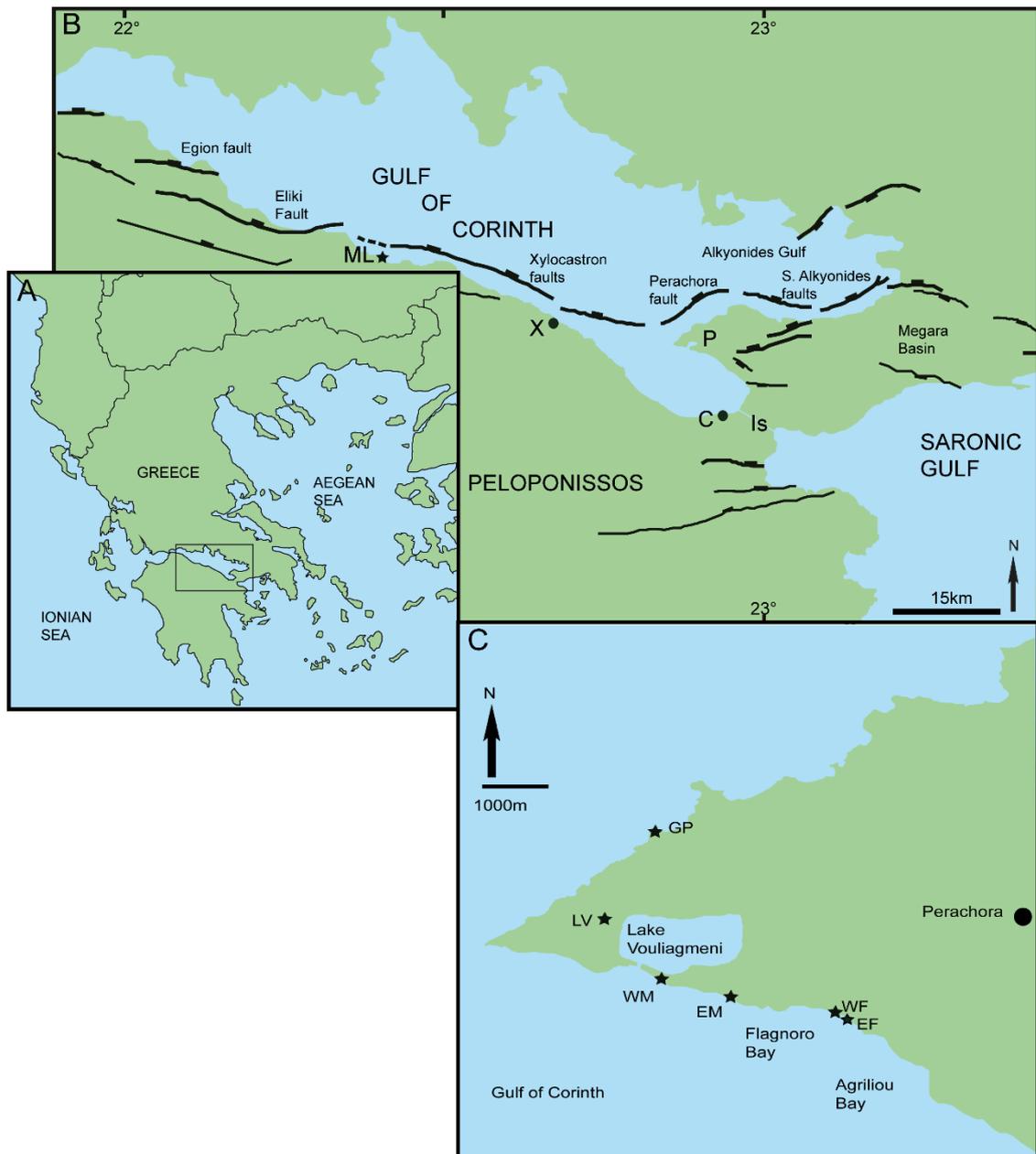
Figure 3.1.4 The Gulf of Corinth with fossil *C. caespitosa* sampling sites. (Clockwise from left) 1A – Greece: Box marks Gulf of Corinth area; 1B – Gulf of Corinth with major faults: ML = Mavra Litharia; X = Xylocastron; C = Corinth; Is = Isthmus of Corinth, P= Perachora; Box marks Perachora Peninsula; 1C – Gulf of Corinth: Stars mark studied localities, GP = Goat Point; LV = Lake Vouliagmeni; WM = West Makrugoaz Ridge; EM = East Makrugoaz Ridge; WF = West Flagnoro Bay; EF = East Flagnoro Bay.

The Gulf of Corinth area is ideal for this kind of study due to its tectonic setting.

The Gulf of Corinth is formed by an active rift system, a half graben (Figure 3.1.4B). The Rift is extending around 13 mm yr^{-1} (Clarke et al., 1997) where

uplift on the footwall of active and dead normal faults has raised marine deposits, including fossil *C. caespitosa*, above sea level in a series of raised Quaternary marine terraces that step up to 600 m above sea level (a.s.l.). The oldest terraces are assigned ages back to at least 450 ka (Keraudren and Sorel, 1987; Collier, 1990). These terraces can be correlated by regional mapping, several at the east end of the rift have been dated by U-series dating of corals (Leeder et al., 2003; Leeder et al., 2005); the older terraces have ages that are more weakly constrained by correlating terrace elevation to sea level highstands and assuming spatially average uplift rates over time (Keraudren and Sorel, 1987; Armijo et al., 1996).

In the eastern parts of the Gulf, around the Perachora Peninsula, average Late Quaternary (post MIS 7) uplift rates of around 0.2-0.3 mm yr^{-1} have raised MIS 5e shorelines to a modern elevation of 25-30 m over an area of >200 km^2 (Leeder et al., 2003; Leeder et al., 2005). It is these well-correlated, dated shallow marine terraces that the *C. caespitosa* samples were collected from. Where possible, samples were collected from the same colony, or proximal colonies to those from which stems were collected for the U-series dating.

Localities were selected where material showed no obvious recrystallization or secondary cement growth visible by hand lens, minimal algal encrustation, endolithic boring or iron staining, and limited sediment infill in corallite cavities. Multiple samples in 'life position' were collected from colonies that had already been screened for mineralogical purity by combined X-ray diffraction (XRD), scanning electron microscopy (SEM) and trace element geochemistry (Leeder et al., 2005; Turner et al., 2010).

3.1.3.   Fossil Italian samples

Fossil and subfossil samples were also collected from various localities around

the South of Italy (Figure 3.1.5) in May 2012 on a field campaign with Dr Jenni

Turner.
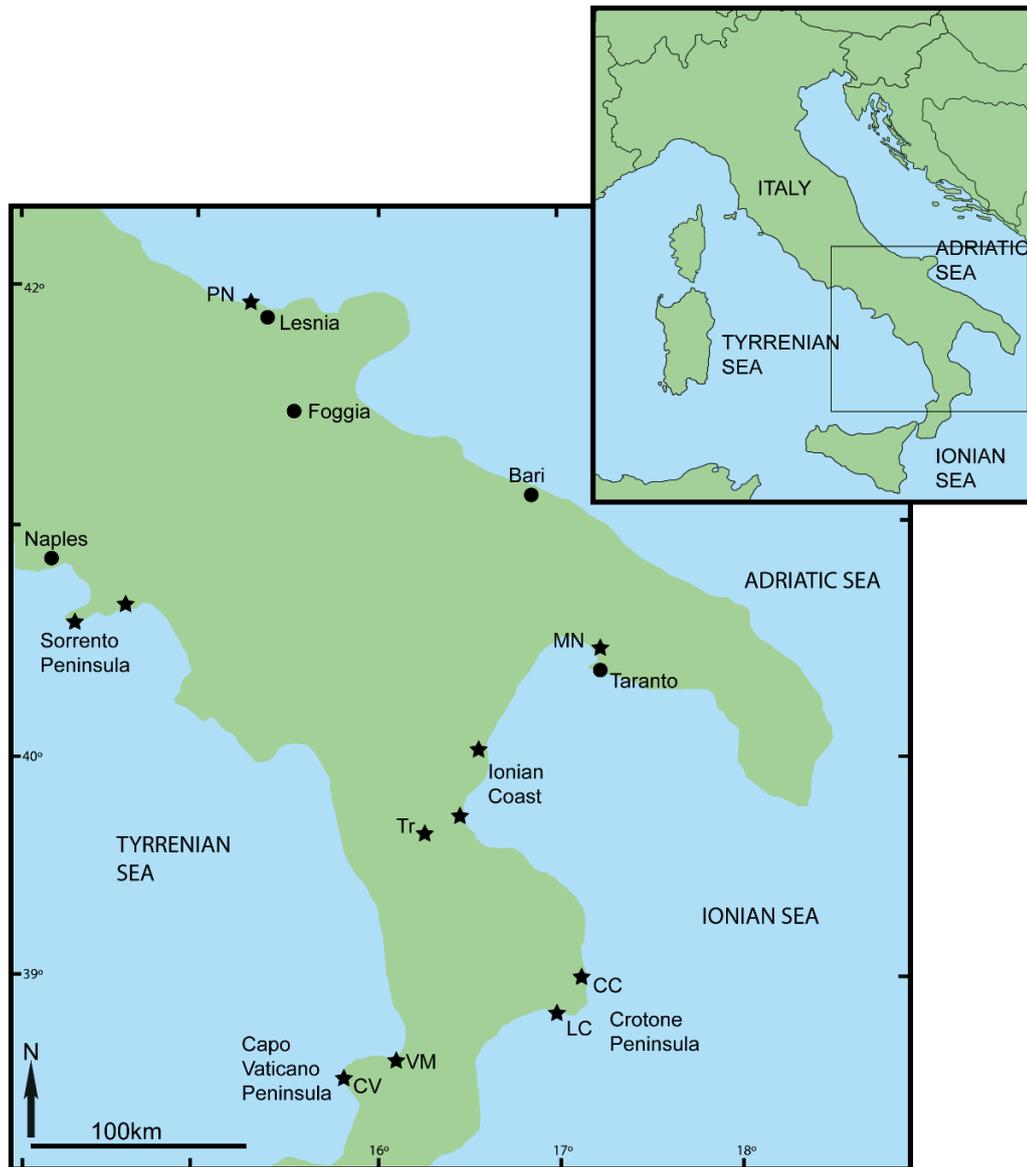
Figure 3.1.5 Locality map of the South of Italy showing sites where fossil *C. caespitosa* are reported in the literature and were targeted on the field campaign. PN = Punta della Pietre Nere; MN = Masseria Natrella reef; Tr = Tarsia; CC = Capo Colonna; LC = Le Castille; VM = Vibo Valentia Marina; CV = Capo Vaticano

Like the Gulf of Corinth, southern Italy was also chosen as a potential study region as (while northern Italy is subsiding) its coastline is uplifting at rates of up to 1.4 mm yr^{-1} with the highest rates towards the southwest (Ferranti et al., 2006) exposing a succession of marine terraces (Cucci and Cinti, 1998; Belluomini et al., 2002; e.g. Santoro et al., 2009).

Areas to target were selected from an extensive review of the literature. Unfortunately, during the field campaign, it was found that the many of the deposits no longer outcrop due to recent building work or were found to not have been described in enough in detail to find amongst the complex architecture of the various terraces' coarser fluvial deposits. Where *C. caespitosa* bearing exposures were found the samples were too poorly preserved to be of any further use to this study. The *C. caespitosa* bearing exposures reported in the literature and visited during the field campaign, and the issues found with each locality are listed in Table 3.1.1.

Table 3.1.1 Details of problems with Italian *C. caespitosa* localities reported in literature

Locality	Reference	Age	Problem
Vibo Valentia Marina	Pirazzoli et al., 1997	MIS 5e	No signs of 50m marine terrace, probably buried under new housing development. Terrace found at 145m but deposits too coarse, possibly terrestrial, for fossil preservation
Capo Vaticano N38°56'59'' E015°50'14''	Pirazzoli et al., 1997	MIS 5e	At grid reference where *C. caespitosa* reported only found coarse igneous basement topped by a non-fossiliferous breccia
Le Castille, N38°54'26.5'' E017°01'21.5'' Elev. 1 m	Zecchin et al., 2004; 2010;	MIS 5a/c	Corals are very rare and only found at the base of the clinoform sequence in the splash zone, corals are shot with calcite alteration visible to the naked eye
Capo Colonna N39°01'21.8'' E017°12'14.4'' Elev. 19 m	Zecchin and Caffau, 2011	MIS 5a/c	Algal cemented reef is very bioturbated, corals are shot with calcite alteration visible to the naked eye
Ionian Coast and Crati Valley	Santoto et al., 2009; Cucci and Cinti, 1998	MIS 1 to 15 terraces	3 or 4 terraces found across area but all seem to be made up of extensive coarse fluvial sediments on top of marl and metamorphic bedrock. Few traces of marine environments with *in situ* oyster beds, clams and scallops but no corals.
'Coral cave' above Tarsia; N39°37'19.2'' E016°16'02.4'' Elev. 224 m	Bernasconi et al., 2002	MIS 11 or older	Corals are very abundant (see Figure 3.1.6) however heavy iron staining, weakness of stems and an age of at least MIS 11 (from the 224m a.s.l. elevation) of the terrace suggest too poor condition so not analysed.
Taranto	Peirano et al., 2009; Belluomini et al., 2002; Ferranti et al., 2006; Mastronuzzi et al., 2003	Holocene, MIS 5a-c, 5e	Dated (107ka) *C. caespitosa* outcrops near Roman Bridge (N40°45'28.4'' E017°41'50.2'') not found, only limestone bedrock and extensive fluvial conglomerates. Santa Teresiola reef not found as on inaccessible private land. Masseria Natrella reef found (N40°30'29.1'' E017°14'28.7''; Elev.16m); major *C. caespitosa* reef with diverse bivalve assemblage however samples are short and poor quality. Holocene and 5a-c beach terraces only found to contain oysters and gastropods in lower parts and extensive cockle beds in upper parts, no corals.
Punta della Pietre Nere; N41°54'57.1'' E015°20'32.1'' Elev. 0.5 m	Mastronuzzi and Sanso, 2002, Gravina et al., 2005	Holocene	Heavily algal cemented and stained black from the splash zone. Preliminary LA-ICP-MS trace element analysis showed to be heavily contaminated by metals, especially Al, Fe.

Figure 3.1.6 Abundant *C. caespitosa* exposed in walls and ceiling of man-made 'coral cave' above Tarsia. The cave roof is approximately 2.5 m high.

Because of the issues in obtaining unaltered material, the analysis of the Italian samples did not go beyond preliminary investigations and these samples are not discussed further.

3.2. Sample pre-screening, SEM analysis

It was necessary to check that samples of *C. caespitosa* were well preserved to ensure that they retained their original geochemical signature. To do this they needed to be visually examined under SEM to check for alteration and contamination.

A sample corallite from each colony was selected for pre-screening and cut parallel to growth direction with a wire saw to expose longitudinal sections.

Samples were pre-screened by petrographic analysis under the SEM in low vacuum back-scatter electron mode (BSEM); the samples could not be gold-coated if they were to be used for geochemical analysis. The skeletal ultra-structure of samples were examined for evidence of alteration of aragonite to the more stable calcite polymorph, secondary cements and detritus trapped within void spaces (Figure 3.2.1, Figure 3.2.2, Figure 3.2.3), all of which are known to alter or contaminate the geochemical signature from that of primary coralline aragonite (Cohen and Hart, 2004; Silenzi et al., 2005; Montaggioni et al., 2006; Montagna et al., 2007).
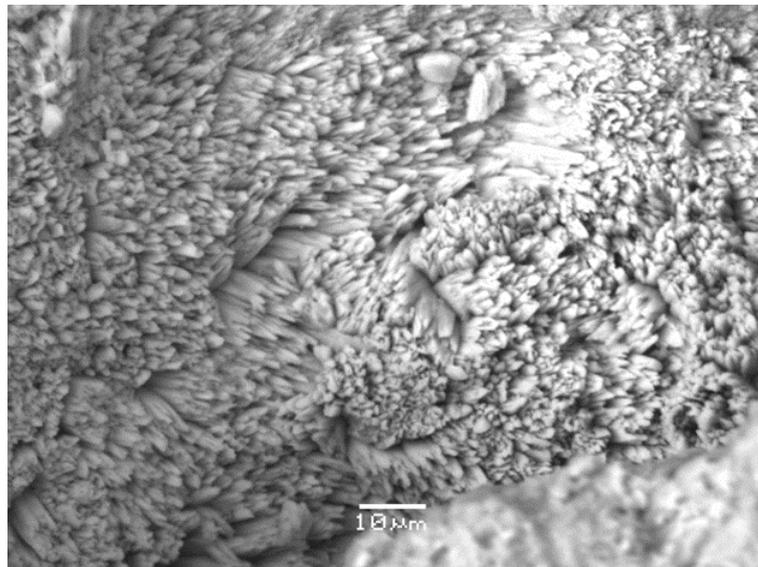
Figure 3.2.1 Uncoated BSEM image of primary aragonite making up the corallite wall of a modern sample of *C. caespitosa*. The sample is from the Gulf of La Spezia, Italy and the aragonite shows well developed fibrous acicular crystal forms with a clear orientation due to the coral's biological control on crystal growth.
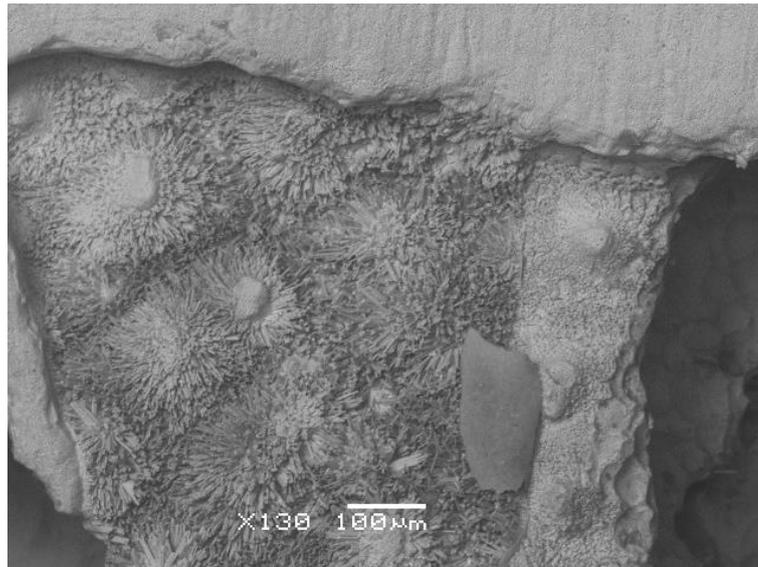
Figure 3.2.2 Uncoated BSEM image of secondary aragonite infilling septal region of a modern sample of *C. caespitosa*. The sample is from the Gulf of La Spezia, Italy and the secondary aragonite shows radiating bundles of acicular crystals developing out from centres of precipitation due to abiological controls on crystal growth. As this sample was collected alive it shows that secondary cements in the septal regions can be an issue in even the best preserved samples. The smooth, darker grey feature to the bottom right of the image is likely some form of detritus.

Figure 3.2.3 Uncoated BSEM image of heavily altered MIS 5a/c *C. caespitosa* with diagenetic calcite growth. The sample is from Italy and was not included in the study due to the high degree of alteration. Abiogenic calcite forms large blocky crystals growing in void spaces between septa.

Alteration and detrital contamination of the septal regions was very common in all but the best preserved (modern and Holocene) samples. The septa also have the added problem that, due to their porous nature, the whole of any

horizon perpendicular to the growth direction may not have formed synchronously due to multiple stages of skeleton growth occurring in skeletal cavities (Figure 3.2.4).
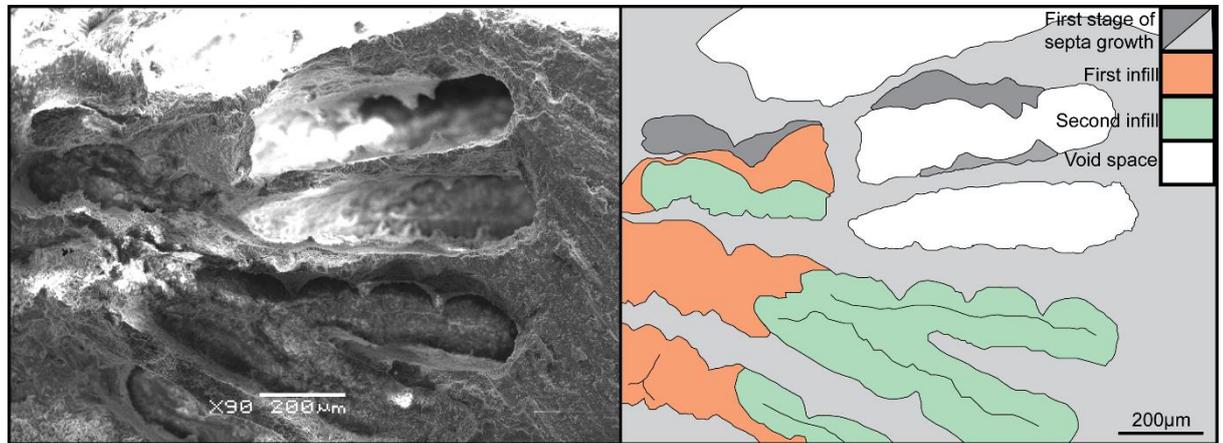
Figure 3.2.4 SEM image and simplified false colour cartoon showing multiple stages of skeletal growth in the septal region of modern *C. caespitosa* (sample PK 21/09/12-07)

The presence of calcite in many samples meant that corallites could not be rejected due to its presence (as Henderson et al. (1993) suggest). This is justified as most samples have relatively pristine corallite walls; this solid region appears resistant to alteration (Montagna et al., 2007) and Sayani et al. (2011) suggest that, even in obviously altered corals, any remaining pristine aragonite skeletal elements may still be useful for palaeoclimate reconstruction. Therefore, only the corallite walls were chosen for analysis, samples that also showed significant contamination of their walls by secondary cements were rejected.

The remaining 'candidate' samples were catalogued using this macro and microscopic petrographic analysis and classified on their likely ability to record original geochemical signatures. This was dependant on their quality of preservation and visible level of diagenesis, allowing the selection of the most

useful samples for analysis. A list of all samples used in this study and the

techniques they were used for is given in Table 3.2.1.

Table 3.2.1 Summary of *C. caespitosa* samples analysed, with collection localities, ages and techniques applied

Sample number	Locality & growth depth	Age	Analytical techniques applied
PK 21/09/12 - 01	Mljet, Croatia (42°46'08''N; 17°22'26''E), 8m depth	Modern, collected alive 21st September 2012	SEM, High resolution IR-MS (C, O), Bulk isotopologues (Δ_{47}), High resolution LA-ICP-MS, water sample IR-MS
PK 21/09/12 - 02	Mljet, Croatia (42°46'08''N; 17°22'26''E), 10m depth	Modern, collected alive 21st September 2012	SEM, High resolution IR-MS (C, O), Bulk isotopologues (Δ_{47}), High resolution LA-ICP-MS, water sample IR-MS
PK 21/09/12 - 05	Mljet, Croatia (42°46'08''N; 17°22'26''E), 11m depth	Modern, collected alive 21st September 2012	SEM, High resolution IR-MS (C, O), Bulk isotopologues (Δ_{47}), High resolution LA-ICP-MS, water sample IR-MS
PK 21/09/12 - 06	Mljet, Croatia (42°46'08''N; 17°22'26''E), 14m depth	Modern, collected alive 21st September 2012	SEM, Bulk isotopologues (Δ_{47}), High resolution LA-ICP-MS, water sample IR-MS
PK 21/09/12 - 07	Mljet, Croatia (42°46'08''N; 17°22'26''E), 15m depth	Modern, collected alive 21st September 2012	SEM, Bulk isotopologues (Δ_{47}), High resolution LA-ICP-MS, water sample IR-MS
AP 05/08/03 – F	Fiascherino (44°05'04''N; 09°44'01'E), 10m depth	Modern, collected alive 05th August 2003	SEM, Bulk isotopologues (Δ_{47})
AP 23/11/94 – MN1	Capo di Montenero (44°05'04''N; 09°44'01''E), 10m depth	Modern, collected alive 23rd November 1994	SEM, Bulk isotopologues (Δ_{47})

UEA 010626-04	Agrilou Bay, Greece (38°00'31.4''N; 22°55'32.5''E)	MIS 5a-c; Deposit U-Th dated to 70-82ka (J. Turner; J. Andrews Pers. comm.s)	SEM, High resolution IR-MS (C, O), Bulk isotopologues (Δ_{47}), High resolution LA-ICP-MS
SHR 02/11/11-02	Lake Vouliagmenis, Greece (38°01'55.2''N; 22°52'14.1''E)	MIS 7a-c; Deposit U-Th dated to 186-195ka (Leeder et al., 2005)	SEM, High resolution IR-MS (C, O), Bulk isotopologues (Δ_{47}), High resolution LA-ICP-MS
SHR 02/11/11-08	West Makrugoaz Ridge , Greece (38°01'21.8''N; 22°52'49.8''E)	MIS 5e; Deposit U-Th dated to 108-133ka (Leeder et al., 2003)	SEM, High resolution IR-MS (C, O), Bulk isotopologues (Δ_{47}), High resolution LA-ICP-MS
SHR 03/11/11-02	Mavra Litharia, Greece (38°08'34.5''N; 22°22'49.0''E)	MIS 1; Reef growth dated to 6-10ka (Kershaw et al., 2005)	SEM, High resolution IR-MS (C, O), Bulk isotopologues (Δ_{47}), High resolution LA-ICP-MS
SHR 04/11/11-10	West Flagnoro Bay, Greece (38°01'11.1''N; 22°53'33.5''E)	5e, correlated to dated terraces by mapping (Leeder et al., 2003; Leeder et al., 2005)	SEM, High resolution IR-MS (C, O), Bulk isotopologues (Δ_{47}), High resolution LA-ICP-MS

3.3. Stable Isotope analysis – δ^{18}O, δ^{13}C

This section describes the sampling and analysis techniques used in the carbon and oxygen stable isotopic analysis of both modern and fossil *C. caespitosa* samples.

3.3.1. Sampling method

Modern samples were bleached in 30% H_2O_2 overnight to loosen and partially oxidise organic tissue, rinsed with deionised water, scraped clean of remaining tissue with a scalpel and further cleaned by sonication in deionised water to ensure all surface organic matter and detritus was removed. This was not

necessary with the fossil samples as their organic tissues had already oxidised over the thousands of years since the death of the coral.

A wire saw was used to cut the corallites in half parallel to their growth direction to expose their longitudinal cross sections. Half of the cut stem was selected for isotope analysis. A 3 mm drill bit attached to a rotary tool and a scalpel were used to remove the septa under a binocular microscope. Any surface contaminants (mostly encrusting calciferous algae and serpulid tubes) were removed and the samples were repeatedly sonicated in deionised water.
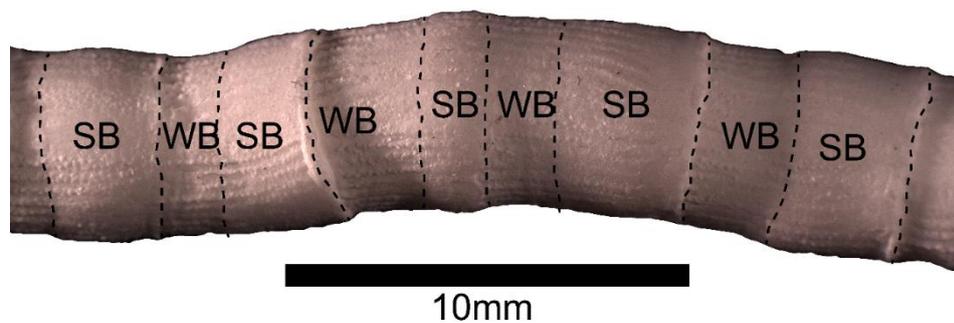
Figure 3.3.1 Modern *C. caespitosa* stem cleaned and annotated to show locations of pronounced summer (SB) and recessed winter (WB) growth bands. Faint colour difference between summer and winter bands cannot be seen in this image.

Isotope sampling was achieved using a diamond file to grind off material perpendicular to the growth direction; visible dissepiments and alternating darker pronounced and lighter recessed growth bands (Figure 3.3.1) served as guides to calculate the growth increment represented by each sample. It was assumed these bands were the summer low-density and winter high-density growth bands described by Peirano et al. (1999), rather than annual features. Therefore a density of ~12 samples per growth band achieved approximately fortnightly temporal resolution, although this was not always possible given the

varying widths and irregularities of the growth bands. Samples of 75±5 µg were weighed out into individual stainless steel capsules using a micro-balance.

3.3.2. Standards

Along with each batch of coral samples 75±5 µg UEACMST (University of East Anglia Carrera Marble Standard) standards of known composition were analysed. Data were reported in per mil (‰) deviation relative to the Vienna Pee Dee Belemnite (UEACMST isotopic composition is: $\delta^{13}C$ = +1.98‰ and $\delta^{18}O$ = −2.04‰). Repeat analysis of the standard shows a measurement precision (1 σ) for $\delta^{18}O$ and $\delta^{13}C$ of 0.09 and 0.08‰ respectively.

3.3.3. Autocarb – Automatic carbonate digestion, CO_2 preparation and introduction system

Sample runs, in batches of 47 (including standards), were loaded into the carousel of the (in house built) Autocarb (automatic carbonate) digestion, CO_2 preparation and introduction system. This system is controlled by the in house AutoPrep 2008 software. Samples individually react with 105% (ρ = 1.92 gml^{-3}) phosphoric acid (H_3PO_4) at 90°C in an on-line common acid bath. CO_2 is then cryogenically purified by removing water vapour by passing the gas through a cold trap at −105°C before being introduced to the mass spectrometer. Purified CO_2 was analysed for carbon and oxygen isotopic composition using the Europa SIRA II dual inlet isotope ratio mass spectrometer (IRMS).

3.3.4. Analysis order

Preliminary analysis found memory effects in the isotope composition of samples which followed the standards. Figure 3.3.2 shows how the composition of triplicates tends away from that of the preceding standards while replicates done before standards (not shown) showed no variation (outside expected error).
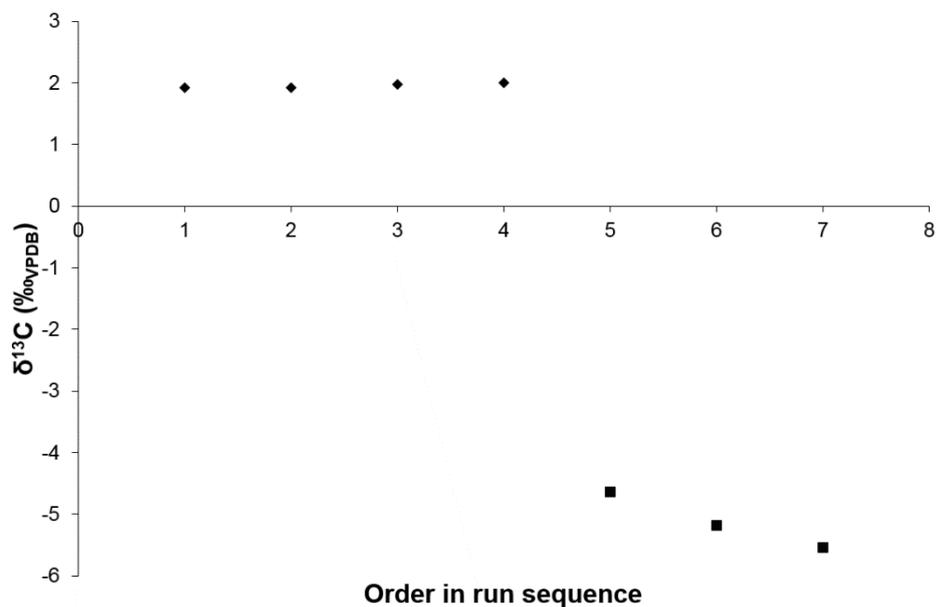
Figure 3.3.2 Memory effects shown by trend of increasing δ^{13}C depletion in one sample analysed in triplicate. UEACMST standards represented by diamonds, JS 11/11/05-03 (08) *C. caespitosa* replicate samples by squares.

This was assumed to be due to the much coarser grain size of the standards (compared to the finely powdered samples) causing them to take longer than their allocated time to digest completely in the acid. This led to some of their CO_2 still entering the mass spectrometer when the following samples were run.

To combat this, various loading patterns were tried, this resulted in all analysis runs following the sequence: 4 standards, 2 blanks (to allow complete degassing of the standards from the acid bath to finish before the samples were

introduced to the acid), all the samples, 4 standards. Replicates of samples were carried out approximately every 15 samples to check reproducibility of the measurements.

3.3.5. Resolution/Sampling strategy

It was initially decided that a resolution of 12 samples per growth band would be ideal as this would give approximately fortnightly resolution. This was tested by selecting two corallites of approximately the same age and locality (MIS 5e, Makrugoaz Ridge, Greece) and sampling one at ≈12 samples per growth band and the other at ≈24 samples per growth band.

Figure 3.3.3 and Figure 3.3.4 show that little useful information is lost by halving the sampling resolution. The strong visible cyclic trend in the isotope composition is still apparent (it actually becomes clearer as noise is reduced) and retains approximately 90% of its amplitude (although this difference may not be significant as the corallites may have actually experienced different environmental conditions). Also, half as many runs on the mass spectrometer were needed to get this lower resolution result, thus twice as many corallites could be analysed for the same amount of time and cost.
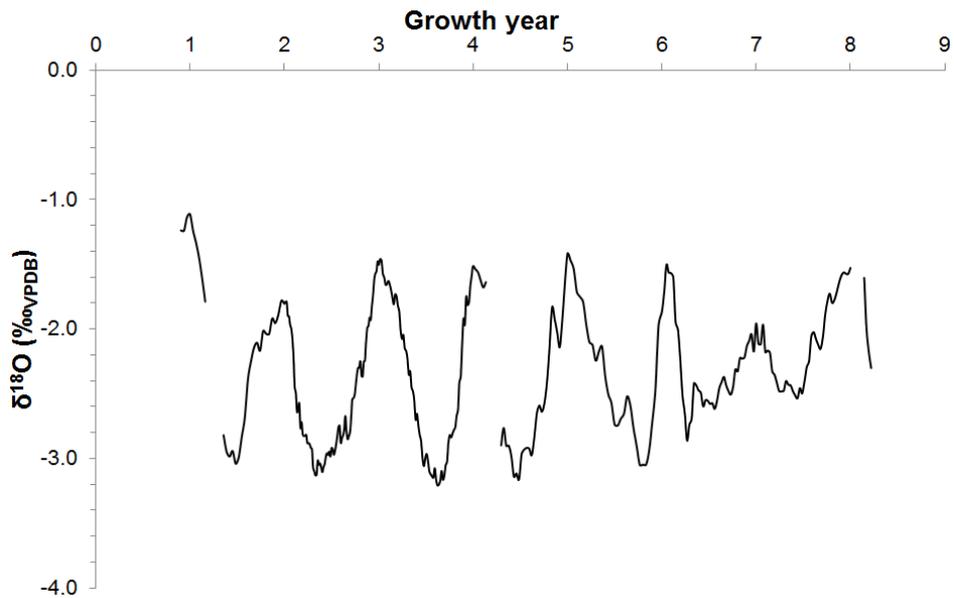
Figure 3.3.3 Stable isotope analysis of *C. caespitosa* **sample SHR 02/11/11-08 (II), unsmoothed but normalised to growth years. Average sample resolution 24 samples per growth band.**
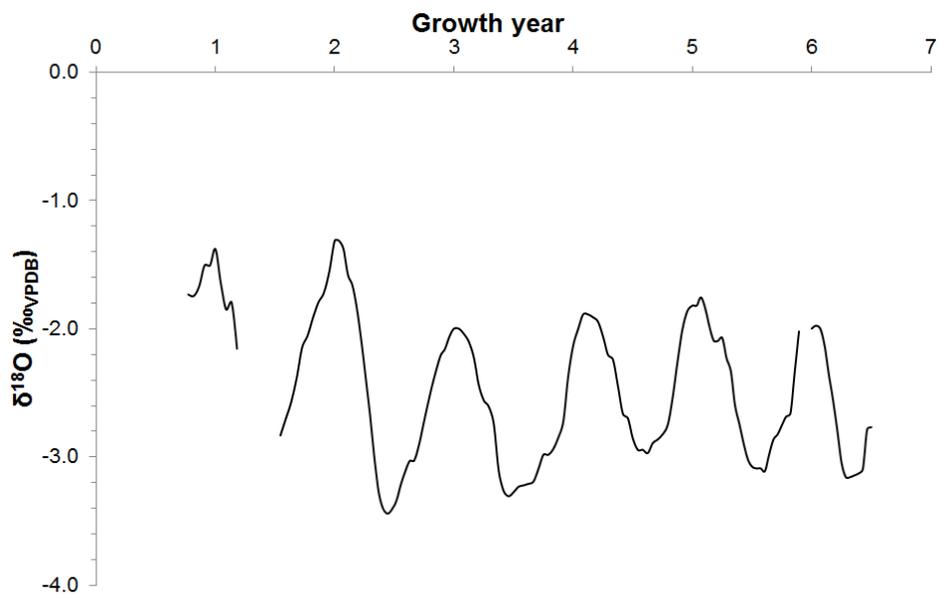
Figure 3.3.4 Stable isotope analysis of *C. caespitosa* **sample SHR 02/11/11-08 I, unsmoothed but normalised to growth years. Average sample resolution 12 samples per growth band.**

3.3.6.   Data analysis techniques

Data processing was carried out offline using Excel. This involved calculating

the isotope composition of the sample carbonate (aragonite) with respect to

VPDB at 25°C, using the measured CO_2 isotope compositions of samples with respect to VPDB at 90°C and the actual UEACMST (internal standard material) compositions, which had previously been calibrated using NBS 19. An empirical correction of 0.287‰ was applied to the $\delta^{18}O$ of the corallite samples to take into account that they are precipitated as aragonite (rather than calcite), based on previous work on this mass spectrometer (A. Marca pers comms).

3.4. Clumped isotope analysis – Δ_{47}

This section describes the sample preparation and analytical techniques involved in the analysis of the clumped isotopic composition of both modern and fossil *C. caespitosa* samples and other MIS 5e carbonates.

3.4.1. Sample preparation

Although bigger samples (10 mg) of fine coralline aragonite powder, rather than 70 μg powders, were needed for this technique, the corallites were prepared and cleaned to remove organic and detrital sediments in exactly the same way as for the previous stable isotopic technique.

Where possible the same sample corallite stems used for high resolution stable isotope analysis were analysed to allow direct comparison between the results from the two techniques. Fine homogenised powders of the corallites were produced by combining the remnants of the sub-samples of corallite that had been produced for the high resolution isotope analysis. These were homogenised by thoroughly mixing the combined samples with a spatula and shaking the vial. Where this was not possible, when powders had not already been produced from the corallites or no powder remained, a corallite from the

same colony was selected and multiple (at least 4) years of growth were ground to a fine powder and homogenised using an agate pestle and mortar. Estimates of the weight percentage of organic matter embedded within a coral skeleton range from 0.01-0.1% (Wainwright, 1963), 1% (Cohen and McConnaughey, 2003) to 2.5-3% (Cuif et al., 2003) with a very heterogeneous distribution (concentrated in calcification centres) (Cuif et al., 2003) in an intermeshing framework of organic material and carbonate nanograins (Barnes, 1970; Cuif and Dauphin, 2005). Because of this nanometre scale intermeshing it is not possible to apply a surface oxidant (e.g. soaking in H_2O_2 as was used on the whole corallites) that can get deep enough into the sample to oxidise all the inter- and intra-crystalline organics. However, these small amounts of organic impurities do not appear to have affected the separate $\delta^{18}O$ and $\delta^{13}C$ measurements, and it has been reported elsewhere that the addition of organic substances have no effect on the isotopic analyses of untreated samples carried out by using the phosphoric acid digestion method (Wierzbowski, 2007). Also, due to its acidic pH and the fine grain size of the carbonate powders, it is unlikely that complete removal of the organic matter by H_2O_2 is possible without some significant dissolution of carbonate material during the bleaching. It is possible that this would preferentially remove carbonate material which is isotopically different from the bulk composition, thus altering the bulk composition of the remaining sample and resulting in an incorrect determination of isotopic composition (White, 1998). Due to this it was decided not to bleach the produced powders with H_2O_2 or attempt any other methods of further organic matter pre-cleaning.

For each sample powder, 10 mg was weighed out into a stainless steel vial using a microbalance and transferred into a Durham tube using a funnel, both the vial and funnel were cleaned to remove any traces of the previous powder between samples.

3.4.2. Sample digestion

Durham tubes containing 10±0.1 mg of sample were placed into reaction vessels along with 1 ml of 105% (ρ = 1.92 gml^{-1}) phosphoric acid (H_3PO_4). The vessels were pumped out to high vacuum ($\geq$ 1·10^6 mbar) while the acid was heated and degassed.

Samples were digested under vacuum in the acid overnight at 25±0.1^{o}C in a water bath so that (the temperature dependant) fractionation of isotopes between the produced CO_2 and the acid remained constant.

3.4.3. CO_2 purification, Prep line

CO_2 produced from this reaction was purified on a dedicated high vacuum manual extraction line to remove all water, non-condensable gases and any organic components. This was achieved by first passing the CO_2 through 2 cold traps held at −115°C to cryogenically remove any water. The CO_2 was then frozen into a cold finger at liquid nitrogen temperature and, after freezing, the non-condensable gases were pumped out. The CO_2 was then passed through a gas chromatography (GC) column filled with Porapak^{TM} porous polymer material, cooled to −25±5°C. This is required to guarantee no interference of hydrocarbons with the mass-47 measurement (Eiler and Schauble, 2004; Zaarur et al., 2011). Finally the CO_2 was refrozen in a sample tube and any

remaining non-condensable gases were pumped out. Between samples the line was pumped at high vacuum at room temperature and the GC column was baked to remove any remaining contaminates.

3.4.4. MIRA

Samples were run on the MIRA (Multi-Isotopologue Ratio Analyser) isotope ratio mass spectrometer (IRMS). Clumped isotope measurements are reported as Δ values (see section 2.4.1) Measured Δ_{47} values are reported standardised to the absolute reference frame (ARF) of Dennis et al. (2011) to account for inter and intra-laboratory differences in standard gases used and mass spectrometric artefacts. Standardisation is based on repeat analysis of heated gases (HG) and water equilibrated gases (WEG), these are CO_2 with known compositions made from BDH marble chips, from a BOC CO_2 cylinder or a combination of both, which are used to construct transfer functions. Standards of UEACMST (University of East Anglia Carrera Marble), UEABEL (University of East Anglia Belemnite) and UEATHC (UEA Turkish Carbonate) are prepared and analysed interspersed with the studied samples to check for consistency. Based on repeat analysis (n=44) of the UEACMST standard, the standard error on this instrument for Δ_{47URF} is 0.005‰ ($2\sigma = 0.064$).

3.5. Water stable isotope measurements

Oxygen and hydrogen isotopic analysis was performed by Dr Sarah Wexler on water samples collected from Lake Veiko Jezero (Croatia) by Dr Petar Kružić (at the same times and localities as the *C. caespitosa* samples he collected) and from around the Perachora Peninsula on water samples collected by Dr Jenni Turner (between the 10th-13th February 2013).

These measurements were performed on filtered samples using a Picarro cavity ring-down spectroscopy (CDRS) laser instrument. Due to memory effects in this type of instrumentation, 2.2 µl of each sample was injected and measured six times. Repeat analyses of the standards Norwich Tap Water (NTW), Greenland Ice Sheet Precipitation (GISP), USGS67400 and USGS64444 were used to calibrate the data and show a measurement precision for $\delta^{18}O$ and δD of 0.16 and 1.05‰ respectively. Data are reported as delta values (‰) with respect to the VSMOW standard.

3.6. Trace elemental analysis

Modern and fossil *C. caespitosa* samples were analysed for trace element compositions with the aim of developing palaeotemperature proxies. This section introduces the technique, describes the process of developing this method to work best with the corallites and the final method and resolution used for analysis.

3.6.1. Laser ablation – inductively coupled plasma – mass spectrometry (LA-ICP-MS)

In situ sampling was carried out by laser ablation-inductively coupled plasma-mass-spectrometry (LA-ICP-MS). Sample corallites were cleaned and cut lengthways (as in the isotope analysis), this method allows the accurate targeting of the corallite wall without the need for removal of the septa. The sampling method was based on the technique of Montagna et al. (2007) who carried out a very similar trace element study on a modern Italian *C. caespitosa*.

 LA-ICP-MS has, over the last few decades, become a popular method for high resolution analysis of the trace elemental composition of a wide range of carbonate and other geological materials (Sinclair et al., 1998; Roberts et al., 1999; Toland et al., 2000; Sinclair, 2005; Hoffmann et al., 2009; Schöne et al., 2010; Sato et al., 2011; Schöne et al., 2011). This is a technique for the direct elemental analysis of solid samples and is described in detail by Arrowsmith (1987) and Gray (1985).

In summary; a focussed pulsed laser beam is used to ablate a solid sample, this produces a plume of fine particulate material which is entrained into a flow of argon gas. Argon is used as it has a very high ionisation potential and so keeps the ablated sample ionised (Sheppard et al., 1990). The gas flow transports the ablated material into an inductively coupled plasma (ICP), ionising the sample, with the resulting ions detected by mass spectrometry.

This is a potentially easy method for sampling as very little sample preparation is necessary, it has application to a wide range of geological (and other) materials, and has a high spatial resolution (≥10μm (Toland et al., 2000)) due to the potential for very fine focussing of the laser beam.

It is this potential for extremely high resolution analysis and the fact that sampling can be carried out *in situ* that makes LA-ICP-MS ideal for sclerochronology. These features are advantageous as they (theoretically) allow for the study of small compositional changes over very short distances/time periods.

In this study, samples were analysed on a Thermo-Electron X Series ICP-MS using a New Wave Research UP-213 Laser Ablation System and argon carrier gas.

3.6.2. Method development

There were many unknowns associated with analysing this type of coralline aragonite by LA-ICP-MS and so preliminary experiments were conducted to develop a reliable and reproducible method.

3.6.2.1. Standards

Standards (of known compositions) are necessary to calibrate the laser to allow semi-quantitative intensities of isotope mass detection to be turned into absolute concentrations.

In a preliminary study, pre-ablated samples of pure calcite ($CaCO_3$), NIST 610 and NIST 612 (silicate reference glasses) were used as calibration standards. The pure calcite was used to calibrate calcium content of the samples as well as the reference glasses. This was an attempt to avoid matrix effects induced by the laser coupling differently with the carbonate sample and silicate glass standards (cf Sinclair et al. (1998) and Montagna et al. (2007)). However, even with these differences in coupling, no difference was found in the sample's concentration data calibrated with or without the calcite and so this standard was removed as an unnecessary step with the NIST glasses being deemed as sufficient.

3.6.2.2. Laser ablation spot size calibration experiment

Preliminary work consistently reported trace element concentrations which were anomalously high compared to published work (Rong Min et al., 1995; Alibert and McCulloch, 1997; Sinclair et al., 1998; Marshall and McCulloch, 2002; Silenzi et al., 2005; Montagna et al., 2007). It was hypothesised that the accuracy of the data may be a function of laser spot size and power. Too large spots would create too much ablated material overloading the detectors in the mass spectrometer, too small a spot size and not enough ablated material would be present for the detectors to analyse. The intensity of the laser was also an important variable; too much power exerted onto too small an area caused the laser to burn holes, causing fragmentation of the sample; too little power over too wide an area and the laser would not couple well with the sample surface. Because of this, an experiment was necessary to determine the effects of spot size on the data produced.

Method

Standard addition analysis (solution-mode)

To get a bulk analysis of the average composition of *C. caespitosa* without the effects of any laser variables, G. Chilvers used a homogenised sample of SHR 04/11/11-11, an unaltered and clean Greek MIS 5e *C. caespitosa,* to create a calibration standard solution which was analysed with the ICP-MS in solution mode to gain accurate average Sr and Ca concentrations by standard addition. The other trace elements present in this standard could not be accurately measured due to the method of standard addition necessary to gain accurate figures for these 2 elements leading to interference in the other, less abundant,

trace element signals. This gave average concentrations of 8166ppm and 38.11% for ^{86}Sr and ^{43}Ca respectively, both in the regions of what have been found by other studies (e.g. Rong Min et al., 1995; Alibert and McCulloch, 1997; Sinclair et al., 1998; Marshall and McCulloch, 2002; Silenzi et al., 2005; Montagna et al., 2007).

Laser ablation analysis

Various spot sizes were used to analyse pre-ablated regions of NIST 612 and 610 and the corallite wall of *C. caespitosa* sample SHR 04/11/11-11 (Table 3.6.1). Each size of spot was used to analyse the same 3 points on the coral, these points were all taken 500 µm apart in a transect normal to the growth direction of the coral. This ensured that they all related to the same temporal horizon and so changes in trace element content of the coralline aragonite over time should not have affected the results; averaging the results of the 3 points for each spot size was done to further minimise the effects of any heterogeneity between microstructural domains in the corallite.

The NIST glass standards were used to calibrate the laser to allow intensities of trace element mass detection to be turned into concentrations so that the following results and discussion all relate to *C. caespitosa* sample SHR 04/11/11-11.

Laser settings

Pre-ablation settings: 250 µm spot size, 90% laser output, 12 Hz repetition rate, 10 µms^{-1} scan speed, 5 µm depth per pass.

Table 3.6.1 Analysis settings for laser calibration experiment

Spot Size (µm)	Laser Output (%)	Repetition Rate (Hz)	Dwell Time (s)
250	90	12	40
75	55	4	40
40	60	4	40

Results and analysis

As hypothesised, spot size did affect the concentration of elements picked up by the detectors. Figure 3.6.1, which shows the laser-analysed concentration data, shows how increasing spot size increased concentration for the majority of elements detected. This is especially obvious for ^{43}Ca and ^{86}Sr which at the 250 µm spot size make up approximately 500% and 75,000ppm of the sample respectively. These concentrations are over an order of magnitude too large, both standard addition data and other, published, studies on various species of corals (Rong Min et al., 1995; Alibert and McCulloch, 1997; Sinclair et al., 1998; Marshall and McCulloch, 2002; Silenzi et al., 2005; Montagna et al., 2007) show that ^{43}Ca makes up around 38% of aragonite and ^{86}Sr should be present at 5000-10,000 ppm. Although there are not really enough data points for a reliable conclusion; it does appear that there is a positive linear relationship between spot size and reported concentration. It can also be seen that the different elements have somewhat different gradients to their lines suggesting that not all are affected to the same degree. Concentrations from the 40 µm spot appear as though they may be anomalously low as, from the real-time signal readout on the mass spectrometer, there did not appear to be enough material being ablated for the detectors to pick up some of the lower concentration elements (like manganese); as the signal to noise ratio was very low.
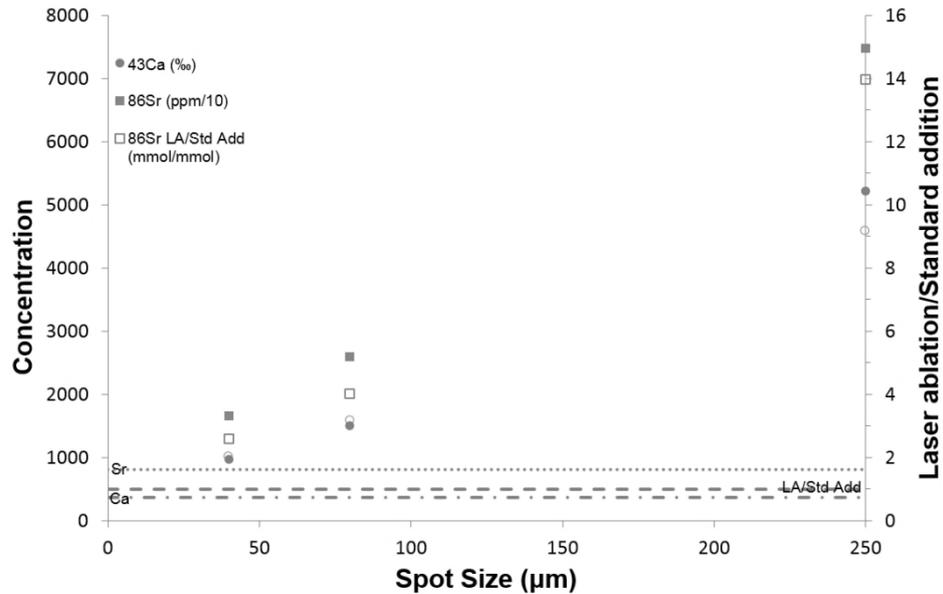
Figure 3.6.1 [43]Ca, [86]Sr laser ablation trace element concentration and laser ablation/standard addition concentration ratios at various spot sizes for *C. caespitosa* sample SHR 04/11/11-11. Varying units are used for the different elements to allow them all to be shown on one graph and these are noted in the key. Concentration levels from standard addition data (no spot size, solution analysed) are plotted as dashed lines for comparison.

Figure 3.6.2 shows the same laser ablation data as Figure 3.6.1, however this has been normalised in an attempt to cancel out the effects of the varying spot size. To normalise the data to 100% aragonite, [43]Ca = 38% has been used as an internal standard (following the data from standard addition). Plotted at 0 µm spot size are the [86]Sr composition data gained by standard addition. As can be seen, the [86]Sr standard addition value is slightly higher than the normalised values, which appear to tend towards it with decreasing spot size, although there are not enough data points for this to be a statistically significant trend.
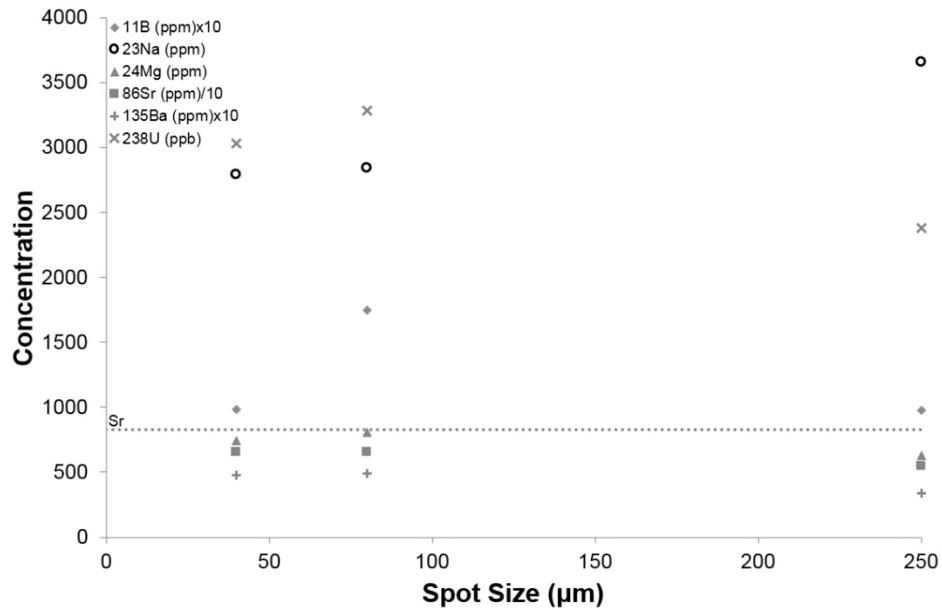
Figure 3.6.2 Laser ablation trace element concentration for a selection of the most common trace elements for *C. caespitosa* sample SHR 04/11/11-11 at various spot sizes normalised to 100% CaCO$_3$, so that ^{43}Ca=38%. The standard addition composition data (no spot size, solution analysed) from sample SHR 04/11/11-10 for ^{86}Sr is plotted as a dashed line for comparison. Varying units are noted in the key.

Figure 3.6.3 and Figure 3.6.4 show the normalised data reported in the standard notation of trace element/calcium ratios to allow the comparison of the data with published work, which is shown in Figure 3.6.4. Even though the samples have been normalised and all concentrations are reported as a ratio of the concentration over a constant value of 38% of ^{43}Ca, there are still significant differences between the concentration values gained from different spot sizes.
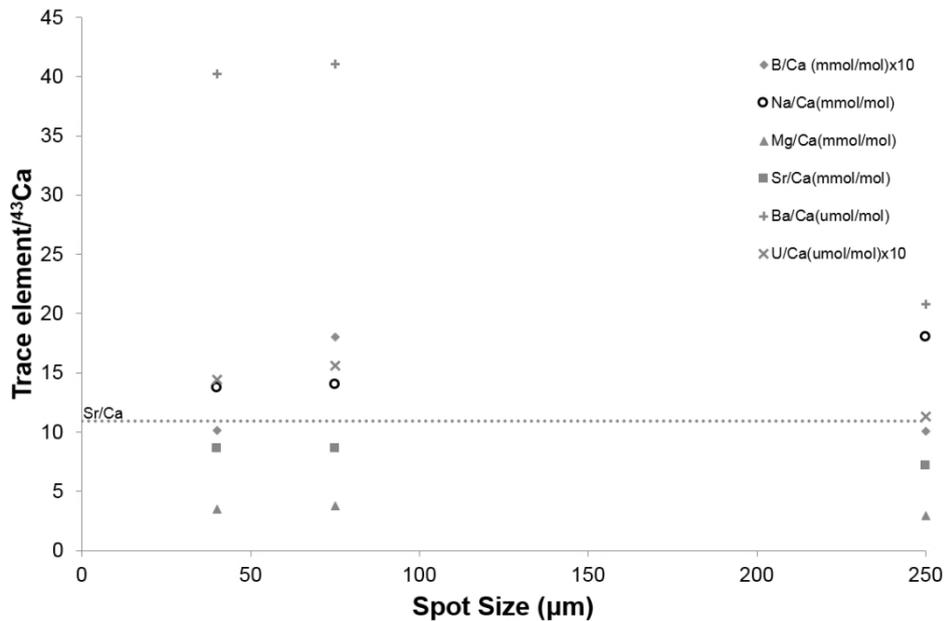
Figure 3.6.3 Normalised laser ablation trace element concentration for *C. caespitosa* sample SHR 04/11/11-11 at various spot sizes reported as ratios of trace element/^{43}Ca. Sr standard addition composition data from sample SHR 04/11/11-10 is shown at 0 µm spot size. Varying units are noted in the key.
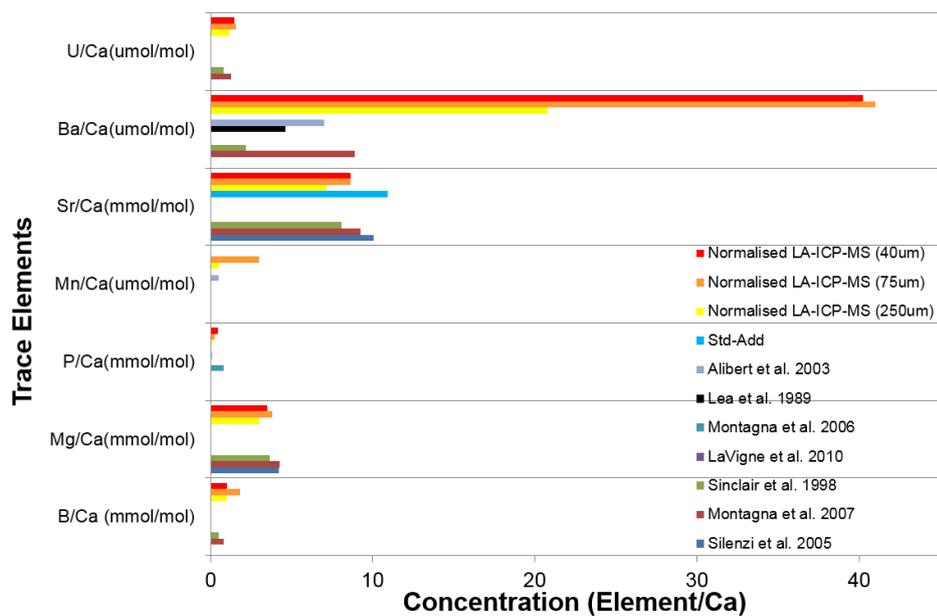
Figure 3.6.4 A comparison of the trace element composition data from the various spot sizes of laser ablation of sample SHR 04/11/11-11, standard addition of sample SHR 04/11/11-10 and from data reported from coral analysis in the literature. Data is only shown for those elements that have published data available for comparison. Only Montagna (2007) and Silenzi (2005) refer to *C. caespitosa* samples, the other studies looked at tropical or deep water species.

Conclusions on spot size

The hypothesis that the accuracy of the data may be a function of laser spot

size and power was supported; smaller spot sizes produce more reliable data.

Normalising the data to represent 100% $CaCO_3$, by using $^{43}Ca=38\%$ as an internal standard, brings all the various spot size data into a reasonable range but there are still differences in the concentrations and subsequent trace element/Ca ratios. Because of this, larger margins of error will be caused by larger spot sizes as the corrections applied will be larger.

The detectors do, however, need a minimum volume of ablated material to be produced to work effectively and this can be seen in the 40 µm data for the elements present in minute amounts. Lithium and manganese values drop dramatically at this spot size. It was also noted that there was a very poor signal-to-noise ratio for this spot size compared to the larger spot sizes.

As, for all elements other than Ba, the normalised laser ablation data seems to be within the range of values expected from previously published work, it seems that using a small spot size and normalising the data in this way is a reliable method of gaining trace elemental data. The 75 µm spot was the best size that avoided overloading the detectors while still producing enough ablated material.

In conclusion, the settings for the 75 µm spot size were used in all subsequent analysis and the data is calibrated by using $^{43}Ca = 38\%$ as an internal standard.

3.6.2.3. Sampling strategy

The use of a smaller spot size does increase levels of variability, as a small spot is more likely to resolve the micro-structural heterogeneities within the coral. Preliminary work followed the technique of Montagna et al. (2007) in analysing a continuously ablated line. Even with pre-ablation the signal was too noisy to pick out any meaningful trends, also, the sheer volume of data produced by

analysing a continuous line makes manipulation and analysis unwieldy and overly time consuming without any clear advantage.

Based on the sampling strategy employed for the stable isotopic analysis, it was decided to use spot analysis at an average of 12 samples per growth band to give approximately fortnightly resolution. Unfortunately it was not possible to see the growth bands under the laser's targeting microscope, due to relatively poor quality optics, and so a constant sampling resolution of 200 μm was selected. This resolution was chosen as it would give the closest resolution to an average 12 samples per band as the growth bands generally range in size from 1.5 to 3.5 mm.

3.6.3. Analysis method

The LA-ICP-MS was calibrated using the (pre-ablated) NIST 610 and 612 with known compositions so intensity values at the detectors could be automatically converted to concentration values. However, due to the laser coupling better with the carbonate of the samples than the silicate glass, these values would be overestimations only valid in relation to each other and so would need a second step of calibration, offline, post-analysis.

Following the optimal techniques outlined by the preliminary work, the samples were pre-ablated in a continuous tract down one wall of the corallite to remove any surface contamination, especially any traces of metals left behind from cutting the samples.

Pre-ablation settings: 250 μm spot size, 90% laser output, 12 Hz repetition rate, 10 μms^{-1} scan speed, 5 μm depth per pass.

Sample analysis was carried out using individual discrete laser spots rather than the continuous tract favoured by Montagna et al. (2007). A relatively small spot size and low laser power was used based on the best results gained in the calibration experiment.

Analysis settings: 75 µm spot size, 55% laser output, 4 Hz repetition rate, 40 s dwell time

Laser spots were placed every 200 µm along the corallite wall, parallel to the direction of growth and starting at the basal end of the corallite so that the data would also produce a clear time series.

The detectors in the mass spectrometer were set up to record the concentrations of the stable isotopes: ^{7}Li, ^{11}B, ^{23}Na, ^{24}Mg, ^{25}Mg, ^{27}Al, ^{31}P, ^{39}K, ^{43}Ca, ^{44}Ca, ^{54}Fe, ^{55}Mn, ^{56}Fe, ^{65}Cu, ^{66}Zn, ^{86}Sr, ^{88}Sr, ^{135}Ba, ^{137}Ba, ^{238}U.

As noted above, the concentration data produced by the mass spectrometer software's online calibrations were only semi-quantitative. Therefore, further calibrations were also necessary; these were carried out offline using Microsoft Excel. ^{43}Ca = 38% was used as an internal standard to normalise all the other trace element concentrations to be representative of a sample made up of 100 % $CaCO_3$ (aragonite).

The calibrated concentrations were converted into the standard trace element/^{43}Ca notation to allow comparison to values from the literature.

4. Stable isotope analysis – Results and discussion

In this chapter data is presented and discussed from the stable isotopic analysis of all analysed samples. Modern Croatian *C. caespitosa* sample data, along with measured temperature and water isotope data are used to assess the reliability of applying published carbonate-water fractionation equations (i.e. $\delta^{18}O$ palaeothermometers) to this species and a new species-specific palaeotemperature equation is proposed. This species-specific equation is compared to other published equations and both are applied to the fossil Greek *C. caespitosa* samples to assess their utility in producing reliable palaeotemperatures for the Pleistocene interglacials. The newly calibrated species-specific equation, when used alongside estimates for the palaeo-$\delta^{18}O_{seawater}$ of the Gulf of Corinth, produces palaeotemperatures for each interglacial in line with the climatic conditions found by other studies.

4.1. Modern Croatian samples – Isotope results

4.1.1. *C. caespitosa* samples

Table 4.1.1 describes the *C. caespitosa* samples collected from the Mljet bank sampling stations (see Figure 3.1.2 and Table 3.1.1) that were analysed for stable isotope composition. The $\delta^{18}O$ and $\delta^{13}C$ stable isotopic data profiles for these corallites are shown in Figure 4.1.1.

Table 4.1.1 Modern Croatian *C. caespitosa* samples analysed for stable isotope composition, sampling station numbers relate to those shown in Figure 3.1.2.

Sample	Sampling station	Growth depth (m)	Corallite length (mm)	Growth bands
PK 21/09/12-01	1	8	49	20 (19 sampled)
PK 21/09/12-02	2	10	33	19 (17 sampled)
PK 21/09/12-05	5	11	38	20 (20 sampled)
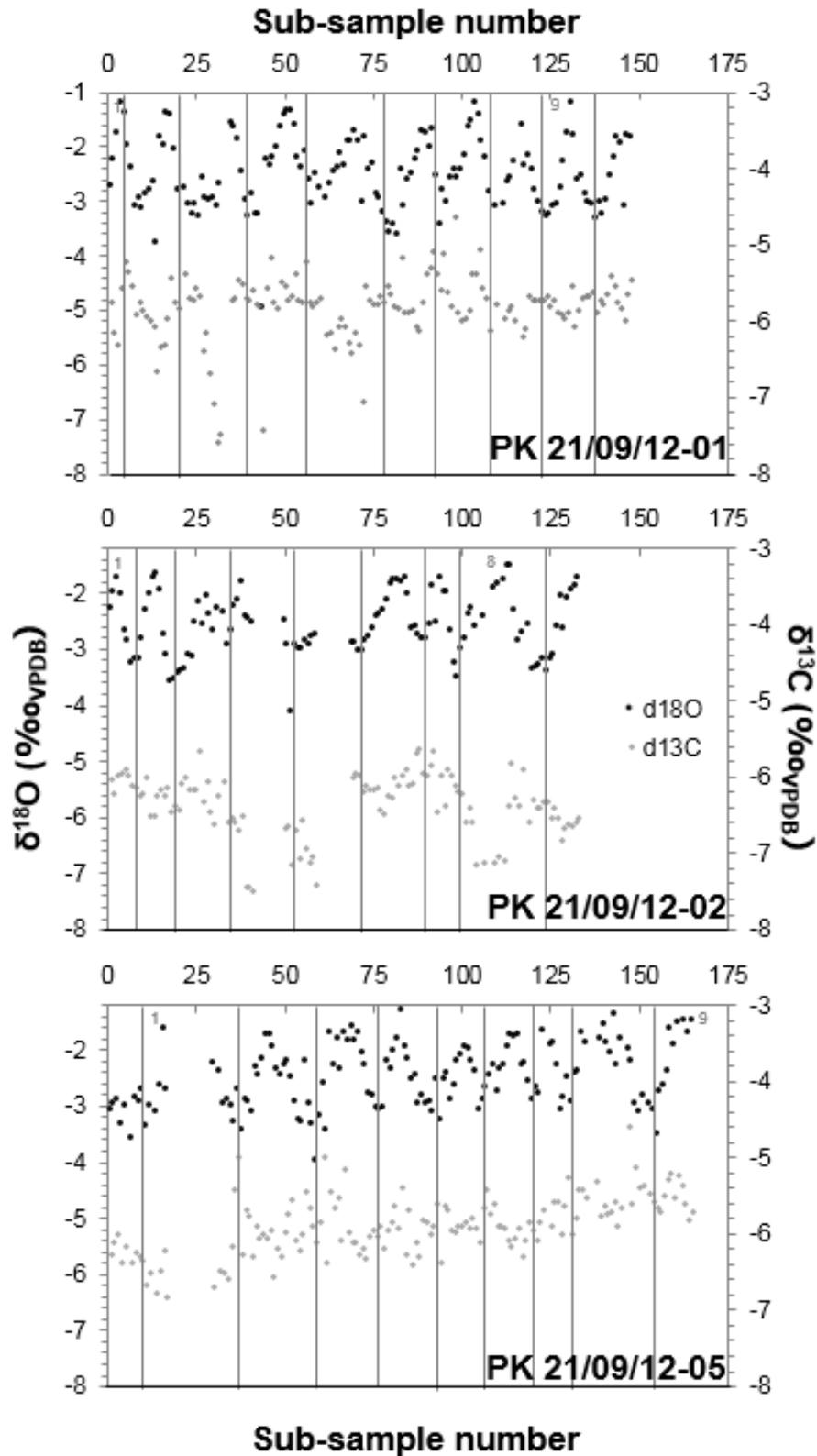
Figure 4.1.1 Stable isotope data from Mljet *C. caespitosa* samples, vertical lines have been added to separate complete cycles based on minima in the δ¹⁸O trace.

4.1.1.1. Sample comparison

The three modern Croatian *C. caespitosa* samples analysed all show very similar $\delta^{18}O$ patterns and values. A clear $\delta^{18}O$ sinusoidal cyclicity is observed in all samples with approximately the same number of cycles present as pairs of seasonal growth bands. This suggests that $\delta^{18}O$ cyclicity is an annual-scale feature in these corals and is presumably linked to the same factors that cause growth band development. In all samples the $\delta^{13}C$ data are complex, hints of cyclicity can be seen however the cycles are at varying scales patterns. Data from the modern Croatian samples are summarised in Table 4.1.2 and plots of the isotope profiles are shown in Figure 4.1.1.

Table 4.1.2 Summary of isotopic data from modern Croatian *C. caespitosa* samples and water isotopic data collected from the same sample sites (average water data also includes measurements from Stations 6 (14m, $\delta^{18}O$ = 1.2, δD = 8.9) and 7 (15m, δ18O = 1.2, δD = 9.3), water values are expressed in ‰ VSMOW while aragonite values are expressed in ‰ VPDB

	PK 21/09/12-01	PK 21/09/12-02	PK 21/09/12-05	Average
Growth depth (m)	8	10	11	N/A
Water $\delta^{18}O$	+1.0	+1.2	+1.2	+1.2 (2σ = 0.2)
Water δD	+7.6	+9.1	+9.0	+8.8 (2σ = 1.4)
Average $\delta^{18}O$	−2.5	−2.6	−2.5	−2.5 (2σ = 0.1)
$\delta^{18}O$ cycles	9.5	8	9	
Av. $\delta^{18}O$ max.	−1.4 (2σ = 0.4)	−1.7 (2σ = 0.2)	−1.7 (2σ = 0.4)	−1.6 (2σ = 0.3)
Av. $\delta^{18}O$ min.	−3.3 (2σ = 0.3)	−3.3 (2σ = 0.6)	−3.3 (2σ = 0.6)	−3.3 (2σ = 0.1)
Av. $\delta^{18}O$ range	−1.8 (2σ = 0.3)	−1.6 (2σ = 0.7)	−1.7 (2σ = 0.7)	−1.7 (2σ = 0.1)
Average $\delta^{13}C$	−5.8	−6.4	−5.9	−6.0 (2σ = 0.6)

As seen in Table 4.1.2 all the samples are very similar to each other in their overall $\delta^{18}O$ average and average trough (low 2σ values: 4.4% and 1.6% of their respective means) and only slightly more variable in their average peak and average amplitude values (2σ values: 18.8 and 16.1% respectively).

Because of this it seems reasonable to assume that all of these samples have experienced similar controls on their aragonitic δ^{18}O values.

4.1.2. Water samples

Water samples collected at the same times and monitoring stations as the Mljet corals were analysed for oxygen and hydrogen isotopic composition; the results are reported in Table 4.1.2. These data are also plotted in Figure 4.1.2 and Figure 4.1.3; there is no significant difference between the stations. This indicates that the upper 15m of the water column is well mixed.
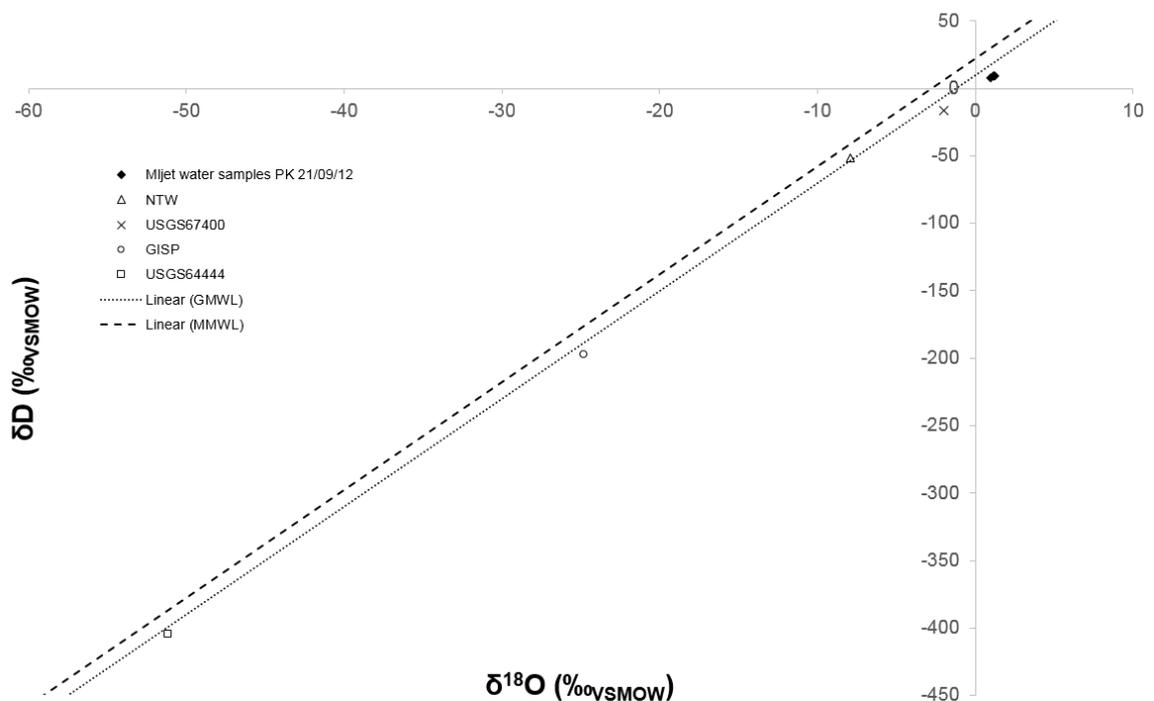
Figure 4.1.2 Mljet water and analysed standards stable isotopic compositions, (error is 0.16‰ for δ^{18}O and 1.05‰ for δD). Global meteoric water line (Craig, 1961) (dotted line) and Eastern Mediterranean meteoric water line (Gat et al., 1996) (dashed line) shown for comparison.
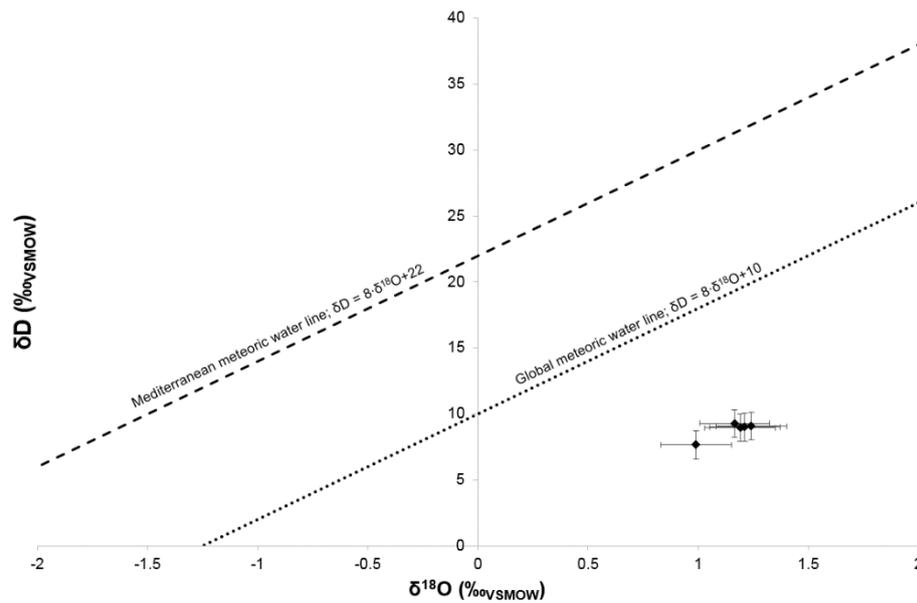
Figure 4.1.3 Expanded view of the Mljet water stable isotopic compositions in Figure 4.1.2, error bars show one standard deviation (0.16‰ for δ^{18}O and 1.05‰ for δD). Global meteoric water line (Craig, 1961) (dotted line) and Eastern Mediterranean meteoric water line (Gat et al., 1996) (dashed line) shown for comparison.

4.2. Modern Croatian samples – Analysis

4.2.1. Calibrating the data to a normalised time series

The *C. caespitosa* aragonite data sets were smoothed with a 4-point running median (following Montagna et al. 2007) to emphasise the cyclic trend and the profiles were normalised to a time series. When seawater δ^{18}O is constant, the primary control on coralline aragonite δ^{18}O is water temperature (Beck et al., 1992; Gagan et al., 1994; McCulloch et al., 1994; Correge, 2006); with carbonate δ^{18}O showing a negative correlation with temperature (McCrea, 1950; Epstein et al., 1953). The clear cyclicity in δ^{18}O profiles is thus attributed to an annual temperature-driven signal.
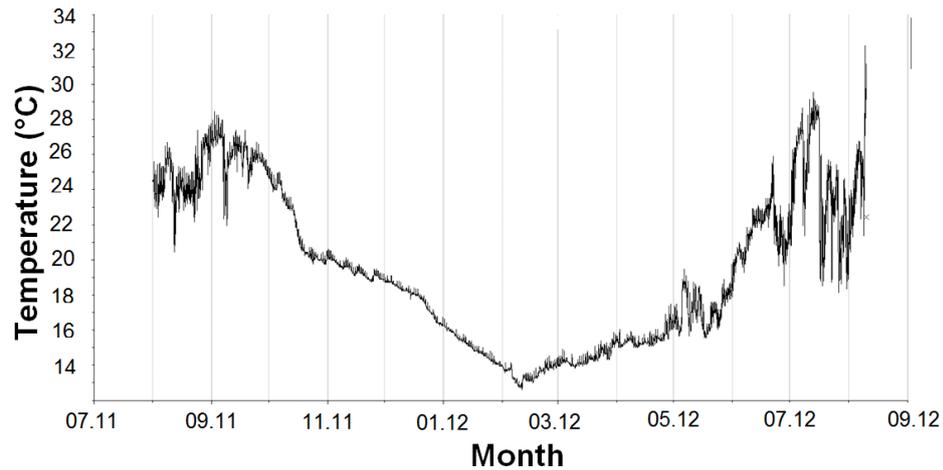
Figure 4.2.1 2012 temperature record from 15m depth on Mljet coral bank (modified from Kružić, pers comms)

Temporal adjustment was achieved assuming peak maxima corresponded to the time of the year with lowest seawater temperatures (February/March at this locality; Figure 4.2.1) and minima corresponding to the highest seawater temperatures (August/September at this locality). As these samples were collected alive in September 2012 the youngest winter growth band corresponded to winter 2011/2012; preceding peak maxima were then assigned years counting backwards from this point. Mid-points between peak maxima/mid-winters were equally spaced using a 1/n formulation where n is the number of sample points between maxima. Figure 4.2.2 shows the smoothed and adjusted profiles aligned for ease of comparison; it can be seen that, while the values are similar overall, the profiles themselves are not identical.
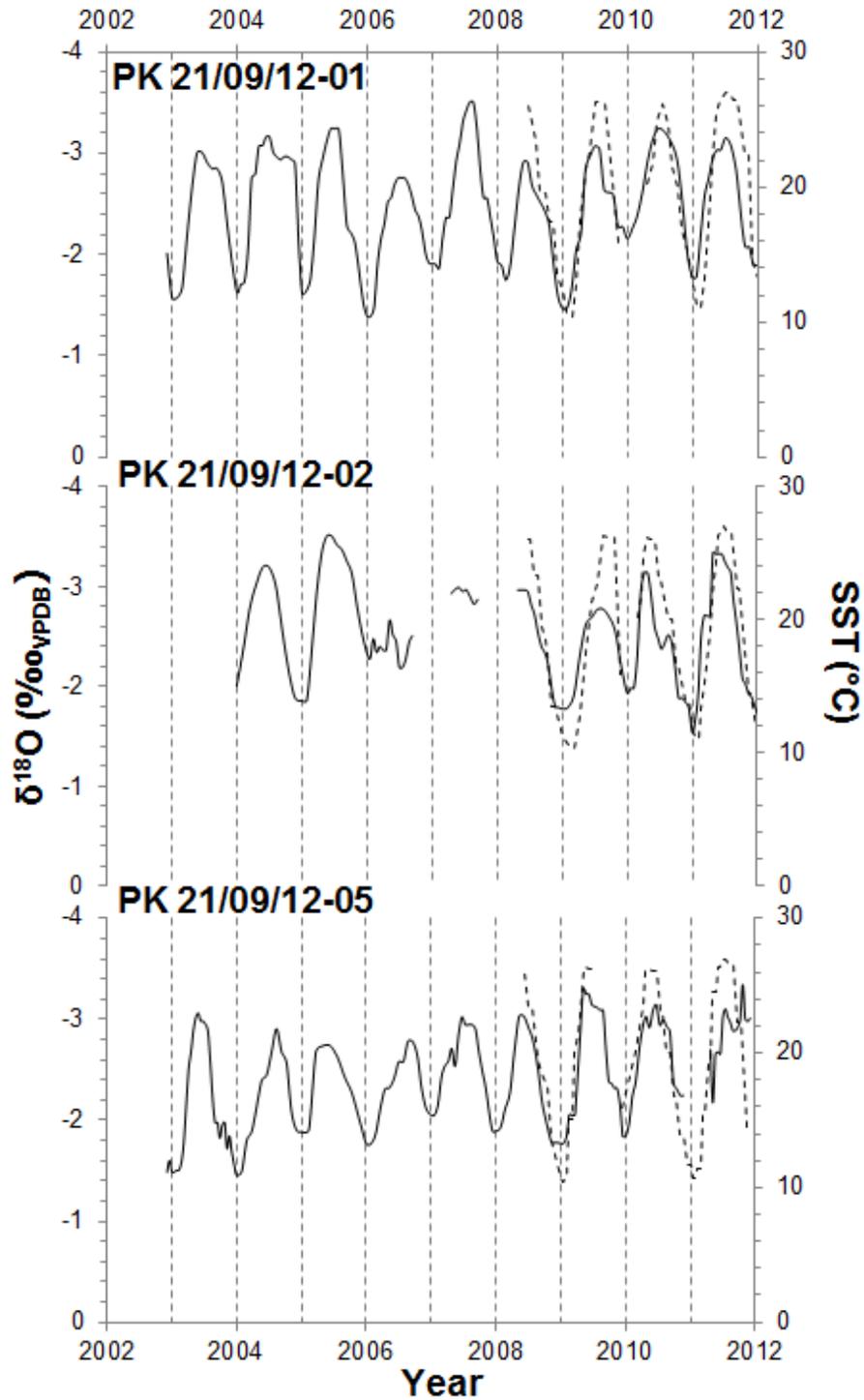
Figure 4.2.2 Modern Croatian *C. caespitosa* aragonite δ¹⁸O profiles smoothed and adjusted to time series, mean monthly in situ measured SST data included for reference (obtained from the Croatian Meteorological and Hydrological Institute). The δ¹⁸O x-axis is reversed for ease of comparison between the two series.

4.2.2. Discussion of carbon stable isotopic data
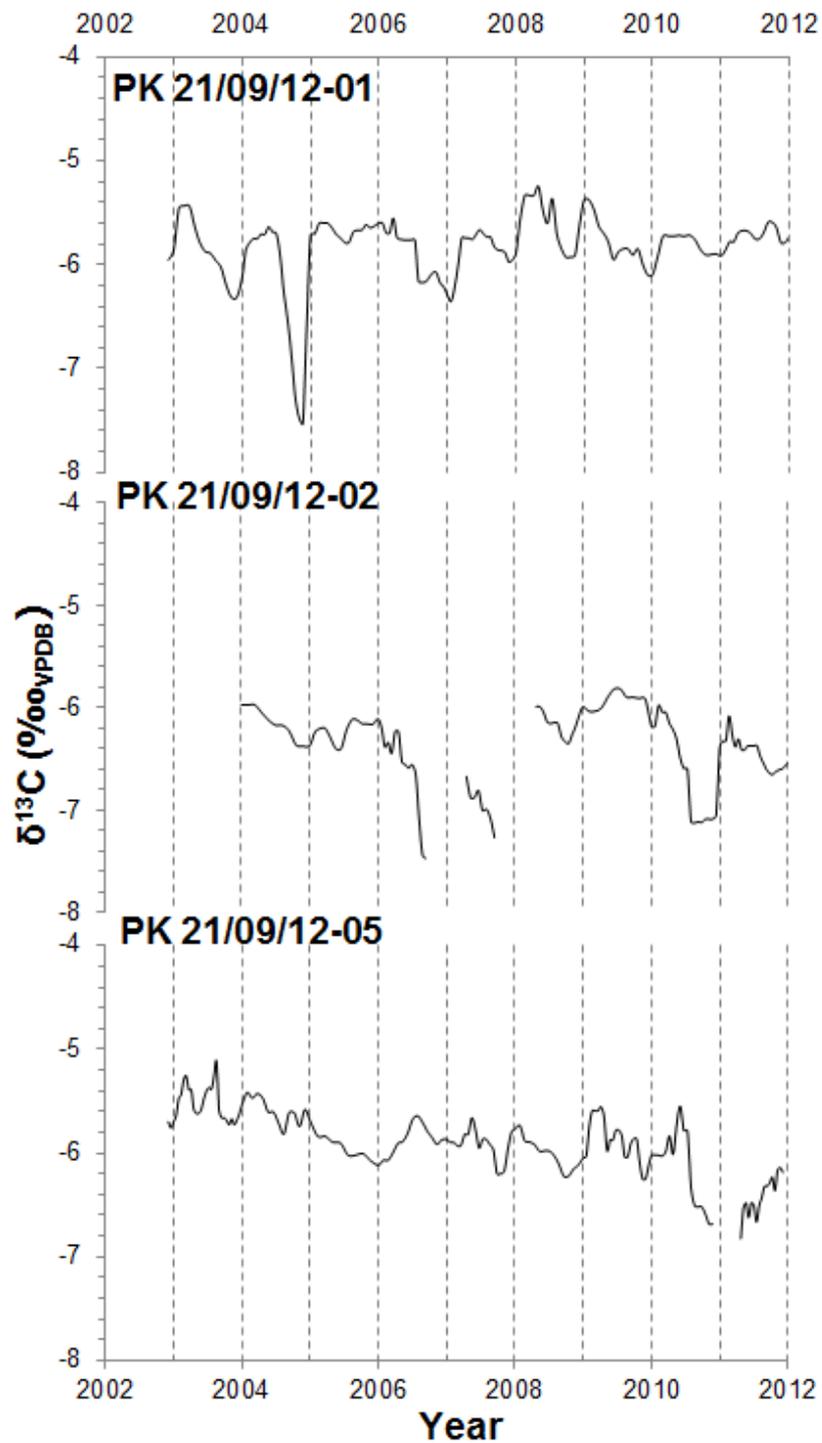
Figure 4.2.3 Modern Croatian coral δ^{13}C profiles smoothed and adjusted to time series

Figure 4.2.3 shows the smoothed and normalised δ^{13}C profiles from the Croatian *C. caespitosa* aragonite. Informed by the δ^{18}O cyclicity, it appears as

though there is some semblance of annual-scale cyclicity in the profiles. However, this is overprinted by a great degree of variability, even after smoothing, and there are no regions where any of the curves show any clear similarities to each other. Some years in some profiles have multiple peaks while others have none. Moreover, comparison of the two isotope profiles (Figure 4.2.4) shows that sometimes the $\delta^{13}C$ follows the $\delta^{18}O$, sometimes it appears to oppose it and sometimes there is no relationship.
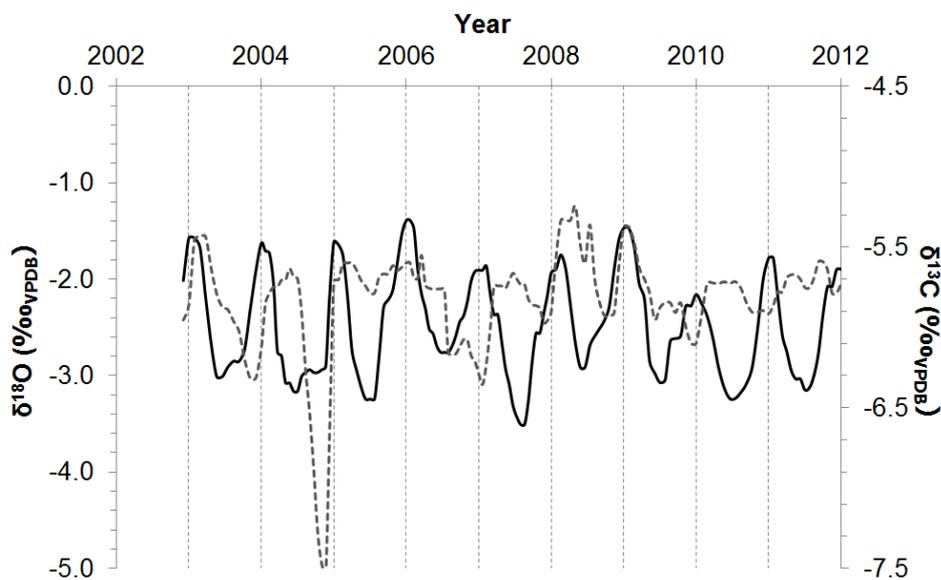
Figure 4.2.4 Comparison of $\delta^{18}O$ and $\delta^{13}C$ profiles overlain for *C. caespitosa* sample PK 21/09/12-01

This suggests that controls on coralline aragonite $\delta^{13}C$ are more complex than those that control $\delta^{18}O$. Corals acquire skeletal carbon from two main pools: (1) from dissolved inorganic carbon (DIC) in seawater via respiration of carbon acquired by photosynthesis by their symbiotic zooxanthellae and (2) via respiration of heterotrophically acquired carbon from capture of zooplankton. These two sources of carbon have very different isotopic signatures, DIC $\delta^{13}C \approx$ 0‰ and zooplankton $\delta^{13}C \approx$ −14 to −30‰ (Rau et al., 1989). Changes in the amount of importance of the two, caused by environmental factors, will alter the

coral's metabolic fractionation and be recorded by changes in the coral's skeletal $\delta^{13}C$. For example, decreasing light intensity or increasing the availability of zooplankton has been shown to significantly decrease skeletal $\delta^{13}C$ levels due to an increased reliance on heterotrophy (Grottoli and Wellington, 1999).

As the $\delta^{13}C$ of the coralline aragonite mainly range between −5 and −7‰, this shows that these corals gain their carbon from both their diet of zooplankton and from DIC in the seawater as this range in somewhere between the two end member values. It could be inferred that the main source of carbon for skeletal precipitation comes from DIC as the aragonite values are closer to this than to organic carbon (from zooplankton).

Although it is highly variable, the annual-scale cyclicity to the $\delta^{13}C$ data suggests that the relative importance of these two sources of carbon vary throughout the year. It appears that, generally, the coral aragonite's $\delta^{13}C$ is higher in the summer, consistent with the study by Ferrier-Pages et al. (2011). In this study, the authors measured the $\delta^{13}C$ and $\delta^{15}N$ of the organic tissue and symbiotic zooxanthellae of a *C. caespitosa* colony as well as in plankton, the coral's potential heterotrophic food source. In the summer the $\delta^{13}C$ of the coral's organic tissue was close to that of the zooxanthellae whereas in the winter it was close to that of the plankton. They concluded that in the summer the corals are mainly autotrophic in their carbon acquisition, relying on their photosynthetic zooxanthellae, whereas in winter most of the coral's carbon comes from heterotrophic feeding with predation on planktonic organisms. This was further backed by winter enrichment of the $\delta^{15}N$ suggesting greater feeding at this time of the year.

Changes in the $\delta^{13}C$ of ambient seawater DIC have been found to overprint the heterotrophic/autotrophic driven signal (Swart et al., 1996). The DIC of riverine waters is usually lower in $\delta^{13}C$ than seawater (Swart, et al., 1996) and so changes in the amount of riverine input to a coastal area will cause depletion of $\delta^{13}C$ in the seawater DIC and be recorded in the coralline aragonite (e.g. Moyer and Grottoli, 2011). Therefore the annual cyclicity, with summer enrichment and winter depletion in $\delta^{13}C$, could be caused by increased winter time riverine input, driven by winter recharge. This region of Croatia has a typical maritime climate with the majority of the annual rainfall falling in the winter (Vreča et al., 2006) .

However, these speculations are not supported by statistically significant relationships with $\delta^{18}O$ (the average R^2 value for a correlation between $\delta^{18}O$ and $\delta^{13}C$ in the samples is 0.03 and P value for the relationship is 0.14). If both $\delta^{18}O$ and $\delta^{13}C$ are predominately controlled by the same seasonal changes then it would be expected that they would have a significant relationship with each other. Due to the negative correlation between temperature and $\delta^{18}O$ values and the summer enrichment and winter depletion in $\delta^{13}C$ in the coralline aragonite, a negative correlation would be expected between the two isotopes. As this is not seen it demonstrates that the $\delta^{18}O$ and $\delta^{13}C$ compositions of the coralline aragonite are not coupled with each other, a change in one does not effect on the other, with both controlled by separate, external factors.

 As the processes which may affect both the $\delta^{13}C$ of seawater DIC and the metabolic fractionation of coral skeletal $\delta^{13}C$ are both primarily controlled by seasonal changes in climate (Moyer and Grottoli, 2011); it is beyond the scope of this study to attempt to unravel the relative influences of these two factors on

the carbon isotopic signature of the corals, this limits the potential use of $\delta^{13}C$ as a palaeoclimate/palaeo-DIC tracer for the fossil samples as there is no way of knowing which is the main control on $\delta^{13}C$. Therefore, the $\delta^{13}C$ data will not be discussed in any further detail.

4.2.3. Application of published $\delta^{18}O$ carbonate-water palaeothermometers to data

It is widely accepted that one of the main controls on the $\delta^{18}O$ composition of a precipitating carbonate is the temperature of precipitation and the $\delta^{18}O$ composition of the water from which it is precipitating from (McCrea, 1950; Epstein et al., 1953). As a clear annual trend is visible in the $\delta^{18}O$ profiles of all the Croatian samples it seems reasonable to assume that this is an annual temperature-driven signal. Therefore these corals are likely recording a signal of water temperature as they grow.

The average annual sea surface temperature at Mljet over the period 2003-2010 (which covers the majority of the growth years analysed) was 20.3°C (Kružić et al., 2012), the average monthly mean temperature reached during the summer months is 27.5°C (Kružić, 2002) and the average lowest monthly mean temperature reached during winter is 11°C (Kružić, 2002). The range is reduced somewhat by the lowest points of the coral bank (around 15m) with average monthly temperatures ranging from ≈ 26 to 14°C at this depth (Figure 4.2.1).

By inputting both the $\delta^{18}O$ carbonate data from the profiles and the measured $\delta^{18}O$ water values from the relevant sampling station into the Goodwin et al. (2001) modified Grossman and Ku (1986) palaeotemperature equation for

aragonite precipitated in equilibrium (Equation 2.3.8 repeated below) it should, in theory, be possible to calculate the water temperatures the coral grew at, if a constant δ¹⁸O water value over the growth period is assumed, with the results being within the range of values recorded at the site.

$$T = 20.60 - 4.34(\delta^{18}O_A - (\delta^{18}O_W - 0.20))$$

<div align="right">**Equation 2.3.8 (repeated)**</div>

The Goodwin et al. (2001) version of the Grossman and Ku (1986) equation was selected for use over other published aragonite-water fractionation equations as it has been used on other biogenic aragonites with some success (Goodwin et al., 2001; Goodwin et al., 2003; Schöne et al., 2005). The correction applied by Goodwin et al. accounts for the original work of Grossman and Ku reporting water values as SMOW minus 0.2‰.

However, Figure 4.2.5 shows that palaeotemperatures calculated using this equation are much too high to be realistic. The results for the calculated temperatures are summarised in Table 4.2.1.

These temperatures are unrealistically high to have been recorded at this locality. Also, *C. caespitosa* polyps can only survive for limited periods when the sea surface temperature reaches 28°C (Kružić, 2007; Rodolfo-Metalpa et al., 2006, 2008). If the water temperature at the growth depth remains above this limit for up to a month extensive bleaching occurs (Kružić, Sršen, & Benković, 2012; Rodolfo-Metalpa, Bianchi, Peirano, & Morri, 2005). Coral bleaching is a phenomenon where the coral loses its colour due to the expulsion of the symbiotic zooxanthellae algae, leading to decreased growth and increased

mortality (Douglas, 2003). Therefore, it is unrealistic for this species to record

an average annual water temperature of around 35.5°C.

Table 4.2.1 Temperatures calculated from modern corals using the Grossman and Ku (1986) palaeotemperature equation

	Average temperature (°C)	Average Maximum (°C)	Average Minimum (°C)	Average Amplitude (°C)
PK 21/09/12-01	34.8	37.6	31.4	6.2
PK 21/09/12-02	36.1	38.8	33.2	5.4
PK 21/09/12-05	35.5	38.0	32.7	5.4
Average	35.5	38.1	32.4	5.7
2σ	1.4	1.2	1.8	1.0
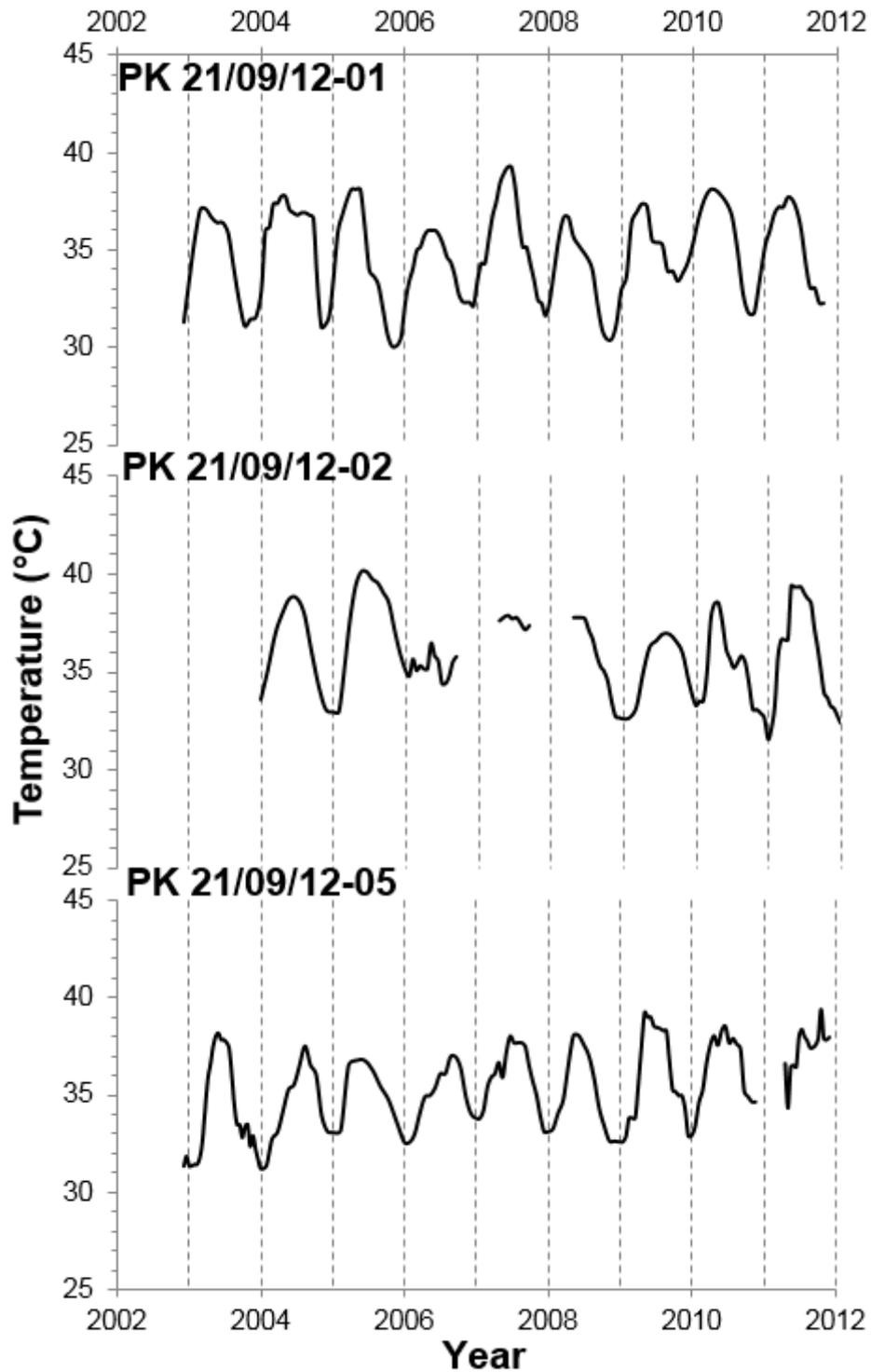
Figure 4.2.5 Calculated temperatures from modern Croatian corals using the Goodwin et al. (2001) modified Grossman and Ku (1986) palaeotemperature equation

4.2.4. Development of a calibrated *C. caespitosa* δ^{18}O carbonate-water palaeothermometer

A new *C. caespitosa* δ^{18}O carbonate-water palaeothermometer was calibrated using the Mljet coral and water oxygen isotopic data. The average 2003-2010 measured SST of 20.3°C (Kružić et al., 2012) was used as a basis for this as SSTs at this locality are a reasonable approximation of the temperature over the depths of the bank (Kružić & Pozar-Domac, 2002; Kružić et al., 2012).

To recalibrate the Goodwin et al. (2001) modified Grossman and Ku (1986) equation to take into account the offset of the coralline δ^{18}O$_A$ from equilibrium due to the coral's vital effects; the following sequence of equations was carried out for each sample:

$$_{Average\ calculated}T = 20.60 - 4.34 \left[\left(_{Average\ measured}\delta^{18}O_A - (\delta^{18}O_W - 0.20) \right) \right]$$

Equation 4.2.2 Average Grossman and Ku (1986) calculated temperatures

Equation 4.2.2 gave temperatures much too high to be realistic, therefore Equation 4.2.3 is as follows:

$$_{Average\ measured}T \ll 20.60 - 4.34 \left[\left(_{Average\ measured}\delta^{18}O_A - (\delta^{18}O_W - 0.20) \right) \right]$$

Equation 4.2.3 Average measured temperature is significantly lower than average calculated temperature

It is known that corals precipitate their aragonite out of equilibrium, with vital effects causing a depletion in aragonite δ^{18}O. Therefore the aragonite δ^{18}O must be the term that needs correcting to calibrate the equation for the offset from equilibrium; Equation 4.2.4.

$$_{Average\ measured}T$$

$$= 20.60$$

$$- 4.34\big[\big(_{Average\ measured}\delta^{18}O_A + \delta^{18}O_A\text{depletion}\big) - \big(\delta^{18}O_W - 0.20\big)\big]$$

Equation 4.2.4 Calibrating equation for taking into account the depletion of aragonite δ^{18}O from 'vital effects'

By rearranging Equation 4.2.4 it is possible to calculate aragonite δ^{18}O if the coral precipitated in equilibrium; Equation 4.2.5

$$\frac{_{Average\ measured}T - 20.60}{-4.34} + (\delta^{18}O_W - 0.20) = {}_{Average\ equillibrium}\delta^{18}O_A$$

Equation 4.2.5 Rearranged (modified) Grossman and Ku (1986) equation to allow calculation of expected equilibrium δ^{18}O from measured temperature

The difference between the calculated average equilibrium aragonite δ^{18}O and the average measured aragonite δ^{18}O will indicate how much the coral's 'vital effects' cause a depletion of the δ^{18}O value in the coralline aragonite; Equation 4.2.6

$$_{Average\ equillibrium}\delta^{18}O_A - {}_{Average\ measured}\delta^{18}O_A = \delta^{18}O_A\ depletion$$

Equation 4.2.6 Calculating depletion of δ^{18}O due to 'vital effects'

Further modifying the Goodwin et al. (2001) modified Grossman and Ku (1986) equation to take into account the depletion of the coralline aragonite from the equilibrium value, results in an equation that describes the calibrated δ^{18}O carbonate-water palaeothermometer; Equation 4.2.7

$$T = 20.60 - 4.34\big[\big(_{measured}\delta^{18}O_A + \delta^{18}O_A depletion\big) - \big(\delta^{18}O_W - 0.20\big)\big]$$

Equation 4.2.7 Calibrated δ¹⁸O carbonate-water palaeothermometer

Table 4.2.2 reports the values calculated for each coral using this sequence of equations:

Table 4.2.2 Average oxygen isotopic values from Croatian corals used in palaeothermometer calibration

Coral sample	Average measured $\delta^{18}O_A$	$\delta^{18}O_W$	Average equilibrium $\delta^{18}O_A$	$\delta^{18}O_A$ depletion	Average measured temperature	Calibrated average calculated temperature
PK 21/09/12 - 01	−2.5	1.0	0.9	3.3	20.3	20.4
PK 21/09/12-02	−2.5	1.2	1.1	3.6	20.3	20.6
PK 21/09/12-02	−2.4	1.2	1.1	3.5	20.3	20.6
Average	−2.5 (2σ=0.1)	1.1 (2σ=0.3)	1.0 (2σ=0.3)	3.5 (2σ=0.3)	20.3 (2σ=0)	20.5 (2σ=0.2)

Using the average isotopic data from each sample a calibrated palaeothermometer for each sample was derived; using the average depletion values from those individual palaeothermometers, a general palaeotemperature equation can be constructed from the Croatian *C. caespitosa*; Equation 4.2.8

$$T = 20.60 - 4.34\big[(\delta^{18}O_A + 3.5(\pm 0.15)) - (\delta^{18}O_W - 0.20)\big]$$

Equation 4.2.8 Croatian *C. caespitosa* calibrated δ¹⁸O carbonate-water

palaeothermometer

4.2.1.   The need for a calibrated palaeothermometer

It is unsurprising that the Goodwin et al. (2001) modified Grossman and Ku (1986) equation does not produce the actual range of temperatures the corals

grew in. This equation was calibrated for aragonite growing in isotopic equilibrium and it is well established that corals do not precipitate their aragonitic skeleton in isotopic equilibrium (Weber and Woodhead, 1972; Rollion-Bard et al., 2003b), instead demonstrating an isotopic depletion due to biologically controlled vital effects (see Section 2.3.3).

However, if the amount of disequilibrium caused by the vital effect is constant the coral's isotopic composition may still be a useful indicator of palaeotemperature (Weil et al., 1981). This vital effect appears to be species specific so that coral palaeotemperature equations must also be species specific. There are many reported $\delta^{18}O$ carbonate-water palaeotemperature equations for tropical species reported in the literature, but only one for *C. caespitosa*: by Silenzi et al. (2005) (Equation 4.2.1).

$$SST(°C) = (\delta^{18}O_A - 0.91(\pm1.42)) \div -0.15(\pm0.09)$$

Equation 4.2.1 Silenzi et al. (2005) *C. caespitosa* $\delta^{18}O_c$-SST relationship

This equation does not take into account changes in the oxygen isotopic value of the water and has error limits that are wider than the observed temperature range at the study locality. In the Silenzi et al. (2005) study this was found to be a non-statistically significant relationship as there were significant variations in the oxygen isotopic value of the seawater during the time period analysed due to varying levels of rainfall.

Because of this, a new species-specific palaeothermometer is required to allow the analysis of *C. caespitosa's* $\delta^{18}O$ record for potential as a palaeoclimate archive.

4.2.2. Testing the new *C. caespitosa* δ^{18}O carbonate-water palaeothermometer

Using the high resolution δ^{18}O data from the Croatian corals and Equation 4.2.8 it is possible to re-construct semi-quantitative temperature ranges: Table 4.2.3 and Figure 4.2.6.

Table 4.2.3 Summary of modern Croatian corals calculated temperatures using the newly calibrated palaeotemperature equation

	Average temperature (°C)	Average Maximum (°C)	Average Minimum (°C)	Average Amplitude (°C)
PK 21/09/12-01	19.6	23.1	15.1	8.0
PK 21/09/12-02	20.8	23.9	17.2	6.6
PK 21/09/12-05	20.3	24.1	17.0	7.1
Average	20.2 (2σ=1.2)	23.7 (2σ=1.1)	16.4 (2σ=2.3)	7.2 (2σ=1.4)
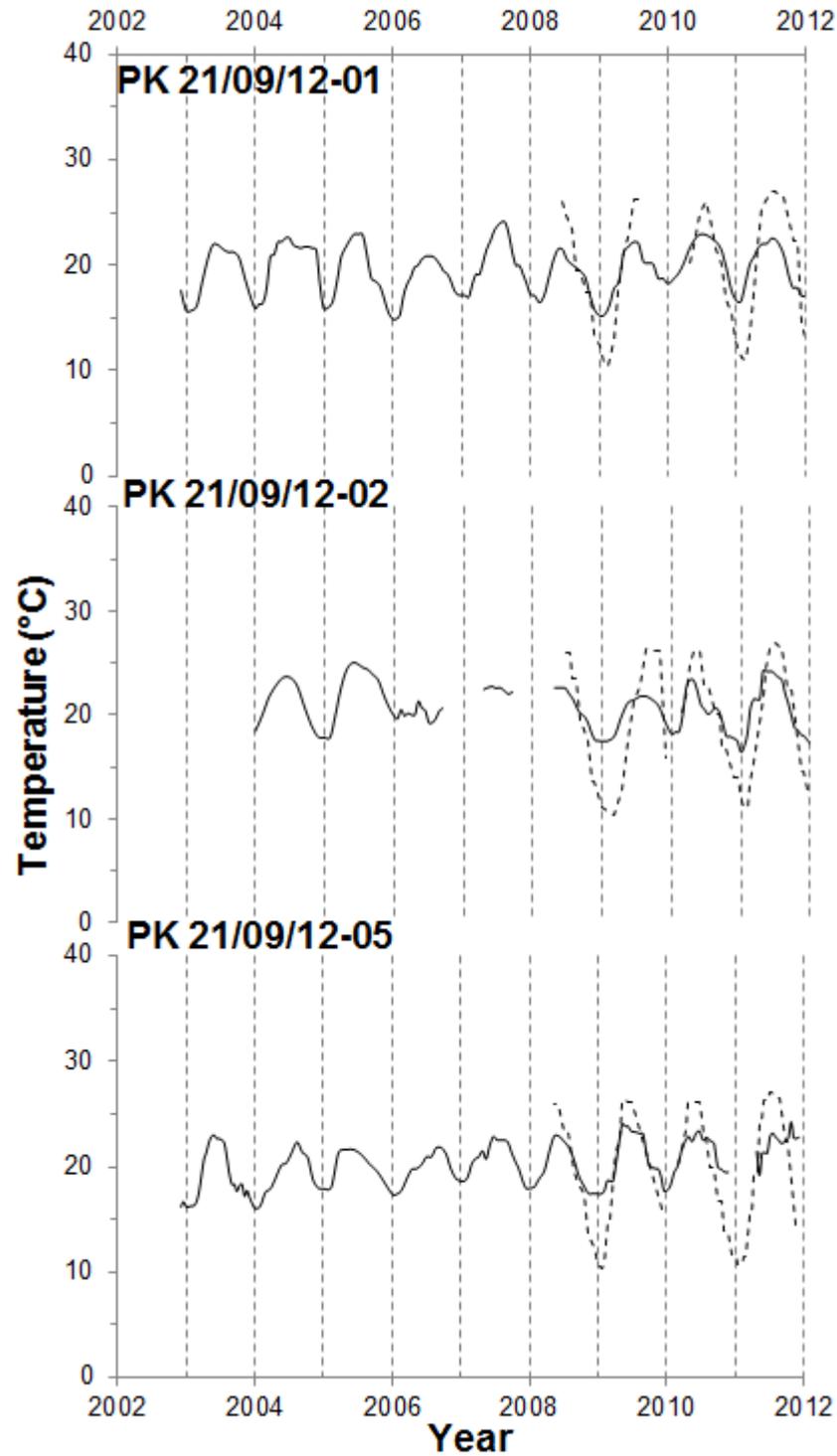
Figure 4.2.6 Modern Croatian corals calculated temperatures using the newly calibrated palaeotemperature equation, mean monthly in situ measured SST data included for reference (obtained from the Croatian Meteorological and Hydrological Institute).

The calculated temperatures reproduce the mean temperatures well, although the calculated ranges are lower than the actual annual water temperature ranges measured at the site, both at the sea surface (which can be seen very clearly in Figure 4.2.6) and at 15 m depth. There are two possible explanations for this:

1. The calculated *C. caespitosa* $\delta^{18}O$ aragonite-water palaeotemperature relationship is not correct, and as well as being isotopically depleted relative to equilibrium aragonite, coralline aragonite $\delta^{18}O$ is less sensitive to changes in temperature of precipitation than aragonite precipitated in isotopic equilibrium.

2. The calculated *C. caespitosa* $\delta^{18}O$ aragonite-water palaeotemperature relationship is correct but the corals either do not calcify, or calcify very slowly, when water temperatures are >24°C or <15°C, such that only a restricted range of water temperatures is recorded.

Explanation 2 is most likely because at temperatures between 14-16°C, *C. caespitosa* is unable to precipitate aragonite, such that the lowest winter temperatures are not recorded in skeletal aragonite (Montagna et al., 2007). Tank experiments and field observations also show that after 2 weeks of constant water temperatures of 28°C, high levels of tissue necrosis occur, and even after 5 weeks at 24°C the corals show signs of stress (Rodolfo-Metalpa et al., 2005; Kružić et al., 2014). We thus infer that growth temperatures outside the 15-24°C range are unlikely to be recorded due to heavily decreased, or cessation of, corallite growth, in agreement with Montagna et al. (2007). As well as this it is likely that the extreme values are somewhat moderated by a

'smoothing' effect due to some calcification occurring deeper within the tissue layer, rather than all at the upper surface (Gagan et al., 2012). It is unlikely that extreme values are significantly moderated by increased runoff from winter rainfall (isotopically negative) decreasing seawater $\delta^{18}O$ during winter/spring, and/or increased summer aridity/evaporation increasing salinity and seawater $\delta^{18}O$. If there was a major seasonal change in the isotope composition of the water, caused by riverine/groundwater input, then changes in the coralline $\delta^{18}O$ and $\delta^{13}C$ would be coupled, as increased riverine input would decrease both $\delta^{18}O$ and $\delta^{13}C$ values, and there would also be a greater annual range in salinity.

4.2.3. Increasing the range of values produced by the palaeothermometer to match expected values

Reconsideration of the equation calibrated using the average annual temperature (Equation 4.2.8) shows that it is possible to adjust the temperature sensitivity of the palaeothermometer by adjusting the second of the constant values (4.34). This allows the range of temperature values produced by the data set to be increased to the range of temperature values that are recorded at the locality. By replacing the original constant with an unknown 'b', the 'stretch factor' and rearranging the equation to solve for this with the relevant maximum, minimum, average monthly $\delta^{18}O$ aragonite values, temperatures and an average $\delta^{18}O$ water value Equation 4.2.9 can be solved:

$$b = -\left[\frac{T_{(\text{min } average)} - 20.60}{\left(\delta^{18}O_{A(\text{max } average)} + 3.5\right) - \left(\delta^{18}O_{W(average)} - 0.2\right)}\right]$$

Equation 4.2.9 palaeotemperature equation re-arranged for calculation of 'b' the stretch

factor

This is also solved for 'b' when T=max average, $\delta^{18}O$ = min average and when

T=average, $\delta^{18}O$ = min average.

An average value for the stretch factor 'b' of 6.457(±0.525) is calculated using

the values in Table 4.2.4.

Table 4.2.4 Average values from modern Croatian samples used for calculation of 'b' value

$\delta^{18}O_A$ average				$\delta^{18}O_W$ average	'b' value
$\delta^{18}O$ average	−2.5	T(°C) average	20.3	1.2	0.3
$\delta^{18}O$ maximum	−1.6	T(°C) maximum	26.0	1.2	6.8
$\delta^{18}O$ minimum	−3.3	T (°C) minimum	15.0*	1.2	6.2
				Average 'b'	6.5 (2σ=1.05)

*15°C is used as a minimum as it is unlikely that significant precipitation occurs below this temperature

(Montagna et al. 2007)

This produces the range calibrated palaeotemperature Equation 4.2.10:

$$T = 20.60 - 6.5\left[\left(_{measured}\delta^{18}O_A + 3.5\right) - \left(\delta^{18}O_W - 0.20\right)\right]$$

Equation 4.2.10 Calibrated $\delta^{18}O$ carbonate-water palaeothermometer stretched for

observed temperature range

Figure 4.2.7 shows this new equation applied to the modern corals with both the

Grossman & Ku (1986) and average-calibrated equations for comparison. This

new range-calibrated equation does stretch the produced range of values,

however, due to the increased number of assumptions and increased use of

average values it is much less reliable than the average-calibrated equation. This is shown by the (relatively) large standard deviation of 'b' and the way it regularly calculates winter temperatures down to 10-12°C.

This suggests that the first explanation, that only a restricted range of temperatures is recorded, is a more reliable conclusion. On this basis the average-calibrated palaeothermometer appears to be a more reliable technique for gaining realistic temperature data from modern and fossil *C. caespitosa* aragonite. This conclusion means that only Equation 4.2.8 will be used in the analysis of the fossil samples.
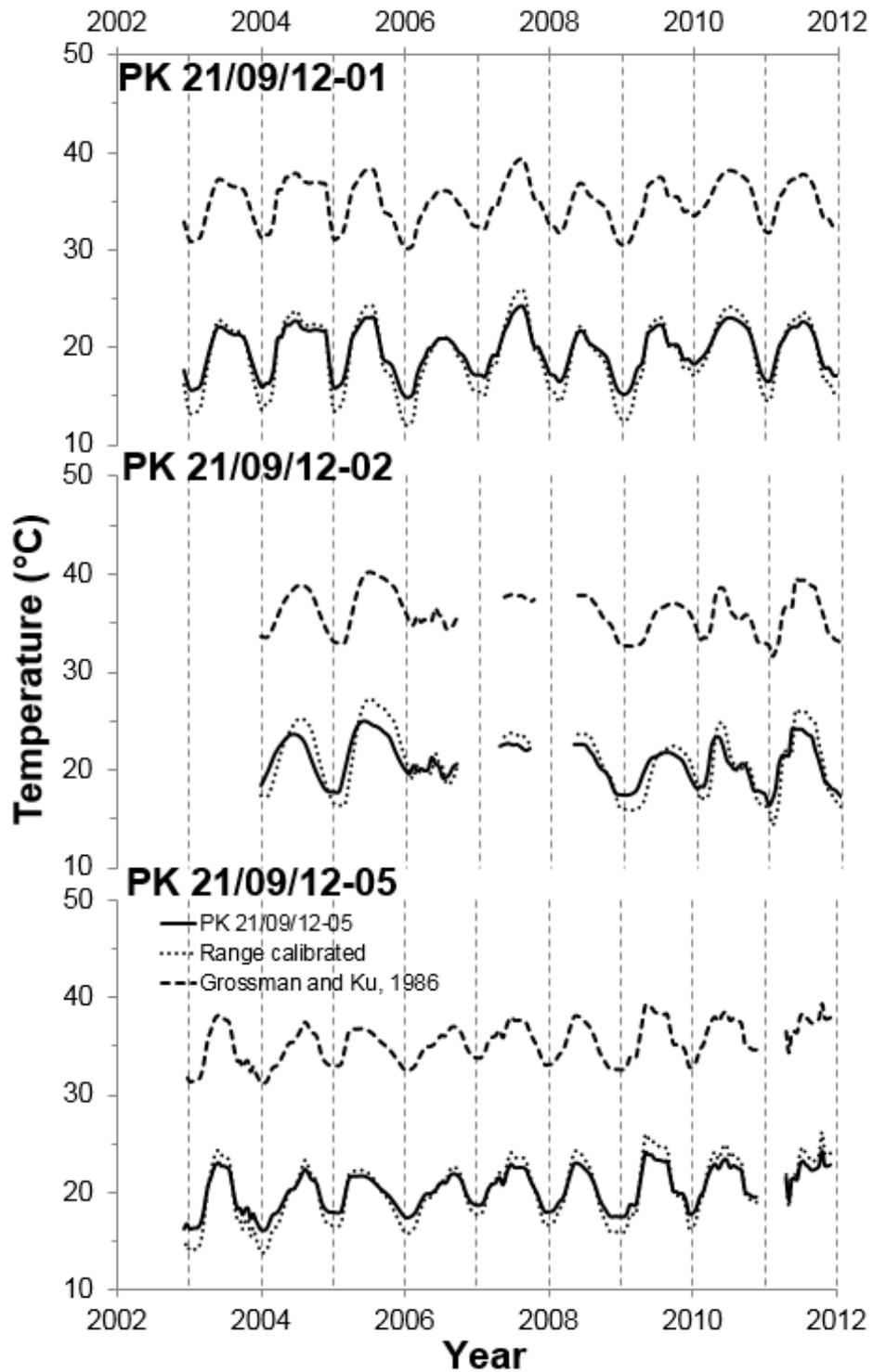
Figure 4.2.7 Modern Croatian corals calculated temperatures using the newly calibrated range based palaeotemperature equation (other palaeotemperature equations used shown for comparison)

4.3. Fossil Greek samples – Isotopic results

Table 4.3.1 describes the *C. caespitosa* samples collected from the Greek

localities (see Figure 3.1.4) that were analysed for stable isotope composition.

The δ^{18}O stable isotopic data profiles for these corallites are shown in Figures

4.3.1 to 4.3.3 with data summarised in Table 4.3.2.

Table 4.3.1 Greek *C. caespitosa* samples analysed for stable isotope composition, see Figure 3.1.4 for locality map.

Sample	Age	Location	Length (mm)	Number of Growth bands	Notes	Fig.
SHR 03/11/11-02	Holocene	Mavra Litharia (38°08'34.5''N; 22°22'49.0''E)	40	20 (18 sampled)	Basal 2 bands avoided due to calcareous algal overgrowth	4.3.1
JEA 010626-04	MIS 5e	Goat Point (38°02'45.2''N; 22°52'49.7''E)	36	14 (11.5 sampled)	Collected by Julian Andrews	4.3.2 (A)
SHR 04/11/11-10	MIS 5e	West Flagnoro Bay (38°01'11.1''N; 22°53'33.5''E)	42	19 (12 sampled)	N/A	4.3.2 (B)
SHR 02/11/11-08 (I)	MIS 5e	Makrugoaz Ridge (38°01'21.8''N; 22°52'49.8''E)	31	13 (12 sampled)	Both collected from the same deposit and presumed to be approximately the same age.	4.3.2 (C)
SHR 02/11/11-08 (II)			45	17 (15 sampled)		4.3.2 (D)
SHR 02/11/11-02 (I)	MIS 7a	West of Lake Vouliagmeni (38°01'55.2''N; 22°52'14.1''E)	46	17 (16 sampled)	Both collected from the same deposit and presumed to be approximately the same age.	4.3.3 (A)
SHR 02/11/11-02 (II)			38	15 (13 sampled)		4.3.3 (B)
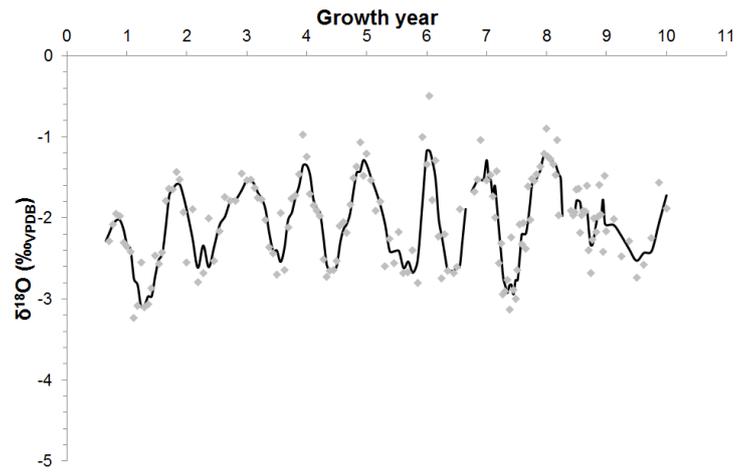
Figure 4.3.1 Holocene *C. caespitosa* sample SHR 03/11/11-02 oxygen isotopic profile, smoothed (using 4-point running median) and adjusted to growth years, unsmoothed data shown as grey diamonds.
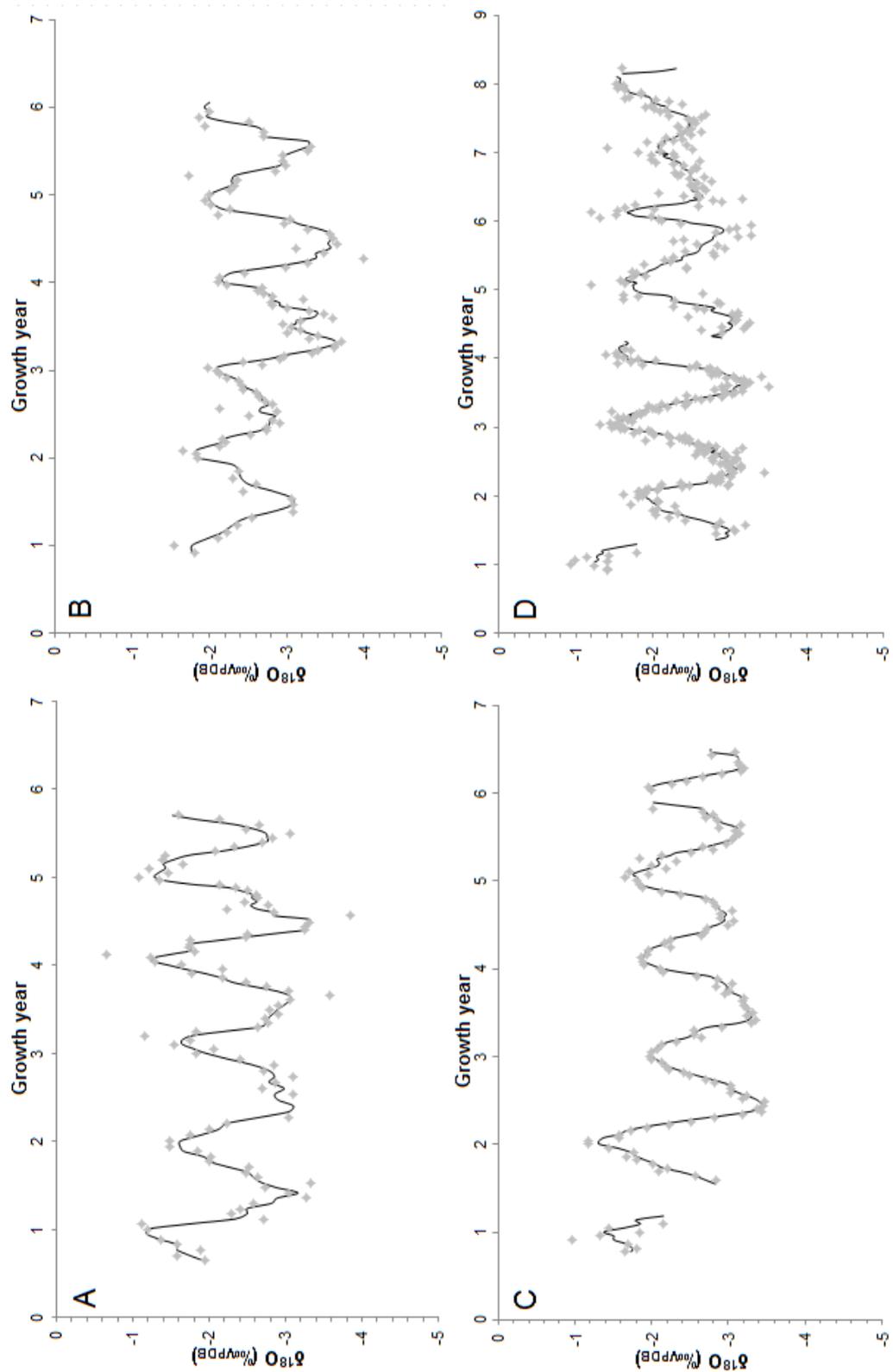
Figure 4.3.2 MIS 5e *C. caespitosa* oxygen isotopic profiles smoothed (using 4-point running median) and adjusted to growth years, unsmoothed data shown as grey diamonds. A: JEA 010626-04; B: SHR 04/11/11-10; C: SHR 02/11/11-08 (I); D: SHR 02/11/11-08 (II), note that this sample has a different y-axis scale and has been smoothed using an 8-point running median due to being sampled at twice the resolution of the others (see Section 3.3.5).
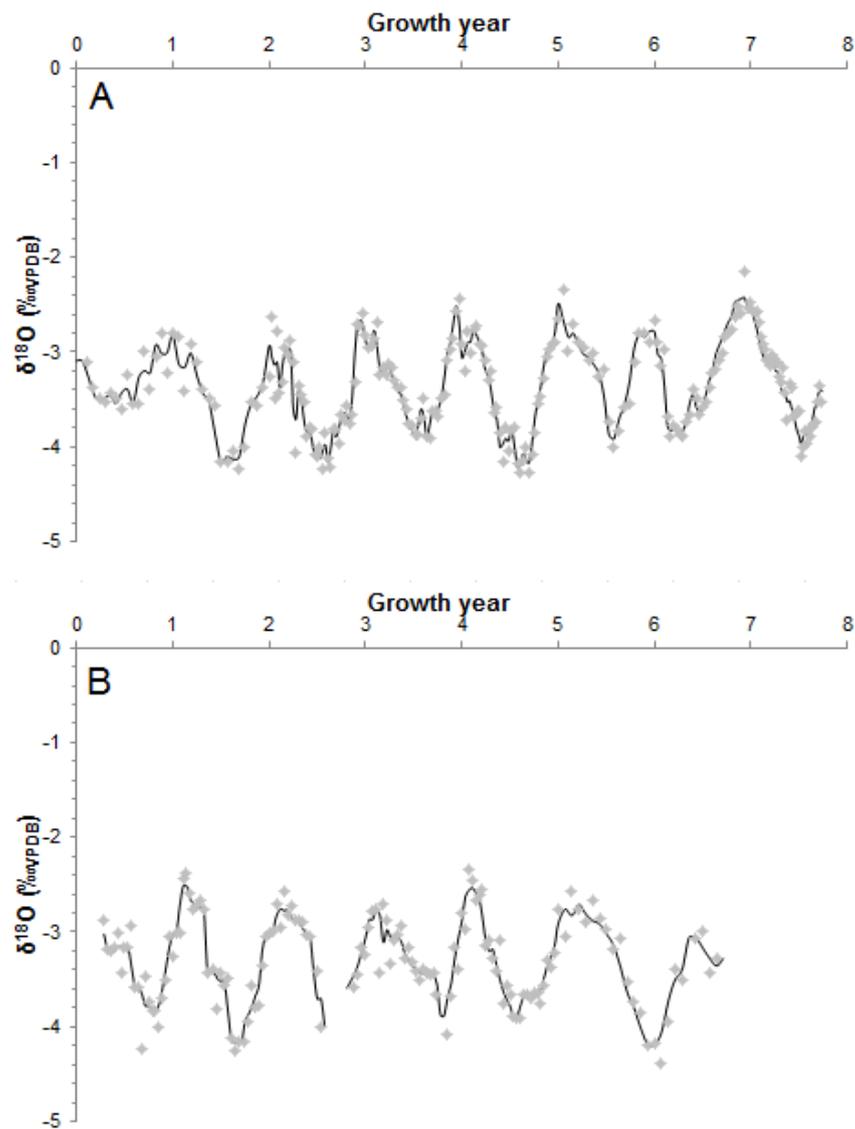
Figure 4.3.3 MIS 7a *C. caespitosa* **oxygen isotopic profiles, smoothed (using 4-point running median) and adjusted to growth years, unsmoothed data shown as grey diamonds. A: SHR 02/11/11-02 (I); (B) SHR 02/11/11-02 (II).**

Table 4.3.2 Summary of isotopic data from all Greek fossil *C. caespitosa* samples, values are expressed in ‰ VPDB.

Sample	Average δ^{18}O (‰)	No. of δ^{18}O annual cycles	Average δ^{18}O peak (‰)	Average δ^{18}O trough (‰)	Average δ^{18}O amplitude (‰)
Holocene					
SHR 03/11/11-02	−2.0	9.5	−1.4 (2σ = 0.6)	−2.7 (2σ = 0.4)	1.3 (2σ = 0.5)
MIS 5e					
JEA 010626-04	−2.2	5.0	−1.4 (2σ = 0.4)	−3.1 (2σ = 0.4)	1.7 (2σ = 0.6)
SHR 04/11/11-10	−2.7	5.5	−2.0 (2σ = 0.3)	−3.3 (2σ = 0.7)	1.3 (2σ = 0.4)
SHR 02/11/11-08(I)	−2.5	6.0	−1.7 (2σ = 0.4)	−3.2 (2σ = 0.4)	1.4 (2σ = 0.8)
SHR 02/11/11-08(II)	−2.4	7.5	−1.5 (2σ = 0.5)	−3.0 (2σ = 0.5)	1.5 (2σ = 0.9)
MIS 5e Average	−2.5 (2σ = 0.4)	N/A	−1.65 (2σ = 0.5)	−3.2 (2σ = 0.3)	1.5 (2σ = 0.3)
MIS 7a					
SHR 02/11/11-02(I)	−3.4	7.5	−2.7 (2σ = 0.4)	−4.1 (2σ = 0.5)	1.4 (2σ = 0.5)
SHR 02/11/11-02(II)	−3.3	6.5	−2.7 (2σ = 0.4)	−4.0 (2σ = 0.3)	1.4 (2σ = 0.5)
MIS 7a Average	−3.4 (2σ = 0.1)	N/A	−2.7 (2σ = 0)	−4.1 (2σ = 0.1)	1.4 (2σ = 0)

4.4. Fossil Greek samples – Discussion

4.4.1. Application of developed *C. caespitosa* $\delta^{18}O$ carbonate-water palaeothermometer to data

As there is a clear cyclicity to the $\delta^{18}O$ data for each profile and the average values for all samples are close to those of the modern samples (−2.5 +0.5/−0.9‰) it can be inferred that an unaltered, or nearly unaltered, isotope signal has been preserved in each sample.

It should thus be possible to calculate water palaeotemperature data for the period each corallite grew by applying the newly calibrated palaeotemperature equation (Equation 4.2.8) to the measured aragonite $\delta^{18}O$. To do this, an assumption about the seawater isotopic composition is required.

4.4.1.1. Water $\delta^{18}O$ value

A water $\delta^{18}O$ value of +1.15‰ VSMOW was used as a first estimation for palaeotemperature calculation. This was based on isotope analysis of a sea water sample (JT 11/02/12-01) collected from Agrillou Bay (38° 00' 09.4"N; 022° 55' 51.0"E), which gave a value of +1.2‰ VSMOW, a measurement of +1.15‰ VSMOW from nearby Cape Heraion by Portman et al. (2005) and other isotopic data for the Gulf of Corinth from the literature (Stahl and Rinow, 1973; Gat et al., 1996; Pierre, 1999). This value was assumed to be an appropriate first approximation for all interglacial periods, although this is clearly a potential source of substantial error.

4.4.1.2. Modern temperatures

Modern average monthly temperatures for the Gulf of Corinth on the coast of the Perachora Peninsula at 10-28 m depth, which covers most of the range of depths *C. caespitosa* inhabits in the present (Rodolfo-Metalpa et al., 2008), are shown in Figure 4.4.1. This data was collected and provided by Yiannis Ligkos of the Crostaceo Dive Centre and Watersports Club, Loutraki.

Water temperature ranges from 16°C in March to 24°C in September with a 19.5°C annual average.
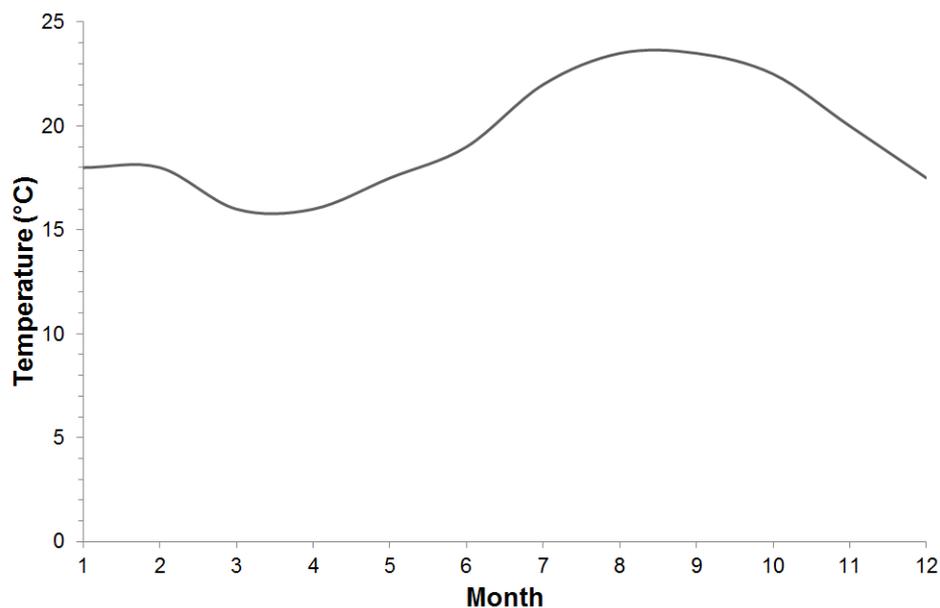
Figure 4.4.1 Modern Gulf of Corinth average monthly water temperature data at 10-28m

4.4.1.3. Fossil sample results and interglacial palaeoclimate

Rather than discuss the samples and the palaeoclimatic interpretation of the data in chronological order, the discussion is started with the MIS 5e records because this interglacial highstand has an extensive literature on inferred climatic conditions. This context is used (1) to help constrain the necessary

assumptions about MIS 5e seawater $\delta^{18}O$ and (2) to give context to the data collected from other interglacials where supporting evidence is less complete.

4.4.1.4. Marine Isotope Stage 5e

Marine isotope stage 5e lasted for approximately 13,000 years from 115-128ka (Thompson and Goldstein, 2005) and the range of dates found for the deposits at the Makrugoaz Ridge sampling site, 108.5-133.4ka (Leeder et al., 2003), are consistent with this. However, the short, 6-8 years, time period covered by each of the four samples means it is very unlikely that the growth periods recorded by individual MIS 5e samples overlap each other. Therefore, together, the samples should provide average values for a longer, approximately 23 year, period. The calculated water temperatures for each sample, using Equation 4.2.8 and assuming $\delta^{18}O_{water}$ = +1.15‰, are shown in Figure 4.4.2 and summarised in Table 4.4.1.
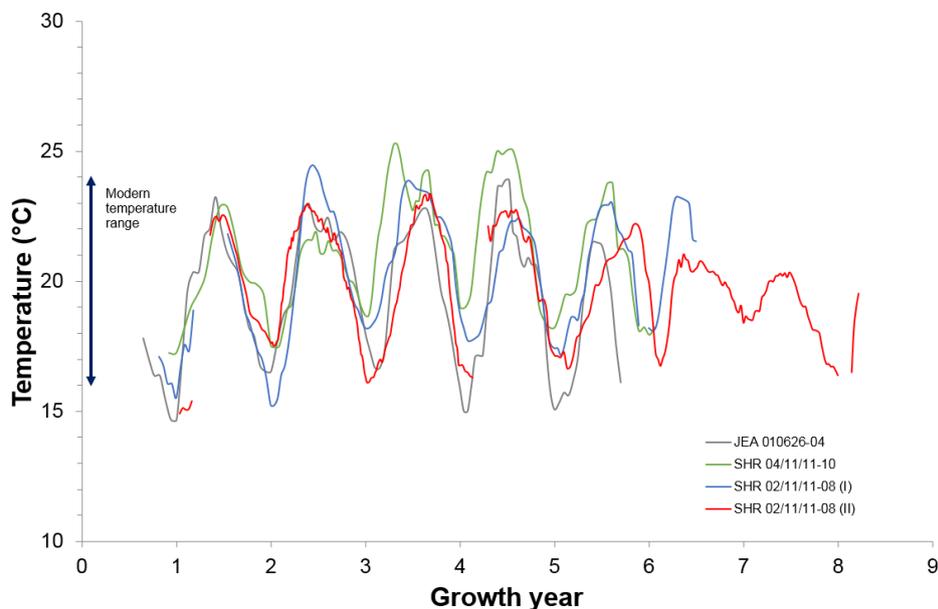
Figure 4.4.2 Overlaid MIS 5e *C. caespitosa* sample calculated water temperatures, using Equation 4.2.8 and assuming $\delta^{18}O_{water}$ = 1.15‰

Table 4.4.1 Summary of calculated temperature data from Greek MIS 5e *C. caespitosa* samples using Equation 4.2.8 and assuming $\delta^{18}O_{water}$ = +1.15‰ VSMOW, values are expressed in °C.

MIS 5e Sample	Average temperature	Average winter minimum	Average summer maximum	Average annual range
JEA 010626-04	19.3	15.6°C (2σ =1.9°C)	22.9°C (2σ =1.8°C)	7.3°C (2σ =2.7°C)
SHR 04/11/11-10	21.2	18.1 (2σ = 1.4)	23.8 (2σ = 2.9)	5.6 (2σ = 1.6)
SHR 02/11/11-08(I)	20.2	17.0 (2σ = 2.6)	23.4 (2σ = 1.6)	6.1 (2σ = 3.6)
SHR 02/11/11-08(II)	19.7	16.2 (2σ = 2.2)	22.5 (2σ = 2.0)	6.3 (2σ = 3.8)

It can be seen that the temperature data from all samples are in good agreement. Averaging the data from the 4 samples: Average temperature is 20.1°C (2σ = 1.6°C), average minimum 16.7°C (2σ =2.2°C), average maximum 23.2°C (2σ =1.1°C), average annual range 6.3°C (2σ =1.4°C).

These temperatures suggest that during MIS 5e water temperatures in the Gulf of Corinth were slightly warmer than they are today, albeit with slightly cooler summers; the average temperature is higher (close to that of the modern temperature at the reef in Mljet) while winters were much milder. This decreased seasonality, with warmer winters and cooler summers, potentially allowed the corals to grow all year round. This created more optimum growing conditions for *C. caespitosa* than are present in the Gulf of Corinth at the present day. This is supported by the extensive, hundreds of metres long and metres thick, *C. caespitosa* dominated biostromes that are a feature of MIS 5e terraces but are absent in the present.

However, other studies have suggested that the climate of the Mediterranean during MIS 5e was significantly warmer than this. The Senegalese fauna

characteristic of MIS 5e deposits throughout the Mediterranean (including around the Gulf of Corinth) are an indicator of warmer than present marine surface waters (Zaso et al., 1993; Bardaji et al., 2009). This fauna is characterised by the presence of the gastropod *Strombus bubonius* which is restricted to equatorial Africa under current climatic conditions. From its present distribution this fauna is known to require a mean annual sea surface temperature (SST) of ≈23-24°C which rarely drops below 19°C in the winter (Bardaji et al., 2009). Other molluscan assemblages independently back this up, suggesting that around Greece winter temperatures were ≈5(±1)°C warmer then present and seasonality was much lower, exhibiting an annual temperature range of ≈6-7°C (Garilli, 2011).

There is a large body of evidence for the first 3-4,000 years (Cheddadi et al., 2005) of the last interglacial being significantly wetter than the Holocene across the Mediterranean region. Molluscan faunal assemblages indicative of reduced salinity, isotopic data from foraminifera and sediment cores suggest that the surface waters of the Mediterranean were significantly diluted with $\delta^{18}O$ values reduced by up to 1.6‰ with respect to modern. This is believed to have been caused by increased precipitation and surface run off (Grazzini et al., 1986; Kallel et al., 2000; Pérez-Folgado et al., 2004; Garilli, 2011). Analysis of water samples collected in February 2013 (by J. Turner, and run alongside the Mljet water samples) showed that modern rainfall over Loutraki has a $\delta^{18}O$ of −2.5‰ and after heavy rain the surface sea water near sources of discharge can be as low as −2.7‰, showing that rainfall can have a significant effect on the composition of the surface waters (at least in the short term). If our *C. caespitosa* had lived in this early part of MIS 5e we can infer that surface water

δ^{18}O would have been lower than modern, which would have the overall effect of lowering our calculated temperatures. Evidence for increased runoff and pluvial conditions at the MIS 5e sample sites pre-date the coral bearing sediment (Portman et al., 2005; Andrews et al., 2007) and the coralline U/Th ages of 108.5-133.4 ka at the Makrugoaz Ridge MIS 5e sample site (Leeder et al., 2003), span the whole of MIS 5e (128 -115 ka; Thompson & Goldstein, 2005). It is thus likely the corals grew later in the interglacial when climatic conditions were more stable, warmer than today, and drier (Cheddadi et al., 2005).

The interpretation that these corals grew during a warmer and drier period (relative to today) is supported by the presence of marine phreatic aragonite cements found within the MIS 5e coral-bearing deposits of the Perachora Peninsula (J. Andrews pers. comm.). The best preserved of these aragonites gave U/Th dates between 113.8±1.6 to 118.0±1.6 ka (Andrews et al., 2007) supporting the younger coral dates. Widespread marine abiotic aragonite cementation does not occur in the Gulf today and with evidence for it restricted to MIS 5e in the study area it suggests conditions for its formation were specialised (J. Andrews pers. comm.). Aragonite marine cementation is promoted by warm SST's and higher supersaturation with respect to $CaCO_3$ (Burton and Walter, 1987), a condition favoured by slight increase in salinity, which requires reduced surface water runoff and thus aridity. Aridity would be consistent with a more positive seawater δ^{18}O compared to modern: although we cannot constrain the magnitude of enrichment, it would increase the calculated temperatures. The sea level in the Gulf of Corinth was approximately 6m higher than modern during the highstand of MIS 5e (Leeder et al., 2005).

This would have enhanced the connection between the GOC and more open Mediterranean marine waters, this should have decreased the $\delta^{18}O$ of the GOC's seawater. However, the GOC would still be a significantly restricted basin due to the narrowness and shallowness of the Rion Straights, currently 2km wide and 65m deep (Poulos et al., 1996), which link the GOC to the Patraikos Gulf and the more open Ionion Sea of the Mediterranean. However, modern $\delta^{18}O$ of the open Mediterranean surface waters are already enriched due to evaporation and range from +0.76 to +1.66 ‰ (Pierre, 1999), so that the GOC is a restricted basin within a restricted basin. Increased aridity across the Mediterranean would therefore be likely have more effect on increasing the $\delta^{18}O$ of the GOC's seawater than an increase in sea level would on decreasing it. The modern seawater $\delta^{18}O$ value of +1.15‰ $_{VSMOW}$ can thus be viewed as a minimum value. Moreover, *C. caespitosa* cannot survive in an environment where temperature regularly exceeds 28°C for extended periods (providing an absolute maximum for recorded summer temperatures), and taking into account the Senegalese fauna's requirements of a mean annual SST of ≈23-24°C; it is possible to constrain a likely range of values for water $\delta^{18}O$ and therefore also temperature (Table 4.4.2).

Table 4.4.2 Possible range of MIS 5e Gulf of Corinth seawater $\delta^{18}O$ values and calculated temperatures

Calculated temperatures (°C)	Average $\delta^{18}O$ aragonite (‰VPDB)	Estimated $\delta^{18}O$ water (‰VSMOW)				
		+1.15 (modern)	+1.6	+1.8	+2.0	+2.2
Average mean	−2.45	20.2	22.1	22.9	23.9	24.7
Average winter minima	−1.65	16.7	18.6	19.5	20.4	21.3
Average summer maxima	−3.15	23.2	25.2	26.0	26.9	27.8
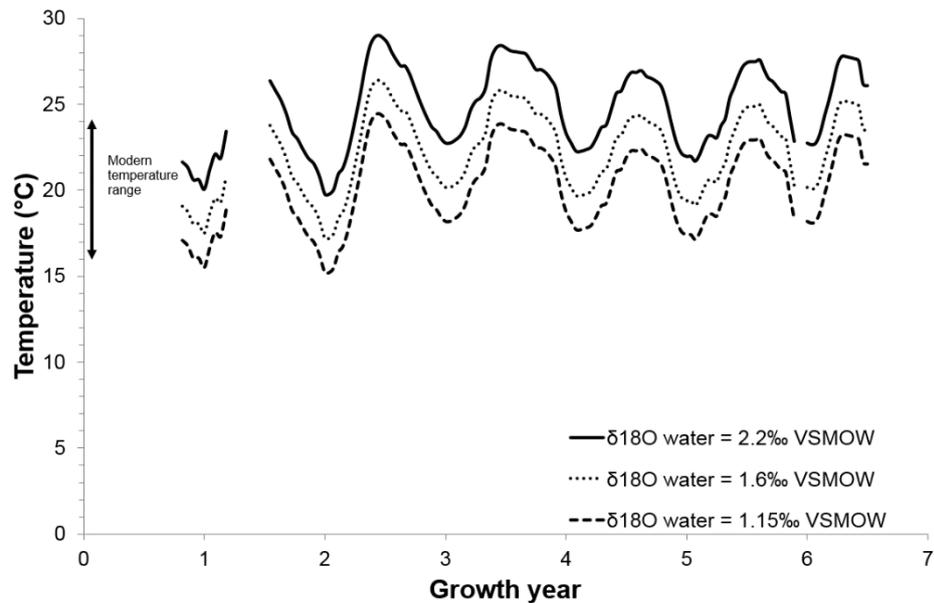
Figure 4.4.3 Range of temperatures calculated from *C. caespitosa* sample SHR 02/11/11-08 (I) using Equation 4.2.8 and the full range of possible seawater $\delta^{18}O$ values for MIS 5e Gulf of Corinth based on all available information. Likely temperature range for MIS 5e is bound by the 1.6‰ and 1.8‰ temperature profiles, the temperatures calculated using the modern 1.15‰ seawater value are included for ease of comparison.

Figure 4.4.3 shows the temperatures calculated, using the $\delta^{18}O$ aragonite data from sample SHR 02/11/10-08 (I), by applying this range of potential seawater $\delta^{18}O$ values. This sample was selected for this as it is has the closest average values to the mean of the 4 analysed samples.

This shows that, taking all the available evidence into account, the Gulf of Corinth seawater in MIS 5e, during the period of corallite growth studied, probably had a $\delta^{18}O$ value between 1.6-2.2‰VSMOW, an average annual water temperature of 22.1-24.7°C, average winter minima of 18.6-21.3°C and an average summer maxima of 26.0-27.8°C. This still suggests a significantly reduced seasonality during MIS 5e and this, combined with the increased temperature, could explain the large banks of *C. caespitosa* present at this time, as the coral would be capable of growing all year round.

4.4.1.5. Marine Isotope Stage 1

Sample SHR 03/11/11-02 came from red algal and coral reef deposits, U-Th dated to between 6-10 ka. The studied *C. caespitosa* was collected from the same height (±1m) as corals dated to 7.5-7.9 ka (Stiros and Pirazzoli, 1998).
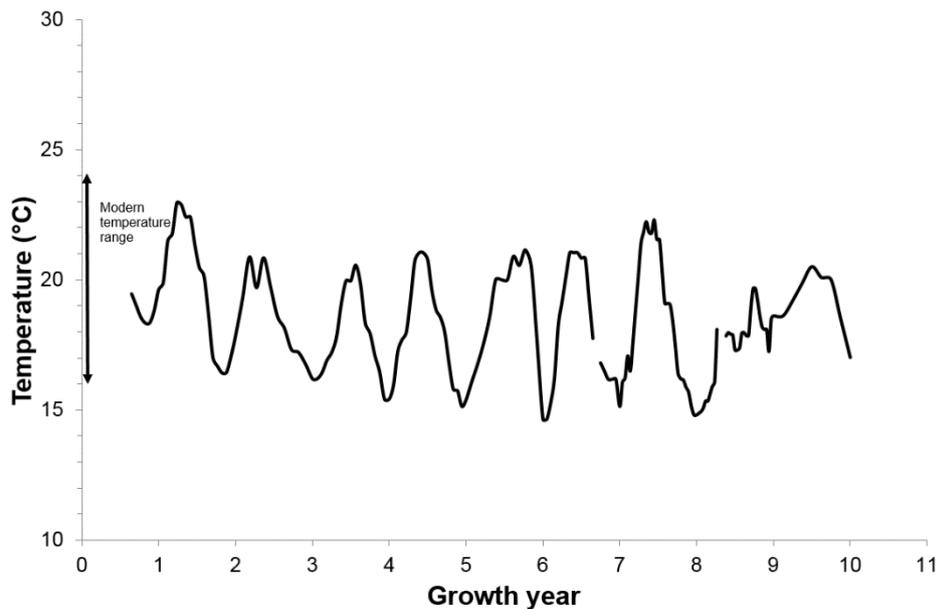
Figure 4.4.4 Holocene *C. caespitosa* sample SHR 03/11/11-02 calculated water temperatures using Equation 4.2.8, and assuming $\delta^{18}O_{water}$ = +1.15‰. Average temperature for MIS 1 *C. caespitosa* sample SHR 03/11/11-02 is 18.3°C, average minimum 15.7°C (2σ = 2.4°C), average maximum 21.4°C (2σ = 1.7°C), average annual range 5.5°C (2σ =2.2°C).

The calculated temperatures in Figure 4.4.4, taken at face value, suggest that Gulf of Corinth seawater in the early-mid Holocene was somewhat cooler than today. The calculated average summer maxima temperatures are around 2.5°C cooler than the maximum average summer temperature that *C. caespitosa* can tolerate without being put under stress and therefore become less able to accurately record temperatures. This suggests that the maxima of the temperature record are not truncated and that summers were significantly

cooler than they are today. However, the average minimum has to be taken as an upper limit to the average winter value as it is in the range of the minimum values that this species can calcify under. Therefore it cannot be stated with confidence that the range of annual temperatures was lower at this time, although this does appear likely, just that they were shifted lower with the minima record truncated.

Using the modern water isotope value appears, as a first approximation, to be justifiable as this coral grew during the same interglacial as the present. However, there is a large body of evidence to suggest that the first half of the Holocene was significantly wetter than the latter part, with a general evolution from wetter to drier conditions throughout this period across the whole of the Mediterranean (Magny et al., 2002). The wettest and coolest period appears to have been between 9000-6500 cal yr BP, corresponding with widespread human settlement and increased lacustrine facies deposition in North Africa (Petit-Maire, 1991), high lake levels in Sicily (Sadori and Narcisi, 2001), wetter conditions in Albania, Israel and Italy (Denèfle et al., 2000; Frumkin et al., 1991; Zanchetta et al., 2007) and the deposition of sapropel 1 which is indicative of increased discharge of freshwater into the Mediterranean due to increased rainfall (Ariztegui et al., 2000; Zanchetta et al., 2007). This cool and wet period encompasses the period these corals are believed to have grown, an increased volume of rainfall and freshwater input into the Gulf of Corinth would reduce the seawater's salinity and therefore lower its $\delta^{18}O$ value, with respect to the modern composition. The sea level of the Gulf of Corinth was approximately 9.5-7.74 m lower than modern during the period of coral growth (Kershaw et al., 2005) so it would still, most likely, be a somewhat restricted basin with a more

enriched isotopic signature than the open ocean. This, along with the limited range of temperatures *C. caespitosa* can tolerate, allows some constraints to be placed on the $\delta^{18}O$ seawater value and the calculated temperatures (Table 4.4.3 and Figure 4.4.5).

Table 4.4.3 Possible range of Early-Mid Holocene Gulf of Corinth seawater $\delta^{18}O$ values and calculated temperatures

Calculated temperatures (°C)	Average $\delta^{18}O$ aragonite (‰ VPDB)	Estimated $\delta^{18}O$ water (‰ VSMOW)				
		+1.15 (modern)	+1.0	+0.9	+0.8	+0.75
Average mean	−2.0	18.3	17.6	17.2	16.8	16.6
Average winter minima	−1.4	15.7	15.1	14.7	14.2	14.0
Average summer maxima	−2.7	21.4	20.7	20.3	19.9	19.7
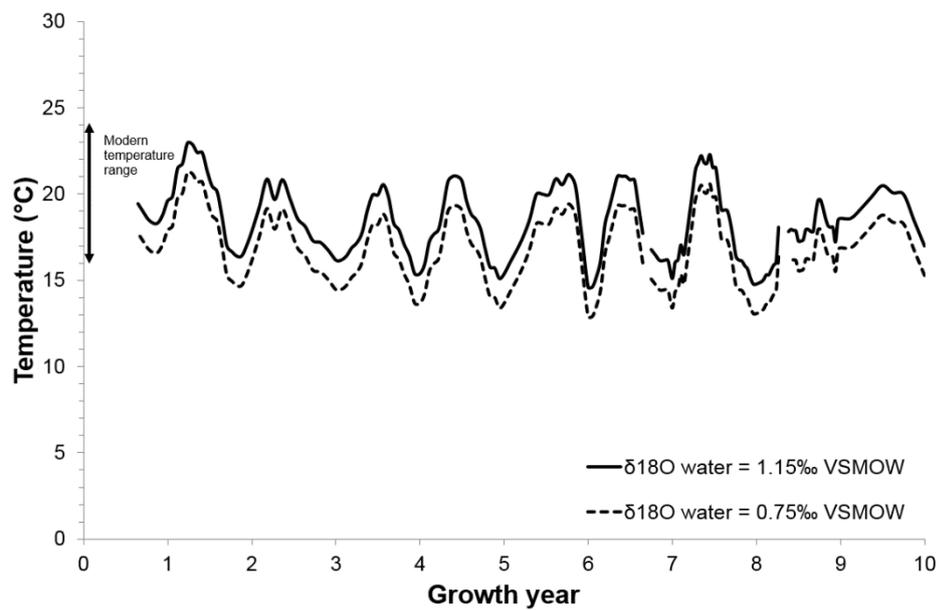
Figure 4.4.5 Range of temperatures calculated from *C. caespitosa* sample SHR 03/11/11-02 using Equation 4.2.8 and the full range of possible seawater $\delta^{18}O$ values for Mid-Early Holocene Gulf of Corinth based on all available information. Likely temperature range for this period is bound by the +0.75‰ and +1.15‰ (modern water value) temperature profiles.

This analysis shows that, taking all the available evidence into account, the Gulf of Corinth seawater between 7.9-7.5ka, during the period of corallite growth, probably had a $\delta^{18}O$ value of +0.75 to +1.15‰ VSMOW, an average recorded water temperature of 16.6-18.3°C, an average recorded summer maxima of 19.7-21.4°C and an average recorded winter temperature of 14.0-15.7°C. As this is in the minimum temperature range this species can record this is most likely a truncated winter record and the winter temperatures were lower than this. Because of this constraint we cannot be confident that this period had a reduced range of temperature; *C. caespitosa* can survive (but not calcify) at winter water temperatures down to at least 6°C (Kružić and Požar-Domac, 2003). However, it does seem likely that both winter and summer temperatures were reduced lower than those today. Average summer temperatures were 2.6-4.3°C cooler while average annual temperatures and winter temperatures were at least 1.2-4.3°C cooler. These findings are in line with the work of Cheddadi et al. (1996) which has shown that the Mediterranean's climate was 2-4°C cooler during around this period based on pollen assemblages.

4.4.1.6. Marine Isotope Stage 7a

Samples SHR 02/11/11-02 (I) and SHR 02/11/11-02 (II) both come from a deposit which U-Th dating ages to 186-195ka, placing them (within error) of MIS 7a (Leeder et al., 2005). Between them, the corals span and provide average data for a period of 14 years. It is, again, unlikely that these 2 samples overlap each other in time. The calculated water temperatures for each sample, using Equation 4.2.8 and assuming $\delta^{18}O_{water}$ = +1.15‰, are shown in Figure 4.4.6 and summarised in Table 4.4.4.
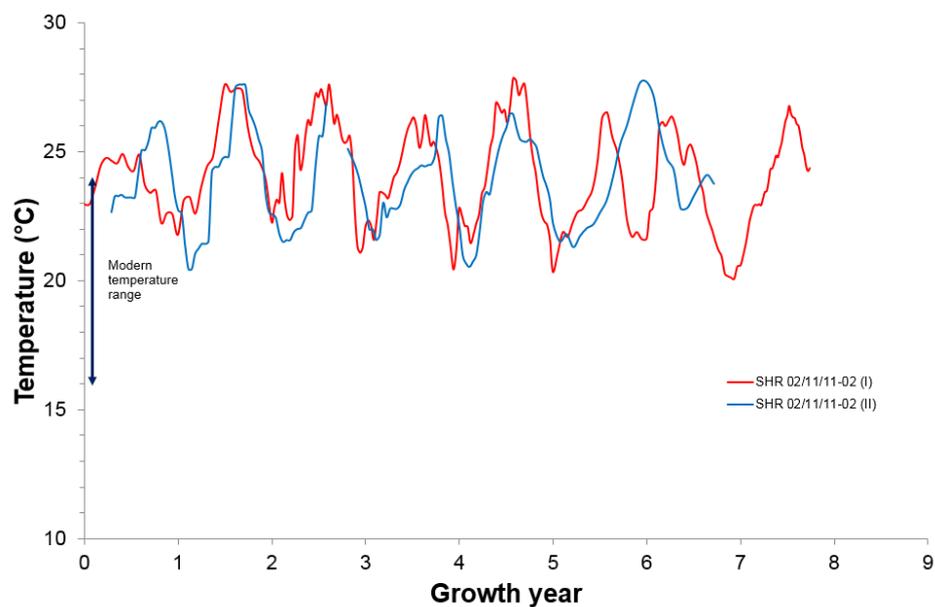
Figure 4.4.6 Overlain MIS 7a *C. cae*spitosa calculated water temperatures, using Equation 4.2.8 and assuming $\delta^{18}O_{water}$ = 1.15‰

Table 4.4.4 Summary of calculated temperature data from Greek MIS 7a-c *C. caespitosa* samples using Equation 4.2.8 and assuming $\delta^{18}O_{water}$ = 1.15‰$_{vsmow,}$ values are expressed in °C.

MIS 7a-c Sample	Average temperature	Average winter minimum	Average summer maximum	Average annual range
SHR 02/11/11-02(I)	24.1	21.8 (2σ = 1.7)	27.3 (2σ = 2.3)	6.2 (2σ = 2.0)
SHR 02/11/11-02(II)	23.9	21.4 (2σ = 1.7)	26.9 (2σ = 1.5)	6.1 (2σ = 2.0)

Temperature data from the two samples are in good agreement; averaging the data from the 2 samples: Average temperature is 24.0°C (2σ = 0.3°C), average minimum 21.2°C (2σ =1.7°C), average maximum 27.1°C (2σ =2.0°C), average annual range 6.2°C (2σ =1.9°C). This is similar to the tropical temperatures experienced by corals on the Great Barrier Reef (Alibert and McCulloch, 1997; Alibert et al., 2003) and it is unlikely that this is a true representation of the water conditions during this period. Even if *C. caespitosa* was better adapted for warmer conditions during previous interglacials and could survive these conditions, no other studies have suggested a tropical climate this far north at this time. Most studies suggest that during this period the Mediterranean was both cooler (Shackleton, 2000; Coope, 2001; Kawamura et al., 2003; Martrat et al., 2004; Cheddadi et al., 2005; Kawamura et al., 2007; Coope, 2010) and wetter (Cheddadi et al., 2005; Roucoux et al., 2008) than either MIS 5e or the present, with lower salinity surface waters due to extensive freshwater input (Thunell and Williams, 1983; Fontugne and Calvert, 1992; Bar-Matthews et al., 2003).

Because of the increased freshwater input, it is possible that the Gulf of Corinth seawater was significantly more depleted in $\delta^{18}O$ than today. Sea level during

the highstands of MIS 7 is believed to have been similar to modern (Leeder et al., 2005), therefore it is also likely that the Gulf of Corinth would still have been a restricted basin and so still have had a δ^{18}O value more enriched than the open ocean, or only slightly depleted. This allows loose constraints to be placed on the δ^{18}O value and the temperature of the seawater at the time (Table 4.4.5 and Figure 4.4.7).

Table 4.4.5 Possible range of MIS 7a Gulf of Corinth seawater δ^{18}O values and calculated temperatures

Calculated temperatures (°C)	Average δ^{18}O aragonite (‰ VPDB)	Estimated δ^{18}O water (‰ VSMOW)				
		1.15	0.3	0.2	0	−0.2
Average mean	−3.4	24.1	20.4	19.9	19.1	18.2
Average winter minima	−2.7	21.3	17.6	17.1	16.3	15.4
Average summer maxima	−4.1	27.1	23.4	23.0	22.1	21.3

As can be seen in Table 4.4.5, with the recorded aragonite δ^{18}O values, the Gulf of Corinth seawater would have to have been significantly depleted in δ^{18}O for calculated temperatures to be lower than the modern; this must suggest that this was a very wet period relative to modern or any of the other periods studied. A depleted δ^{18}O value of +0.3 to −0.2‰VSMOW, gives an average water temperature of 18.2-20.4°C, average winter minima of 15.4-17.6°C and an average summer maxima of 21.3-23.4°C. This all suggests that it was actually the summer temperatures that were the most affected by cooling during this period, while the winters (and average temperatures) were milder than present, significantly reducing the annual temperature range. The only way to produce significantly cooler winter and average temperatures from this data would be to make δ^{18}O water even more negative than the lowest estimate, which seems unlikely given the restricted nature of the Gulf of Corinth.
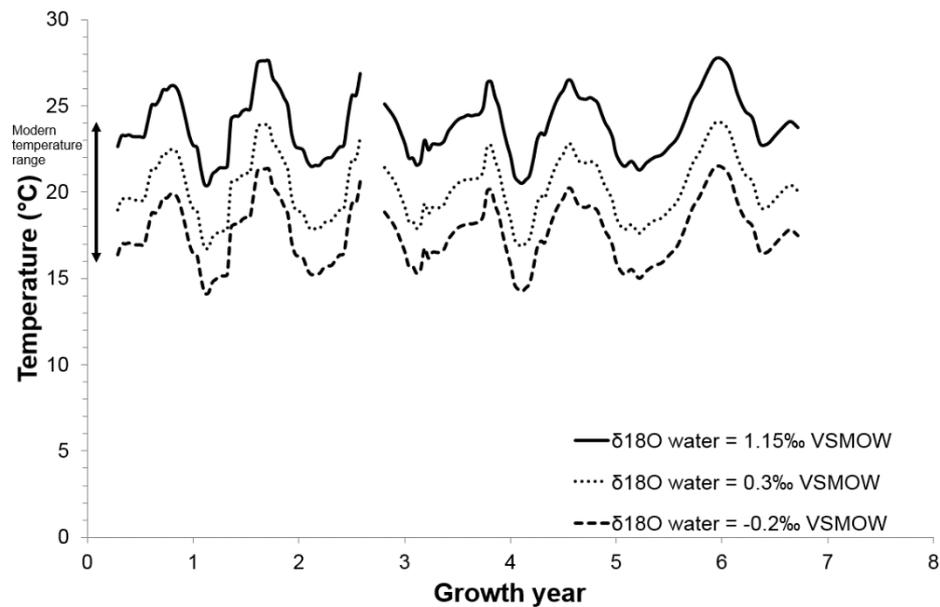
Figure 4.4.7 Range of temperatures calculated from *C. caespitosa* sample SHR 02/11/11-02 (II) using Equation 4.2.8 and the full range of possible seawater $\delta^{18}O$ values for MIS 7a Gulf of Corinth based on all available information. Likely temperature range for MIS 7c is bound by the −0.2‰ and 0.3‰ temperature profiles, the temperatures calculated using the modern 1.15‰ seawater value are included for ease of comparison.

However, due to the age of the samples, it is possible that the depleted aragonite $\delta^{18}O$ values have come about due to diagenetic alteration. Recrystalisation and the growth of secondary cements from meteoric waters would shift the aragonite $\delta^{18}O$ to lower values, due to the more negative water $\delta^{18}O$ value of the rainfall and resulting groundwaters percolating through the corals. However, while evidence of secondary cements and recrystalisation were observed (under SEM) in the highly porous septal regions of these MIS 7 corals, the analysed (low porosity) corallite walls were seen to be alteration free. This coupled with the preservation of very clear annual scale cyclicity in the aragonite $\delta^{18}O$ signals (and well preserved cyclicity in trace elemental signals, which seems to be more susceptible to alteration than $\delta^{18}O$, discussed later) suggests that diagenetic alteration is, however, not the cause of this isotopic shift and so this is an original palaeoclimate signal.

4.4.2.   Summary of inferred palaeotemperatures

Aside from the MIS 7 temperatures, all of the palaeotemperatures calculated using Equation 4.2.8 and using the modern $\delta^{18}O_{water}$ value of 1.15‰$_{vsmow}$ appeared, at face value, to be within a realistic range. However, once they are studied in depth, and other evidence is taken into account, it was found that this was unlikely to be the case. Both the temperatures calculated from modern seawater $\delta^{18}O$ values and the estimated $\delta^{18}O$ values are summarised in Table 4.4.6, and Figure 4.4.8 for ease of comparison.

Table 4.4.6 Summary of temperatures calculated from the Greek *C. caespitosa* samples using Equation 4.2.8 and the modern water $\delta^{18}O$ value of +1.15‰, estimated $\delta^{18}O$ water values based on the literature and recalculated potential temperatures using the estimated water $\delta^{18}O$ values. *Modern measured temperature values included for ease of comparison

| Period | Age (ka) | $\delta^{18}O$ = modern | | | | Full new calculated temperature range | | | |
		Min.	Mean	Max.	Est. $\delta^{18}O$ range	Min.	Mean	Max.	Annual range
Modern*	0	16	19.5	24	+1.15	16	19.5	24	8
Early-Mid Holocene	7.5-7.9	15.7	18.3	21.4	+0.75-+1.15	14	17.45	21.4	5.7
MIS 5e	108.5-133.4	16.7	20.2	23.2	+1.6-+2.2	18.6	23.4	27.8	6.3
MIS 7a	186-196	21.2	24	27.1	−+0.2-+0.3	15.4	19.3	23.4	5.9
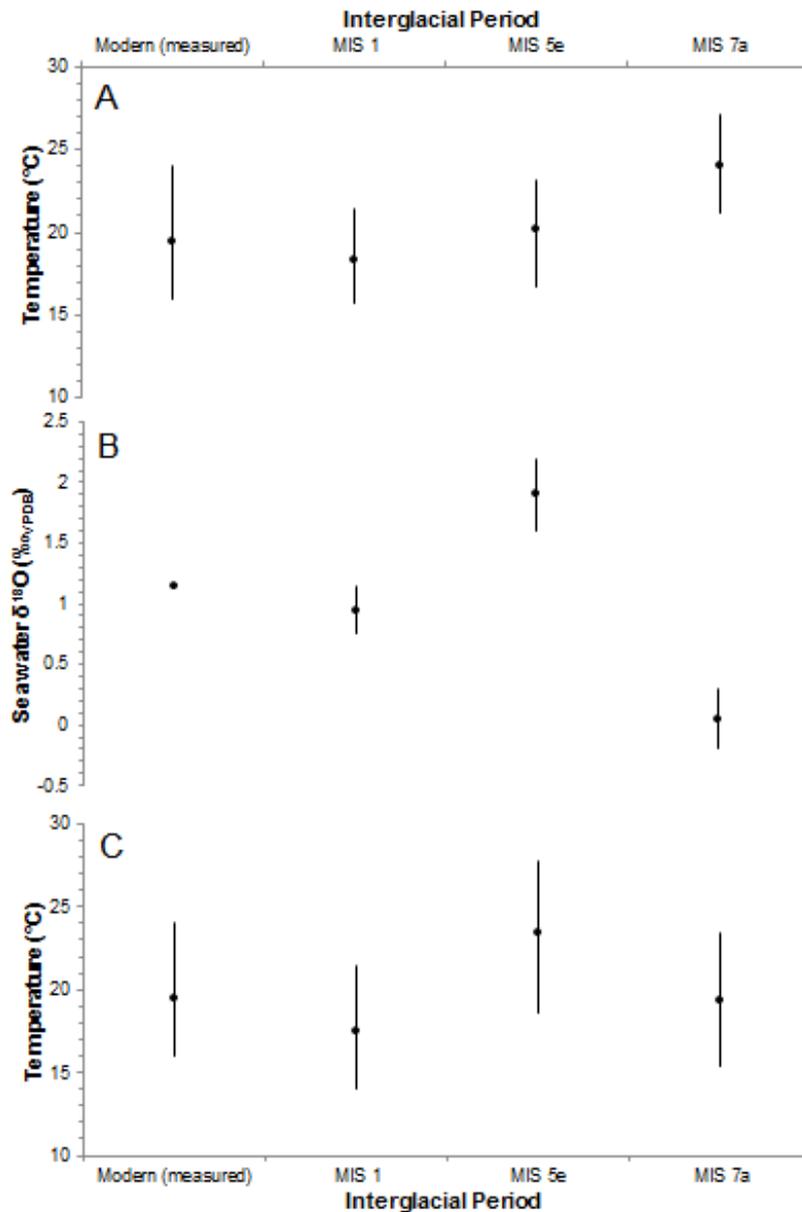
Figure 4.4.8 A: Summarised ranges of temperatures calculated for each period using the modern measured Gulf of Corinth δ^{18}O water value of +1.15‰. Modern measured range shown for ease of comparison; B: Summarised ranges of estimated Gulf of Corinth seawater δ^{18}O for each studied period based on the available literature on climatic conditions during each interglacial. Modern measured value shown for ease of comparison; C: Summarised ranges of annual temperatures calculated for each studied period using the relevant range of estimated Gulf of Corinth seawater δ^{18}O for each studied period based on the available literature on climatic conditions during each interglacial. Range indicates the maximum range of temperatures possible, not the annual range of seawater recorded, see Table 4.4.6. Modern measured range shown for ease of comparison.

By comparing the data on the summary diagrams, it can be seen that if only the

modern δ^{18}O water value was used for all interglacials (Figure 4.4.8a), it would

appear as though there had been a general cooling throughout the last few interglacials: as discussed above, based on the supporting literature, this is not believed to be the case. Figure 4.4.8b and Figure 4.4.8c show that based on the available information, the current conditions in the Gulf of Corinth are approximately average for the interglacial periods of the last 225ka. The warmest studied period of an interglacial was during MIS 5e, this also had the lowest seasonality and was (based on seawater $\delta^{18}O$ values) probably the most arid, The period of the Early-Mid Holocene analysed likely had the coolest conditions experienced by any of the analysed corals while (again based on seawater $\delta^{18}O$ values) it appears as though the analysed period of MIS 7a was the wettest period analysed with the most freshwater input into the Gulf.

However, for these temperatures to be completely reliable, so that real conclusions can be drawn from them, it is necessary to gain more reliable values for the water $\delta^{18}O$ values from each time period to decrease the (currently rather wide) margins of error. This is very important as the equation calculates that there is a 4.4°C increase in temperature per 1‰ enrichment of $\delta^{18}O_{water}$ putting a large potential for error in temperature calculation in any assumption about the $\delta^{18}O$ value of past interglacial Gulf of Corinth seawater.

It is necessary to use clumped isotopic analysis on inorganic carbonates and/or shell samples known to precipitate in equilibrium to find out the $\delta^{18}O_{water}$ applicable to each time period and this will be explored in Chapter 5.

5. Clumped isotopic analysis – Results and discussion

In this chapter I present and discuss data from the clumped isotopic analysis. Average growth temperatures and water $\delta^{18}O$ compositions calculated from modern Croatian *C. caespitosa* sample data are compared to the measured values from the sampling locality and are found to be significantly different. It is concluded that this species of coral calcifies its skeletal aragonite in isotopic disequilibrium with ambient seawater. Well preserved abiotic aragonite seafloor cements and calcite *Pecten* shells from MIS 5e deposits, that are presumed to have grown in equilibrium with the seawater, are found to give reasonable seawater temperatures for the last interglacial.

5.1. Modern *C. caespitosa* samples – clumped isotopic results

Homogenised powders of the modern Croatian *C. caespitosa* samples PK 21/09/12-01, PK 21/09/12-02, PK 21/09/12-02 (II), PK 21/09/12-05, PK 21/09/12-06 were analysed for Δ_{47}, Δ_{48}, Δ_{49}, $\delta^{18}O$ and $\delta^{13}C$ (notations explained in Section 2.4.1, 2.3.2). $\Delta_{47\ (URF)}$ is reported due to its theoretical (and observed) (Ghosh et al., 2006; Dennis et al., 2011; Eiler, 2011) relationship with temperature of carbonate precipitation. Δ_{48} and Δ_{49} are also reported because anomalously high deviations of these values can be used to identify samples contaminated by organic matter. Therefore, samples with anomalous Δ_{48} and Δ_{49} were rejected or viewed with suspicion. The results are shown in Table 5.1.1:

Table 5.1.1 Modern Croatian *C. caespitosa* clumped isotopic bulk sample analysis results, carbonate standards also shown for reference. 'Repeat' identifies a replicate analysis of the same homogenised sample powder. One run of sample PK 21/09/12-02 and is highlighted as positive Δ_{48} and >10 Δ_{49} values suggest contamination, these data are therefore left out when calculating average values for the samples. Full data set is reported in Appendix ii.

Sample	$\Delta_{47 \text{ (URF)}}$	Δ_{48}	Δ_{49}	$\delta^{18}O$	$\delta^{13}C$
PK-21/09/12-01	0.72	−0.26	−45.23	−2.65	−5.84
PK 21/09/12-01 (Repeat)	0.75	-0.28	-36.31	-2.47	-5.93
Average	**0.74** (2σ = 0.04)	**-0.27** (2σ = 0.03)	**-40.77** (2σ = 12.60)	**-2.56** (2σ = 0.26)	**-5.89** (2σ = 0.13)
PK 21/09/12-02	0.76	0.03	13.24	−2.35	−5.30
PK 21/09/12-02 (Repeat)	0.74	-0.08	-17.76	−2.25	−5.39
PK 21/09/12-02 (Repeat)	0.77	-0.23	-59.89	−2.27	−5.35
Average	**0.76** (2σ = 0.44)	**-0.16** (2σ = 0.21)	**-38.83** (2σ = 59.57)	**-2.26** (2σ = 0.03)	**-5.57** (2σ = 0.06)
PK 21/09/12-05	**0.72**	**−0.02**	**−11.89**	**−2.54**	**−5.83**
PK 21/09/12-06	0.72	-0.16	-31.30	-2.47	-6.01
PK 21/09/12-06 (Repeat)	0.69	−0.11	35.74	−2.58	−6.05
PK 21/09/12-06 (Repeat)	0.71	-0.42	-27.83	-2.21	-5.98
Average	**0.70** (2σ = 0.03)	**-0.23** (2σ = 0.33)	**7.80** (2σ = 75.49)	**-2.42** (2σ = 0.38)	**-6.01** (2σ = 0.07)
UEATHC	**0.63**	**-0.02**	**30.20**	**-13.97**	**2.70**
UEABEL	**0.67**	**-0.03**	**39.26**	**0.06**	**2.52**
UEACMST	0.43	-0.47	-19.34	-1.83	1.94
UEACMST (Repeat)	0.41	-0.06	-13.41	-1.80	1.95
UEACMST (Repeat)	0.42	-0.49	58.48	-1.81	1.95
Average	**0.42** (2σ = 0.48)	**-0.34** (2σ = 0.48)	**8.58** (2σ = 86.64)	**-1.81** (2σ = 0.03)	**1.95** (2σ = 0.01)

5.2. *C. caespitosa* samples - Analysis and discussion

5.2.1. Temperature

Temperature of precipitation is believed to be the dominant control on the Δ_{47} composition of all carbonates (Guo et al., 2009a). The majority of carbonates analysed conform to (laboratory specific) Δ_{47}-temperature calibration lines $T(\Delta_{47})$ whether they are biological, natural inorganic or synthetic precipitates (Ghosh et al., 2007; Eiler, 2011; Came et al., 2014). Because of this, it was hypothesised that the bulk analysis of homogenised modern *C. caespitosa* samples would have $T(\Delta_{47})$ values that represent the average water temperature throughout the growth period studied.

The Δ_{47} values appear very similar for all the uncontaminated modern samples (average = 0.73, 2σ = 0.05), although it must be remembered that the relationship between Δ_{47} and temperature is very sensitive; across the commonly used 0-50°C range, Δ_{47} only changes by ≈ 0.2 ‰ (Ghosh et al., 2006) with a temperature sensitivity of −0.00289‰/°C (Guo et al., 2009a). As these samples were run on the University of East Anglia's MIRA mass spectrometer, the in-house Δ_{47}-temperature calibration equation (Equation 5.2.1) was used to calculate temperatures. This calibration line is close to the theoretical one (of Guo et al. (2009a)), with a temperature sensitivity of −0.0034‰/°C.

$$\Delta_{47} = 0.0389 \cdot \frac{10^6}{T^2} + 0.2139$$

Equation 5.2.1 UEA Δ_{47} – temperature calibration line

The calculated $T(\Delta_{47})$ values are shown in Table 5.2.1 and plotted on the UEA

calibration line in Figure 5.2.1.

Table 5.2.1 Modern Croatian *C. caespitosa* average growth temperatures and water $\delta^{18}O$ compositions calculated using the UEA Δ_{47} – temperature calibration line compared to the actual average growth temperatures as recorded at the site (Kružić et al., 2012) and measured water compositions.

Sample	Δ_{47}	Calculated $T(\Delta_{47})$	Actual average temperature (°C)	Calculated water $\delta^{18}O$ (‰VSMOW)	Measured water $\delta^{18}O$ (‰VSMOW)
PK 21/09/12-01	0.73	1.12	20.3	−1.73	1.0
PK 21/09/12-02	0.76	−5.35	20.3	−3.52	1.2
PK 21/09/12-05	0.72	4.71	20.3	−0.92	1.2
PK 21/09/12-06	0.70	8.54	20.3	−0.16	1.2
Average	0.73 (2σ=0.05)	2.26 (2σ=11.72)	20.3	−1.58 (2σ=2.88)	1.15 (2σ=0.1)

It is clear that the $T(\Delta_{47})$ values are unrealistically low to have supported coral

growth. The average water temperature at this locality over the period 2003-

2010 (which covers the majority of the corallite growth analysed) was 20.3°C

(Kružić et al., 2012). It has also been demonstrated that at temperatures below

14-16°C *C. caespitosa* is unable to precipitate aragonite (Montagna et al.,

2007); meaning that temperatures below this cannot be recorded by this

species. These constraints mean the corals could not have grown at the derived

$T(\Delta_{47})$ values. This result was not totally unexpected given that this species of

coral does not calcify in isotopic equilibrium with seawater (Chapter 4).

According to Equation 5.2.1, carbonate precipitated in isotopic equilibrium at an

average temperature of 20.3°C should have a Δ_{47} value of 0.67‰. The

measured values of 0.70-0.76‰ show that the corals are enriched in Δ_{47} by 0.03-0.09‰.
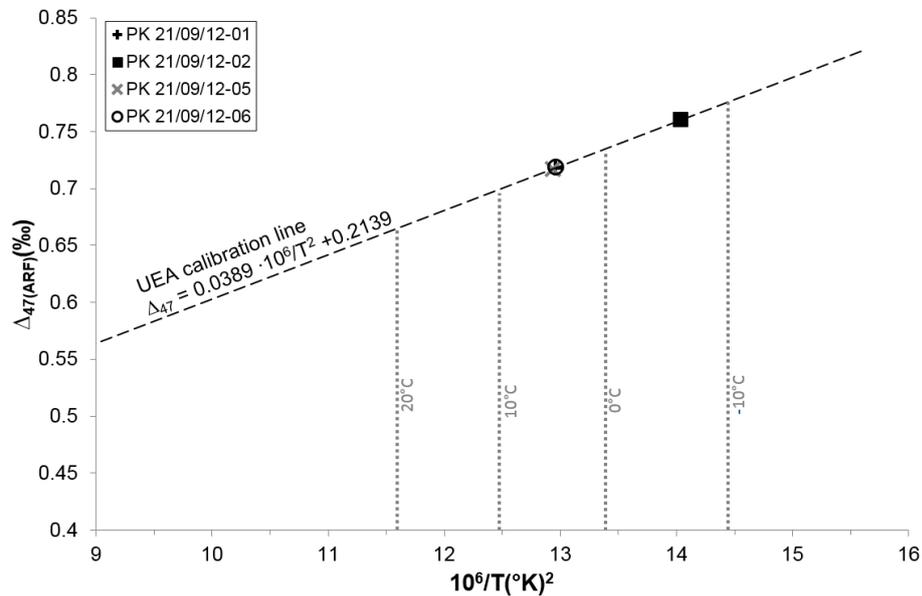
Figure 5.2.1 Modern Croatian *C. caespitosa* clumped isotopic data plotted on the UEA calibration line, x-axis temperatures are also shown in Celsius for ease of comparison.

5.2.2. Comparing the UEA calibration equation to equations derived in other laboratories

The UEA calibration line (black line in Figure 5.2.2) used in this study is closest to the intercept and gradient of the theoretical line of Guo et al. (2009a). Theoretically, there should only be the one relationship between temperature and Δ_{47}, that of Guo et al. (2009a), but in each laboratory there is an offset that probably depends on digestion temperature, preparation and measurement protocol. The equations for the lines of best fit for each laboratory data set at Earth surface temperatures, approximately 0-50°C, are shown in Table 5.2.2 with the lines plotted in Figure 5.2.2. The data discussed here was produced by measurements on MIRA, using the UEA laboratory protocol and calibrated

using the UEA 'line'; however, it is instructive to compare the C. caespitosa data

and the UEA calibration to those of other laboratories.

Table 5.2.2 Published Δ_{47} - temperature calibration equations for earth surface temperatures. Equations published before 2011 have been retrospectively fitted to the absolute reference frame and, where necessary, have been corrected for the difference in fractionation factors between 25 and 90°C by Dennis and Schrag (2011) whereas equations from after 2011 were already fitted to the reference frame and corrected by their respective authors. Also included within the table are the laboratories where the mass spectrometry was carried out, the temperature of phosphoric acid digestion and the $CaCO_3$ material studied for comparison.

Study	Lab	Subject	Reaction T (°C)	Δ_{47} =
UEA cal. line	UEA	Modern brachiopods and inorganic calcite	25	$0.0389\cdot10^6/T^2+0.2139$
Ghosh et al., (2006)	Caltech	Synthetic	25	$0.0636\cdot10^6/T^2-0.0047$
Guo et al., (2009a)	N/A	Theoretical	N/A	$0.0375\cdot10^6/T^2+0.210$
Dennis & Schrag (2010)	Harvard	Synthetic	90	$0.0362\cdot10^6/T^2+0.292$
Eagle et al. (2013)	Caltech	Molluscs	90	$0.0362\cdot10^6/T^2+0.314$
Henkes et al., (2013)	John Hopkins	Molluscs & brachiopods	90	$0.0327\cdot10^6/T^2+0.3286$
Zaarur et al., (2013)	Yale	Synthetic	25	$0.0555\cdot10^6/T^2+0.0780$
Came et al., (2014)	Yale & Caltech	Brachiopods	25	$0.0506\cdot10^6/T^2+0.1453$
Tang et al., (2014)	Tulane & UCLA	Synthetic	25 & 90	$0.0387\cdot10^6/T^2+0.2532$

If the *C. caespitosa* Δ_{47} data is plotted against the known average growth

temperature for these samples, Figure 5.2.2, it is clear the data plot well above

both the UEA and the theoretical (Guo et al., 2009a) calibration line. The other

published calibration lines, derived by various laboratories using slightly

different preparation procedures and types of calcium carbonate are also

plotted up for comparison. The *C. caespitosa* data plot closest to the Ghosh et al (2006) calibration line, which is interesting as this line was derived using skeletal carbonates, and is, in itself, an outlier from the other calibration lines, being much steeper. The samples do still show an enrichment in Δ_{47} for their growth temperatures as is discussed further below.
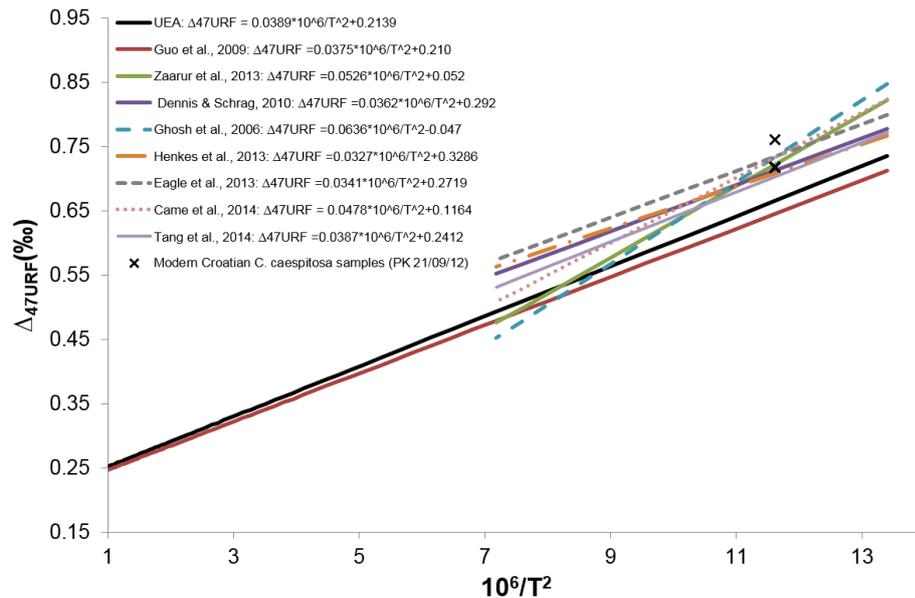
Figure 5.2.2 Published Δ_{47} - temperature calibration equations for CaCO$_3$ precipitated at earth surface temperatures (see Table 5.2.2 for equations). *C. caespitosa* data is plotted against the known growth temperature of 20.3°C for comparison to all temperature calibration lines. The outlier *C. caespitosa* sample is the potentially contaminated PK 21/09/12-02.

5.2.3. Potential sources of contamination – Reliability of data

It could be argued that the anomalous results found in these modern corals were caused by some form of contamination or alteration that affected isotopic composition. It is, for example, well known that coral skeletons have very finely intermeshed organic material within the skeletal carbonate (Barnes, 1970; Cuif and Dauphin, 2005). As surface oxidants were used to clean whole samples,

with the produced powders themselves not being bleached to avoid partial dissolution (White, 1998), it is possible that the Δ_{47} values were compromised by organic contaminants. However, this seems unlikely because laboratory protocols check for the presence of organic contaminants (hydrocarbons, chlorocarbons or sulphur-bearing compounds (Huntington et al., 2011)) that can interfere with mass-47, and therefore compromise temperature calculations (Eiler and Schauble, 2004; Guo and Eiler, 2007; Huntington et al., 2009; Huntington et al., 2011). Routine analysis of mass-48, 49 were carried out alongside mass-47. The presence of heavy species (C-O-H-Cl) recombining with produced H atoms or ions in the source creates highly anomalous mass-48 and/or mass-49 intensities and (less obvious) associated unusual Δ_{47} values (Eiler and Schauble, 2004). Samples where $\Delta_{48,49}$ are more than a few per mil from stochastic distribution can therefore be rejected as contaminated (Huntington et al., 2011): in the UEA laboratory positive Δ_{48} and >10‰ Δ_{49} are indicative of contamination. Samples with these characteristics were thus rejected (reported in Appendix ii). One run of PK 21/09/12-02 shows some signs of organic contamination: its results are reported, however, as a clear outlier for Δ_{47}, yielding lower temperatures than the other samples, it was not included in calculating average values.

SEM analysis (Chapter 3.2) showed these modern corallites to be well preserved, with no secondary marine cementation of septal regions and no recrystallisation of the corallite walls. There is no textural evidence to support diagenetic alteration.

5.3. MIS 5e Fossil Greek samples – clumped isotopic results

Due to the inferred disequilibrium effects in modern *C. caespitosa*, it is not possible to make meaningful palaeotemperature interpretations using fossil corallites without further study of the modern; this is beyond the scope and time constraints of this study. Because of this, plans to analyse multiple samples of fossil Greek *C. caespitosa* from the various deposits were abandoned. Instead, the focus switched to fossil samples where data from a few corals could be compared with both biogenic and abiogenic carbonates that are thought to have formed in near isotopic equilibrium. Material from MIS 5e deposits were best suited to this, containing both appropriate targets and carbonates that had been screened for likely diagenetic alteration (Section 3.2).

One corallite of *C. caespitosa* (SHR 02/11/11-08) from Makrugoaz Ridge, was prepared and ran as a homogenised powder to ascertain whether results from this well-preserved fossil sample were similar to those from modern samples. Along with this I procured: (1), sub-samples of abiogenic syndepositional marine aragonite cements, collected by Professor Julian Andrews from various MIS 5e deposits around the Perachora Peninsula, including the *C. caespitosa*-bearing deposits at Makrugoaz Ridge; and (2) complete radial ribs from two well preserved calcitic *Pecten* (scallop) shells (SHR 02/11/11-07 (I) & (II); Figure 5.3.1), also from Makrugoaz Ridge.

As the aragonite cement is an abiogenic precipitate it is likely to have formed in quasi-equilibrium with seawater, while *Pecten* also precipitate their calcitic shells (Barbin et al., 1991) in near isotopic equilibrium with seawater (Hickson

et al., 1999; Owen et al., 2002; Chauvaud et al., 2005). Therefore, the Δ_{47} of both these carbonates should provide realistic representations of the water temperature and seawater $\delta^{18}O$ composition they grew in.

There are, however, a few issues with assuming these carbonates will be accurate representations of the same MIS 5e shallow marine environment inhabited by the corals. The aragonite cements have formed in sediment or bedrock void spaces, some within sediment or bedrock fractures and some within the *C. caespitosa* bearing biostromes: they are intergrown with serpulids that encrusted firm substrates and are assumed to have grown syndepositionally with the biostromes (rather than post-burial) (J. Andrews, pers. comm.). It is therefore expected that the geochemical signature of these cements will record bottom water conditions representative of those that the corals themselves experienced. However, the association between serpulid worms and the cements suggests that they may have formed within dark sheltered cavities with restricted water flow (Antonioli et al., 2001), which is not the environment zooanthellate corals, such as *C. caespitosa* thrive in, suggesting that the aragonite slightly post-dates the corals it grows between. Therefore the conditions the aragonite cement formed under may have been cooler and may have had slightly different seawater $\delta^{18}O$ compositions than the average seawater the corals grew in.

The *Pecten* specimens, whilst found in association with the *C. caespitosa* biostromes, must also be treated with some caution. Winter growth cessation is a common phenomenon in bivalves, and scallops are no exception to this (Hickson et al., 1999; Owen et al., 2002; Goodwin et al., 2003). Therefore the lowest temperatures of the year may not be recorded in the shell calcites, which

will potentially skew the average growth temperature to higher values. It may also be that during the higher temperatures of MIS 5e, growth actually ceased or slowed during the summer, skewing the temperatures to lower values, which has also been shown to occur (Schöne et al., 2003; Buick and Ivany, 2004). Also, most species of scallops are not wholly sessile organisms, being capable of active swimming (Joll, 1989), this means that they may not simply record the conditions experienced by the sessile corals. The results from the analysis of these samples and replicates of them are shown in Table 5.3.1.

.

Figure 5.3.1 MIS 5e Pecten samples showing well preserved original colouration

Table 5.3.1 Greek MIS 5e fossil sample clumped isotopic bulk sample analysis results. Two runs of pecten sample SHR 02/11/11-07 (i) are highlighted as they show signs that the CO$_2$ fractionated during preparation and so are left out of further analysis.

Sample	Type	$\Delta_{47 \text{ (URF)}}$	Δ_{48}	Δ_{49}	$\delta^{18}O$	$\delta^{13}C$
JEA 10901-01	Abiogenic aragonite	0.66	-0.25	-33.44	-1.28	3.17
JEA 10901-01		0.65	-0.23	3.36	-1.02	3.18
Average		**0.65** (2σ=0.02)	**-0.24** (2σ=0.03)	**-15.04** (2σ= 52.03)	**-1.15** (2σ=0.37)	**3.17** (2σ=0.02)
JEA 26602-02	Abiogenic aragonite	0.68	-0.13	-38.00	1.31	3.78
JEA 26602-02		0.69	-0.16	-7.20	1.76	3.83
Average		**0.69** (2σ=0.01)	**-0.14** (2σ=0.04)	**-22.60** (2σ=43.56)	**1.53** (2σ=0.64)	**3.80** (2σ=0.07)
JEA 9508-01	Abiogenic aragonite	0.66	-0.25	-65.91	1.92	2.77
JEA 9508-01		0.67	-0.24	-38.83	2.01	2.78
Average		**0.67** (2σ=0.02)	**-0.24** (2σ=0.01)	**-52.37** (2σ=38.30)	**1.97** (2σ=0.13)	**2.78** (2σ=0.01)
SHR 02/11/11-07 (i)	Pecten	0.74	-0.01	20.55	0.68	0.23
SHR 02/11/11-07 (i)		0.75	-0.12	0.38	0.79	0.24
SHR 02/11/11-07 (i)		0.69	-0.11	-42.98	0.45	0.19
SHR 02/11/11-07 (i)		0.66	-0.40	-79.32	0.48	0.22
Average		**0.68** (2σ=0.04)	**-0.25** (2σ=0.42)	**-61.15** (2σ=51.40)	**0.46** (2σ=0.04)	**0.20** (2σ=0.04)
SHR 02/11/11-07 (ii)	Pecten	0.69	-0.31	-26.01	1.22	0.51
SHR 02/11/11-07 (ii)		0.71	-0.17	-16.72	1.18	0.50
Average		**0.70** (2σ=0.03)	**-0.24** (2σ=0.20)	**-21.37** (2σ=13.14)	**1.20** (2σ=0.06)	**0.51** (2σ=0.01)
SHR 02/11/11-08	MIS 5e coral	0.75	0.10	8.28	-2.42	-5.09
SHR 02/11/11-08		0.71	-0.13	-17.70	-2.50	-5.25
SHR 02/11/11-08		0.75	-0.08	30.39	-2.29	-5.24
Average		**0.74** (2σ=0.05)	**-0.04** (2σ=0.25)	**6.99** (2σ=48.14)	**-2.41** (2σ=0.21)	**-5.19** (2σ=0.17)

5.4. MIS 5e Greek (fossil) samples – Analysis and discussion

Table 5.4.1 MIS 5e sample average growth temperatures and water δ^{18}O compositions calculated using the UEA Δ_{47} – temperature calibration line. Aragonite sample's water compositions calculated using a rearranged form of the Goodwin et al. (2001) modified version of the Grossman & Ku (1986) palaeotemperature equation for aragonites precipitated in equilibrium, calcite sample's water compositions calculated using the Kim & O'Neil (1997) palaeotemperature equation for calcite precipitated in equilibrium

Sample	Type	Δ_{47} (‰)URF	Calculated temperature (°C)	δ^{18}O (‰$_{VPDB}$)	Calculated water δ^{18}O (‰$_{VSMOW}$)
JEA 26602-02	Abiogenic aragonite	0.69	13.84	1.53	−2.89
JEA 9508-01	Abiogenic aragonite	0.67	20.37	1.97	−1.82
JEA 10901-01	Abiogenic aragonite	0.65	24.06	−1.15	2.15
SHR 02/11/11-07 (i)	*Pecten* calcite	0.68	17.13	0.46	1.16
SHR 02/11/11-07 (ii)	*Pecten* calcite	0.70	9.94	1.20	0.23
SHR 02/11/11-08	*C. caespitosa* aragonite	0.74	-0.54	−2.41	-2.26
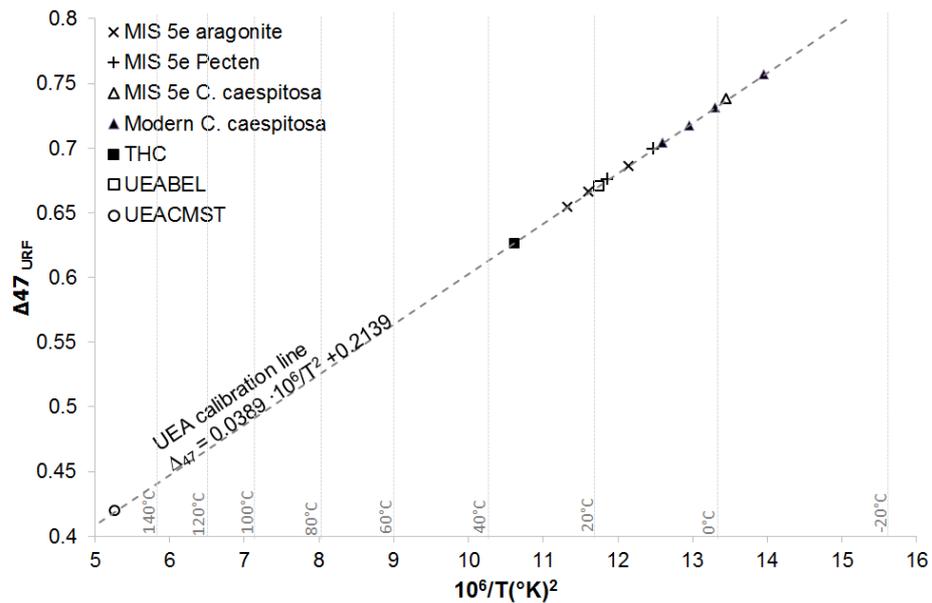
Figure 5.4.1 All clumped isotopic data plotted on the UEA calibration line, temperatures on x-axis also shown in Celsius for ease of reference

5.4.1.   Temperature

Using Equation 5.2.1, the UEA Δ_{47} – temperature calibration, water temperatures $(T(\Delta_{47}))$ have been calculated for MIS 5e and these are reported in Table 5.4.1 and Figure 5.4.1. Values of 14 to 24°C appear to be reasonable for marine cements formed within the bottom sediments or within sheltered cavities (J. Andrews pers. comm.). The higher end of these temperatures may be more representative of the temperature at the bottom of the (shallow) water column, with both JEA 9508-01 and JEA 10901-01 being within error of the average annual temperature that the MIS 5e sea temperature is postulated to have been (22-25°C, Chapter 4).

The *Pecten* shell samples are slightly more complex: SHR 02/11/11-07 (i) has an average $T(\Delta_{47})$ value of 17.1°C, but the individual duplicates give values of 12.6 and 21.9°C, while SHR 02/11/11-07 (ii) gives $T(\Delta_{47})$ values of 6.7 and 13.4°C. The coolest value (6.7°C) is not a likely temperature for last interglacial seawater conditions at this latitude based on all the other

available evidence (Section 4.4.2.1). The T(Δ_{47}) values of 12.5°C and 13.4°C are cooler than anticipated but could reflect the mobility of a *Pecten* that spent much of its life in deeper, colder waters, or that this species actually doesn't calcify in full equilibrium with the seawater. The value of 21.9°C from sample SHR 02/11/11-07(i), however, is consistent with the other available data, being in error of the expected shallow water temperatures for MIS 5e.

In summary the marine aragonite cement data are consistent with precipitation in equilibrium with the seawater, the T(Δ_{47}) values being approximately those expected from cements growing within void spaces in the cooler sediment. Only one of the *Pecten* analyses gave a T(Δ_{47}) value consistent with likely growth conditions for MIS 5e *C. caespitosa*, but this is probably an effect of the small number of samples it was possible to analyse in the time available as it may be that the *Pecten* powders produced were not as well homogenised as thought.

There is substantial variability between T(Δ_{47}) values from replicate analyses; however this is probably an artefact of the highly sensitive Δ_{47} – temperature relationship, with only a small error in the measurement resulting in a large error in the temperature calculated (Guo et al., 2009a). It is clearly preferable to carry out multiple replicates, however, time constraints on the availability of the equipment meant this was not possible in this study.

5.4.2. Water composition

As well as calculating temperature from Δ_{47} data, as the carbonate clumped isotope thermometer is independent of the isotopic composition of the water,

this should also allow the back-calculation of the $\delta^{18}O_{seawater}$ that carbonates formed in. For the aragonite samples this is done by using the measured $\delta^{18}O_{aragonite}$ values and re-arranging Equation 2.3.8, the Goodwin et al. (2001) modified Grossman and Ku (1986) palaeotemperature equation for aragonite precipitated in equilibrium to solve for $\delta^{18}O_w$:

$$\delta^{18}O_W = -1\left(\frac{T - 20.60}{-4.34} - \delta^{18}O_A + 0.20\right)$$

Equation 5.4.1 Goodwin et al. (2001) **modified Grossman and Ku (1986) palaeotemperature equation for aragonite precipitated in equilibrium rearranged to solve for δ^{18}O$_{seawater}$**

For the calcite samples (the *Pecten*) a rearranged version of the Kim and O'Neil (1997) temperature calibration equation for calcite precipitated in equilibrium was used to calculate seawater isotopic compositions (reported in Table 5.4.1).

$$1000 \ln \alpha_{(calcite-water)} = \frac{18030}{T} - 32.42$$

Equation 5.4.2: Kim and O'Neil's (1997) equation for the fractionation factor for calcite precipitated from water at equilibrium, temperature (T) in Kelvins gained from applying the UEA calibration equation (Equation 5.2.1) to the Δ_{47} data.

$$\delta^{18}O_W = \frac{(\delta^{18}O_C + 1000)}{(\alpha - 1000)}$$

Equation 5.4.3: Equation 5.4.1 rearranged to calculate the δ^{18}O value of water, both δ^{18}O$_{water}$ and δ^{18}O$_{calcite}$ are in ‰ (VSMOW)

Most of the calculated seawater compositions from the individual marine aragonite cement replicates (Table 5.4.1) have low values of −2.89 to −1.73‰ (VSMOW). If representative of open Gulf they suggest that MIS 5e Gulf of Corinth seawater was less saline than today (modern seawater in the area has a $\delta^{18}O$ composition around 1.15‰ (VSMOW) (Chapter 4). This argues against

131

most of the other available evidence for a warmer and probably more arid climate during most of the sustained MIS 5e highstand (Chapter 4): instead it suggests higher run off and riverine input and lower evaporation during this period than today. Most of the individual *Pecten* data paints a similar, although less extreme picture, with values for seawater $\delta^{18}O$ between -1.16 to 0.18‰ (VSMOW), again suggesting the water was fresher or the same as modern.

However, the *Pecten* values that yield the lower than expected seawater $\delta^{18}O$ values also produce the uncharacteristically low temperatures (4.6 to 13.4°C). In contrast the highest, and more plausible, *Pecten* growth $T(\Delta_{47})$ (21.9°C) yields a calculated water composition of 2.17‰ (VSMOW), which indicates increased salinity (compared to today) in the Gulf. This is consistent with palaeoecological and coral $\delta^{18}O$ data (Section 4.4.2.1). Shallow marine and estuarine *Pecten* species, are adapted to tolerate of a wide range of salinities (Belding, 1931; Gutsell, 1931; Castagna and Chanley, 1973; Duggan, 1975) some species even being able to survive in freshwater for limited periods of time (Mercaldo and Rhodes, 1982); it is therefore possible that the shells recording lower compositional values could have spent some of their lives in more brackish environments elsewhere.

Explaining the $\delta^{18}O$ seawater values calculated from the aragonite $T(\Delta_{47})$ requires a different approach. It is not yet fully understood in which conditions the aragonites precipitated, only that they typically formed in cavities, voids or fissures within the sediment/bedrock of the seabed (J. Andrews pers. comm.). We need to understand more about the geochemistry of the seawater in these restricted and dark or gloomy cavities, including the possible influence of ophiolite weathering in the catchments which can affect Mg concentration, and

by extension carbonate mineralogy (e.g. Morse et al., 1997), in coastal waters. We do know that one marine aragonite cement that is demonstrably inter-grown with *C. caespitosa* (sample JEA 9508-01; Table 5.4.1), and yields a plausible $T(\Delta_{47})$; it also yields what appears to be a low seawater $\delta^{18}O$ composition of −1.82 ‰ (VSMOW). At present we cannot explain this anomaly.

5.5. Disequilibrium calcification of corals

It is clear from the difference between the known modern temperatures and the $T(\Delta_{47})$ values that *C. caespitosa* does not calcify in equilibrium. Most work on clumped isotopes to date has suggested that the majority of natural calcium carbonates are precipitated in near isotopic equilibrium with respect to Δ_{47}, with little sensitivity to the 'vital effects' that cause $\delta^{18}O$ disequilibrium in many calcifying organisms (Weber and Woodhead, 1972). This implied that the same temperature calibration equation for inorganic carbonate could be universally applied to all biogenic carbonates (Ghosh et al., 2006; Thiagarajan et al., 2011; Eiler, 2011).

The first hints that coral skeleton Δ_{47} might not be in equilibrium were presented in Ghosh et al. (2006), although the anomaly they identified in the winter growth band of a Red Sea *Porites* was attributed to particularly slow growth. Thiagarajan et al. (2011) also found no evidence of vital effects in deep sea corals. However, Saenger et al. (2012) carried out a systematic sub-annual study using multiple species of shallow water corals from various localities. They reported that *Porites* skeletal aragonite is consistently enriched in Δ_{47}, with their samples underestimating growth temperature by ≈8°C, supporting the result found in the present work. Their *Porites* 'offset' when compared on the

UEA calibration line is, however, smaller than that found for here for *C. caespitosa*, suggesting that species specific effects may be important.

It is worth noting that using the Ghosh et al., (2006) equation (corrected to the universal reference frame of Dennis et al. (2011)) the *C. caespitosa* samples of this study have a smaller offset as found for the *Porites* samples in Saenger et al. (2012) – which also used the Ghosh equation. Apparent temperatures of 17.7 to 28.4°C are calculated from the modern *C. caespitosa* corals and 21.5°C from the MIS 5e coral using this calibration, this both covers the range of the actual measured seawater temperatures for the modern samples and the postulated temperature for MIS 5e. The calculated temperature values of the modern corals are generally higher than the annual average measured temperature (of 20.3°C). This could be because the corals cannot grow for the coldest months of the year (Montagna et al., 2007) and grow fastest in the summer (Peirano et al. 1999) and so should give average growth temperatures slightly higher than the actual average annual water temperatures. However, the Ghosh et al. (2006) calibration line is much steeper than all others (except the one by Zaarur et al. (2013)). It seems likely that the data in the present work lends considerable weight to the suggestion that the synthetic carbonates grown and analysed in the Ghosh study were themselves precipitated in disequilibrium (Affek, 2013). Therefore the small offset of the coral data from this calibration line is a product of a co-incidence that the level of disequilibrium found in some corals (by both this study and Saenger et al. (2012)) is approximately the same as the level of disequilibrium in the carbonates analysed by Ghosh, due to rapid calcification. Potential causes for the disequilibrium found here in *C. caespitosa* will be discussed in more detail in

Chapter 7 alongside the mechanisms for disequilibrium in the other geochemical parameters studied.

6. High resolution trace element analysis - Results and discussion

This chapter presents and discusses the high resolution LA-ICP-MS trace elemental data of *C. caespitosa* samples and its potential as a palaeoclimate proxy. Modern Croatian *C. caespitosa* trace element data are used to assess the reliability of this approach using accompanying water temperature data. The modern data is then transformed to temperature using published trace-element/calcium palaeothermometers. The aim is verify the applicability of these equations to samples where growth temperatures are unknown (i.e. fossil material). It is found that there is too much intra-site variability between the modern samples for a single species-specific trace-element/calcium palaeothermometer to be valid, suggesting that this is not a viable approach for high resolution palaeoclimate reconstruction. It is, however, demonstrated that the original annual cyclic variations in numerous trace element concentrations are present in the best preserved fossil (Greek) samples and there is the potential for recording other environmental events. Thus high resolution LA-ICP-MS is a (relatively) rapid, non-destructive, technique for reconstructing aspects of palaeooceanographic and palaeoclimatic variability and in evaluating the preservation quality of samples for other purposes, such as radiometric dating.

6.1. Modern Croatian samples – trace element results

Absolute trace element compositions and the variation in these values along the length of the corallites (i.e. over time) were successfully measured for all analysed modern Croatian *C. caespitosa* samples. SEM analysis of the samples showed well-focused evenly spread laser ablation pits (Figure 6.1.1)
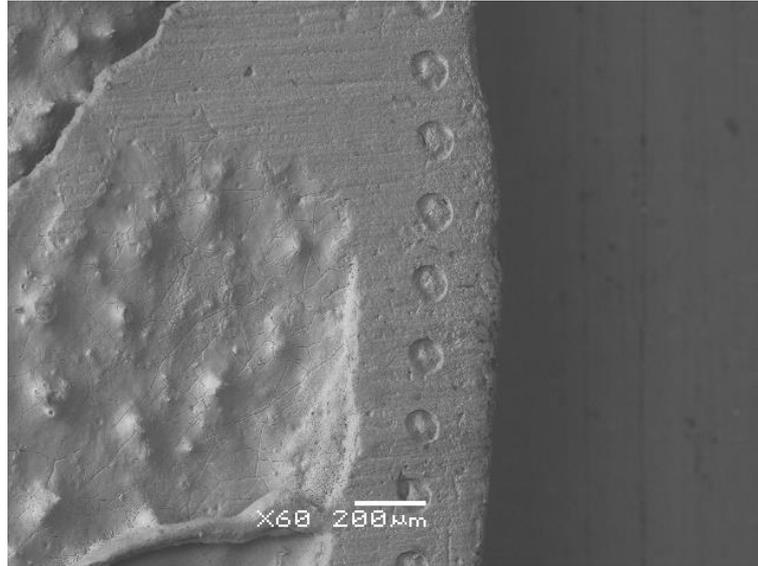
Figure 6.1.1 PK 21/09/12-01, uncoated SEM image, evenly spaced (at 200 µm) laser ablation pits following the corallite wall showing well focussed, circular ablation

By plotting the trace element/^{43}Ca values against distance from the base of the corallites (i.e. the start of the analysed transect) changes in trace element composition over the length of a corallite can be examined; these are shown for each sample in turn. These trace element profiles have been smoothed using a 4-point running median (black line in figures), to reduce noise and to highlight trends over seasonal scales. Figure 6.1.2 to Figure 6.1.8 show that, for the majority of trace elements found to be present in measureable concentrations, there are seemingly significant variations in their distribution along the length of the corallite. These data are also summarised in Table 6.1.1.

In all samples, the most abundant trace elements are Na, Sr, Mg with these three elements generally present in concentrations at least an order of magnitude higher than other elements.

6.1.1.1. PK 21/09/12-01

C. caespitosa collected at Mljet Bank sampling station 1 (see Figure 3.1.2 and Table 3.2.1), 8m growth depth. The last 9 years' worth of growth, based on the positioning of the last 9 pairs of seasonal growth bands up to the tip of the corallite's calyx wall, corresponding to approximately 45 mm of the corallite, was analysed.
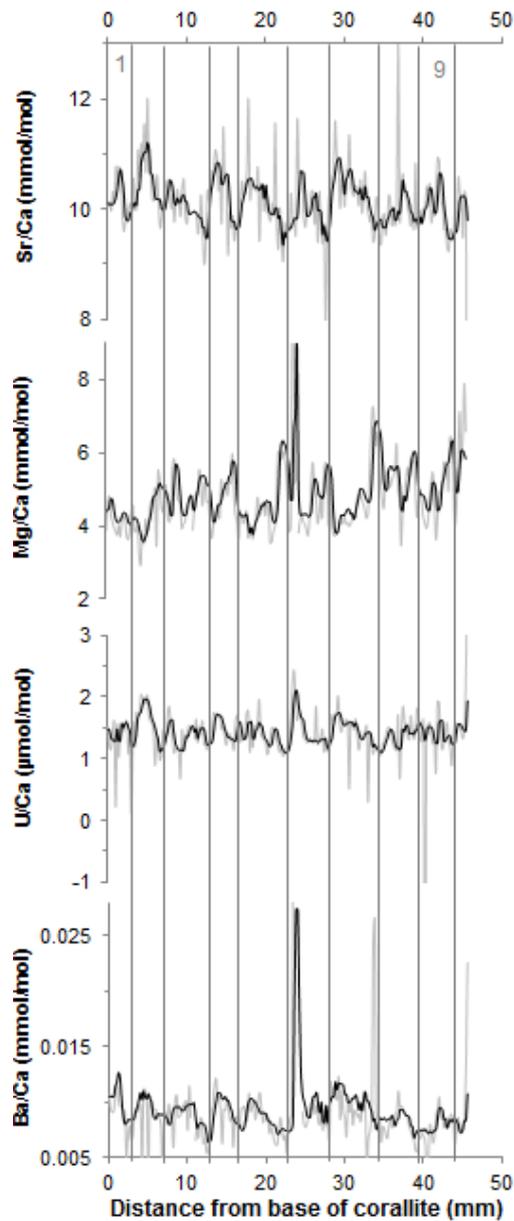
Figure 6.1.2 PK 21/09/12-01, trace element profiles dominated by a cyclic trend. 9.5 cycles are visible and these are most obvious in Ba and Sr. Vertical lines have been added to separate complete cycles.
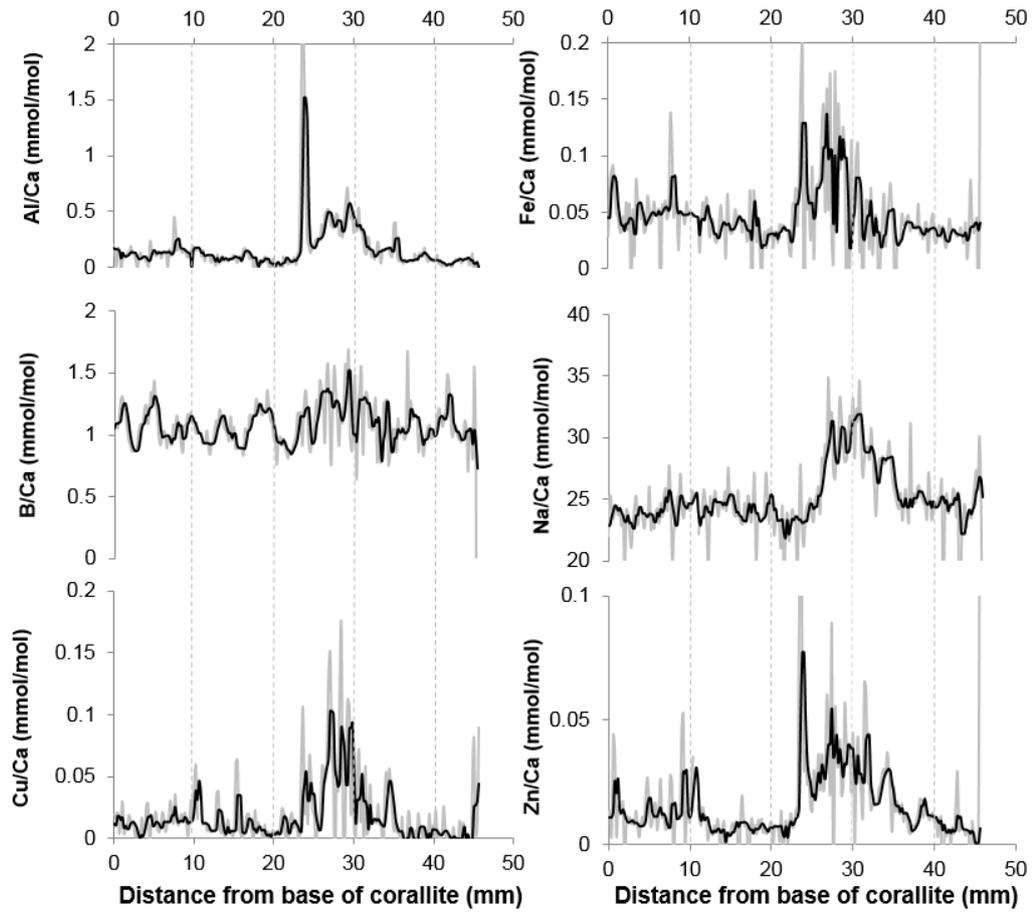
Figure 6.1.3 PK 21/09/12-01, trace element profiles dominated by a large high magnitude, low amplitude spike. B shows a degree of cyclicity until this is partially overprinted by the spike (K/Ca and P/Ca shown separately in Figures 6.2.5 and 6.2.6).

6.1.1.2. PK 21/09/12-01(II)

C. caespitosa collected at Mljet Bank sampling station 1 (see Figure 3.1.2 and Table 3.2.1), 8m growth depth. 23mm, equating to 7 years of growth, analysed.
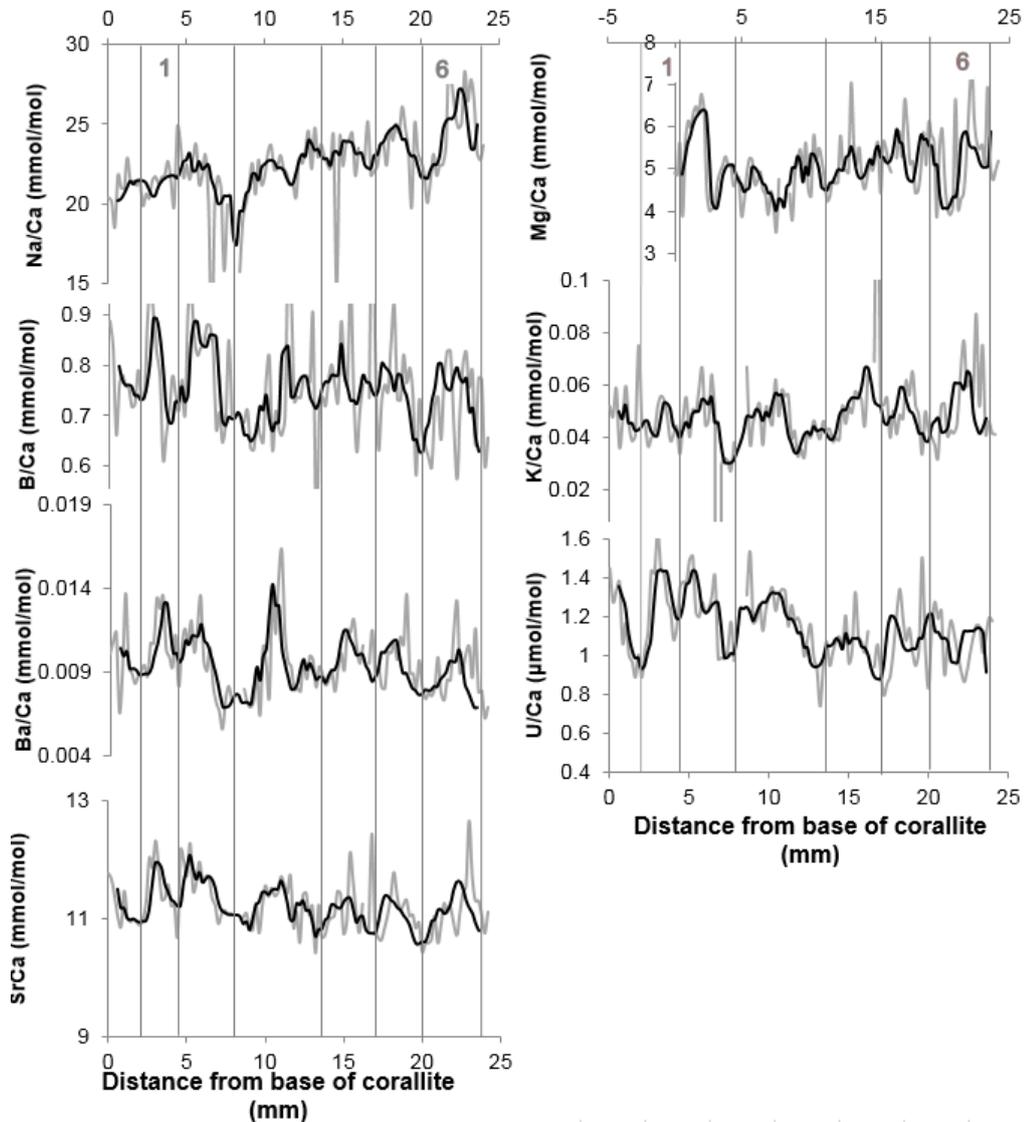
Figure 6.1.4 PK 21/09/12-01 (II), trace element profiles dominated by a cyclic trend, 6 whole cycles are visible, clearest in Sr, B, Ba. Vertical lines have been added to separate complete cycles.

6.1.1.3. PK 21/09/12-02(II)

C. caespitosa collected at Mljet Bank sampling station 2 (see Figure 3.1.2 and Table 3.2.1), 10m growth depth. 31mm, equating to 8 years of growth, analysed.
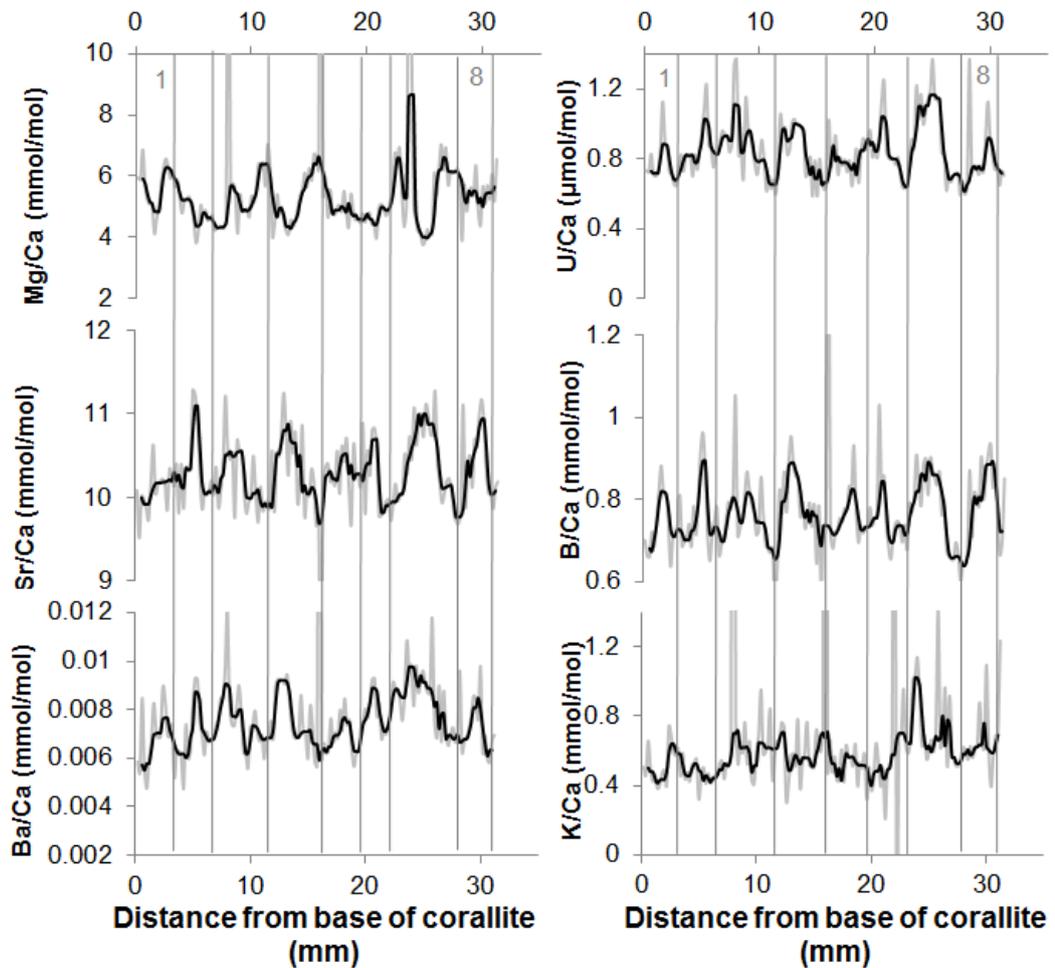
Figure 6.1.5 PK 21/09/12-02 (II), trace element profiles dominated by a cyclic trend, 8 cycles are apparent these are most obvious in Sr and B. Vertical lines have been added to separate complete cycles.

6.1.1.4. PK 21/09/12-05

C. caespitosa collected at Mljet Bank sampling station 5 (see Figure 3.1.2 and Table 3.2.1), 11m growth depth. 21mm, equating to 6 years of growth, analysed.
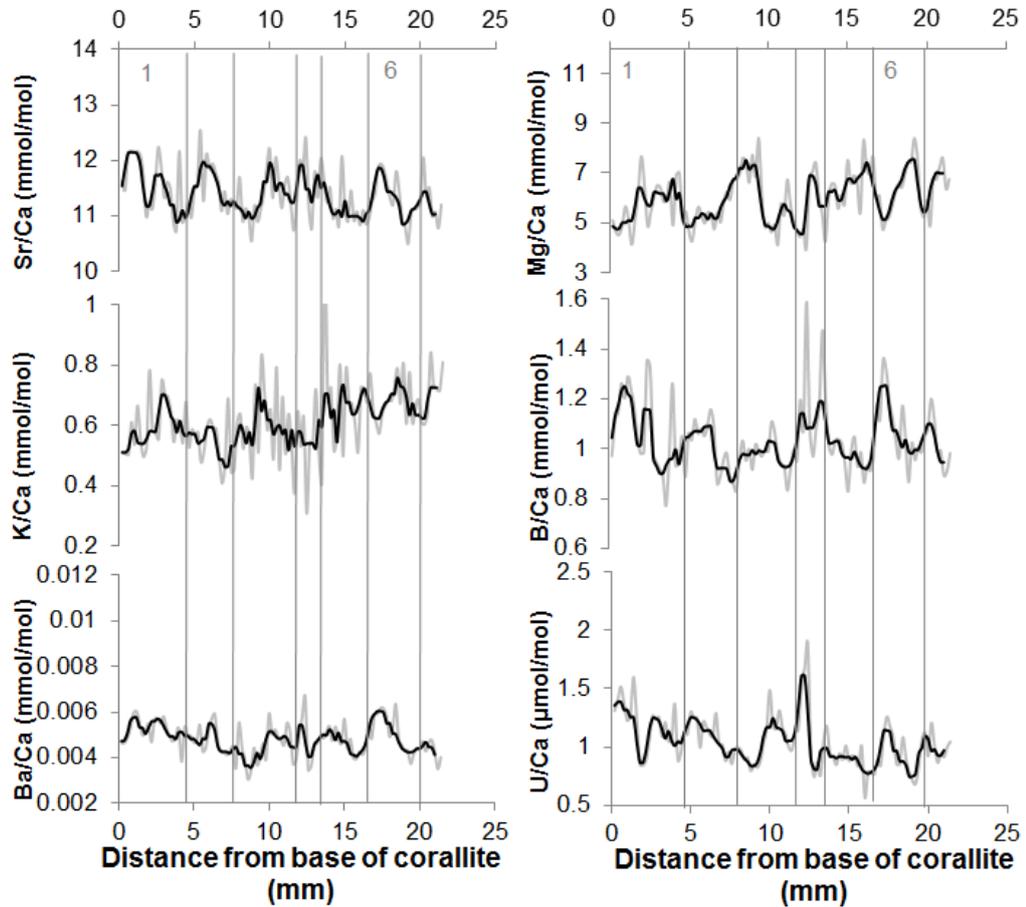
Figure 6.1.6 PK 21/09/12-05, trace element profiles dominated by a cyclic trend, 6 whole cycles are apparent. Vertical lines have been added to separate complete cycles.

6.1.1.5. PK 21/09/12-06

C. caespitosa collected at Mljet Bank sampling station 6 (see Figure 3.1.2 and Table 3.2.1), 14m growth depth. 22mm. equating to 6 years of growth, analysed.
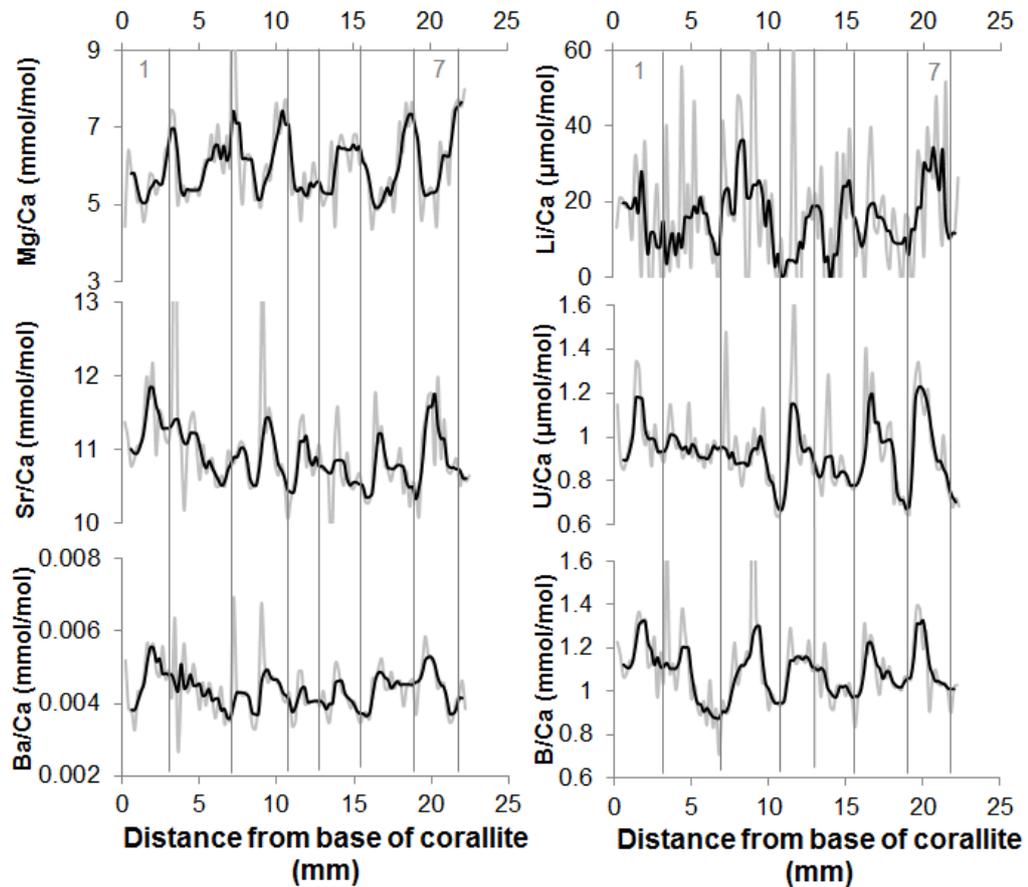
Figure 6.1.7 PK 21/09/12-06, trace element profiles dominated by a cyclic trend with 7 cycles apparent. Vertical lines have been added to separate complete cycles.
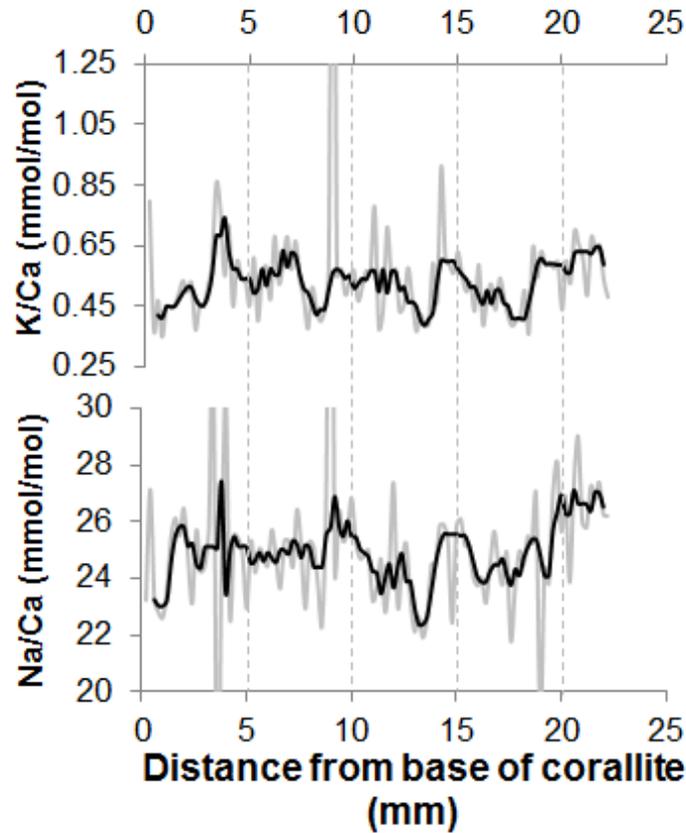
Figure 6.1.8 PK 21/09/12-06, trace element profiles dominated by a lower resolution cyclic trend with 4 possible cycles.

As can be seen in in the figures and Table 6.1.1, patterns seen in the distribution of trace elements in all samples can generally be grouped into three categories:

1. Those elements that show a clear cyclicity: Sr, Mg, Ba, B and U are the clearest of these in most samples. These elements exhibit a number of cycles approximately matching the number of years' growth of the corallite (based on the location of pairs of bi-annual growth bands following Peirano et al. (2005). Thus these cycles are interpreted as annual features related to the development of the growth bands and suggesting that there is a temperature, or other annual-scale, signal preserved by trace element content. Within each sample these elements

generally show similar patterns suggesting a common control on their uptake.

2. Elements with a signal dominated by a low frequency, high magnitude spike, this is only present in the sample PK 21/09/12-01(I) and overprints some of the signals that would (based on other samples) otherwise be cyclic.

Elements that are present in measureable quantities but show no discernible trends, the signal of these traces is apparently high frequency 'noise'. These are not shown in the figures but are listed in Table 6.1.1.

Table 6.1.1 Summary of the average trace element concentrations and main trends of trace element distribution in all LA-ICP-MS analysed modern Croatian *C. caespitosa* samples. Concentrations are shown as ratios of trace element/^{43}Ca (varying units shown in table) after calibration to 100% aragonite (CaCO$_3$) using internal standard ^{43}Ca = 38%. Mg and Sr are highlighted as they are the trace elements this study is most interested in. Key to trend abbreviations: A.S.C. = Annual Scale Cyclicity, the following number shows number of cycles recorded, (N.) shows that the annual signal is noisy; L.F.C = Low Frequency Cyclicity, the following number shows number of cycles recorded; Spike = the signal is dominated by a high magnitude, low frequency spike; H.F.N. = High Frequency Noise (i.e. no obvious trend).

Element	PK 21/09/12-01(I) Conc.	Trend	PK 21/09/12-01(II) Conc.	Trend	PK 21/09/12-02(II) Conc.	Trend	PK 21/09/12-05 Conc.	Trend	PK 21/09/12-06 Conc.	Trend
^{7}Li (μmol/mol)	-	-	12.23	H.F.N.	11.86	H.F.N.	17.90	H.F.N.	15.26	A.S.C. 6/7
^{11}B (mmol/mol)	1.08	Spike	0.75	A.S.C. 7	0.76	A.S.C. 8	1.02	H.F.N.	1.08	A.S.C. 6/7
^{23}Na (mmol/mol)	25.16	Spike	22.48	H.F.N.	27.87	A.S.C. 8	25.12	H.F.N.	24.92	L.F.C. 4
^{24}Mg (mmol/mol)	4.89	A.S.C. (N.) 9.5	5.04	A.S.C. 7 (N.)	5.30	A.S.C. 8 (N.)	6.00	A.S.C. 6/7	5.99	A.S.C. 6/7
^{27}Al (mmol/mol)	0.16	Spike	0.01	H.F.N.	0.02	H.F.N.	0.02	H.F.N.	0.03	-
^{31}P (mmol/mol)	-	-	-	H.F.N.	0.1	H.F.N.	0.02	H.F.N.	0.02	-
^{39}K (mmol/mol)	1.41	Spike	0.05	H.F.N.	0.58	H.F.N.	0.61	A.S.C. 6/7	0.53	L.F.C. 4
^{55}Mn (mmol/mol)	-	-	-	-	-	-	-	-	0.01	-
^{56}Fe (mmol/mol)	0.04	Spike	-	-	-	-.	0.01	-	0.01	H.F.N.
^{65}Cu (mmol/mol)	0.02	Spike	-	-	-	-	-	-	-	-
^{66}Zn (mmol/mol)	0.02	Spike	-	-	-	-	-	-	-	-
^{86}Sr (mmol/mol)	10.13	A.S.C. 9.5	11.19	A.S.C. 7	10.29	A.S.C. 8	11.38	A.S.C. 6/7	10.92	A.S.C. 6/7
^{135}Ba (mmol/mol)	0.01	A.S.C. 9.5	0.01	A.S.C. 7	0.01	A.S.C. 8	0.01	A.S.C. 6/7	0.01	A.S.C. 6/7
^{238}U (μmol/mol)	1.42	A.S.C. 9.5	1.14	A.S.C. 7 (N.)	0.83	A.S.C. 8 (N.)	1.03	A.S.C. 6/7	0.93	A.S.C. 6/7

6.2. Modern Croatian samples – Analysis

6.2.1.   Calibrating the data to a normalised time series

The *C. caespitosa* trace element profiles were normalised to a time series (Figure 6.2.1, 6.2.2). As all corallites were collected alive on the 21st September 2012 and data was collected as close to the growth tip of the corallite wall as possible, it could be assumed that the last measured point of each profile corresponded to September 2012. In each set of corallite profiles, there were multiple elements showing assumed annual scale cyclicity. The strongest annual scale variable is likely to be seasonal variation in water temperature and it has been shown that this is the primary control on the uptake of numerous trace elements (Beck et al., 1992; Rong Min et al., 1995; Silenzi et al., 2005; Montagna et al., 2007). This means that the observed trace element cycles could be used to match up the growth period with various times of the year. Strontium and magnesium were used as, in most cases, these elements demonstrated the clearest cyclic signal with minimal smaller scale variation. Moreover, these are the two trace elements most commonly used as palaeothermometers in coralline aragonite (e.g. Beck et al., 1992; McCulloch et al., 1994; Mitsuguchi et al., 1996; Marshall and McCulloch, 2002).

Strontium uptake in coralline aragonite has a negative correlation with seawater temperature (Weber, 1973; Beck et al., 1992; de Villiers et al., 1994; Alibert and McCulloch, 1997; Marshall and McCulloch, 2002; Silenzi et al., 2005; Montagna et al., 2007; Sayani et al., 2011) and magnesium uptake a positive correlation (Mitsuguchi et al., 1996; Sinclair et al., 1998; Silenzi et al., 2005; Montagna et al., 2007). Thus temporal normalisation of the data was carried out by assuming

that each Sr peak maxima/Mg peak minima corresponded to the time of the year with the lowest seawater temperatures at this locality (February/March) and each Sr trough minima/Mg peak maxima corresponded to the time of the year with the highest seawater temperatures (August/September).

This technique was successfully applied to the $\delta^{18}O$ data in Chapter 4.2, by assuming $\delta^{18}O$ maxima corresponded to temperature minima and $\delta^{18}O$ minima corresponded to temperature maxima. Therefore, by comparing the temporally normalised trace element and $\delta^{18}O$ profiles for the one corallite it was possible to obtain both analysis from, it can be seen that it also works well for this technique, as the profiles appear very similar (Figure 6.2.1).
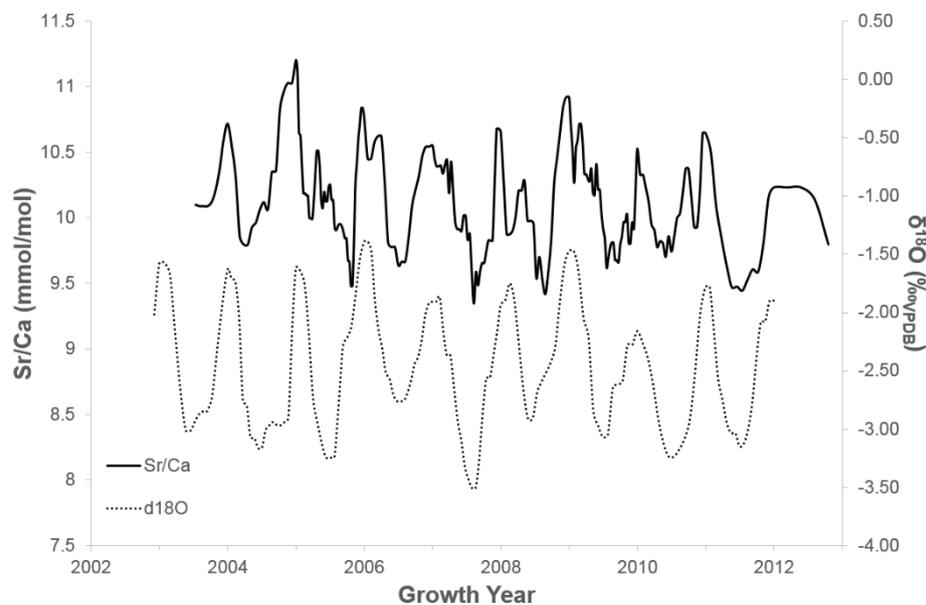
Figure 6.2.1 Sr/Ca and $\delta^{18}O$ profiles of modern Croatian *C. caespitosa* sample PK 21/09/12-01 (I) profiles normalised to the same time series; both profiles show very similar annual sinusoidal cycles, interperted as mainly water temperature change.

It can be seen in Figure 6.2.2 that this technique works well; with similar magnitude and shape patterns visible in separate samples. This is especially obvious with the high amplitude 2008-2009 'summer' peak and the particularly low amplitude 2009-2010 'summer' peak, both correlative between samples.

This suggests that the controls on relative concentrations of Sr and Mg are the same for each corallite, a promising observation for their use in palaeothermometry.
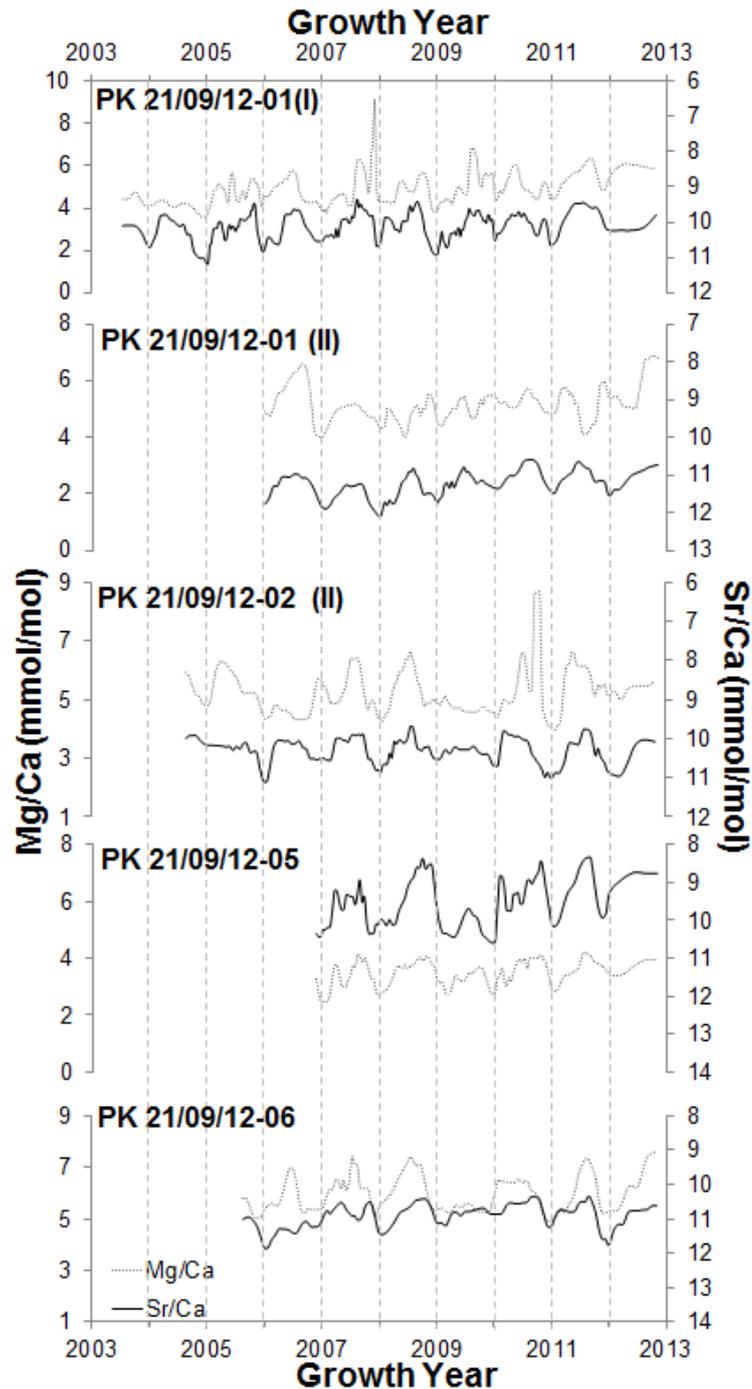
Figure 6.2.2 Modern Croatian *C. caespitosa* samples (PK 21/09/12) Sr/Ca and Mg/Ca profiles normalised to a time series. Intra-year trends can be matched up between corallite samples, e.g. the high amplitude 2008-2009 'summer' peak and the particularly low amplitude 2009-2010 'summer' peak can both be seen in the majority of samples. Sr

profiles are shown with an inverse Y-axis to highlight similarity with Mg profiles due to Sr's negative correlation with SST. R^2 values for Mg/Ca against Sr/Ca are as follows: PK 21/09/12-01 (I): 0.35; PK 21/09/12-01 (II); 0.15; PK 21/09/12-02 (II): 0.16; PK 21/09/12-05: 0.57; PK 21/09/12-06: 0.23.

6.2.2. Application of published trace elemental palaeothermometers

The modern samples come from a well-studied locality where temperatures, both at the sea surface and at the depth of coral growth, are available throughout the majority of the growth period (up to 2010). It should thus be possible to use these samples to test the validity of published *C. caespitosa* trace element/Ca palaeothermometers and their viability for use on ancient samples where growth conditions are unconstrained.

The average annual sea surface temperature at Mljet over the period 2003-2010 (which covers the majority of the growth years analysed) was 20.3°C (Kružić et al., 2012), the average monthly mean temperature reached during the summer months is 27.5°C (Kružić, 2002) and the average lowest monthly mean temperature reached during winter is 11.0°C (Kružić, 2002). The range is reduced somewhat at the deepest parts of the coral bank (around 15 m) with average monthly temperatures ranging from approximately 26 to 14°C at this depth (Figure 4.2.1). It was therefore expected that the temperatures derived from previously published equations for the *C. caespitosa* trace element-SST relationship, using the measured Sr/Ca and Mg/Ca data, would be within this range for all samples.

Sr/Ca

The negatively correlated temperature dependence of strontium incorporation into inorganically grown carbonates was first demonstrated by Kinsman and

Holland (1969) and Weber (1973) found a similar relationship in coralline aragonite (in direct contrast to previous studies which had found no relationship (e.g. Thompson and Chow, 1955; Thompson and Livingston, 1970)). Sr has since been the most commonly used trace element for carbonate thermometry (e.g. Beck et al., 1992; de Villiers et al., 1994; de Villiers et al., 1995; Allison et al., 2001). It has been widely observed that strontium is one of the most abundant trace elements in corals (Silenzi et al., 2005). Sr^{2+} substitutes directly and ideally for Ca^{2+} with only a small (2%) dilation of the site and no evidence has been found for clustering into strontianite ($SrCO_3$) nanodomains within the aragonite crystal lattice (Finch and Allison, 2007), which could potentially affect the reliability of the Sr/Ca palaeothermometer at high resolutions. Incorporation of Sr into the coralline aragonite is believed to be controlled mainly by the Sr/Ca activity of seawater and the Sr/Ca distribution coefficient between aragonite and seawater (D^A_{SR}) which are both controlled by temperature (Beck et al., 1992). While many studies have looked at the Sr/Ca – temperature relationship of tropical corals (Beck et al., 1992; McCulloch et al., 1994; de Villiers et al., 1994; de Villiers et al., 1995; e.g. Alibert and McCulloch, 1997) only two equations have been published for the relationship between Sr/Ca and SST for *C. caespitosa*:

Equation 6.1: $Sr/Ca(mmol/mol) = 11.25(\pm 0.38) - 0.079(\pm 0.026) \cdot SST(^oC)$

(Silenzi et al., 2005)

Equation 6.2: $Sr/Ca(mmol/mol) = 10.50(\pm 0.13) - 0.073(\pm 0.006) \cdot SST(°C)$

(Montagna et al., 2007)

By applying these equations to the modern samples' Sr/Ca compositions and comparing the calculated SSTs to those recorded at Mljet National Park (Kružić, 2002; Kružić et al., 2012) their validity for calculating palaeotemperatures can be assessed. The produced temperature profiles are shown in Figure 6.2.3.
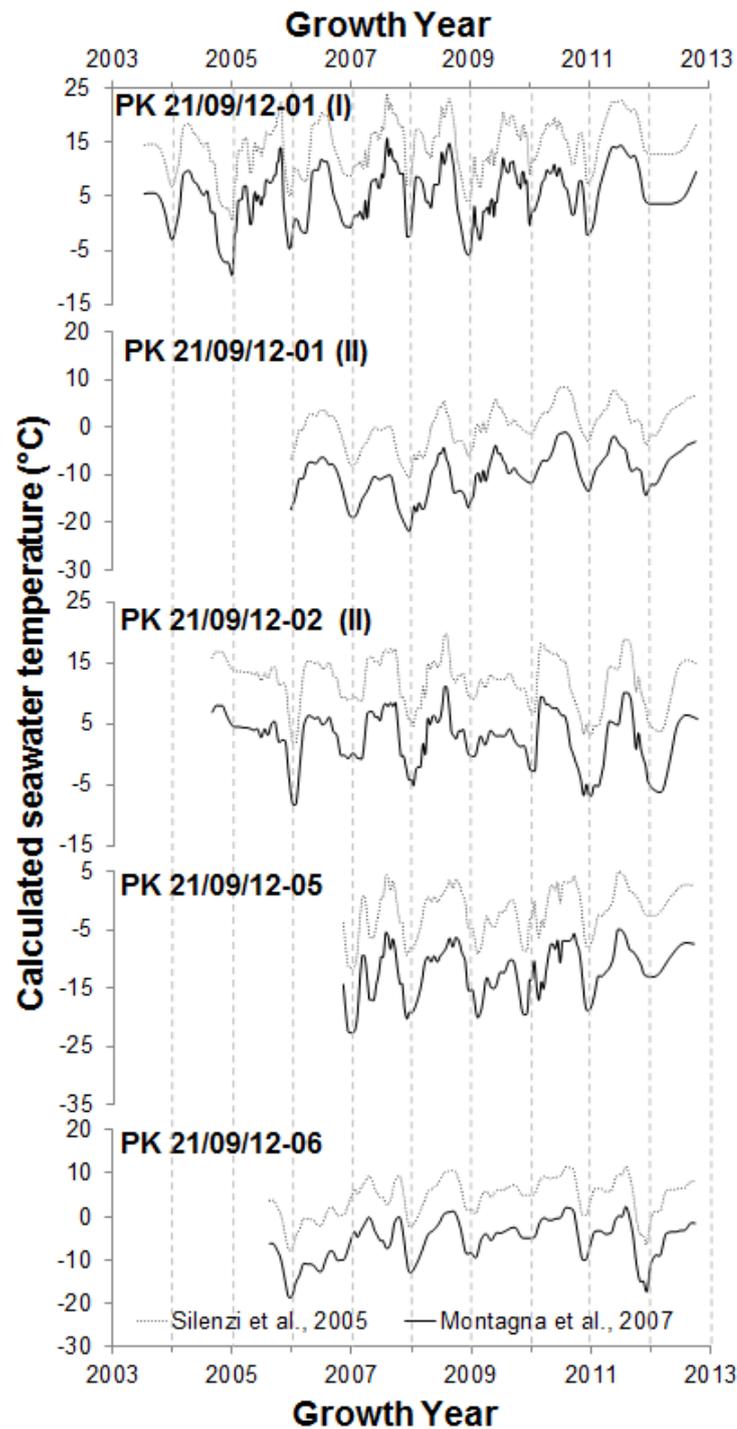
Figure 6.2.3 Sr/Ca calculated palaeotemperatures using equations published by Silenzi et al. (2005) and Montagna et al. (2007)

Figure 6.2.3 shows that the temperatures produced by Equations 6.1 and 6.2 are significantly different from each other, in all samples the Montagna et al. (2007) equation consistently results in temperatures around 10°C lower. It is also clear that both equations produce temperatures, for these modern samples, that are too low to be realistic, with temperatures below freezing 'recorded' in all samples. In an isolated sample this may not be a problem as it would be possible to re-calibrate the equation for the sample, as was done for the isotopic compositions in Chapter 4. This is not possible in practice, however, as the different samples show large degrees of intra-site variation in their Sr compositions, ranging from 10.13 to 11.38 mmol/mol (

Table 6.1.1), therefore producing very different temperatures when the same equation is applied to all. It is not just the calculated temperatures that are different; the annual ranges are different for each corallite; for example PK 21/09/12-01 (I) shows annual variation of around 15-20°C whereas PK 21/09/12-02 (II) shows a variation of just 8-15°C. As all the corals have grown within metres of each other on the same bank they should have experienced very similar growth conditions; clearly they are not recording actual temperatures in their Sr composition.

Mg/Ca

The distribution of Mg/Ca also showed a strong seasonal signal and again this relationship has been used extensively as a proxy for growth temperature of carbonate organisms (Mitsuguchi et al., 1996; Sinclair et al., 1998; Silenzi et al., 2005; Montagna et al., 2007). SST and Mg/Ca have repeatedly been shown to have a significant positive correlation with each other, allowing for the calibration of Mg/Ca palaeothermometers (Mitsuguchi et al., 1996; Sinclair et al., 1998; Silenzi et al., 2005; Montagna et al., 2007; Armid et al., 2011; Schöne et al., 2011), in some cases more sensitive to changes (Mitsuguchi et al., 1996) and more reliable (Kamenos et al., 2008) than the Sr/Ca – SST relationship.

For *C. caespitosa* two equations have been published for the relationship between Mg/Ca and SST:

Equation 6.3: Mg/Ca (mmol/mol) = −4.41(±3.10) +0.55(±0.21) · SST (^{o}C)

(Silenzi et al., 2005)

Equation 6.4: Mg/Ca (mmol/mol) = 1.66(±0.28) + 0.121(±0.013) · SST ($^{\circ}$C)

154

(Montagna et al., 2007)

Again, by applying these equations to the modern samples' Mg/Ca compositions and comparing the calculated SSTs to those recorded at Mljet National Park (Kružić, 2002; Kružić et al., 2012) their utility for calculating palaeotemperatures can be assessed (Figure 6.2.4).
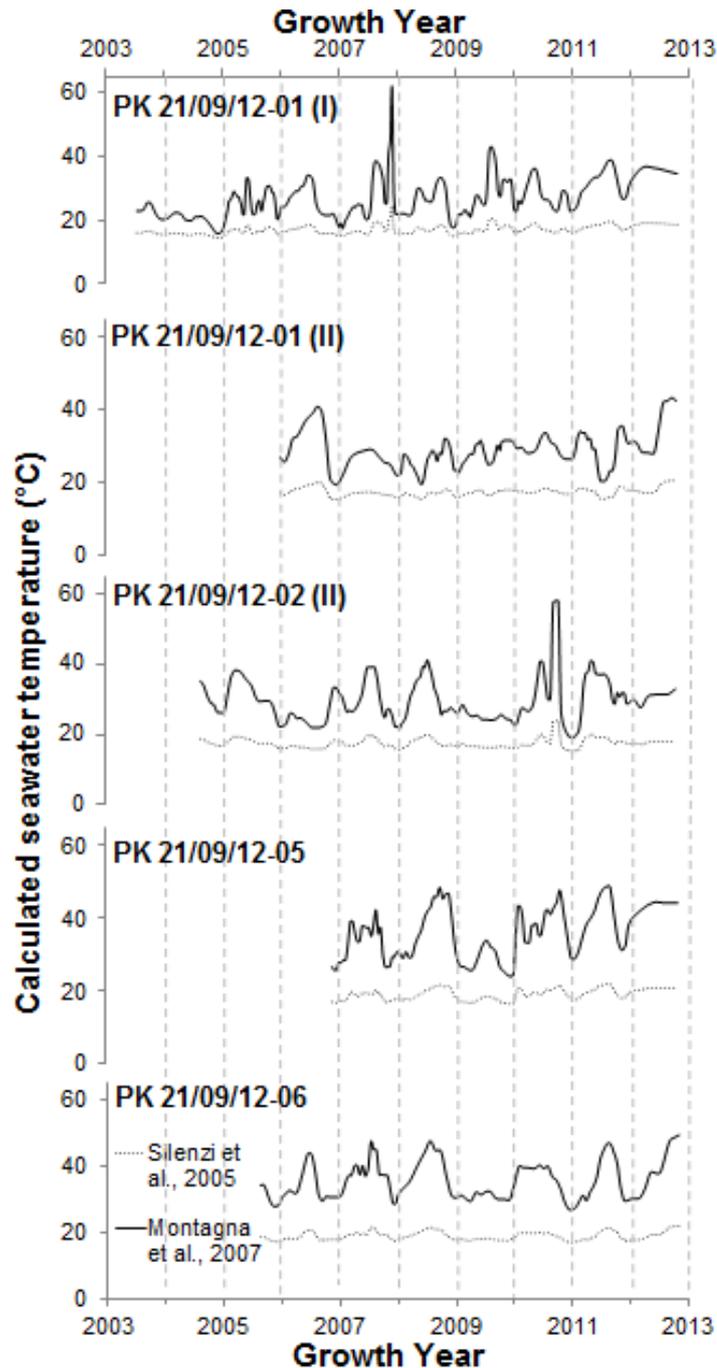
Figure 6.2.4 Mg/Ca calculated palaeotemperatures using equations published by Silenzi et al. (2005) and Montagna et al. (2007)

The most obvious feature of the temperatures produced by these equations is that the Silenzi et al. (2005) equation, while providing a reasonable average temperature for each sample, calculates a very narrow seasonal range with less than 5°C variation over the whole of each profile. The Montagna et al. (2007) equation is somewhat closer to the expected degree of variation, with most

years in all samples showing a seasonal variation of between 15-20°C, but with temperatures which are too high, the majority of temperatures between 20 and 45°C. The large difference in the seasonal temperature range calculated by the two equations may partly be explained by the way Silenzi et al. (2005) produced their calibration equation; using only the winter growth bands of a *C. caespitosa* corallite and looking at average seasonal temperatures. This means that they only applied a narrow range of temperatures and Mg/Ca values in their calculation of their calibration equations so that there is a lot of extrapolation involved in applying their equation(s) to a full year's Mg/Ca (or Sr/Ca) data. A calculated 9°C variability in the average temperatures between all the samples shows a high degree of intra-site variability in Mg uptake which cannot be explained by differences in temperature experienced over the growth period.

6.2.3.   Intra-site variability in trace elemental composition

The Mg and Sr data from the modern Croatian samples is summarised in Table 6.2.1. There is a high degree of intra-site variation between the average compositions of the samples and the temperatures calculated from those compositions for both Sr and Mg.

Table 6.2.1 Summary of modern Croatian (PK 21/09/12) Sr and Mg compositions and the temperatures calculated from them using the published Silenzi et al. (2005) and Montagna et al. (2007) equations to show the wide degree of intra-site variation.

	Average compositions (mmol/mol)		Average Sr/Ca calculated temperatures (°C)		Average Mg/Ca calculated temperatures (°C)		Actual measured temperature (°C)
	Sr/Ca	Mg/Ca	Silenzi et al., 2005	Montagna et al., 2007	Silenzi et al., 2005	Montagna et al., 2007	Kružić et al., 2012
PK 21/09/12-01(I)	10.12	4.89	14.22	5.12	16.92	26.72	20.3
PK 21/09/12-01(II)	11.19	5.04	0.70	−9.52	17.19	28.67	20.3
PK 21/09/12-02(II)	10.29	5.01	12.15	2.88	17.13	30.09	20.3
PK 21/09/12-05	11.38	6.00	−1.65	−12.06	18.92	35.85	20.3
PK 21/09/12-06	10.92	5.99	4.24	−5.69	18.90	35.76	20.3

There is also wide intra-site variability in all the other trace elements analysed, as shown in Table 6.2.1. This variation suggests that each coral exhibits a strong metabolic control, a 'vital effect' (Weber and Woodhead, 1972), over the uptake and incorporation of trace elements from the seawater into its calcifying skeleton. This means that there is no constant, species-specific offset from equilibrium and any temperature-trace element relationships would need to be colony specific, which is unsuitable for palaeotemperature reconstruction. A reliable proxy for temperature requires the amount of disequilibrium to be constant at least at the genus or species level (Marshall and McCulloch, 2002).

These findings of intra-site variability in trace element uptake are in agreement with some studies on tropical corals, such as *Porites*, where analysis of multiple colonies has shown there are issues with reproducibility of a constant Sr/Ca calibration between studies and even within the same study. For example, de Villers et al. (1994) analysed the Sr/Ca ratio of 3 specimens of *Porites lobata* from the same reef in Hawaii. SST, Sr/Ca$_{seawater}$ and growth rate were found to be the same at all localities; however, a different trend of Sr/Ca and therefore a different calibration to SST was found for each specimen. This meant that SST calculations varied by as much as 2-3°C.

Intra-specific variation may be related to variations in the photosynthetic variability of the symbiotic zooxanthellae (Cohen et al., 2002). Increased water temperature and increased photosynthesis both have an inverse relationship with the Sr/Ca of skeletal aragonite. As well as causing variations between corals this may also exaggerate seasonality in individual corals where zooxanthellae are much more active in the summer than winter (Cohen et al., 2002). This will clearly affect non-tropical corals such as *C. caespitosa*. It seems reasonable, then, to infer that the effect of photosynthesis on ion uptake may extend to, and explain the variance in, other trace elements. As *C. caespitosa* is particularly well adapted to living in turbid waters due to its combined reliance on autotrophy and heterotrophy (Peirano et al., 2004), the amount of each that a particular colony relies on during any period could be highly variable, depending on the flow of particulates (both edible and non-edible sediment) around the coral bank, and also how shady the growth locality is.

It has also been shown that (tropical) corals under stress do not conform to the normal rules for trace element-SST relationships. At high or low temperatures

highly anomalous results with a breakdown in relationship have been recorded (Marshall and McCulloch, 2002). This is a factor which may be quite important for the study of *C. caespitosa* as, at this locality, much of the winter is spent at temperatures near or below the minimum temperature for calcification (Montagna et al., 2007) while, during the summer, temperatures often peak at around the maximum levels this species can tolerate (Rodolfo-Metalpa et al., 2005; Kružić, 2007).

These issues with intra-site/inter-corallite variability in trace element uptake were not encountered in the papers of Montagna et al. (2007) and Silenzi et al. (2005) as these studies focussed their efforts onto a single corallite. However, the fact that the same data set (from any one of the Croatian corallites) produces such different temperatures from their two sets of equations (Silenzi et al., 2005; Montagna et al., 2007) suggests that the corallites studied in these papers did also exhibit differing trace element-temperature relationships.

It is also noteworthy that the published *C. caespitosa* trace element – seawater temperature thermometers incorporate a level of error in the equations that allows a range of temperatures to be calculated. For example, using the Silenzi et al., (2005) equation and an Mg/Ca value of 6.0 mmol/mol, temperatures ranging from 9.6 to 39.7°C may be calculated. This ≈20°C error range is larger than the ≈17°C actual annual temperature range recorded over the year at the locality (Kružić and Požar-Domac, 2002; Kružić et al., 2012). Similar errors are found for the other equations; this is shown in Figure 6.2.5 using the Silenzi et al. (2005) Sr/Ca – temperature relationship and PK 21/09/12-02(II) as an example.
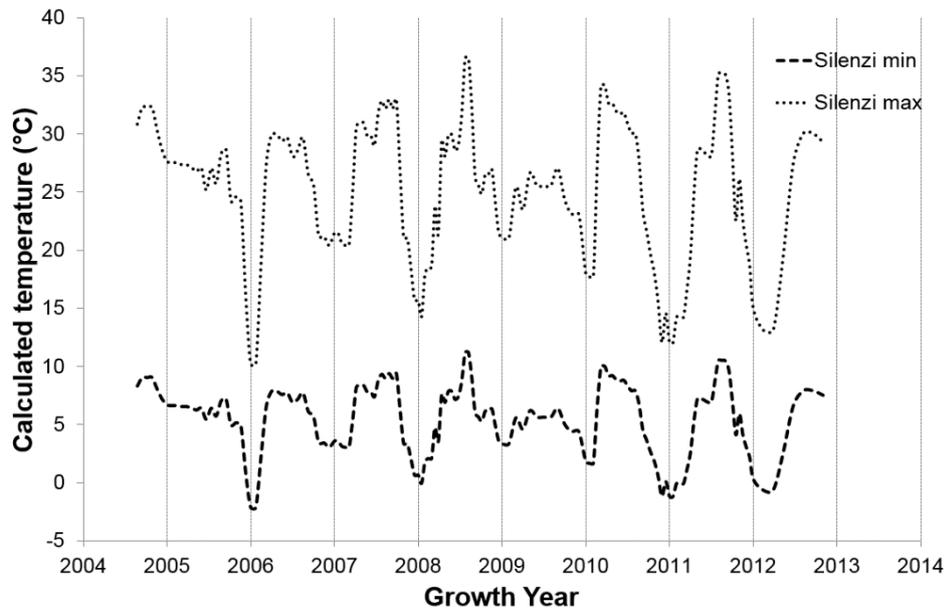
Figure 6.2.5 Range of temperatures that can be calculated from the Silenzi et al. (2005) Sr/Ca – temperature relationship equation for *C. caespitosa* sample PK 21/09/12-02(II) when the full range of uncertainty in the equation is taken into account. The line 'Silenzi min.' plots the minimum values that can be attained, using the equation: SST = (Sr/Ca−10.87)/−0.105; 'Silenzi max' plots the maximum values that can be attained, using the equation: SST = (Sr/Ca−11.63)/−0.053.

As both of these studies only examined a single individual corallite, this shows that there is a large degree of internal variation of the trace element – temperature relationship within each corallite. This further demonstrates that this is not a reliable technique for palaeothermometry.

6.2.4. Other potential uses for trace element analysis of *C. caespitosa* samples

6.2.4.1. Other palaeoenvironmental indicators

While it appears that intra-site, and possibly even intra-colony/corallite, variability means that the trace elemental composition of *C. caespitosa* cannot provide a reliable quantitative palaeotemperature record, it is clear, from the repeated cyclicity and patterns that can be traced between corallites, that *C. caespitosa* does record some essence of the environmental conditions in its

trace element record as it grows. Therefore there may be the potential to procure other, non-quantitative, information.

The non-cyclic profiles of PK 21/09/12-01 are dominated by a large asymmetrical spike (Figure 6.1.3). Figure 6.2.6 shows one of the strongest spike dominated signals, K/Ca, after time series calibration. The spike is much too low frequency to have any relationship with an annual phenomena such as temperature; however, the spike clearly starts in late 2007.

As the spike is broadly asymmetric, being steeper on the basal (older) side and tailing off more gradually over time, it appears there was an influx of elements into the aragonite-seawater system towards the end of 2007 which subsequently decreased over time. This points to a sudden, singular event, injecting a high concentration of these elements into the water which then gradually dispersed, settling into the sediment or taken up by organisms. Indeed the shape could be a composite of at least three smaller spikes, suggesting multiple (linked) injection events.
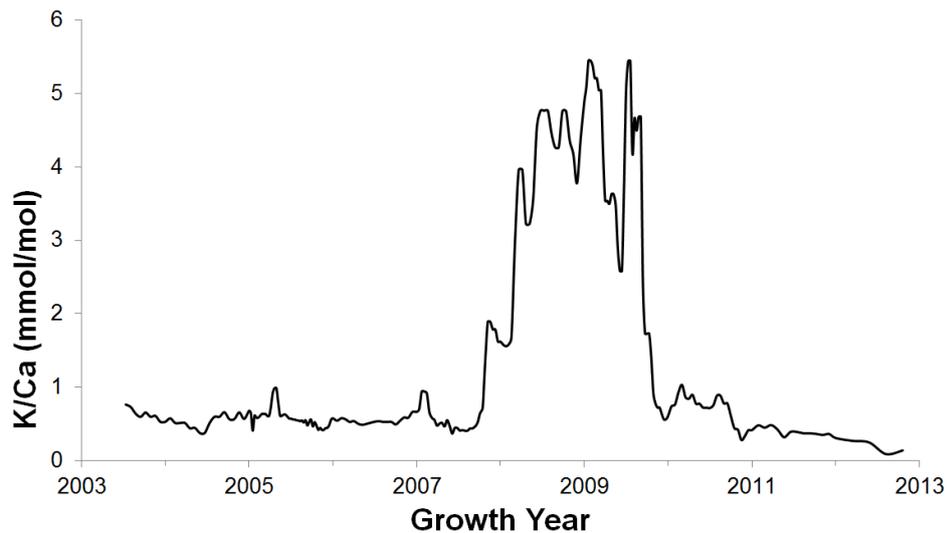
Figure 6.2.6 K/Ca profile of PK 21/09/12-01 showing the high magnitude, low amplitude spike in the signal which is believed to be related to a large influx of sediment into the seawater.
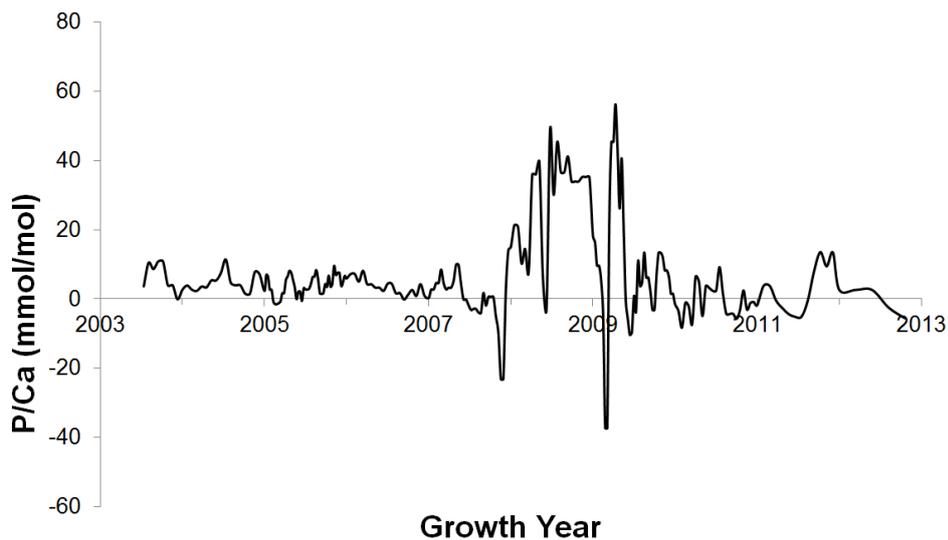
Figure 6.2.7 Unquantified P/Ca profile of PK 21/09/12-01 showing the high magnitude, low amplitude spike in the signal which is believed to be related to a large influx of sediment into the seawater. Note negative concentrations showing that the signal is not correctly calibrated.

Of the elements recorded in this 'event', Al, Fe, Cu, Zn, Na are all common rock forming elements; it would thus be expected that the seawater content of these elements would be higher at times of increased sediment input. An even larger similar shaped (unquantified) spike in the P signal was also observed, the shape of this profile is presented in Figure 6.2.7 but the data is not truly

quantitative as P content could not be calibrated accurately with the standards used in this study. Changes in the P/Ca content of corals have been shown to reflect the phosphorous content of seawater (Montagna et al., 2006b; LaVigne et al., 2010) which often reflects changes in biological productivity and cycling of the water column. In the Mediterranean, however, increases in phosphate activity are mainly related to river-runoff and sediment supply (Béthoux et al., 1998). It is unusual that high Ba content is not recorded in this event, only a very short frequency, initial spike being recorded in the Ba/Ca profile. Alibert et al. (2003) and Montaggioni et al. (2006) both found that Ba/Ca ratios in modern near shore corals are related to the sediment load of rivers which discharge into the coastal zone, such that discrete peaks in Ba/Ca coincide with flood events, masking the normal temperature related signal. As all the elements that record this event are those common in both detrital sediments and organic matter (especially P and K), it suggests that during 2007 an event introduced larger than normal volumes of both inorganic and organic detritus into the shallow marine environment around Croatia.

If this signal was found in an ancient sample without other supporting information, the cause of an increased sediment discharge event would be rather ambiguous. However, for this recent sample there are reliable supporting historical records. During the late summer of 2007, following a particularly long heat wave in Southern and Eastern Europe, widespread wildfires burned through coastal regions of Croatia affecting a total area of 1590km[2] (BBC, 2007; U.S. Agency for International Development, 2007; CRED, 2009) It is well known that after fires have destroyed vegetation, terrestrial sediments are destabilised. This means that during the following rainy season(s) water runoff

and erosion of soils was enhanced. This effect will last until the hinterland vegetation is re-established, which can take years (e.g. Abram et al., 2003).

Increased sediment supply due to increased soil erosion following the 2007 wild fires fits very well with the trace elemental data from this sample. Further evidence for this is the presence of organic, woody matter (possibly charcoal) preserved embedded in the inner edge of the corallite wall of PK 21/09/12-01, Figure 6.2.8. This is only present at one horizon in the corallite at approximately 21.5mm from the base; within error this is the right place to be entrapped debris from the 2007 fires.
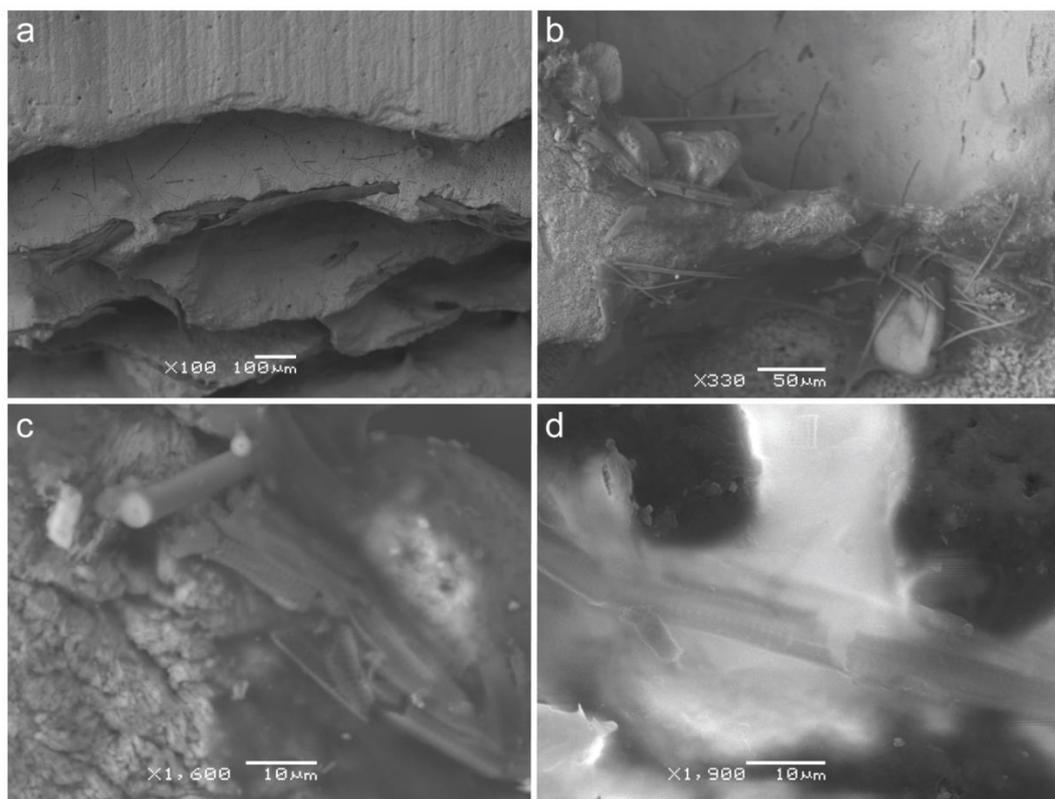
Figure 6.2.8 PK 21/09/12-01, secondary electron images of organic detritus at various magnifications. (a) Twig fragments embedded in the corallite wall, (b-d) smaller woody tissues. Only d is gold-coated, the rest were imaged under low vacuum due to difficulties with applying an even covering of gold to the complex microstructure of the corallite.

In both the Mg and (inverse) Sr traces in all samples, except PK 21/09/12-01(II), the peak believed to correspond to the summer of 2007 is a high, broad peak

with little variation compared to other years. This suggests that this was a (relatively) long, hot summer with water temperatures kept consistently high for the whole season, consistent with reports of the long heat wave which preceded the fires (BBC, 2007; Wikipedia, 2007).

This demonstrates the potential for coastal corals to be used as palaeo-fire indicators, although other events could lead to a similar increase of soil erosion and sediment and organic detritus input into the sea, for example increased periods of rainfall and flooding. Without the presence of the charcoaled wood fragments, preserved within this sample, it could be difficult to tell what the causal event was. This event is not recorded in the other samples from the colony, which suggest corallite growth position was key; presumably corals that did not record the event grew in less turbid areas, sheltered from the increased sediment flux. As the 'spike' is not recorded in other corallites, there is the possibility that it is an analytical artefact, potentially produced by a fluctuation in the energy of the laser. However, due the observation of detritus embedded in the corallite wall (under SEM) at approximately the same position as the 'spike' is recorded, it is believed that this is a real phenomenon recording the wildfire event.

6.2.4.2. Indicator of preservation quality

These modern samples were all very well preserved, with SEM images (Figure 6.2.9) showing no syndepositional marine cement growth (cf. Montagna et al., 2007). This was observed in other modern samples from the Gulf of La Spezia, Italy (Figure 6.2.10) however these were not analysed further.

Such syndepositional marine aragonite cementation precipitated within skeletal cavities is important to quantify as it typically has significantly higher average Sr/Ca and U/Ca than coralline skeletal aragonite (e.g. Cohen and Hart, 2004; Montaggioni et al., 2006): growing corals appear to discriminate against uranium and strontium incorporation, while marine cements, which form either syndepositionally or subsequently while the coral is immersed in seawater (Montagna et al., 2007) are not biologically controlled and so are significantly enriched in uranium (Gvirtzman et al., 1973). The presence of marine aragonite cements may thus significantly change derived SST towards cooler temperatures (Montaggioni et al., 2006; Sayani et al., 2011) as Sr/Ca and U/Ca ratios are negatively correlated with temperature.
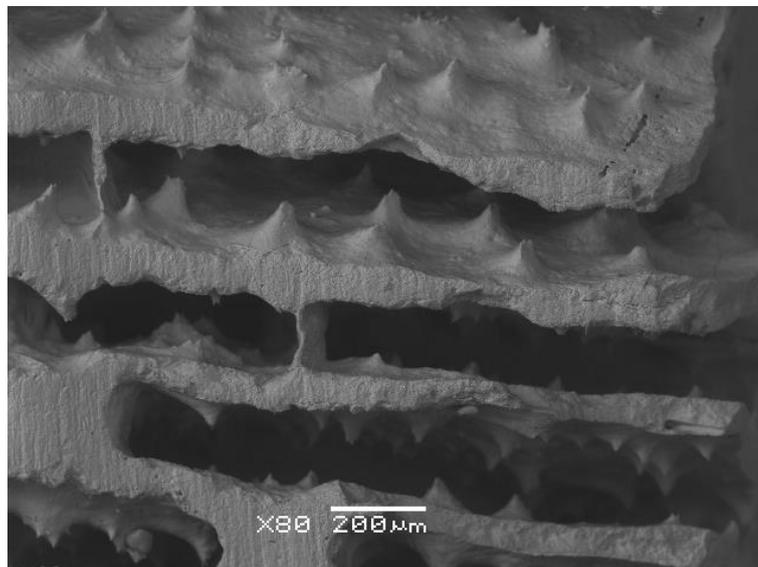
Figure 6.2.9 Septal region of modern Croatian *C. caespitosa*, pore spaces free of syndepositional cement growth and no signs of alteration (uncoated secondary electron image)
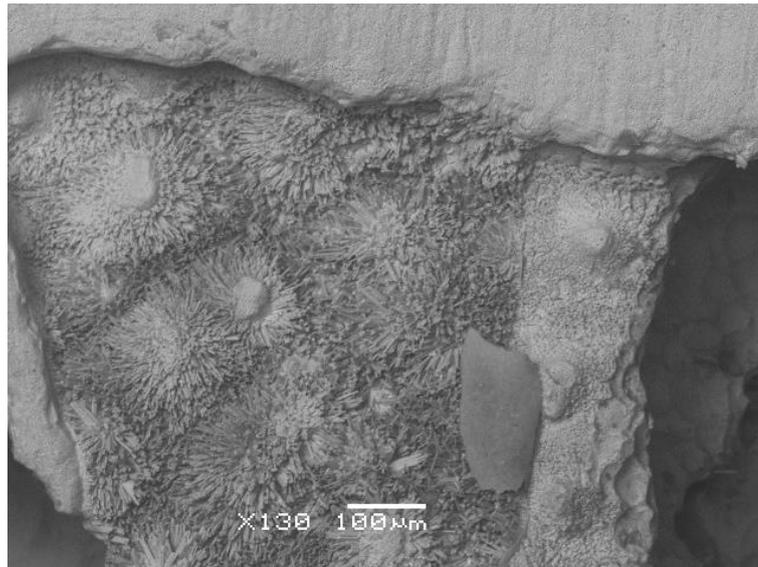
Figure 6.2.10 Radial syndepositional marine aragonite cements in a modern Italian *C. caespitosa*; secondary electron image, uncoated.

As no cements were found, however, the geochemical profiles in the modern Croatian samples are interpreted as original signals recorded at the time of growth. This need not be the case for fossil or sub fossil samples which may have typically had many thousands of years exposed to percolating meteoric waters or exposed in the marine supratidal splash zone where open system conditions allow elemental remobilisation, partial dissolution and cementation, collectively termed 'stabilization'.

Depending on the properties of the particular element, there are a number of ways in which trace elements become incorporated into coralline skeletal aragonite, some of these more stable than others. Trace elements are incorporated by substituting for Ca^{2+} ions in aragonite (Finch and Allison, 2007), however, they need not be lattice-bound, instead forming organo-metal complexes or being adsorbed onto crystal faces (Amiel et al., 1973). Trace elements may co-precipitate with the aragonite by occlusion, being trapped in crystal defects or micro-domains (Sinclair, 2005). Small trace-element enriched organic or inorganic particles may also become trapped between skeletal

spines when stresses cause coral tissue to retract (Brown et al., 1991). Those elements (such as Mg) which are only bound loosely in the aragonite crystal lattice will be more easily affected by diagenesis (Silenzi et al., 2005); original geochemical trends will thus potentially be lost by redistribution of the weakly-bound trace elements during stabilization. Even elements held securely within the crystal lattice can be affected by alteration and stabilization.

The (relatively) quick, inexpensive and non-destructive LA-ICP-MS analysis of fossil and sub-fossil coral samples is therefore be a robust way of testing corallites for significant levels of alteration, before using them for dating or other analytical purposes. Because of this, the collected LA-ICP-MS data from fossil corals (below) is focussed on testing their preservation quality and the subsequent robustness of any palaeothermometry and wider environmental signals such as detrital input.

6.3. Fossil Greek samples – trace elemental results and discussion

Fossil *C. caespitosa* corallites were selected to provide a range of preservation qualities and ages to test how the cyclic signals seen in modern corals might degrade over time with alteration of the corallite. The Greek fossil corallites examined were: an obviously altered MIS 5e sample JEA 010626-04 from Goat Point; two (visibly) well preserved MIS 5e samples SHR 02/11/11-08(II) and SHR 04/11/11-10 from West Makrugoaz Ridge and West Flagnoro Bay respectively; two (visibly) well preserved MIS 7a samples, SHR 02/11/11-02 (I) and (II) from Lake Vouliagmenis (see Table 3.2.1 and Figure 3.1.4 for locality details). The average trace element concentrations measured and types of trends shown are summarised in Table 6.3.1; the majority of samples do

preserve annual scale cyclicity in Sr, Mg, B, Ba and U as seen in the modern corallites.

The number of each corallite's seasonal growth band pairs were compared against the number of cycles (if any) in the Sr and Mg profiles, and if these numbers were similar (±1) then it was assumed that annual cyclicity was preserved and the profile was set to a time series in the same way as the modern samples (see above). If there was no annual scale cyclicity present in Sr or Mg then it was necessary to attempt to set the trace element profile to a time series by attempting to match up the distances along the ablation transect with the spacings of the growth bands, assuming each growth band was representative of the same period of time (5 months for the winter, recessed, bands and 7 months of the summer, pronounced, bands (Peirano et al., 1999)). This is a much more time consuming and less accurate method; the individual bands are often not very distinct, they are hard to measure and the transect was not always completely parallel to growth direction (as holes and bends had to be compensated for), introducing error in the time series.

Table 6.3.1 Summary of the average trace element concentrations and main trends of trace element distribution in selected LA-ICP-MS analysed fossil Greek *C. caespitosa* samples. Concentrations are shown as ratios of trace element/^{43}Ca (varying units shown in table) after calibration to 100% aragonite (CaCO$_3$) using internal standard ^{43}Ca = 38%. Mg and Sr are highlighted as they are the trace elements this study is most interested in. Key to trend abbreviations: A.S.C. = Annual Scale Cyclicity, the following number shows number of cycles recorded, (N.) shows that the annual signal is noisy; S.C. = Some Cyclicity, a degree of an original cyclicity has been preserved; L.T.G. = Long Term Gradient, the signal is dominated by an overall increase or decrease in the signal; H.F.N. = High Frequency Noise (i.e. no obvious trend).

Element	SHR 02/11/11-08(II)		SHR 04/11/11-10		SHR 02/11/11-02(I)		SHR 02/11/11-02(II)		JEA 010626-04	
	Conc.	Trend	Conc.	Trend	Conc.	Trend	Conc.	Trend	Conc.	Trend
^{7}Li (μmol/mol)	73.82	H.F.N.	104.87	H.F.N.	7.00	H.F.N.	3.82	H.F.N.	29.81	H.F.N.
^{11}B (mmol/mol)	0.81	A.S.C. 8	0.93	A.S.C. 8	1.02	A.S.C. 7	1.00	A.S.C. 8	1.08	S.C. 6/7
^{23}Na (mmol/mol)	25.61	H.F.N	31.18	H.F.N.	16.70	S.S. 6/7	13.67	H.F.N.	24.56	L.T.G.
^{24}Mg (mmol/mol)	4.37	A.S.C. 8	5.14	A.S.C. 8	5.82	A.S.C. 7	5.97	A.S.C. 8	4.98	H.F.N.
^{27}Al (mmol/mol)	-	-	-	-	-	-	-	-	0.07	H.F.N.
^{31}P (mmol/mol)	0.25	H.F.N.	0.34	H.F.N.	0.20	H.F.N.	0.09	H.F.N.	0.22	H.F.N.
^{39}K (mmol/mol)	0.23	H.F.N.	0.32	H.F.N.	0.54	H.F.N.	0.45	H.F.N.	0.48	H.F.N.
^{55}Mn (mmol/mol)	0.01	H.F.N.	0.01	H.F.N.	-	-	-	-	0.04	H.F.N.
^{56}Fe (mmol/mol)	0.02	H.F.N.	0.21	H.F.N.	0.04	H.F.N.	0.03	H.F.N.	0.05	H.F.N.
^{65}Cu (mmol/mol)	-	-	0.01	H.F.N.	-	-	-	-	-	-
^{66}Zn (mmol/mol)	-	-	-	-	-	-	-	-	-	-
^{86}Sr (mmol/mol)	9.06	A.S.C. 8	7.97	A.S.C. 8	10.35	A.S.C. 7	10.65	A.S.C. 8	13.30	S.C. 6/7
^{135}Ba (mmol/mol)	0.04	A.S.C. 8	0.02	H.F.N.	0.02	A.S.C. 7	0.03	H.F.N.	0.06	S.C. 6/7
^{238}U (μmol/mol)	1.06	A.S.C. 8	0.69	A.S.C. 8	0.02	A.S.C. 7	2.04	A.S.C. 8	1.80	L.T.G. 6/7

6.3.1.   Well preserved samples – MIS 5e and MIS 7a

Samples as old as 225 ka still preserve clear annual-scale signals in Sr and Mg,

as shown in Figure 6.3.1 to Figure 6.3.4.
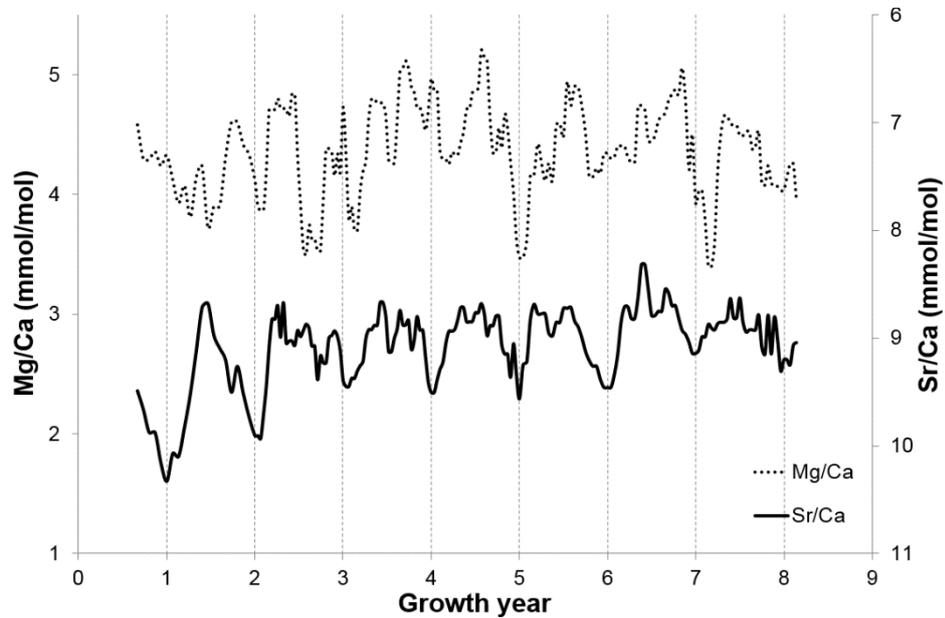
Figure 6.3.1 SHR 02/11/11-08(II), Mg/Ca and Sr/Ca profiles through MIS 5e corallite showing clear, annual-scale cyclicity
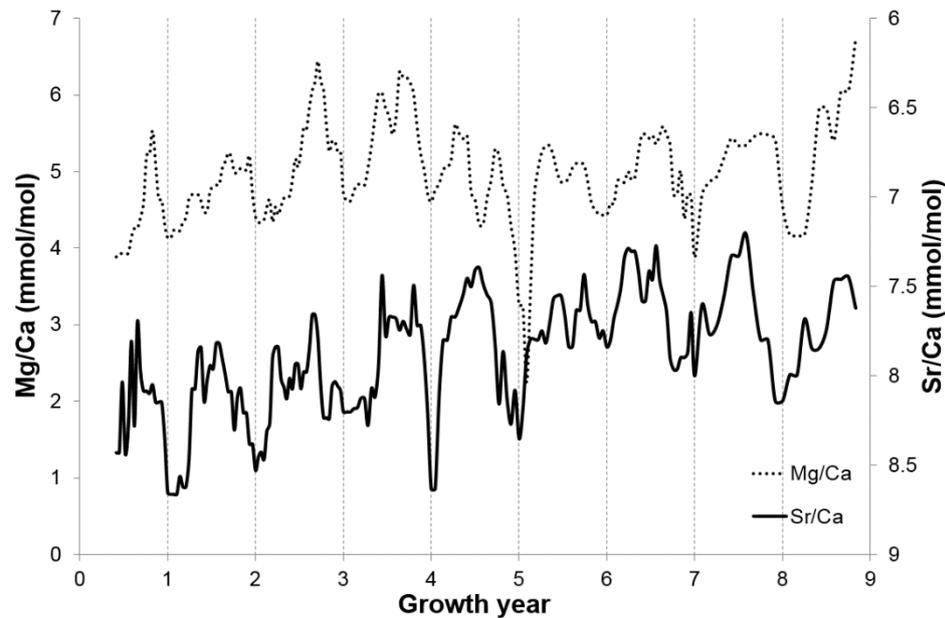
Figure 6.3.2 SHR 04/11/11-10, Mg/Ca and Sr/Ca profiles through MIS 5e corallite showing clear, annual-scale cyclicity
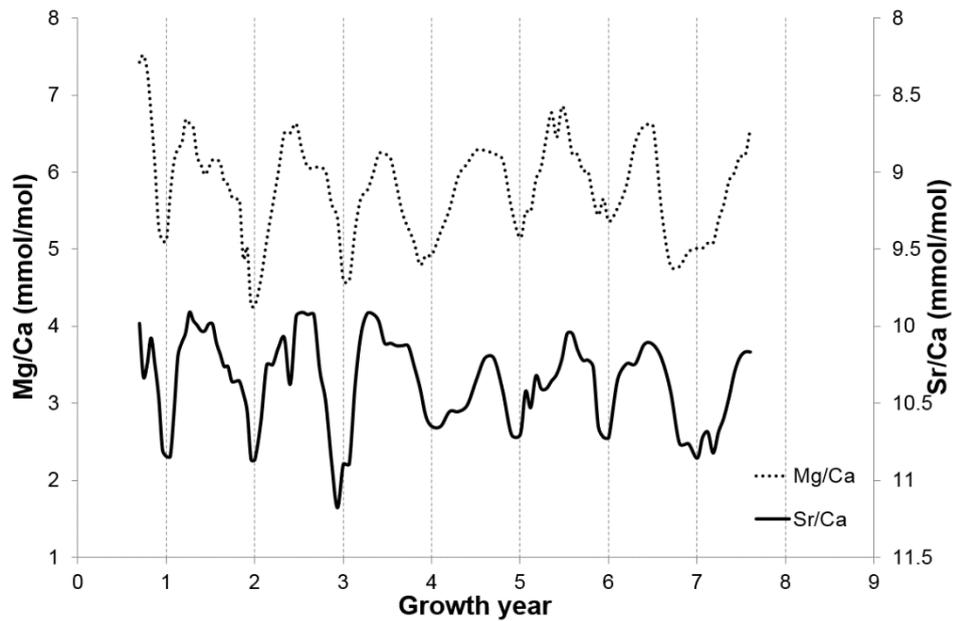
Figure 6.3.3 SHR 02/11/11-02(I), Mg/Ca and Sr/Ca profiles through MIS 7c corallite showing clear, annual-scale cyclicity
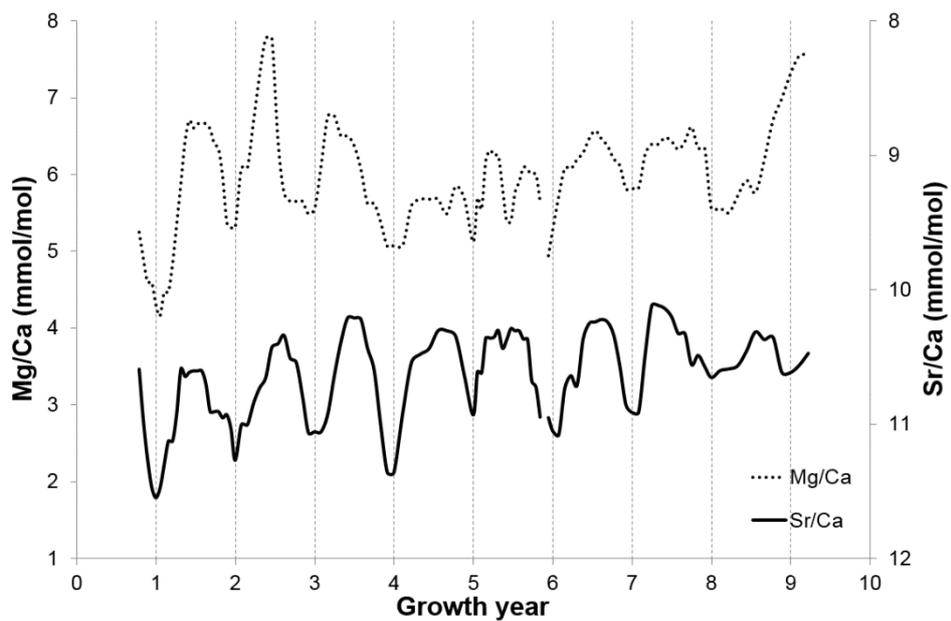
Figure 6.3.4 SHR 02/11/11-02(II), Mg/Ca and Sr/Ca profiles through MIS 7c corallite showing clear, annual-scale cyclicity

The clear annual-scale cyclicity and similar values and ranges in the data in these fossil samples to the modern samples show they are still preserving their original geochemical signature: this is supported by well-preserved aragonite skeletal crystals visible in SEM images (Figure 6.3.5). This should make them

173

candidates for providing reliable U-Th dates, as it is often difficult to identify

reliable, unaltered, material by other methods.
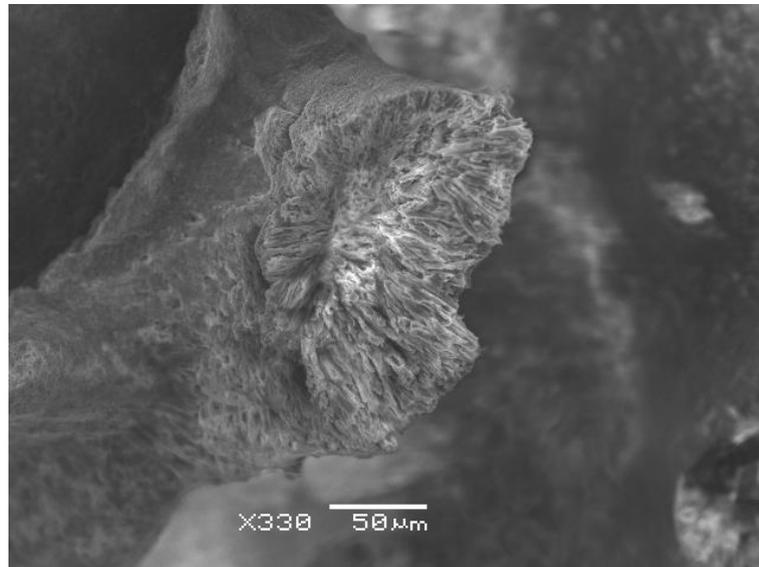
Figure 6.3.5 Well preserved acicular aragonite exposed in broken septa in MIS 5e *C. caespitosa* sample SHR 02/11/11-08(II) confirms lack of diagenetic alteration; gold coated secondary electron image.

6.3.2.   Altered sample – MIS 5e
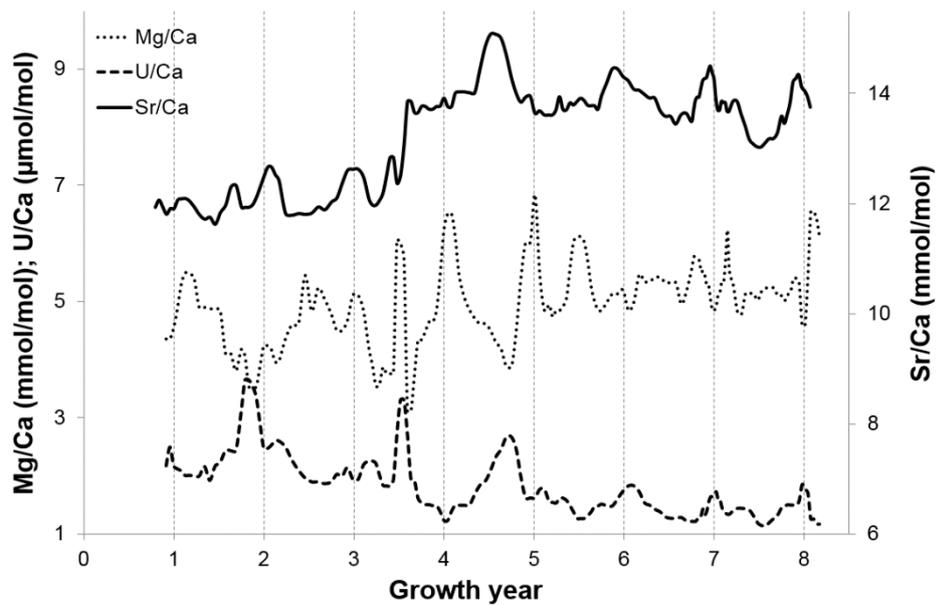
Figure 6.3.6 JEA 010626-04 Mg/Ca and Sr/Ca profiles through MIS 5e corallite showing hints of annual-scale cyclicity, however this is mostly lost in apparently random, higher frequency 'noise'. U/Ca is also shown for comparison with Sr/Ca.

The complexities of the trace element/Ca trace (Figure 6.3.6) for this sample are probably an example of complex partial alteration in a coral with an unusually complex post-depositional history. The sample was collected at about 5 m modern elevation in the modern seawater splash zone. Based on regional uplift models (Leeder et al., 2005; 2003), Figure 6.3.7, Figure 6.3.8, the fossil was probably emergent for 20-30 ka after death (at about ~125 ka), before being re-immersed in seawater during the sea-level highstands of MIS 5c and 5a, due to ~20m down-throw from local faulting (Figure 6.3.8; J. Andrews pers. comm.). Following 5a the coral became emergent again during the lowstands of MIS 2 and 3, but situated close to sea-level (and thus in the marine splash zone) during the 7 thousand years as Holocene sea-levels approached modern elevations. The local down-throw associated with faulting is key as this allows this sample to be re-emerged in seawater twice during its history and to be situated close to modern sea level throughout the Holocene.
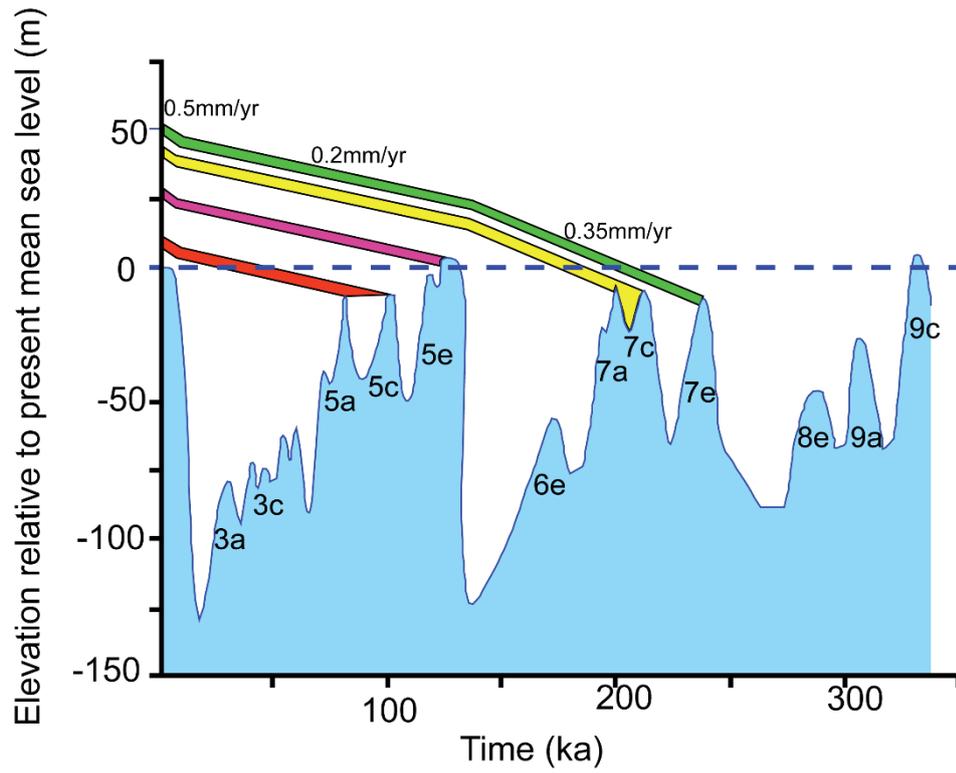
Figure 6.3.7 Eustatic Sea level curve adapted from Leeder et al. (2003) showing changing rates of uplift experienced by the marine terraces of the Perachora Peninsula relative to modern sea level
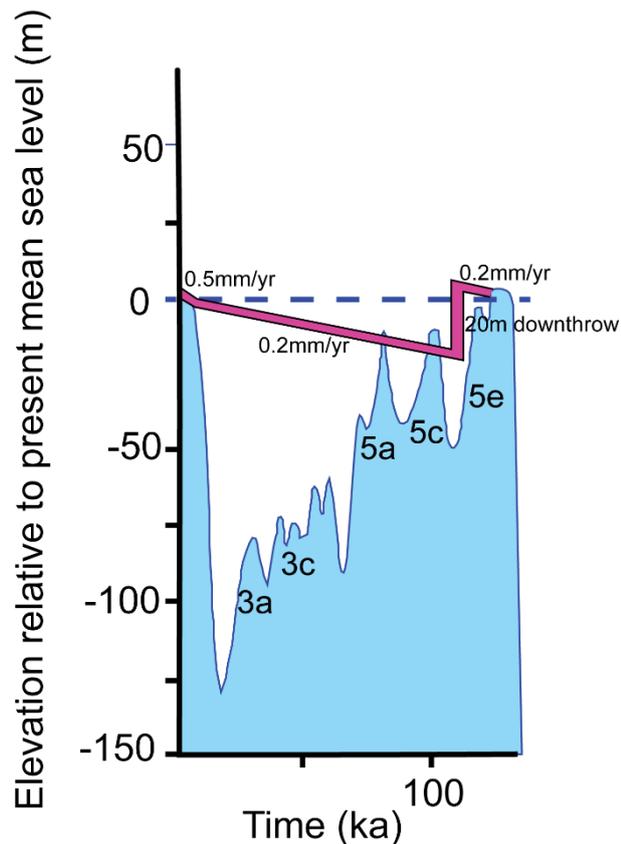
Figure 6.3.8 Post depositional history diagram for the MIS 5e sample JEA 010626-04 from Goat Point. This deposit was downthrown ≈20m between 5e and 5c (based on field relationships) before uplift recommenced. Because of this the corals were re-submerged during the highstands of MIS 5c and 5a, exposed to the splash zone throughout the Holocene and to meteoric fluids during other times, a partially open system where stabilisation to calcite may have occurred during any of these situations.

Annual scale cyclic trends in Mg/Ca and U/Ca for the first two growth years of this coral decrease in amplitude thereafter, with the overall Mg/Ca content increasing and the trend completely disappearing into 'noise' for the rest of the record. The cyclic trend of Sr is noisy in growth years 1 and 2 and then shows increased Sr content thereafter. Partial stabilization of aragonite to calcite explains the Mg data, the younger part of the coral having been partially stabilized from aragonite to calcite with concomitant accommodation of Mg in calcite. This is supported by the range of levels of diagenetic calcite in the SEM images, going from regions of (visibly) unaltered primary aragonite through to complete replacement by calcite (Figure 6.3.9 and Figure 6.3.10). The Sr and U data could reflect partial stabilization following episodes of marine diagenesis

(see diagenetic history above) when immersion allowed precipitation of marine

aragonite cements with higher Sr/Ca and U/Ca than the skeletal aragonite (e.g.

Cohen and Hart, 2004; Montaggioni et al., 2006) however, no aragonite

cements were seen under SEM. Instead, it is suggested that the Sr and U data

may simply show that partial alteration was not fully open-system leaving calcite

domains where Sr and U liberated from the dissolving aragonite, were forced to

be accommodated.
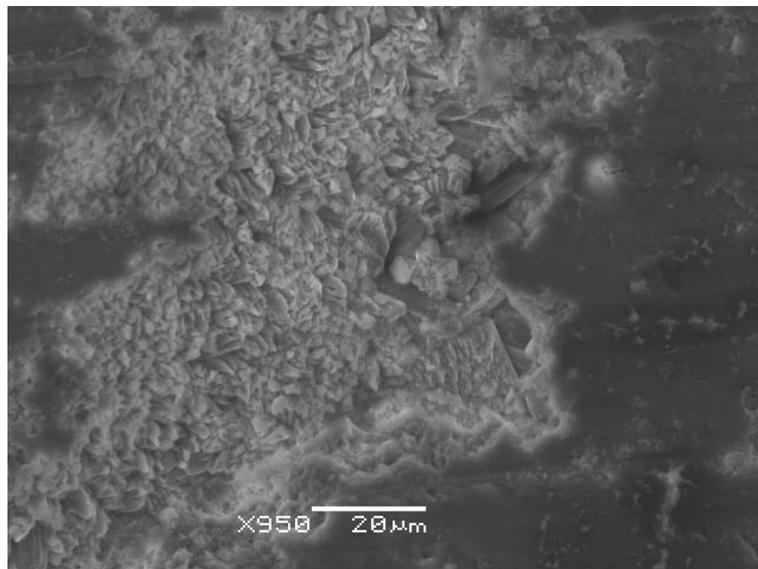
Figure 6.3.9 *C. caespitosa* sample JEA 010626-04 showing partially altered corallite wall, mostly made up of acicular aragonite crystals but blocky calcite crystals are also present, gold coated secondary electron image

Figure 6.3.10 Uncoated BSEM image of JEA 010626-04 showing patch of corallite wall completely altered to blocky calcite crystals

6.4. Conclusions

6.4.1. Potential of this technique for palaeoclimate research

As there is so much inter-site variability in the modern samples, it is concluded that there is little potential for the trace elemental composition of *C. caespitosa* to be used as a high resolution palaeothermometer. However, it is shown that original depositional geochemical signatures can be preserved in corallites up to at least MIS 7a age, with the conditions that the corallite is exposed to (e.g. time in the splash zone) being more important for preservation than age alone.

Partial alteration of the corallite wall (apparently due to prolonged exposure in the marine splash zone) to calcite and the growth of secondary cements destroys original cyclic signals. Therefore analysis of samples by LA-ICP-MS to identify the presence of annual scale cyclicity could be a quick way of testing

preservation quality, allowing the selection of corallites for U-Th dating which requires unaltered material.

A solitary modern sample (PK 21/09/12-01), shows that there is potential for these corals to record singular events of sediment discharge, in this case linked to fires but also including floods However, as this was only seen in one sample from the bank, and each corallite analysed only records a few years of growth, it would be lucky to find evidence for these rare events in the fossil record.

6.4.2.   Comparisons with the findings of Montagna et al., 2007

Montagna et al. (2007) concluded that '*C. caespitosa has the potential to provide an important new archive of high-resolution climate variability in the Mediterranean Sea*'. The authors reach this conclusion after finding close relationships between the trace element concentrations of B, Ba, Sr, U and (to a lesser extent) Mg in 6 years' worth of growth of a solitary corallite with weekly-fortnightly *in situ* measured SST. This study finds the strongest correlation with SST to be with boron, claiming it not to be affected by changes in salinity or river run off, while U and Ba are more affected by river runoff.

In contrast, the current study finds, from analysing multiple corallites, that there is too much intra-site variability in the geochemical composition of corallites for their use as archives of high-resolution climate variability in the Mediterranean Sea. Clearly SST controlled cycles in trace element composition, for the same elements as in the work of Montagna, were found in all samples. If each sample was taken separately then it would be concluded that there was promise for this species as a palaeoenvironmental archive. However, when looked at together,

there are large differences in both the absolute concentration and range of concentrations of trace elements between samples which grew on the same bank, under (presumably) identical climatic conditions. This shows the importance of analysing multiple samples before making an assumption that all will give the same results; the uptake of trace elements by the growing coral clearly has an unpredictable metabolic control or vital effect (discussed in more detail in Chapter 7.1).

7. Discussion & Review

In this chapter I discuss the findings of this study, focusing on complications arising from disequilibrium precipitation in coralline aragonite.

7.1. Disequilibrium calcification in *C. caespitosa*

The modern samples of *C. caespitosa* aragonite were calculated to be depleted (from equilibrium values) in $\delta^{18}O$ by an average $\approx 3.5‰$ and enriched in Δ_{47} by 0.07‰ using the UEA calibration. This apparently negative relationship in disequilibrium between Δ_{47} and $\delta^{18}O$ must be caused by a 'vital effect' (Weber and Woodhead, 1972).

7.1.1. Coral Calcification

To be able to properly discuss the potential mechanisms that cause the observed disequilibrium calcification, it is first necessary to review how corals form their aragonite skeleton.
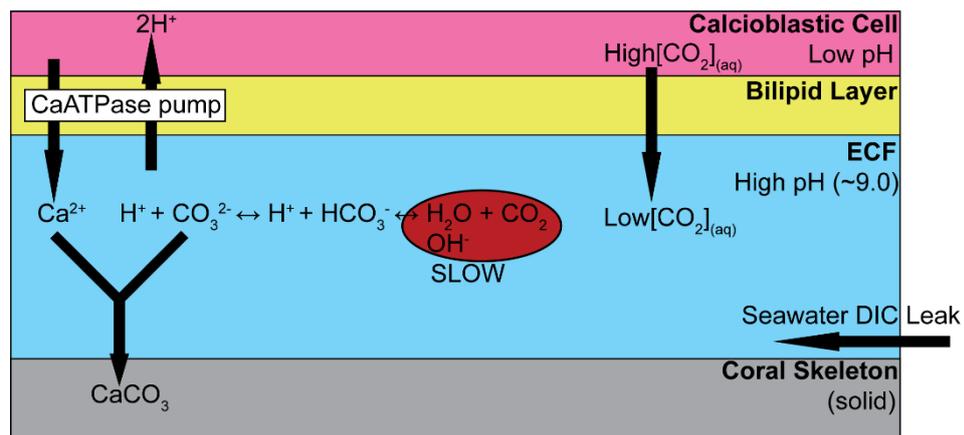
Figure 7.1.1 Simplified schematic diagram of coral calcification (modified from Saenger et al., 2012 and Adkins et al. 2003). See text for a detailed explanation. Not to scale.

All coralline skeletal solids calcify from a closed, or semi-enclosed extracellular calcifying fluid (ECF) located between the existing skeleton and the coral's

calcioblastic membrane (Cohen and McConnaughey, 2003; Adkins et al., 2003; Saenger et al., 2012) (Figure 7.1.1). Therefore all $CaCO_3$ is deposited in association with the calcioblastic tissue and so is organically mediated (Ghosh et al., 2006). At seawater concentrations, calcium becomes supersaturated in the calcifying space via a Ca-ATPase enzyme pump that actively expels two hydrogen protons for each Ca^{2+} pumped in across the membrane; Figure 7.1.1. This removal of H^+ also increases pH at the calcification site, to significantly alkaline values, ≈ 9.0 (Holcomb et al., 2009), causing a shift in dissolved organic carbon (DIC) speciation from HCO_3^- to CO_3^{2-}, further increasing the aragonite saturation state of the ECF (Cohen and McConnaughey, 2003). The removal of H^+ from the calcification site reduces the partial pressure of CO_2 within the ECF, initiating a net diffusion of respired $CO_{2(aq)}$ across the permeable calcioblastic membrane (McConnaughey, 1989) into the calcifying space. This metabolic CO_2 reacts with H_2O and OH^- to produce more HCO_3^- and CO_3^{2-} via hydration and/or hydroxylation reactions (Cohen and McConnaughey, 2003; Saenger et al., 2012):

Hydration: $CO_2 + H^2O \leftrightarrow H_2CO_3 \leftrightarrow H^+ + HCO_3^- \leftrightarrow H^+ + CO_3^{2-}$
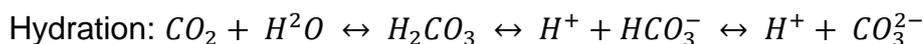
Equation 7.1.1. Hydration reaction forming carbonate ions in coralline ECF

Hydroxylation: $CO_2 + OH^- \leftrightarrow HCO_3^- \leftrightarrow H^+ + CO_3^{2-}$
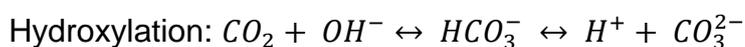
Equation 7.1.2. Hydroxylation reaction forming carbonate ions in coralline ECF

Also, as the calcifying space is not a perfectly closed system, additional seawater DIC may leak into the calcifying space (see Figure 7.1.1); an additional carbon source to react (Saenger et al., 2012). This calcification

mechanism has the potential to produce very high aragonite supersaturations in the ECF (Cohen and McConnaughey, 2003).

7.1.2.   Potential mechanisms for isotopic vital effects

There are numerous steps in the model for the precipitation of coralline aragonite where vital effects could introduce disequilibrium and a number of explanations have been put forth for $\delta^{18}O$, $\delta^{13}C$, Δ_{47} and trace metal concentrations, based on this model.

7.1.2.1. Kinetic isotope effects

McConnaughey (1989a; 1989b) developed a kinetic explanation to explain the observed depletion from equilibrium values in both $\delta^{18}O$ and $\delta^{13}C$ in corals. This theory suggests that rapid precipitation of aragonite outpaces the rate that light metabolic CO_2 entering the ECF reaches isotopic equilibrium. In this system, equilibrium is attained through the back-and-forth hydration/dehydration and hydroxylation/dehydroxylation reactions of Equations 7.1.1 and 7.1.2. Exchange of oxygen isotopes between dissolved CO_3^{2-} and H_2O is slow at the high pH of the ECF and so this process takes hours to reach equilibrium (Cohen and McConnaughey, 2003). This is slow when compared to rates of precipitation so that CO_3^{2-} units in the aragonite crystal lattice are buried before they can isotopically equilibrate with H_2O. Due to discrimination against the heavier isotopes during hydration and hydroxylation this leads to lower skeletal $\delta^{18}O$ when coral growth is rapid (McConnaughey, 1989a; McConnaughey, 1989b; Saenger et al., 2012).

7.1.2.2. Equilibrium isotope effects

Through high resolution analysis of a deep sea coral, Adkins et al. (2003) found that $\delta^{13}C$ vs. $\delta^{18}O$ trends in coralline aragonite are linear until the lightest values where $\delta^{18}O$ continues to decrease but $\delta^{13}C$ does not change. This cannot be explained by the kinetic model as a change in slope of the $\delta^{13}C$ vs. $\delta^{18}O$ cannot be explained by a single kinetic fractionation process governing both isotopes. In addition, these authors argue that, the presence of the enzyme carbonic anhydrase (identified in corals by Ip et al., (1991)) ensures that the inorganic carbon system in the ECF is at equilibrium by catalysing the slow step in the precipitation reaction where bicarbonate is converted to $CO_{2(aq)}$.

To explain these discrepancies, Adkins et al., (2003) proposed a new model for oxygen isotopic fractionation (separate to that of the carbon isotopic fractionation which is not discussed here) where the level of oxygen fractionation is the result of the pH in the ECF. The $\delta^{18}O$ of precipitating carbonate solids shows a dependence on the pH of the solution it is precipitating from, solutions with a higher pH create more depleted $\delta^{18}O$ values in the precipitating carbonate (assuming all other variables are constant) (McCrea, 1950). This is because oxygen atoms in each of the separate DIC species (carbonate ion, bicarbonate ion and carbonic acid) have separate isotopic offsets from water. CO_3 is the lightest of these species, although all are more enriched than seawater, (Usdowski and Hoefs, 1993) and therefore solutions with higher CO_3^{2-} are isotopically lighter than more acidic waters. As the $\delta^{18}O$ of the carbonate solid formed is determined by the total number of ^{18}O and ^{16}O atoms attached to available DIC species and this number is dependent on the DIC speciation, then the $\delta^{18}O$ of the solid must be directly dependent on

the pH of the solution, which is at equilibrium with itself (Zeebe, 1999; Adkins et al., 2003). Less $\delta^{18}O$ depleted aragonite is deposited by the coral when the ECF DIC is dominated by normally fractionated seawater leaking in (Figure 7.1.1) and lowering the pH when calcification rates are low. At high calcification rates, the DIC of the ECF is dominated by isotopically light CO_2 that passively diffuses across the calcification membrane because of the large pH and diffusion gradients induced by the highly active Ca-ATPase pump (Figure 7.1.1). This increases the proportion of isotopically light oxygen from CO_3 and causes the aragonite $\delta^{18}O$ to be lighter, thus increasing the offset from equilibrium (Adkins et al., 2003).

7.1.2.3. Combined kinetic and equilibrium effects

Rollion-Bard et al. (2003a; 2003b) proposed a combination of the kinetic and equilibrium models to explain large changes in $\delta^{18}O$ that they observed at micrometre scale in coralline aragonite. Boron isotopic data was used as a proxy for pH and this, along with the pH levels corals can reach, does not allow for the very high pH levels the purely equilibrium model explanation (Adkins et al., 2003) calls for.

As with the equilibrium model, the authors use the pH control of both the relative concentrations of DIC speciation and the respective roles of hydration and hydroxylation reactions in the formation of bicarbonate. Because the kinetics of hydration and hydroxylation reactions are different, with the slower hydroxylation being the dominant reaction at high pH (Johnson, 1982), the rate that the system attains equilibrium is lower when pH is high; this brings a pH controlled kinetic control to attaining equilibrium in the system.

In this model, oxygen isotopic equilibrium between CO_3^{2-} – H_2O is reached in ≈1 hour at pH 7 but takes ≈12 hours at pH 9. Therefore, when the Ca-ATPase pump is highly active, creating a high pH and increasing the rate of calcification, the coralline aragonite preserves a $\delta^{18}O$ value farther from equilibrium, with the offset decreasing as residence time of DIC in the ECF increases/calcification rate decreases. As the activity of the Ca-ATPase pump and calcification rates are higher at times of increased photosynthesis (Rollion-Bard et al., 2003b; Al-Horani et al., 2003a; Rollion-Bard et al., 2011) then the activity of the photosynthetic zooxanthellae has a direct effect on the $\delta^{18}O$ of the coral skeleton, with greater offset from equilibrium in aragonite precipitated during the day than the night.

7.1.2.4. Application of a combined kinetic and equilibrium model to explain the observed disequilibrium in both Δ_{47} and $\delta^{18}O$

A combined kinetic and equilibrium model can also be applied to the Δ_{47} data as differences in clumped isotopic composition between DIC species could lead to pH effects in Δ_{47} as with $\delta^{18}O$ (Saenger et al., 2012). The carbonate ion is estimated to be lower in Δ_{47} than bicarbonate so that departures from apparent equilibrium due to increased pH should result in lower values in both $\delta^{18}O$ and Δ_{47}. pH increasing from 8 to 9, typical for coral calcifying fluid, should lower $\delta^{18}O$ by 3.7‰ and slightly decrease Δ_{47} by 0.01‰ (Saenger et al., 2012). This does not explain the positive Δ_{47} offset observed in the present study or others (Ghosh et al., 2006; Saenger et al., 2012) so a purely pH control is not the cause of the vital effect.

The $CO_2 - H_2O$ oxygen isotope exchange rate for Δ_{47} is similar to that for $\delta^{18}O$ (Affek and Ayalon, 2009; Affek, 2013) so that any $\delta^{18}O$ kinetic effects associated with incomplete DIC-H_2O equilibrium through hydration/dehydration and hydroxylation/dehydroxylation (Equations 7.1.1 and 7.1.2) should be accompanied by proportional Δ_{47} offsets with an increase of 0.01-0.05‰ for every 1‰ decrease in $\delta^{18}O$ (Guo et al., 2009b; Saenger et al., 2012). These hypothetical offsets are consistent with the range observed in both the current study and by Saenger et al., (2012) suggesting that this may be the primary cause of Δ_{47} offsets in hermatypic corals.

As hydration/hydroxylation kinetics only influence metabolic CO_2, any influence of this effect on Δ_{47} would depend on the ratio of metabolic CO_2 to seawater DIC in the calcification space (Saenger et al., 2012). As fast growing hermatypic corals gain the majority of their skeletal carbonate from metabolic CO_2 (Adkins et al., 2003), this will increase the positive Δ_{47} and negative $\delta^{18}O$ offsets when the rate of calcification is faster than DIC equilibration. Therefore slower growing corals, with longer DIC residence times, will have smaller offsets.

In the presence of the enzyme carbonic anhydrase, experiments have shown that, isotopic equilibrium between $CO_2 - H_2O$ can be reached in approximately 20 minutes at pH 8 compared to approximately 3 hours at pH 9 (Uchikawa and Zeebe, 2012), as the residence time of calcifying fluid can be anywhere between 30 minutes and 12 hours (McConnaughey, 1989b) kinetic effects could allow for the observed offset even in the presence of carbonic anhydrase (Saenger et al., 2012). Differences between the observed Δ_{47} offsets between

the *C. caespitosa* (of this study) and the *Porites* (of Saenger et al. (2012)) could therefore be caused by inter-species differences in CA activity and/or ECF DIC residence times caused by differences in Ca-ATPase activity and calcification rate.

Therefore, a growth rate controlled combination of differing ECF pH (which leads to negative $\delta^{18}O$ without impacting Δ_{47} significantly) and ratios of hydration/hydroxylation reactions (which underestimates $\delta^{18}O$ depletion relative to the observed Δ_{47} offsets) may lead to species-specific (or potentially site-specific if growth rate is significantly different) Δ_{47} offsets, this agrees with the conclusions of Saenger et al. (2012).

7.1.3.   Differences in trace element concentration

The large intra-site variation in the trace element concentration of the modern samples of *C. caespitosa* may also be explained by differences in growth rate and photosynthetic activity. Due to it being the most commonly studied and most promising trace element for palaeothermometry, this discussion will focus on the strontium data. The majority of points can be applied equally to any trace element, although the transport pathways of other elements through the calcioblastic membrane have been less well studied.

7.1.3.1. Strontium incorporation into coralline aragonite

Experiments have shown that strontium incorporation into aragonite is inversely related to temperature (Kinsman and Holland, 1969; Rimstidt et al., 1998); however, studies have shown that in corals the average slope of the Sr/Ca – SST relationship is twice that for inorganic aragonite precipitating at equilibrium (Weber, 1973; Cohen et al., 2002).

Experiments with inhibitors and saturation levels have shown that strontium ions are transported to the calcifying space both actively, sharing the Ca-ATPase pathway with Ca^{2+} (Ferrier-Pagès et al., 2002; Cohen and McConnaughey, 2003) and passively as seawater leaks into the calcifying space (Ip and Krishnaveni, 1991) so that the incorporation of Sr is partially biologically mediated Figure 7.1.2b.

7.1.3.2. Kinetic controls on Sr/Ca; Ca-ATPase and photosynthesis

Along with this study which has found wide variation in Sr/Ca, other work has shown that there is considerable inter-colony variation in slopes and intercept values of the Sr/Ca – SST calibration for different species, the same species at different localities (see Table 2.5.1) and the same species at the same locality (de Villiers et al., 1994). This inter and intra-species and even intra-site variation suggests that there is some control other than just temperature on the vital effect.

Some sort of kinetic control linked to growth rate (Cohen et al., 2001) has been established as the most likely cause for the different degrees of vital effects

observed. This is because faster growing corals have been observed to have lower skeletal Sr/Ca than slower growing corals at the same site (de Villiers et al., 1995; Goodkin et al., 2007) and within a single colony low density skeleton has a higher mean Sr/Ca than higher density skeleton from the same aged growth horizon (Alibert and McCulloch, 1997).

As Ca-ATPase has a higher affinity for Ca than Sr (Yu and Inesi, 1995), when this pump is highly active, leading to higher calcification rates, the ECF will have a depleted Sr/Ca ratio compared to seawater (due to active discrimination of the Sr ion), Figure 7.1.2a. When the pump is switched off, or slow, then the ECF's Sr content will approach that of seawater due to passive diffusion of seawater into the calcifying space (Ip and Krishnaveni, 1991; Cohen et al., 2001)), Figure 7.1.2b.

The Ca-ATPase pump is activated by the exposure of the polyp to light, as ATP from photosynthesis is needed for this active ion transport, although it is light rather than just energy which triggers Ca^{2+} uptake (Al-Horani et al., 2003b; Al-Horani et al., 2003a). Corals with higher rates of photosynthesis will therefore have lower Sr/Ca values.
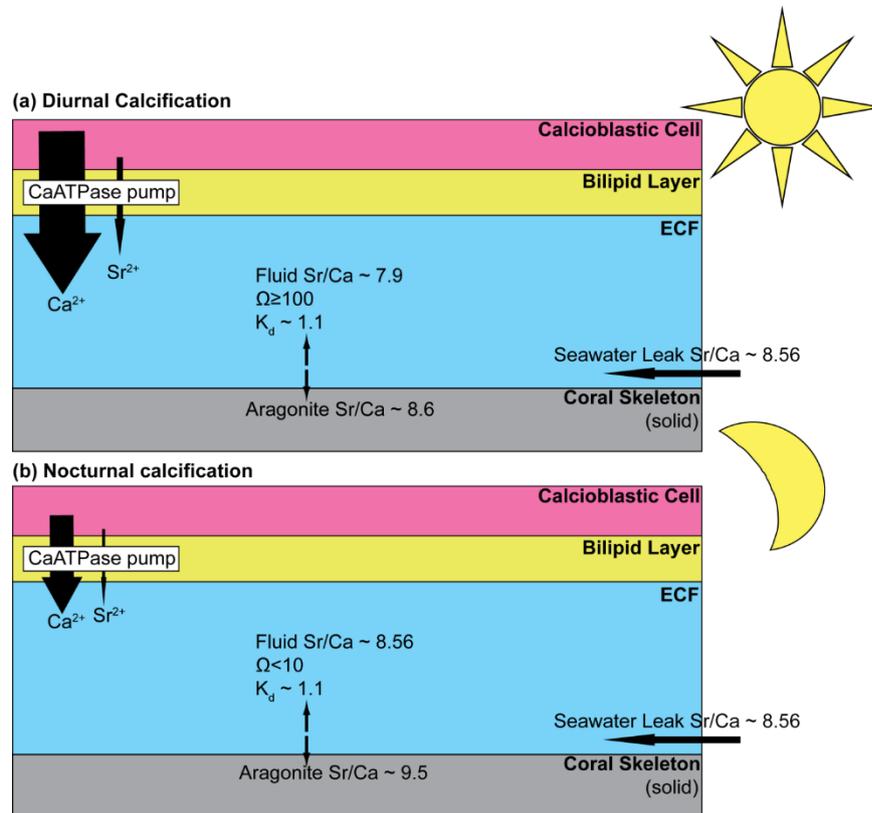
Figure 7.1.2 Simplified schematic diagram showing differing pathways for strontium ion uptake during coral calcification (modified from Adkins et al, 2003; Cohen and McConnaughey, 2003; Saenger et al., 2012). In (a) the Ca-ATPase pump is activated during the day by light, this leads to a highly fractionated Sr/Ca concentration between the seawater and the depleted extracellular calcifying fluid (ECF). Calcification rates are rapid and the precipitating aragonite is depleted in Sr/Ca compared to inorganic values (the fractionation factor for Sr into aragonite (Kd) >1 (Kinsman & Holland, 1969)). In (b) the Ca-ATPase pump is slow or switched off during the night, this leads to the Sr/Ca concentration in the ECF approaching that of the seawater by passive diffusion into the calcifying space. Calcification rates are slow and the precipitating aragonite Sr/Ca is approximately the same as what would be expected from inorganic values (the fractionation factor for Sr into aragonite (Kd) >1 (Kinsman & Holland, 1969)) Not to scale.

Increased photosynthesis may be caused by either being exposed to more light – in shallower, less turbid or less shaded patches of the colony - or because they have higher concentrations of/more active symbiotic zooxanthellae. It is conceivable that these variables could be different within one colony, for example if some corallites are shaded by the others, or change within a corallite over time if the coral grows out of shade, is shaded by other corals or plants, or if sediment input changes (*C. caespitosa* is quite tolerant of high levels of turbulence (Tremblay et al., 2011)).

Zooplankton biomass has been shown to be significantly different between different parts and at various depths on reefs (Alldredge and King, 1977) and so the differences in availability of this food source will also impact Sr/Ca levels. Night time calcification rate (when Sr and Ca are delivered to the ECF at near equilibrium levels due to the dominate transport process being passive (Figure 7.1.2)) are primarily controlled by the availability of zooplankton (Houlbrèque et al., 2003) as energy from the respiration of food is necessary to synthesise organic molecules (Al-Horani et al., 2003b) for the framework to calcify onto when photosynthesis is not an option.

Therefore, as well as a temperature control on the Sr/Ca content of the precipitating aragonite, there is also a growth rate control. This is controlled by rate of photosynthesis, which can itself be altered by temperature (Jacques et al., 1983), light levels and symbiont activity, and so greatly complicates any attempts at creating a universal calibration equation due to intra-site variability.

7.1.4. A combined kinetic vital effect

It appears that all of the observed issues with vital effects in the stable isotopes, clumped isotopes and trace elements can all be linked primarily to changes in the composition of the ECF due to complications brought about by varying degrees of photosynthetic activity altering the activity of the Ca-ATPase pump and in turn the growth rate of the corallite.
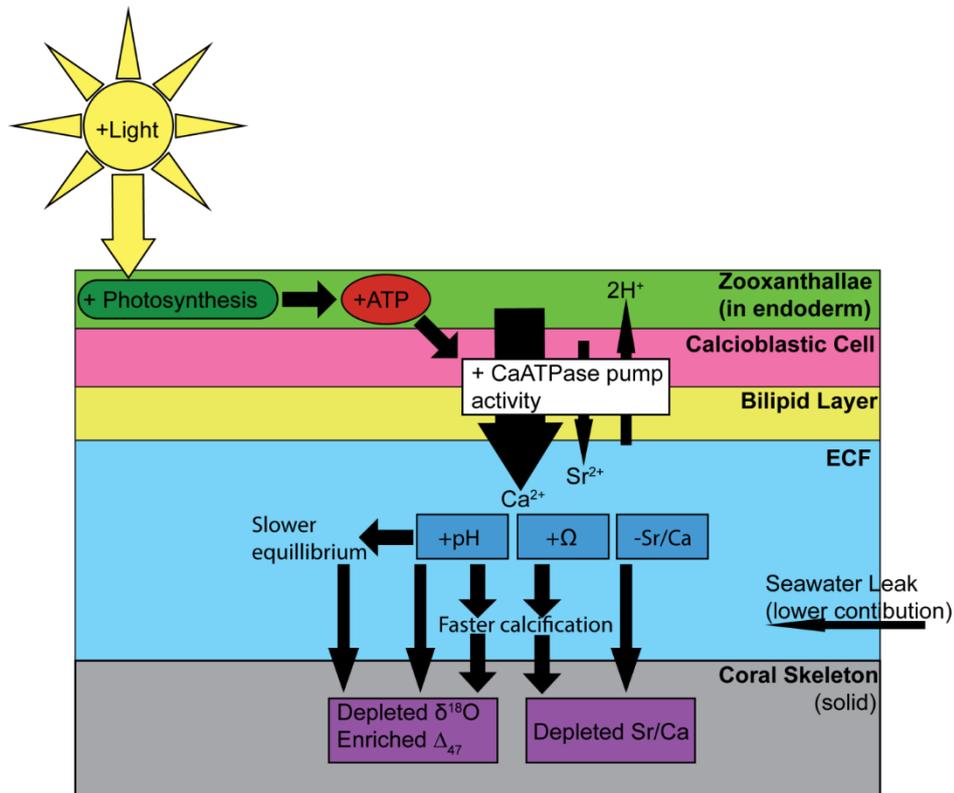
Figure 7.1.3 Flow diagram demonstrating how increasing light leads to increased 'vital effect' offsets from equilibrium values in oxygen isotopes, clumped isotopes and strontium concentration in the precipitating aragonite skeleton, full explanation in text. '+' and '-' denote an increase or decrease in rate, availability or value. Coral cell structure is greatly simplified, for example mesogloea is not shown between endoderm and calcioblastic cells for simplicity and diagram is not to scale.

A flow diagram summarising the steps leading to the varying vital effects observed in the offsets from equilibrium values for the isotopes and strontium concentrations is shown in Figure 7.1.3. As light is increased the rate of photosynthesis in the symbiotic zooxanthellae increases, this produces more energy (in the form of ATP) which fuels the Ca-ATPase ion transport pump. Active transport preferentially pumps Ca ions into the calcification space while discriminating against Sr ions and removing hydrogen ions. This increases the pH and saturation state of the ECF while decreasing its Sr/Ca ratio to lower than that of the seawater. The high pH fluid is dominated by the isotopically light carbonate ion (as opposed to heavier bicarbonate and carbonic acid ions). The higher pH slows the rate that the ECF can attain isotopic equilibrium by shifting

the dominant process of bicarbonate production to hydroxylation whilst also increasing calcification rate (along with the increased saturation state (Ω)) so that the fluid doesn't have time to equilibrate with the seawater. This biologically altered disequilibrium ECF composition, and the rate of precipitation of aragonite from it, is what leads to all of the observed vital effects. This explains the depleted $\delta^{18}O$ and enriched Δ_{47} (which are representative of the high pH ECF) and the depleted Sr/Ca which are representative of the values in the ECF.

7.2. Potential of *C. caespitosa* as a high resolution palaeoclimate archive

The high resolution analysis of the oxygen isotopes and some trace element (Sr, Mg, U, etc) compositions of the corallites returned clear, annual-scale cyclic variation which can be best explained as a seasonal temperature signal. These original depositional geochemical signatures are found to be preserved in corallites up to at least MIS 7a age, with the early diagenetic conditions that the corallite is exposed to (e.g. time in the splash zone) being more important for signal preservation than age.

While there was too much intra-site variation in the modern coral's trace element data to use this technique in any quantifiable way, it is apparently possible to identify major, discrete events that inject large quantities of sediment/organic matter into the seawater (such as fires or floods) where the corals are living, if those corals are exposed to the increased particulate matter. This could be used to look at the frequency of these types of events changing between different periods as increased fires would suggest greater aridity while increased flooding would indicate greater rainfall. Unfortunately with only finding

one sample with evidence of the 2007 Croatian wildfires it is not yet possible to distinguish between different types of event (aside from charcoal fragments embedded in the corallite wall as was found), further work on modern corallites from different localities may, however, allow this.

The modern coralline aragonite oxygen isotopes, while not in equilibrium with the seawater, suffered from much less intra-site variation than the trace elements. This allowed a species-specific aragonite-water $\delta^{18}O$ temperature calibration equation to be calculated, which appeared to be effective for estimating the ranges of temperature and isotopic compositions of the seawater when used in conjunction with constraints set out by the growth limits of *C. caespitosa* and previous work from the literature.

This suggests that, as long as some limits on absolute water temperature and/or water $\delta^{18}O$ can be set by other methods, this species can be used to look at high resolution palaeo-SST to infer changes in seasonality and climate between various interglacial periods.

7.3. Limitations and problems with using this species

7.3.1. Clumped isotopes

It was originally expected that the clumped data would provide definitive temperatures and water $\delta^{18}O$ compositions agreeing with the measured data for the modern Croatian samples and provide sensible values for the previous interglacials from the fossil samples, however, this field progressed throughout the course of the study, with the most recent work finding that disequilibrium occurs equally in both $\delta^{18}O$ and Δ_{47} (Affek, 2013) and corals generally show

disequilibrium in both (Saenger et al., 2012). The findings of this study agree with those of the most recent work. Both modern and fossil samples were depleted in Δ_{47}, resulting in the underestimation of growth temperatures. The level of offset from equilibrium values in the modern samples did however have a relatively low degree of intra-site variability between corallites. This means that a species specific Δ_{47} – temperature calibration may be possible, although not within the time constraints of the present study.

7.3.2. Trace element analysis

The wide degree of intra-site variability found in the trace element compositions of the modern samples means that there is little potential for the trace elemental composition of *C. caespitosa* to be used as a high resolution palaeothermometer. This is in contrast to the findings of Montagna et al. (2007) who concluded that '*C. caespitosa has the potential to provide an important new archive of high-resolution climate variability in the Mediterranean Sea*'. This shows the importance of analysing multiple samples before making an assumption that all will give the same results; the uptake of trace elements by the growing coral clearly has an unpredictable metabolic control or 'vital effect'.

7.4. Mediterranean palaeoclimate

7.4.1. Comparing the climate of previous interglacials with that of the modern

From the oxygen isotope data, it appears as though the current conditions in the Gulf of Corinth are approximately average for the interglacial periods of the last 225 ka. The warmest period studied was MIS 5e, which also had lower

seasonality than today and was (based on inferred seawater $\delta^{18}O$ values) probably the most arid. The Early-Mid Holocene probably experienced the coolest temperatures while conditions in MIS 7a/c, whilst most similar to today in terms of temperature, were probably the wettest with most freshwater input into the Gulf. These findings are in line with work carried out in other studies.

7.4.2. MIS 5e: A multi-proxy approach, bringing the high resolution *C. caespitosa* oxygen record and (non-coral) clumped isotopic data together

If the high resolution *C. caespitosa* $\delta^{18}O$ and the bulk average Δ_{47} data are looked at together, it appears as though some of the clumped data supports the findings of the high resolution study. *Pecten* sample SHR 02/11/11-07 (i) and aragonite sample JEA 10901-01 provided T(Δ_{47}) values of 24.1°C and 21.9°C and water compositions of 2.2‰ and 2.2‰ VSMOW; these values are within error of those calculated using the $\delta^{18}O$ data. Aragonite sample JEA 9508-01 gave a temperature of 20.4°C, but an anomalously low water $\delta^{18}O$ values. As all of the other *Pecten* and aragonite T(Δ_{47}) and $\delta^{18}O_{water}$ values were unfeasibly low, this good agreement between these calculated temperatures and water compositions and the $\delta^{18}O$ findings suggests that with time to get more replicates from well preserved MIS 5e *Pecten* shells similar values would be gained. With the observed spread in values being due to the small sample size (due to time constraints) and the relative newness of the clumped isotopic technique meaning that the method still needs refining to get consistent, fully reproducible data. It is, however, also possible that the mobile *Pecten* records slightly lower temperatures, not quite representative of SST, due to having

migrated to deeper, cooler waters during the hottest periods of the warm MIS 5e summer, while the conditions the aragonites precipitated in are not fully understood.

7.5. Future work

If there was time available to expand this study there are a few potential avenues of research that it would be interesting to explore.

7.5.1. Further clumped isotope work

As there was little inter-corallite variation in the offset from Δ_{47} equilibrium, it would be interesting to measure more modern corallites, that are known to have grown under varying temperature conditions, to attempt to produce a species-specific Δ_{47} – temperature calibration equation for *C. caespitosa* that could then be applied to the fossil samples.

The most important future clumped work, however, is to test the reliability of the MIS 5e *Pecten* data through replication and analysis of modern samples with known growth temperatures. If found to be accurate palaeotemperature and palaeo-$\delta^{18}O_{seawater}$ records as some of the data suggests, it would then be ideal to find and analyse *Pecten* samples from the other interglacials to further constrain conditions in those periods.

7.5.2. Further trace element work

While the trace element content of *C. caespitosa* was not found to be useful for high resolution palaeotemperature analysis, evidence of palaeo-fires, and presumably palaeo-floods, was found to be potentially well recorded. As

evidence for the 2007 Croatian wildfires was only found in a single corallite, it would be useful to analyse more corallites from Mljet – maybe more rapidly at a lower resolution – to show that this event was more widely recorded. If possible it would then be interesting to analyse corallites from an area where recent flooding has taken place, to see if the injection of increased sediment load from this type of event is also recorded and to see if the two types of event (fires and floods) can be distinguished from each other. This could be by the types of trace elements that are increased in the coralline aragonite and the actual shape of the signal in the element's profile – it could be expected that flood signals will show more discrete spikes than fires as the terrestrial sediment may be unstabilised for years after a fire until vegetation is fully re-established (Abram et al., 2003).

8. References

Abram N. J., Gagan M. K., McCulloch M. T., Chappell J. and Hantoro W. S. (2003) Coral reef death during the 1997 Indian Ocean dipole linked to Indonesian wildfires. *Science.* **301**, 952–955.

Adkins J. F., Boyle E. A., Curry W. B. and Lutringer A. (2003) Stable isotopes in deep-sea corals and a new mechanism for "vital effects." *Geochim. Cosmochim. Acta* **67**, 1129–1143.

Affek H. P. (2013) Clumped isotopic equilibrium and the rate of isotope exchange between CO2 and water. *Am. J. Sci.* **313**, 309–325.

Affek H. P. and Ayalon A. (2009) Kinetic effects in `clumped isotopes': application to Soreq cave speleothems. *AGU Fall Meet. Abstr.*

Aguirre J. and Jimenez A. P. (1998) Fossil analogues of present-day *Cladocora caespitosa* coral banks: Sedimentary setting, dwelling community, and taphonomy (Late Pliocene, W Mediterranean). *Coral Reefs* **17**, 203–213.

Al-Horani F. A., Al-Moghrabi S. M. and de Beer D. (2003a) Microsensor study of photosynthesis and calcification in the scleractinian coral, *Galaxea fascicularis*: active internal carbon cycle. *J. Exp. Mar. Bio. Ecol.* **288**, 1–15.

Al-Horani F. A., Al-Moghrabi S. M. and de Beer D. (2003b) The mechanism of calcification and its relation to photosynthesis and respiration in the scleractinian coral *Galaxea fascicularis*. *Mar. Biol.* **142**, 419–426.

Alibert C., Kinsley L., Fallon S. J., McCulloch M. T., Berkelmans R. and McAllister F. (2003) Source of trace element variability in Great Barrier Reef corals affected by the Burdekin flood plumes. *Geochim. Cosmochim. Acta* **67**, 231–246.

Alibert C. and McCulloch M. T. (1997) Strontium/calcium ratios in modern *Porites* corals from the Great Barrier Reef as a proxy for sea surface temperature: Calibration of the thermometer and monitoring of ENSO. *Paleoceanography* **12**, 345–363.

Alldredge A. L. and King J. M. (1977) Distribution, abundance, and substrate preferences of demersal reef zooplankton at Lizard Island Lagoon, Great Barrier Reef. *Mar. Biol.* **41**, 317–333.

Allison N. and Finch A. A. (2004) High-resolution Sr/Ca records in modern *Porites lobata* corals: Effects of skeletal extension rate and architecture. *Geochemistry Geophys. Geosystems* **5**, 1–10.

Allison N., Finch A. A., Sutton S. R. and Newville M. (2001) Strontium heterogeneity and speciation in coral aragonite: Implications for the strontium paleothermometer. *Geochim. Cosmochim. Acta* **65**, 2669–2676.

Amiel A. J., Friedman G. M. and Miller D. S. (1973) Distribution and nature of incorporation of trace-elements in modern aragonitic corals. *Sedimentology* **20**, 47–64.

Anderson T. F. and Arthur M. A. (1983) Stable isotopes of oxygen and carbon and their applications to sedimentologic and paleoenvironmental problems. In *Stable Isotopes in Sedimentary Geology, Society of Economic Paleontologists and Mineralogists, Short Course Notes* (ed. A. M. A. et al). pp. 1–151.

Andrews J. E., Portman C., Rowe P. J., Leeder M. R. and Kramers J. D. (2007) Sub-orbital sea-level change in early MIS 5e: New evidence from the Gulf of Corinth, Greece. *Earth Planet. Sci. Lett.* **259**, 457–468.

Antonioli F., Silenzi S. and Frisia S. (2001) Tyrrhenian Holocene palaeoclimate trends from spelean serpulids. *Quat. Sci. Rev.* **20**, 1661–1670.

Ariztegui D., Asioli A., Lowe J. J., Trincardi F., Vigliotti L., Tamburini F., Chondrogianni C., Accorsi C. A., Bandini Mazzanti M., Mercuri A. M., Van der Kaars S., McKenzie J. A. and Oldfield F. (2000) Palaeoclimate and the formation of sapropel S1: inferences from Late Quaternary lacustrine and marine sequences in the central Mediterranean region. *Palaeogeogr. Palaeoclimatol. Palaeoecol.* **158**, 215–240.

Armid A., Asami R., Fahmiati T., Sheikh M. A., Fujimura H., Higuchi T., Taira E., Shinjo R. and Oomori T. (2011) Seawater temperature proxies based on D(Sr), D(Mg), and D(U) from culture experiments using the branching coral *Porites cylindrica*. *Geochim. Cosmochim. Acta* **75**, 4273–4285.

Armijo R., Meyer B., King G. C. P., Rigo A. and Papanastassiou D. (1996) Quaternary evolution of the Corinth Rift and its implications for the Late Cenozoic evolution of the Aegean. *Geophys. J. Int.* **126**, 11–53.

Arrowsmith P. (1987) Laser ablation of solids for elemental analysis by inductively coupled plasma mass-spectrometry. *Anal. Chem.* **59**, 1437–1444.

Barbin V., Schein E., Roux M., Decrouez D. and Ramseyer K. (1991) Stries de croissance révéléespar cathodoluminescence dans la coquille de *Pecten maximus* (L.) récent de la rade de Brest (Pectinidae, Bivalvia). *Geobios* **24**, 65–70.

Bardaji T., Goy J. L., Zazo C., Hillaire-Marcel C., Dabrio C. J., Cabero A., Ghaleb B., Silva P. G. and Lario J. (2009) Sea level and climate changes during OIS 5e in the Western Mediterranean. *Geomorphology* **104**, 22–37.

Bar-Matthews M., Ayalon A., Gilmour M., Matthews A. and Hawkesworth C. J. (2003) Sea-land oxygen isotopic relationships from planktonic foraminifera and speleothems in the Eastern Mediterranean region and their implication

for paleorainfall during interglacial intervals. *Geochim. Cosmochim. Acta* **67**, 3181–3199.

Barnes D. J. (1970) Coral skeletons - An explanation of their growth and structure. *Science).* **170**, 1305–1308.

BBC (2007) Dubrovnik fire threat subsiding. Available at: http://news.bbc.co.uk/1/hi/world/europe/6932578.stm.

Beck J. W., Edwards R. L., Ito E., Taylor F. W., Recy J., Rougerie F., Joannot P. and Henin C. (1992) Sea-surface temperature from coral skeletal strontium/calcium ratios. *Science.* **257**, 644–647.

Belding D. (1931) The scallop fishery of Massachusetts: including an account of the natural history of the common scallop. *Massachusetts Div. Fish. Game, Mar. Fish. Sect.* **5**, 1–51.

Belluomini G., Caldara M., Casini C., Cerasoli M., Manfra L., Mastronuzzi G., Palmentola G., Sanso P., Tuccimei P. and Vesica P. L. (2002) The age of Late Pleistocene shorelines and tectonic activity of Taranto area, Southern Italy. *Quat. Sci. Rev.* **21**, 525–547.

Bernasconi M. P., Corselli C. and Carobene L. (1997) A bank of the scleractinian coral *Cladocora caespitosa* in the Pleistocene of the Crati valley (Calabria, Southern Italy) growth verses environmental conditions. *Boll. della Soc. Paleontol. Ital.* **36**, 53–62.

Béthoux J. P., Morin P., Chaumery C., Connan O., Gentili B. and Ruiz-Pino D. (1998) Nutrients in the Mediterranean Sea, mass balance and statistical analysis of concentrations with respect to environmental change. *Mar. Chem.* **63**, 155–169.

Bevan D. J. M., Rossmaith E., Mylrea D. K., Ness S. E., Taylor R. M. and Cuff C. (2002) On the structure of aragonite - Lawrence Bragg revisited. *Acta Crystallogr. Sect. B-Structural Sci.* **58**, 448–456.

Brown B. E., Tudhope A. W., Letissier M. D. A. and Scoffin T. P. (1991) A novel mechanism for iron incorporation into coral skeletons. *Coral Reefs* **10**, 211–215.

Buick D. P. and Ivany L. C. (2004) 100 years in the dark: Extreme longevity of Eocene bivalves from Antarctica. *Geology* **32**, 921.

Burton E. and Walter L. (1987) Relative precipitation rates of aragonite and Mg calcite from seawater: Temperature or carbonate ion control? *Geology* **15**, 111–114.

Came R. E., Brand U. and Affek H. P. (2014) Clumped isotope signatures in modern brachiopod carbonate. *Chem. Geol.* **377**, 20–30.

Came R. E., Eiler J. M., Veizer J., Azmy K., Brand U. and Weidman C. R. (2007) Coupling of surface temperatures and atmospheric CO2 concentrations during the Palaeozoic era. *Nature* **449**, 198–201.

Castagna M. and Chanley P. (1973) Salinity tolerance of some marine bivalves from inshore and estuarine environments in Virginia waters on the western mid-Atlantic coast. *Malacologia* **12**, 47–96.

Chassefi B. and Kremer Y. (1972) Presence of Cladocora caespitosa in recent marine level of Gulf of Saint Tropez (Var, France). *Comptes Rendus Hebd. Des Seances L Acad. Des Sci. Ser. D* **275**, 1951.

Chauvaud L., Lorrain A., Dunbar R. B., Paulet Y.-M., Thouzeau G., Jean F., Guarini J.-M. and Mucciarone D. (2005) Shell of the Great Scallop *Pecten maximus* as a high-frequency archive of paleoenvironmental changes. *Geochemistry, Geophys. Geosystems* **6**, 1–15.

Cheddadi R., de Beaulieu J.-L., Jouzel J., Andrieu-Ponel V., Laurent J.-M., Reille M., Raynaud D. and Bar-Hen A. (2005) Similarity of vegetation dynamics during interglacial periods. *Proc. Natl. Acad. Sci. U. S. A.* **102**, 13939–43.

Cheddadi R., Yu G., Guiot J., Harrison S. P. and Prentice I. C. (1996) The climate of Europe 6000 years ago. *Clim. Dyn.* **13**, 1–9.

Chintiroglou C. C. (1996) Feeding guilds of polychaetes associated with *Cladocora caespitosa* (L.) (Anthozoa, Cnidaria) in the north Aegean sea. *Isr. J. Zool.* **42**, 261–274.

Clarke P. J., Davies R. R., England P. C., Parsons B. E., Billiris H., Paradissis D., Veis G., Denys P. H., Cross P. A., Ashkenazi V. and Bingley R. (1997) Geodetic estimate of seismic hazard in the Gulf of Korinthos. *Geophys. Res. Lett.* **24**, 1303–1306.

Clayton R. N., Goldsmith J. R., Karel K. J., Mayeda T. K. and Robert C. N. (1975) Limits on the effect of pressure on isotopic fractionation. *Geochim. Cosmochim. Acta* **39**, 1197–1201.

Cohen A. L. and Hart S. R. (2004) Deglacial sea surface temperatures of the western tropical Pacific: A new look at old coral. *Paleoceanography* **19**, 1–6.

Cohen A. L., Layne G. D., Hart S. R. and Lobel P. S. (2001) Kinetic control of skeletal Sr/Ca in a symbiotic coral: Implications for the paleotemperature proxy. *Paleoceanography* **16**, 20–26.

Cohen A. L. and McConnaughey T. A. (2003) Geochemical perspectives on coral mineralization. In *Biomineralization* (eds. P. M. Dove, J. J. DeYoreo, and S. Weiner). Mineralogical Soc Amer, Chantilly. pp. 151–187.

Cohen A. L., Owens K. E., Layne G. D. and Shimizu N. (2002) The effect of algal symbionts on the accuracy of Sr/Ca paleotemperatures from coral. *Science).* **296**, 331–333.

Collier R. (1990) Eustatic and tectonic controls upon Quaternary coastal sedimentation in the Corinth Basin, Greece. *J. Geol. Soc. London.* **147**, 301–314.

Coope G. R. (2001) Biostratigraphical distinction of interglacial coleopteran assemblages from southern Britain attributed to Oxygen Isotope Stages 5e and 7. *Quat. Sci. Rev.* **20**, 1717–1722.

Coope G. R. (2010) Coleoptera from the Cromerian Type Site at West Runton, Norfolk, England. *Quat. Int.* **228**, 46–52.

Correge T. (2006) Sea surface temperature and salinity reconstruction from coral geochemical tracers. *Palaeogeogr. Palaeoclimatol. Palaeoecol.* **232**, 408–428.

Craig H. (1961) Isotopic Variations in Meteoric Waters. *Science.* **133**, 1702–3.

Craig H. (1965) The measurement of oxygen isotope paleotemperatures. *Stable Isot. Oceanogr. Stud. Paleotemp.* **23**, 1–24.

CRED (2009) EM-DAT: The OFDA/CRED International Disaster Database. Available at: http://www.emdat.be/search-details-disaster-list [Accessed March 20, 2014].

Cucci L. and Cinti F. R. (1998) Regional uplift and local tectonic deformation recorded by the Quaternary marine terraces on the Ionian coast of northern Calabria (southern Italy). *Tectonophysics* **292**, 67–83.

Cuif J. P. and Dauphin Y. (2005) The Environment Recording Unit in coral skeletons - a synthesis of structural and chemical evidences for a biochemically driven, stepping-growth process in fibres. *Biogeosciences* **2**, 61–73.

Cuif J. P., Dauphin Y. Y., Doucet J., Salome M. and Susini J. (2003) XANES mapping of organic sulfate in three scleractinian coral skeletons. *Geochim. Cosmochim. Acta* **67**, 75–83.

Denèfle M., Lézine A.-M., Fouache E. and Dufaure J.-J. (2000) A 12,000-year pollen record from Lake Maliq, Albania. *Quat. Res.* **54**, 423–432.

Dennis K. J., Affek H. P., Passey B. H., Schrag D. P. and Eiler J. M. (2011) Defining an absolute reference frame for "clumped" isotope studies of CO2. *Geochim. Cosmochim. Acta* **75**, 7117–7131.

Dennis K. J. and Schrag D. P. (2010) Clumped isotope thermometry of carbonatites as an indicator of diagenetic alteration. *Geochim. Cosmochim. Acta* **74**, 4110–4122.

Douglas A. E. (2003) Coral bleaching—how and why? *Mar. Pollut. Bull.* **46**, 385–392.

Duggan W. P. (1975) Reactions of the Bay Scallop, *Argopecten irradians*, to Gradual Reductions in Salinity. *Chesap. Sci.* **16**, 284.

Dunbar R. B., Wellington G. M., Colgan M. W. and Glynn P. W. (1994) Eastern Pacific sea surface temperature since 1600 A.D.: The δ18O record of climate variability in Galápagos Corals. *Paleoceanography* **9**, 291–315.

Eagle R. A., Eiler J. M., Tripati A. K., Ries J. B., Freitas P. S., Hiebenthal C., Wanamaker A. D., Taviani M., Elliot M., Marenssi S., Nakamura K., Ramirez P. and Roy K. (2013) The influence of temperature and seawater saturation state on 13C–18O bond ordering in bivalve mollusks. *Biogeosciences* **10**, 4591–4606.

Eagle R. A., Schauble E. A., Tripati A. K., Tütken T., Hulbert R. C. and Eiler J. M. (2010) Body temperatures of modern and extinct vertebrates from (13)C-(18)O bond abundances in bioapatite. *Proc. Natl. Acad. Sci. U. S. A.* **107**, 10377–82.

Eiler J. M. (2011) Paleoclimate reconstruction using carbonate clumped isotope thermometry. *Quat. Sci. Rev.* **30**, 3575–3588.

Eiler J. M. and Schauble E. (2004) 18O13C16O in Earth's atmosphere. *Geochim. Cosmochim. Acta* **68**, 4767–4777.

Epstein S., Buchsbaum R., Lowenstam H. A. and Urey H. C. (1953) Revised carbonate-water isotopic temperature scale. *Geol. Soc. Am. Bull.* **64**, 1315–1325.

Faure G. and Mensing T. (2005) Hydrogen and Oxygen. In *Isotopes Principles and Applications* John Wiley & Sons, Inc, Hoboken, New Jersey. pp. 693–744.

Ferranti L., Antonioli F., Mauz B., Amorosi A., Dai Pra G., Mastronuzzi G., Monaco C., Orrù P., Pappalardo M., Radtke U., Renda P., Romano P., Sansò P. and Verrubbi V. (2006) Markers of the last interglacial sea-level high stand along the coast of Italy: Tectonic implications. *Quat. Int.* **145–146**, 30–54.

Ferrier-Pagès C., Boisson F., Allemand D. and Tambutté E. (2002) Kinetics of strontium uptake in the scleractinian coral *Stylophora pistillata*. *Mar. Ecol. Prog. Ser.* **245**, 93–100.

Finch A. A. and Allison N. (2007) Coordination of Sr and Mg in calcite and aragonite. *Mineral. Mag.* **71**, 539–552.

Fontugne M. R. and Calvert S. E. (1992) Late Pleistocene variability of the carbon isotopic composition of organic matter in the eastern mediterranean: monitor of changes in carbon sources and atmospheric CO2 concentrations. *Paleoceanography* **7**, 1–20.

Fornos J. J., Baron A. and Pons G. x. (1996) Arrecifes de coral hermatipicos (*Cladocora caespitosa*) en el relleno holoceno de la zona de Es Grau (Menorca, Mediterraneo Occidental). *Geogaceta* **20**, 303–306.

Frumkin A., Magaritz M., Carmi I. and Zak I. (1991) The Holocene climatic record of the salt caves of Mount Sedom, Israel. *Holocene* **1**, 191–200.

Gaetani G. A. and Cohen A. L. (2006) Element partitioning during precipitation of aragonite from seawater: A framework for understanding paleoproxies. *Geochim. Cosmochim. Acta* **70**, 4617–4634.

Gagan M. K., Chivas A. R. and Isdale P. J. (1994) High-resolution isotopic records from corals using ocean temperature and mass-spawning chronometers. *Earth Planet. Sci. Lett.* **121**, 549–558.

Gagan M. K., Dunbar G. B. and Suzuki A. (2012) The effect of skeletal mass accumulation in Porites on coral Sr/Ca and δ 18 O paleothermometry. *Paleoceanography* **27**, n/a–n/a.

Garilli V. (2011) Mediterranean Quaternary interglacial molluscan assemblages: Palaeobiogeographical and palaeoceanographical responses to climate change. *Palaeogeogr. Palaeoclimatol. Palaeoecol.* **312**, 98–114.

Gat J. R., Shemesh A., Tziperman E., Hecht A., Georgopoulos D. and Basturk O. (1996) The stable isotope composition of waters of the eastern Mediterranean Sea. *J. Geophys. Res.* **101**, 6441–6451.

Ghosh P., Adkins J., Affek H., Balta B., Guo W., Schauble E. A., Schrag D. and Eiler J. M. (2006) 13C–18O bonds in carbonate minerals: A new kind of paleothermometer. *Geochim. Cosmochim. Acta* **70**, 1439–1456.

Ghosh P., Eiler J., Campana S. E. and Feeney R. F. (2007) Calibration of the carbonate "clumped isotope" paleothermometer for otoliths. *Geochim. Cosmochim. Acta* **71**, 2736–2744.

Gladfelter E. H., Monahan R. K. and Gladfelter W. B. (1978) Growth rates of five reef-building corals in the Northeastern Caribbean. *Bull. Mar. Sci.* **28**, 7.

Goodkin N. F., Hughen K. A. and Cohen A. L. (2007) A multicoral calibration method to approximate a universal equation relating Sr/Ca and growth rate to sea surface temperature. *Paleoceanography* **22**, PA1214.

Goodwin D. H., Flessa K. W., Schöne B. R. and Dettman D. L. (2001) Cross-calibration of daily growth increments, stable isotope variation, and temperature in the gulf of california bivalve mollusk *Chione cortezi*: Implications for paleoenvironmental analysis. *Palaios* **16**, 387–398.

Goodwin D. H., Schöne B. R. and Dettman D. L. (2003) Resolution and fidelity of oxygen isotopes as paleotemperature proxies in bivalve mollusk shells: Models and observations. *Palaios* **18**, 110–125.

Goy J. L., Hillaire-Marcel C., Zazo C., Ghaleb B., Dabrio C. J., Gonzalez A., Bardaji T., Civis J., Preda M., Yebenes A. and Forte A. M. (2006) Further evidence for a relatively high sea level during the penultimate interglacial: open-system U-series ages from La Marina (Alicante, East Spain). *Geodin. Acta* **19**, 409–426.

Gray A. L. (1985) Solid sample introduction by laser ablation for inductively coupled plasma source mass spectrometry. *Analyst* **110**, 551–556.

Grazzini C. V, Devaux M. and Znaidi J. (1986) Stable isotope anomalies in Mediterranean Pleistocene records. *Mar. Micropaleontol.* **10**, 35–69.

Grossman E. L. and Ku T. L. (1986) Oxygen and carbon isotope fractionation in biogenic aragonite: Temperature effects. *Chem. Geol.* **59**, 59–74.

Guo W. and Eiler J. M. (2007) Temperatures of aqueous alteration and evidence for methane generation on the parent bodies of the CM chondrites. *Geochim. Cosmochim. Acta* **71**, 5565–5575.

Guo W., Kim S., Thiagarajan N., Adkins J. F. and Eiler J. M. (2009) Mechanisms for "Vital Effects" in Biogenic Carbonates: New Perspectives Based on Abundances of 13C-18O Bonds. *AGU Fall Meet. Abstr.* **-1**, 07.

Guo W., Mosenfelder J. L., Goddard W. and Eiler J. M. (2009) Isotopic fractionations associated with phosphoric acid digestion of carbonate minerals: Insights from first-principles theoretical modeling and clumped isotope measurements. *Geochim. Cosmochim. Acta* **73**, 7203–7225.

Gutsell J. (1931) Natural history of the bay scallop. *Bull. United States Bur. Fish.* **45**, 569–632.

Henderson G. M., Cohen A. S. and O' Nions R. K. (1993) 234U/238U ratios and 230TH ages for Hateruma Atoll corals - implications for coral diagenesis and seawater 234U/238U ratios. *Earth Planet. Sci. Lett.* **115**, 65–73.

Henkes G. A., Passey B. H., Wanamaker A. D., Grossman E. L., Ambrose W. G. and Carroll M. L. (2013) Carbonate clumped isotope compositions of modern marine mollusk and brachiopod shells. *Geochim. Cosmochim. Acta* **106**, 307–325.

Hickson J. A., Johnson A. L. ., Heaton T. H. . and Balson P. S. (1999) The shell of the Queen Scallop *Aequipecten opercularis* (L.) as a promising tool for palaeoenvironmental reconstruction: evidence and reasons for equilibrium stable-isotope incorporation. *Palaeogeogr. Palaeoclimatol. Palaeoecol.* **154**, 325–337.

Hoefs J. (2004) 1 Theorectical and Experimental Principles. In *Stable Isotope Geochemistry* Springer-Verlag Berlin Heidelberg New York. pp. 1–29.

Hoffmann D. L., Spoetl C. and Mangini A. (2009) Micromill and in situ laser ablation sampling techniques for high spatial resolution MC-ICPMS U-Th dating of carbonates. *Chem. Geol.* **259**, 253–261.

Holcomb M., Cohen A. L., Gabitov R. I. and Hutter J. L. (2009) Compositional and morphological features of aragonite precipitated experimentally from seawater and biogenically by corals. *Geochim. Cosmochim. Acta* **73**, 4166–4179.

Houghton S. L., Roberts G. P., Papanikolaou I. D., McArthur J. M. and Gilmour M. A. (2003) New 234U/230Th coral dates from the western Gulf of Corinth: Implications for extensional tectonics. *Geophys. Res. Lett.* **30**.

Houlbrèque F., Tambutté E. and Ferrier-Pagès C. (2003) Effect of zooplankton availability on the rates of photosynthesis, and tissue and skeletal growth in the scleractinian coral *Stylophora pistillata*. *J. Exp. Mar. Bio. Ecol.* **296**, 145–166.

Huntington K. W., Budd D. A., Wernicke B. P. and Eiler J. M. (2011) Use of Clumped-Isotope Thermometry to Constrain the Crystallization Temperature of Diagenetic Calcite. *J. Sediment. Res.* **81**, 656–669.

Huntington K. W., Eiler J. M., Affek H. P., Guo W., Bonifacie M., Yeung L. Y., Thiagarajan N., Passey B., Tripati A., Daëron M. and Came R. (2009) Methods and limitations of "clumped" CO2 isotope (Delta47) analysis by gas-source isotope ratio mass spectrometry. *J. Mass Spectrom.* **44**, 1318–29.

Ip Y. K. and Krishnaveni P. (1991) Incorporation of strontium (90Sr2+) into the skeleton of the hermatypic coral *Galaxea fascicularis*. *J. Exp. Zool.* **258**, 273–276.

Ip Y. K., Lim A. L. L. and Lim R. W. L. (1991) Some properties of calcium-activated adenosine triphosphatase from the hermatypic coral *Galaxea fascicularis*. *Mar. Biol.* **111**, 191–197.

Jacques T. G., Marshall N. and Pilson M. E. Q. (1983) Experimental ecology of the temperate scleractinian coral *Astrangia danae*. *Mar. Biol.* **76**, 135–148.

Johnson A. L. A., Hickson J. A., Bird A., Schöne B. R., Balson P. S., Heaton T. H. E. and Williams M. (2009) Comparative sclerochronology of modern and

mid-Pliocene (c. 3.5Ma) *Aequipecten opercularis* (Mollusca, Bivalvia): an insight into past and future climate change in the north-east Atlantic region. *Palaeogeogr. Palaeoclimatol. Palaeoecol.* **284**, 164–179.

Johnson K. S. (1982) Carbon dioxide hydration and dehydration kinetics in seawater. *Limnol. Oceanogr.* **27**, 849–855.

Joll L. M. (1989) Swimming behaviour of the saucer scallop *Amusium balloti* (Mollusca: Pectinidae). *Mar. Biol.* **102**, 299–305.

Kallel N., Duplessy J. C., Labeyrie L., Fontugne M., Paterne M. and Montacer M. (2000) Mediterranean pluvial periods and sapropel formation over the last 200,000 years. *Palaeogeogr. Palaeoclimatol. Palaeoecol.* **157**, 45–58.

Kawamura K., Nakazawa T., Aoki S., Sugawara S., Fujii Y. and Watanabe O. (2003) Atmospheric CO2 variations over the last three glacial–interglacial climatic cycles deduced from the Dome Fuji deep ice core, Antarctica using a wet extraction technique. *Tellus B* **55**, 126–137.

Kawamura K., Parrenin F., Lisiecki L., Uemura R., Vimeux F., Severinghaus J. P., Hutterli M. A., Nakazawa T., Aoki S., Jouzel J., Raymo M. E., Matsumoto K., Nakata H., Motoyama H., Fujita S., Goto-Azuma K., Fujii Y. and Watanabe O. (2007) Northern Hemisphere forcing of climatic cycles in Antarctica over the past 360,000 years. *Nature* **448**, 912–6.

Keraudren B. and Sorel D. (1987) The terraces of Corinth (Greece) — A detailed record of eustatic sea-level variations during the last 500,000 years. *Mar. Geol.* **77**, 99–107.

Kershaw S., Guo L. and Braga J. C. (2005) A Holocene coral-algal reef at Mavra Litharia, Gulf of Corinth, Greece: structure, history, and applications in relative sea-level change. *Mar. Geol.* **215**, 171–192.

Kim S.-T. and O'Neil J. R. (1997) Equilibrium and nonequilibrium oxygen isotope effects in synthetic carbonates. *Geochim. Cosmochim. Acta* **61**, 3461–3475.

Kinsman D. J. J. and Holland H. D. (1969) Co-precipitation of cations with CACO3-IV. The co-precipitation of Sr2+ with aragonite between 16 and 96 degrees C. *Geochim. Cosmochim. Acta* **33**, 1–17.

Kružić P. (2002) Marine fauna of the Mljet National Park (Adriatic Sea, Croatia). 1. Anthozoa. *Nat. Croat.* **11**, 265–292.

Kružić P. (2007) Polyp expulsion of the coral *Cladocora caespitosa* (Anthozoa, Scleractinia) in extreme sea temperature conditions. *Nat. Croat.* **16**, 211–214.

Kružić P. and Benković L. (2008) Bioconstructional features of the coral *Cladocora caespitosa* (Anthozoa, Scleractinia) in the Adriatic Sea (Croatia). *Mar. Ecol. Evol. Perspect.* **29**, 125–139.

Kružić P., Lipej L., Mavrić B. and Rodić R. (2014) Impact of bleaching on the coral *Cladocora caespitosa* in the eastern Adriatic Sea. *Mar. Ecol. Prog. Ser.* **509**, 193–202.

Kružić P. and Požar-Domac A. (2003) Banks of the coral *Cladocora caespitosa* (Anthozoa, Scleractinia) in the Adriatic Sea. *Coral Reefs* **22**, 536.

Kružić P. and Požar-Domac A. (2002) Skeleton growth rates of coral bank of *Cladocora caespitosa* (Anthozoa, Scleractinia) in Lake Veliko Jezero (Mljet National Park). *Period. Biol.* **104**, 123–129.

Kružić P., Sršen P. and Benković L. (2012) The impact of seawater temperature on coral growth parameters of the colonial coral Cladocora caespitosa (Anthozoa, Scleractinia) in the eastern Adriatic Sea. *Facies* **58**, 477–491.

Kružić P., Žuljević A. and Nikolić V. (2008) Spawning of the colonial coral *Cladocora caespitosa* (Anthozoa, Scleractinia) in the Southern Adriatic Sea. *Coral Reefs* **27**, 337–341.

Laborel J. (1987) Marine biogenic constructions in the Mediterranean: a review. *Sci. Reports Port Cros Natl. Park* **13**, 97–126.

LaVigne M., Matthews K. A., Grottoli A. G., Cobb K. M., Anagnostou E., Cabioch G. and Sherrell R. M. (2010) Coral skeleton P/Ca proxy for seawater phosphate: Multi-colony calibration with a contemporaneous seawater phosphate record. *Geochim. Cosmochim. Acta* **74**, 1282–1293.

Lea D. W., Shen G. T. and Boyle E. A. (1989) Coralline barium records temporal variability in Equatorial Pacific upwelling. *Nature* **340**, 373–376.

Leeder M. R., McNeill L. C., Collier R. E. L., Portman C., Rowe P. J., Andrews J. E. and Gawthorpe R. L. (2003) Corinth rift margin uplift: New evidence from Late Quaternary marine shorelines. *Geophys. Res. Lett.* **30**, 1–4.

Leeder M. R., Portman C., Andrews J. E., Collier R. E. L., Finch E., Gawthorpe R. L., McNeill L. C., Pérez-Arlucea M. and Rowe P. (2005) Normal faulting and crustal deformation, Alkyonides Gulf and Perachora peninsula, eastern Gulf of Corinth rift, Greece. *J. Geol. Soc. London.* **162**, 549–561.

Lewis S. E., Shields G. A., Kamber B. S. and Lough J. M. (2007) A multi-trace element coral record of land-use changes in the Burdekin River catchment, NE Australia. *Palaeogeogr. Palaeoclimatol. Palaeoecol.* **246**, 471–487.

Linnaeus C. (1767) *Systema naturae per regna tria naturae, secundum classes, ordines, genera, species, cum characteribus, differentiis, synonymis, locis*. 12th ed., Stockholm.

Magny M., Miramont C. and Sivan O. (2002) Assessment of the impact of climate and anthropogenic factors on Holocene Mediterranean vegetation in Europe on the basis of palaeohydrological records. *Palaeogeogr. Palaeoclimatol. Palaeoecol.* **186**, 47–59.

Marriott C. S., Henderson G. M., Belshaw N. S. and Tudhope A. W. (2004) Temperature dependence of δ7Li, δ44Ca and Li/Ca during growth of calcium carbonate. *Earth Planet. Sci. Lett.* **222**, 615–624.

Marshall J. F. and McCulloch M. T. (2002) An assessment of the Sr/Ca ratio in shallow water hermatypic corals as a proxy for sea surface temperature. *Geochim. Cosmochim. Acta* **66**, 3263–3280.

Martrat B., Grimalt J. O., Lopez-Martinez C., Cacho I., Sierro F. J., Flores J. A., Zahn R., Canals M., Curtis J. H. and Hodell D. A. (2004) Abrupt temperature changes in the Western Mediterranean over the past 250,000 years. *Science.* **306**, 1762–5.

Mastronuzzi G., Sanso P., Tuccimei P. and Vesica P. L. (2003) Stop 3.3.1 - The *Cladocora caespitosa* bank of Santa Teresiola locality. In *Project IGCP 437 - Coastal environmental change during sea-level highstands: a global synthesis with implication for management of future coastal change: Puglia 2003 final conference, Quaternary coastal morphology and sea level changes - Field Guide GI2S* (eds. G. Mastronuzzi and P. Sanso). pp. 85–100.

Mauz B., Buccheri G., Zöller L. and Greco A. (1997) Middle to Upper Pleistocene morphostructural evolution of the NW-coast of Sicily: thermoluminescence dating and palaeontological-stratigraphical evaluations of littoral deposits. *Palaeogeogr. Palaeoclimatol. Palaeoecol.* **128**, 269–285.

McConnaughey T. (1989a) 13C and 18O isotopic disequilibrium in biological carbonates: I. Patterns. *Geochim. Cosmochim. Acta* **53**, 151–162.

McConnaughey T. (1989b) 13C and 18O isotopic disequilibrium in biological carbonates: II. In vitro simulation of kinetic isotope effects. *Geochim. Cosmochim. Acta* **53**, 163–171.

McCrea J. M. (1950) On the isotopic chemistry of carbonates and a paleotemperature scale. *J. Chem. Phys.* **18**, 849–857.

McCulloch M. T., Fallon S., Wyndham T., Hendy E., Lough J. and Barnes D. (2003) Coral record of increased sediment flux to the inner Great Barrier Reef since European settlement. *Nature* **421**, 727–730.

McCulloch M. T., Gagan M. K., Mortimer G. E., Chivas A. R. and Isdale P. J. (1994) A high resolution Sr/Ca and δ18O coral record from the Great Barrier Reef, Australia, and the 1982-1983 El-Nino. *Geochim. Cosmochim. Acta* **58**, 2747–2754.

Mercaldo R. S. and Rhodes E. W. (1982) Influence of reduced salinity on the Atlantic bay scallop *Argopecten irradians* (Lamarck) at various temperatures. *J. Shellfish Res.* **2**, 177–181.

Mitsuguchi T., Matsumoto E., Abe O., Uchida T. and Isdale P. J. (1996) Mg/Ca thermometry in coral-skeletons. *Science (80-.).* **274**, 961–963.

Montaggioni L. F., Le Cornec F., Correge T. and Cabioch G. (2006) Coral barium/calcium record of mid-Holocene upwelling activity in New Caledonia, South-West Pacific. *Palaeogeogr. Palaeoclimatol. Palaeoecol.* **237**, 436–455.

Montagna P., McCulloch M. T., Mazzoli C., Silenzi S. and Odorico R. (2007) The non-tropical coral Cladocora caespitosa as the new climate archive for the Mediterranean: high-resolution (~ weekly) trace element systematics. *Quat. Sci. Rev.* **26**, 441–462.

Montagna P., McCulloch M. T., Mazzoli C., Silenzi S. and Schiaparelli S. (2006) Li/Ca ratios in the Mediterranean non-tropical coral *Cladocora caespitosa* as a potential paleothermometer. *Geophys. Res. Abstr.* **8**.

Montagna P., McCulloch M. T., Taviani M., Mazzoli C. and Vendrell B. (2006) Phosphorus in cold-water corals as a proxy for seawater nutrient chemistry. *Science.* **312**, 1788–1791.

Morse J. W., Wang Q. and Tsio M. Y. (1997) Influences of temperature and Mg:Ca ratio on CaCO3 precipitates from seawater. *Geology* **25**, 85–87.

Nier A. (1950) A redetermination of the relative abundances of the isotopes of carbon, nitrogen, oxygen, argon, and potassium. *Phys. Rev.* **77**, 789–793.

Owen R., Kennedy H. and Richardson C. (2002) Experimental investigation into partitioning of stable isotopes between scallop (*Pecten maximus*) shell calcite and sea water. *Palaeogeogr. Palaeoclimatol. Palaeoecol.* **185**, 163–174.

Pedley M. and Grasso M. (2002) Lithofacies modelling and sequence stratigraphy in microtidal cool-water carbonates: a case study from the Pleistocene of Sicily, Italy. *Sedimentology* **49**, 533–553.

Peirano A., Abbate M., Cerrati G., Difesca V., Peroni C. and Rodolfo-Metalpa R. (2005) Monthly variations in calix growth, polyp tissue, and density banding of the Mediterranean scleractinian *Cladocora caespitosa* (L.). *Coral Reefs* **24**, 404–409.

Peirano A., Kružić P. and Mastronuzzi G. (2009) Growth of Mediterranean reef of *Cladocora caespitosa* (L.) in the Late Quaternary and climate inferences. *Facies* **55**, 325–333.

Peirano A., Morri C. and Bianchi C. N. (1999) Skeleton growth and density pattern of the temperate, zooxanthellate scleractinian *Cladocora caespitosa* from the Ligurian Sea (NW Mediterranean). *Mar. Ecol. Prog. Ser.* **185**, 195–201.

Peirano A., Morri C., Bianchi C. N., Aguirre J., Antonioli F., Calzetta G., Carobene L., Mastronuzzi G. and Orru P. (2004) The Mediterranean coral *Cladocora caespitosa*: a proxy for past climate fluctuations? *Glob. Planet. Change* **40**, 195–200.

Peirano A., Morri C., Bianchi N. and Rodolfo-Metalpa R. (2001) Biomass, carbonate standing stock and production of the Mediterranean coral *Cladocora caespitosa* (L.). *Facies* **44**, 75–80.

Peirano A., Morri C., Mastronuzzi G. and Bianchi C. N. (1998) The coral *Cladocora caspitosa* (Anthozoa, Scleractinia) as a bioherm builder in the Mediterranean Sea. *Mem. Descr. della Cart. Geol. d'Italia* **52**, 59–74.

Pérez-Folgado M., Sierro F. J., Flores J. A., Grimalt J. O. and Zahn R. (2004) Paleoclimatic variations in foraminifer assemblages from the Alboran Sea (Western Mediterranean) during the last 150 ka in ODP Site 977. *Mar. Geol.* **212**, 113–131.

Petit-Maire N. (1991) Recent quaternary climatic change and man in the Sahara. *J. African Earth Sci.* **12**, 125–132.

Pierre C. (1999) The oxygen and carbon isotope distribution in the Mediterranean water masses. *Mar. Geol.* **153**, 41–55.

Pirazzoli P. A., Mastronuzzi G., Saliege J. F. and Sanso P. (1997) Late Holocene emergence in Calabria, Italy. *Mar. Geol.* **141**, 61–70.

Portman C., Andrews J. E., Rowe P. J., Leeder M. R. and Hoogewerff J. (2005) Submarine-spring controlled calcification and growth of large *Rivularia* bioherms, Late Pleistocene (MIS 5e), Gulf of Corinth, Greece. *Sedimentology* **52**, 441–465.

Poulos S. E., Collins M. B., Pattiaratchi C., Cramp A., Gull W., Tsimplis M. and Papatheodorou G. (1996) Oceanography and sedimentation in the semi-enclosed, deep-water Gulf of Corinth (Greece). *Mar. Geol.* **134**, 213–235.

Quinn T. M., Crowley T. J., Taylor F. W., Henin C., Joannot P. and Join Y. (1998) A multicentury stable isotope record from a New Caledonia coral: Interannual and decadal sea surface temperature variability in the southwest Pacific since 1657 A.D. *Paleoceanography* **13**, 412–426.

Rimstidt J. D., Balog A. and Webb J. (1998) Distribution of trace elements between carbonate minerals and aqueous solutions. *Geochim. Cosmochim. Acta* **62**, 1851–1863.

Roberts G. P., Houghton S. L., Underwood C., Papanikolaou I., Cowie P. A., van Calsteren P., Wigley T., Cooper F. J. and McArthur J. M. (2009) Localization of Quaternary slip rates in an active rift in 105 years: An example from central Greece constrained by 234U-230Th coral dates from uplifted paleoshorelines. *J. Geophys. Res.* **114**, B10406.

Roberts M. S., Smart P. L., Hawkesworth C. J., Perkins W. T. and Pearce N. J. G. (1999) Trace element variations in coeval holocene speleothems from GB cave, southwest England. *Holocene* **9**, 707–713.

Rodolfo-Metalpa R., Bianchi C., Peirano A. and Morri C. (2005) Tissue necrosis and mortality of the temperate coral *Cladocora Caespitosa*. *Ital. J. Zool.* **72**, 271–276.

Rodolfo-Metalpa R., Peirano A., Houlbreque F., Abbate M. and Ferrier-Pages C. (2008) Effects of temperature, light and heterotrophy on the growth rate and budding of the temperate coral *Cladocora caespitosa*. *Coral Reefs* **27**, 17–25.

Rodolfo-Metalpa R., Richard C., Allemand D., Bianchi C. N., Morri C. and Ferrier-Pages C. (2006) Response of zooxanthellae in symbiosis with the Mediterranean corals *Cladocora caespitosa* and *Oculina patagonica* to elevated temperatures. *Mar. Biol.* **150**, 45–55.

Rollion-Bard C., Blamart D., Cuif J. P. and Juillet-Leclerc A. (2003) Microanalysis of C and O isotopes of azooxanthellate and zooxanthellate corals by ion microprobe. *Coral Reefs* **22**, 405–415.

Rollion-Bard C., Chaussidon M. and France-Lanord C. (2011) Biological control of internal pH in scleractinian corals: Implications on paleo-pH and paleo-temperature reconstructions. *Comptes Rendus Geosci.* **343**, 397–405.

Rollion-Bard C., Chaussidon M. and France-Lanord C. (2003) pH control on oxygen isotopic composition of symbiotic corals. *Earth Planet. Sci. Lett.* **215**, 275–288.

Rong Min G., Lawrence Edwards R., Taylor F. W., Recy J., Gallup C. D. and Warren Beck J. (1995) Annual cycles of U/Ca in coral skeletons and U/Ca thermometry. *Geochim. Cosmochim. Acta* **59**, 2025–2042.

Roucoux K. H., Tzedakis P. C., Frogley M. R., Lawson I. T. and Preece R. C. (2008) Vegetation history of the marine isotope stage 7 interglacial complex at Ioannina, NW Greece. *Quat. Sci. Rev.* **27**, 1378–1395.

Sadori L. and Narcisi B. (2001) The Postglacial record of environmental history from Lago di Pergusa, Sicily. *The Holocene* **11**, 655–671.

Saenger C., Affek H. P., Felis T., Thiagarajan N., Lough J. M. and Holcomb M. (2012) Carbonate clumped isotope variability in shallow water corals:

Temperature dependence and growth-related vital effects. *Geochim. Cosmochim. Acta* **99**, 224–242.

Sander P. M. and Klein N. (2005) Developmental plasticity in the life history of a prosauropod dinosaur. *Science.* **310**, 1800–2.

Santoro E., Mazzella M. E., Ferranti L., Randisi A., Napolitano E., Rittner S. and Radtke U. (2009) Raised coastal terraces along the Ionian Sea coast of northern Calabria, Italy, suggest space and time variability of tectonic uplift rates. *Quat. Int.* **206**, 78–101.

Sato K., Santosh M., Tsunogae T., Chetty T. R. K. and Hirata T. (2011) Subduction-accretion-collision history along the Gondwana suture in southern India: A laser ablation ICP-MS study of zircon chronology. *J. Asian Earth Sci.* **40**, 162–171.

Sayani H. R., Cobb K. M., Cohen A. L., Elliott W. C., Nurhati I. S., Dunbar R. B., Rose K. A. and Zaunbrecher L. K. (2011) Effects of diagenesis on paleoclimate reconstructions from modern and young fossil corals. *Geochim. Cosmochim. Acta* **75**, 6361–6373.

Schiller C. (1993) Ecology of the symbiotic coral *Cladocora caespitosa* (L.) (Faviidae, Scleractinia) in the Bay of Piran (Adriatic Sea): I. Distribution and biometry. *Mar. Ecol.* **14**, 205–219.

Schöne B. R., Fiebig J., Pfeiffer M., Gleβ R., Hickson J., Johnson A. L. A., Dreyer W. and Oschmann W. (2005) Climate records from a bivalved Methuselah (*Arctica islandica*, Mollusca; Iceland). *Palaeogeogr. Palaeoclimatol. Palaeoecol.* **228**, 130–148.

Schöne B. R., Oschmann W., Rossler J., Castro A. D. F., Houk S. D., Kroncke I., Dreyer W., Janssen R., Rumohr H. and Dunca E. (2003) North Atlantic oscillation dynamics recorded in shells of a long-lived bivalve mollusk. *Geology* **31**, 1037–1040.

Schöne B. R., Zhang Z. J., Jacob D. E., Gillikin D. P., Tutken T., Garbe-Schonberg D., McConnaughey T. and Soldati A. (2010) Effect of organic matrices on the determination of the trace element chemistry (Mg, Sr, Mg/Ca, Sr/Ca) of aragonitic bivalve shells (*Arctica islandica*) - Comparison of ICP-OES and LA-ICP-MS data. *Geochem. J.* **44**, 23–37.

Schöne B. R., Zhang Z. J., Radermacher P., Thebault J., Jacob D. E., Nunn E. V and Maurer A. F. (2011) Sr/Ca and Mg/Ca ratios of ontogenetically old, long-lived bivalve shells (*Arctica islandica*) and their function as paleotemperature proxies. *Palaeogeogr. Palaeoclimatol. Palaeoecol.* **302**, 52–64.

Schuhmacher H. and Zibrowius H. (1985) What is hermatypic - a redefination of ecological groups in corals and other organisms. *Coral Reefs* **4**, 1–9.

Shackleton N. J. (2000) The 100,000-Year Ice-Age Cycle Identified and Found to Lag Temperature, Carbon Dioxide, and Orbital Eccentricity. *Science.* **289**, 1897–1902.

Sheppard B. S., Shen W. L., Davidson T. M. and Caruso J. A. (1990) Helium-argon inductively coupled plasma for plasma source-mass spectrometry. *J. Anal. At. Spectrom.* **5**, 697–700.

Silenzi S., Bard E., Montagna P. and Antonioli F. (2005) Isotopic and elemental records in a non-tropical coral (*Cladocora caespitosa*): Discovery of a new high-resolution climate archive for the Mediterranean Sea. *Glob. Planet. Change* **49**, 94–120.

Sinclair D. J. (2005) Non-river flood barium signals in the skeletons of corals from coastal Queensland, Australia. *Earth Planet. Sci. Lett.* **237**, 354–369.

Sinclair D. J., Kinsley L. P. J. and McCulloch M. T. (1998) High resolution analysis of trace elements in corals by laser ablation ICP-MS. *Geochim. Cosmochim. Acta* **62**, 1889–1901.

Stahl W. and Rinow U. (1973) Sauerstoffisotopenanalysen an Mittelmeerwassen. Ein Beitrag zur Problematik von Palaotemperaturbestimmungen "Meteor" Forschungsergeb. . *Reich C* **14**, 55–59.

Stamatopoulos L., Belluomini G., Branca M., Manfra L. and Voltaggio M. (1998) 230Th/234U and isoleucine epimerization dating of quaternary marine deposits in western Peloponnesus (Greece). *Zeitschrift Fur Geomorphol.* **42**, 245–253.

Stecher III H. A., Krantz D. E., Lord III C. J., Luther III G. W. and Bock K. W. (1996) Profiles of strontium and barium in *Mercenaria mercenaria* and *Spisula solidissima* shells. *Geochim. Cosmochim. Acta* **60**, 3445–3456.

Stiros S. C. and Pirazzoli P. A. (1998) Late Quaternary coastal changes in the Gulf of Corinth, Greece: tectonics earthquake, archaeology. In *Guidebook for the Gulf of Corinth Field Trip, 14–16 September 1998, Patras University, Greece, Patras* p. 49.

Swart P. K., Leder J. J., Szmant A. M. and Dodge R. E. (1996) The origin of variations in the isotopic record of scleractinian corals .2. Carbon. *Geochim. Cosmochim. Acta* **60**, 2871–2885.

Thiagarajan N., Adkins J. and Eiler J. (2011) Carbonate clumped isotope thermometry of deep-sea corals and implications for vital effects. *Geochim. Cosmochim. Acta* **75**, 4416–4425.

Thompson W. G. and Goldstein S. L. (2006) A radiometric calibration of the SPECMAP timescale. *Quat. Sci. Rev.* **25**, 3207–3215.

Thompson W. G. and Goldstein S. L. (2005) Open-system coral ages reveal persistent suborbital sea-level cycles. *Science.* **308**, 401–404.

Thunell R. C. and Williams D. F. (1983) Paleotemperature and paleosalinity history of the estern Mediterranean during the Late Quaternary. *Palaeogeogr. Palaeoclimatol. Palaeoecol.* **44**, 23–39.

Toland H., Perkins B., Pearce N., Keenan F. and Leng M. J. (2000) A study of sclerochronology by laser ablation ICP-MS. *J. Anal. At. Spectrom.* **15**, 1143–1148.

Tremblay P., Peirano A. and Ferrier-Pages C. (2011) Heterotrophy in the Mediterranean symbiotic coral *Cladocora caespitosa*: comparison with two other scleractinian species. *Mar. Ecol. Prog. Ser.* **422**, 165–177.

Tripati A. K., Eagle R. A., Thiagarajan N., Gagnon A. C., Bauch H., Halloran P. R. and Eiler J. M. (2010) 13C–18O isotope signatures and "clumped isotope" thermometry in foraminifera and coccoliths. *Geochim. Cosmochim. Acta* **74**, 5697–5717.

Trotter J., Montagna P., McCulloch M., Silenzi S., Reynaud S., Mortimer G. E., Martin S., Ferrier-Pagès C., Gattuso J. P. and Rodolfo-Metalpa R. (2011) Quantifying the pH "vital effect" in the temperate zooxanthellate coral *Cladocora caespitosa*: Validation of the boron seawater pH proxy. *Earth Planet. Sci. Lett.* **303**, 163–173.

Turner J. A., Leeder M. R., Andrews J. E., Rowe P. J., Van Calsteren P. and Thomas L. (2010) Testing rival tectonic uplift models for the Lechaion Gulf in the Gulf of Corinth rift. *J. Geol. Soc. London.* **167**, 1237–1250.

U.S. Agency for International Development (2007) Southeast Europe - Wildfires and Drought. *Fact Sheet #1, Fisc. Year 2007*, 2. Available at: http://reliefweb.int/sites/reliefweb.int/files/resources/11D630DB90C5BC274 925735B00019D36-Full_Report.pdf [Accessed February 6, 2015].

Uchikawa J. and Zeebe R. E. (2012) The effect of carbonic anhydrase on the kinetics and equilibrium of the oxygen isotope exchange in the CO2–H2O system: Implications for δ18O vital effects in biogenic carbonates. *Geochim. Cosmochim. Acta* **95**, 15–34.

Urey H. C. (1947) The thermodynamic properties of isotopic substances. *J. Chem. Soc.*, 562–581.

Usdowski E. and Hoefs J. (1993) Oxygen isotope exchange between carbonic acid, bicarbonate, carbonate, and water: A re-examination of the data of McCrea (1950) and an expression for the overall partitioning of oxygen isotopes between the carbonate species and water. *Geochim. Cosmochim. Acta* **57**, 3815–3818.

De Villiers S., Nelson B. K. and Chivas A. R. (1995) Biological-controls on coral Sr/Ca and δ18O reconstructions of sea-surface temperatures. *Science.* **269**, 1247–1249.

De Villiers S., Shen G. T. and Nelson B. K. (1994) The Sr/Ca-temperature relationship in coralline aragonite: Influence of variability in (Sr/Ca)seawater and skeletal growth parameters. *Geochim. Cosmochim. Acta* **58**, 197–208.

Vreča P., Bronić I. K., Horvatinčić N. and Barešić J. (2006) Isotopic characteristics of precipitation in Slovenia and Croatia: Comparison of continental and maritime stations. *J. Hydrol.* **330**, 457–469.

Wainwright S. A. (1963) Skeletal organisation in coral, Pocillopora damicornis. *Q. J. Microsc. Sci.* **104**, 169–183.

Watson E. B. (2004) A conceptual model for near-surface kinetic controls on the trace-element and stable isotope composition of abiogenic calcite crystals. *Geochim. Cosmochim. Acta* **68**, 1473–1488.

Watson E. B. and Liang Y. (1995) A simple model for sector zoning in slowly grown crystals: Implications for growth rate and lattice diffusion, with emphasis on accessory minerals in crustal rocks. *Am. Mineral.* **80**, 1179–1187.

Weber J. N. (1973) Incorporation of strontium into reef coral skeletal carbonate. *Geochim. Cosmochim. Acta* **37**, 2173–2190.

Weber J. N. and Woodhead P. M. (1972) Temperature dependance of oxygen-18 concentration in reef coral carbonates. *J. Geophys. Res.* **77**, 463–473.

Weil S. M., Buddemeier R. W., Smith S. V and Kroopnick P. M. (1981) The stable isotopic composition of coral skeletons - control by environmental variables. *Geochim. Cosmochim. Acta* **45**, 1147–1153.

White R. (1998) Oxygen isotope systematics of the freshwater mollusc *Lymnaea peregra.* Thesis, University of East Anglia.

Wierzbowski H. (2007) Effects of pre-treatments and organic matter on oxygen and carbon isotope analyses of skeletal and inorganic calcium carbonate. *Int. J. Mass Spectrom.* **268**, 16–29.

Wikipedia (2007) 2007: Croatian coast fires. **2013**. Available at: http://en.wikipedia.org/w/index.php?title=2007_Croatian_coast_fires&action =history.

Yu X. and Inesi G. (1995) Variable Stoichiometric Efficiency of Ca2+ and Sr2+ Transport by the Sarcoplasmic Reticulum ATPase. *J. Biol. Chem.* **270**, 4361–4367.

Zaarur S., Affek H. P. and Brandon M. T. (2013) A revised calibration of the clumped isotope thermometer. *Earth Planet. Sci. Lett.* **382**, 47–57.

Zaarur S., Olack G. and Affek H. P. (2011) Paleo-environmental implication of clumped isotopes in land snail shells. *Geochim. Cosmochim. Acta* **75**, 6859–6869.

Zanchetta G., Drysdale R. N., Hellstrom J. C., Fallick A. E., Isola I., Gagan M. K. and Pareschi M. T. (2007) Enhanced rainfall in the Western Mediterranean during deposition of sapropel S1: stalagmite evidence from Corchia cave (Central Italy). *Quat. Sci. Rev.* **26**, 279–286.

Zaso C., Goy J. L., Dabrio C. J., Bardaji T., Somoza L. and Silva P. G. (1993) The last interglacial in the Mediterranean as a model for the present interglacial. *Glob. Planet. Change* **7**, 109–117.

Zecchin M., Caffau M., Civile D. and Roda C. (2010) Anatomy of a late Pleistocene clinoformal sedimentary body (Le Castella, Calabria, southern Italy): A case of prograding spit system? *Sediment. Geol.* **223**, 291–309.

Zecchin M., Nalin R. and Roda C. (2004) Raised pleistocene marine terraces of the Crotone peninsula (Calabria, southern Italy): facies analysis and organization of their deposits. *Sediment. Geol.* **172**, 165–185.

Zeebe R. E. (1999) An explanation of the effect of seawater carbonate concentration on foraminiferal oxygen isotopes. *Geochim. Cosmochim. Acta* **63**, 2001–2007.